School of Medicine

Understanding Proteolytic Processing of Melanoma Cell Adhesion Molecule (MCAM) in Cutaneous Melanoma

Tenielle George

0000-0002-5746-0214

This thesis is presented for the Degree of

Doctor of Philosophy

Curtin University

June, 2023

Declaration

To the best of my knowledge and belief this thesis contains no material previously published by any other person except where due acknowledgment has been made. This thesis contains no material which has been accepted for the award of any other degree or diploma in any university.

Signature: [redacted]

Date: 17/06/2023

Abstract

Cutaneous melanoma is one of the most common cancers in Australia. Typically, patients with melanoma have a high survival rate when tumours are detected and treated early. However, the aggressive nature of melanoma means tumours can rapidly spread and become difficult to treat, and patients with metastatic melanoma have significantly poorer survival rates. Melanoma cell adhesion molecule (MCAM/CD146/MUC18) is a transmembrane glycoprotein that contributes to the metastatic progression of melanoma and is associated with lower survival rates. MCAM exists as multiple isoforms, including a long and short isoform that are generated by alternative splicing. A soluble isoform (sMCAM) also exists, which is functionally relevant in melanoma progression and has potential as a therapeutic target. Indeed, sMCAM is released from melanoma cells and can influence both endothelial cells (paracrine) and tumour cells (autocrine) to foster tumour progression.

To date, most of the knowledge pertaining to sMCAM production and function has been studied in endothelial cells. Harnessing the therapeutic potential of sMCAM in melanoma will require a clearer understanding of how it is generated in these cells. Evidence suggests that MCAM undergoes sequential proteolytic cleavage, referred to as “regulated intramembrane proteolysis” (RIP), to generate both the soluble isoform and a C-terminal fragment (MCAM-CTF). The aim of this research was to firstly investigate the proteolysis of MCAM, including the role of metalloproteinases in generating sMCAM by ectodomain shedding, and secondly to determine the fate of the MCAM-CTF in melanoma cells *in vitro*. Finally, we aimed to improve our understanding of different mechanisms that may regulate ectodomain shedding and CTF cleavage.

Our data suggest that full-length MCAM is susceptible to metalloproteinase (MP)-mediated ectodomain shedding, and that different melanoma cell lines have varying abilities to release sMCAM into the cell culture media. This is possibly associated with the expression of ADAM10 and/or ADAM17, which are members of the MP family, since these were differentially expressed by melanoma cell lines. The MCAM-

CTF is the second product of ectodomain shedding and is hypothesised to undergo sequential internalisation and proteolytic processing mediated by the gamma (γ)-secretase complex. In our hands the MCAM-CTF accumulated in the juxtanuclear region of various melanoma cell lines, where it localised within LAMP2-positive vesicles. Further accumulation was observed when these cells were treated with a broad-spectrum γ-secretase inhibitor. Meanwhile knockout of either of the proteolytic components of the γ-secretase complex - presenilin (PS)1 or-2 - altered the expression of full-length MCAM but did not inhibit cleavage of the MCAM-CTF, suggesting PS1 and PS2 may function interchangeably. Collectively, these results provide evidence that MCAM in melanoma cells undergoes sequential proteolytic processing involving a member of the MP family, followed by PS1 and/or PS2. This is also one of the first studies to identify MCAM as a substrate of γ-secretase.

Regulation of these cleavage events can occur at either the substrate level or the protease level. Since the overexpression of ADAM10 and ADAM17 did not appear to enhance MCAM cleavage in melanoma cell lines, we investigated whether various post-translational modifications or intracellular binding proteins could inhibit or promote MCAM proteolysis. Specifically, palmitoylation and glycosylation were not associated with enhanced MCAM ectodomain shedding, whilst binding of the intracellular proteins, moesin and calmodulin, to the MCAM-CTF could not be proven to reciprocally regulate MCAM ectodomain shedding due to experimental issues.

Overall, this research has contributed to the understanding of MCAM processing in melanoma cells, which may assist in overcoming barriers in the generation of MCAM-targeted therapies for melanoma.

Acknowledgements

I would first like to thank my primary supervisor, Dr Danielle Dye, for being an incredible mentor and role model. Your support during difficult times (of which there were many!), and your unwavering faith in my ability has havee this all possible. You have gone above and beyond to help me achieve my goals, and for that, I will always be grateful. I would also like to say thank you to you, and to Professor Deirdre Coombe, for not hesitating to take me on as a PhD student. It has been an honour to work in your lab, and I am so grateful to have learned from such incredible researchers.

To my lab-mates who have come and gone over the years- thank you for sharing the journey and making challenging times in the lab more bearable. I am particularly grateful to those who have shared the laughs and the tears, and whom I have built lasting friendships with. I would especially like to thank Jessica Bennett and Michelle Schwager, who were always available for chats, coffees, or snacks. You are each incredibly smart and strong women, and I am grateful to have had you in my support network over the past few years.

A heartfelt thank you must also be extended to the late Beverley Kinnear, an amazing teacher and friend who instilled to me all her knowledge of tissue culture. Thank you for making me a better scientist.

To my colleagues and peers, journey has been long and hard, but it is always reassuring to have people around who understand the challenges and who will not hesitate to provide support where it is needed. And a special shout out to Melissa Eccles, a good friend, and an incredible researcher. It is a rare pleasure to come across such an intelligent, motivated, and generous individual, and I am so thankful for all the help you have given me, and the huge contribution you have made to my thesis.

I would also like to recognise the financial support I received from the Australian Government Research Training Program (RTP) Scholarship and the Curtin University Higher Degree by Research (HDR) Scholarship.

I would like to acknowledge all those who have given me support outside the university, including my employers and colleagues. I am especially thankful to my manager, Ian Sproul, for his generosity in providing me with the flexibility to work while I complete my thesis, and no shortage of encouraging words and witty humour. To my other colleagues and managers at AGC, thank you for giving me the chance to learn new skills, build friendships, and for supporting me throughout this long journey.

To my family, especially my parents, who have encouraged and supported me every step of the way. You have provided the love and care that I needed to make it this far in life. Thanks, Dad, for your wise words of encouragement, and for always sharing your M&Ms. And thanks Mum, for helping me maintain my sanity with chocolate, coffee, and the occasional board game or two. This endeavour would not have been possible without you both. Thank you also to my sister, Courtney. I consider myself extremely fortunate to have had someone by my side throughout this entire experience. We have had some amazing adventures and have overcome some incredible challenges. Thank you for showing me it is possible.

Thank you to my friends, especially Ashleigh and Emily, for reminding me to have fun from time-to-time, and for ensuring I reach my monthly cookie quota!

And finally, thank you to my wonderful fiancé, Nick. If not for you, I may never have been “ready” to submit my thesis. It has been challenging for us both, but your patience and encouragement have meant the world to me. You are truly one in a million.

Attribution Statement

Publications

A publication is currently being prepared from data in this thesis, namely from Chapter 5 (presenilin cleavage).

Attribution

Apart from that listed below, all laboratory work and data analysis presented in this thesis was undertaken by Tenielle George. Resources or techniques used in this thesis, that were created, developed, or performed by colleagues, were:

Plasmids

pCDNA3.1-MCAM plasmid was provided by Dr Stéphane Karlen (Dermatological Clinic, Inselspital, Berne, Switzerland).

pSpCas9(BB)-2A-GFP plasmids containing guide sequences were cloned by Ms Melissa Eccles (Curtin Medical School, Curtin University).

Cell lines

The SB2 cell series (SB2 14.1, SB2 LP and SB2 YG) used throughout this thesis were generated by Dr Danielle Dye (Curtin Medical School, Curtin University).

The MM253 presenilin knock out/knock down cells used in Chapter 5 were generated by Dr Danielle Dye (Curtin Medical School, Curtin University).

The HEK293 presenilin knock out/knock down cells used in Chapter 5 were generated by Ms Melissa Eccles (Curtin Medical School, Curtin University).

Presenilin quantification method

The method to quantitate presenilin 1 and 2 protein expression, and directly compare the two, was developed and performed by Ms Melissa Eccles (Curtin Medical School, Curtin University).

Acknowledgement of Country

We acknowledge that Curtin University works across hundreds of traditional lands and custodial groups in Australia, and with First Nations people around the globe. We wish to pay our deepest respects to their ancestors and members of their communities, past, present, and to their emerging leaders. Our passion and commitment to work with all Australians and peoples from across the world, including our First Nations peoples are at the core of the work we do, reflective of our institutions' values and commitment to our role as leaders in the Reconciliation space in Australia.

List of Abbreviations

Degrees Celsius	^{o}C
2-BP	2-bromohexadecanoic acid
ACE2	Angiotensin-converting enzyme 2
ACTAB	Beta actin
AD	Alzheimer's disease
ADAM	A disintegrin and metalloproteinase
AGRF	Australian genome research facility
AICD	APP intracellular domain
AKT	Protein kinase B
ALCAM	Activated leukocyte cell adhesion molecule
Amot	Angiomotin
AP-2	Apetala 2
Aph-1	Anterior pharynx defective
APP	Amyloid precursor protein
APS	Ammonium persulfate
APT	Acyl protein thioesterase
AR	Amphiregulin
ATF-3	Activating transcription factor 3
Aβ	Amyloid beta
BACE	beta-site amyloid precursor *protein* cleaving enzyme
BCA	Bicinchoninic acid
BSA	Bovine serum albumin
Ca^{2+}	Calcium
$CaCl_2$	Calcium chloride

CAF	Cancer associated fibroblast
CAM	Cell adhesion molecule
CaM/*CALM*	Calmodulin
CAMK	Calmodulin-dependent kinases
CASC3	Cancer susceptibility candidate 3
Cat	Catalogue number
CDCP1	CUB-domain-containing protein 1
CHX	Cycloheximide
CLCP1	CUB and LCCL domain containing protein 2
CO_2	Carbon dioxide
Coding DNA	cDNA
Co-IP	Co-immunoprecipitation
COPD	Chronic obstructive pulmonary disease
CPI	cOmplete™ EDTA-free protease inhibitors
CSC	Cancer stem cell
CSL	CBF1, Suppressor of Hairless, Lag-1
CTF	C-terminal fragment
DAPI	4’6-diamidine-2’-phenylindole
DAPT	*N*-[*N*-(3,5-difluorophenacetyl)-L-alanyl]-(*S*)-phenylglycine t-butyl ester
ddH_2O	Double distilled water
DDR1	Discoidin domain receptor 1
DMEM	Dulbecco’s Minimum Essential Medium
DMJ	Deoxymannojirimycin
DMSO	Dimethyl sulfoxide
DN	Dominant negative

DNA	Deoxyribonucleic acid
dKO	Double knockout
DTT	Dithiothreitol
E.coli	*Escherichia coli*
ECD	Extracellular domain
ECGS	Endothelial cell growth supplement
ECM	Extracellular matrix
EDTA	Ethylenediaminetetraacetic acid
EGF	Epidermal growth factor
EMT	Epithelial-mesenchymal transition/transformation
eNOS	Endothelial nitric oxide synthase
EpCAM	Epithelial cell adhesion molecule
ER	Endoplasmic reticulum
ERBB4	Erb-B2 receptor tyrosine kinase 4
ERK1/2	Extracellular signal related kinase 1/2
ERM	Ezrin-Radixin-Moesin
EtOH	Ethanol
FAK	Focal adhesion kinase
FADD	Fas-associated Death Domain
FBS	Foetal bovine serum
FC	Flow cytometry
FGF	Fibroblast growth factor
FITC	Flourescein Isothiocyanate
FYN	Proto-oncogene tyrosine kinase
γ-secretase	Gamma secretase
GAPDH	Glyceraldehyde 3-phosphate dehydrogenase

GalNAc	N-acetylgalactosamine
GCNT3	glycosyltransferase β-1,3-galactosyl-oglycosyl-glycoprotein-β-1,6-N-acetylglucosaminyltransferase-3
GFP	Green fluorescent protein
GST	Glutathione S-transferase
g	Grams
GTP	Guanosine 5’-triphosphate
HA	Haemagglutinin
HB-EGF	Heparin binding EGF-like growth factor
HBS	Hepes-buffered saline
HCl	Hydrochloric acid
HEK	Human embryonic kidney
Hepes	4-(2-hydroxyethyl)-1-piperazineethanesulfonic acid
HIS	Heat-inactivated serum
HPLC	High performance liquid chromatography
HRP	Horse radish peroxidase
HUVEC	Human umbilical vein endothelial cell
I.F.	Immunofluorescence
ICD	Intracellular domain
iCliPs	Intramembrane cleaving proteases
Id-1	Inhibitor of DNA binding 1
Ig	Immunoglobulin
IgSF	Immunoglobulin superfamily
IL-R	Interleukin receptor
iPLA2	Phospholipase A2
IPTG	Isopropyl ß-D-1-thiogalactopyranoside

IQGAP1	IQ motif containing GTPase activating protein 1
KD	Knockdown
kDa	Kilodalton
KO	Knockout
KRAS	Kirsten rat sarcoma viral oncogene homolog
L	Litres
LAMP	Lysosome-associated membrane protein
LB	Luria-Bertani
LE	Late endosome
LPA	Lysophosphatidic acid
Lyso	Lysosome
M	Molar
mAb	Monoclonal antibody
mAmp	MilliAmperes
MAPK	Mitogen-activated protein kinase
MCAM	melanoma cell adhesion molecule
MCAM-l	MCAM-long
MCAM-sh	MCAM-short
MCS	Multiple cloning site
MFI	Mean fluorescent intensity
MGAT3	Beta-1,4-mannosyl-glycoprotein 4-beta-N-acetylglucosaminyl-transferase
MGAT5	Alpha-1,6-mannosylglycoprotein 6-beta-N-acetylglucosaminyl-transferase A
mg	Milligrams
$MgCl_2$	Magnesium chloride
µM	Micromolar

miRNA	Micro RNA
mL	Millilitres
mM	Millimolar
MMP	Matrix metalloproteinase
mRNA	Messenger RNA
MT-MMP	Membrane-type MMP
MVB	Multi-vesicular body
$NaCl_2$	Sodium chloride
NaPyr	Sodium pyruvate
NCAM	Neural cell adhesion molecule
NFκB	Nuclear factor kappa-light-chain-enhancer of activated B cells
NICD	Notch intracellular domain
nM	Nanomolar
NOF	Neurite outgrowth factor
NP40	Nonidet P40
NRG	Neuregulin
NTF	N-terminal fragment
O/N	Overnight
PAGE	Polyacrylamide gel electrophoresis
PBS	Phosphate-buffered saline
PBS/BSA	Phosphate-buffered saline/bovine serum albumin
PBST	Phosphate-buffered saline-Tween20
PCR	Polymerase chain reaction
PDGF	Platelet-derived growth factor
PDGFR	Platelet-derived growth factor receptor
PECAM	Platelet endothelial cell adhesion molecule

Pen-2	Presenilin enhancer 2
PFA	Paraformaldehyde
PI3K	Phosphoinositide 3-kinase
PKC	Protein kinase C
PMA	Phorbol-12-myristate-13-acetate
PMSF	Phenylmethylsulfonyl fluoride
PRMI	Roswell Park Memorial Institute Medium
PS/PSEN	Presenilin
PTK	Protein tyrosine kinase
PVDF	Polyvinylidene difluoride
qPCR	Quantitative polymerase chain reaction
RAGE	Receptor for advanced glycation end products
ROS	Reactive oxygen species
RHBDL2	Rhomboid-like 2
RiP	Regulated intramembrane proteolysis
RNA	Ribonucleic acid
RPS2	Ribosomal protein S2
RT	Room temperature
SD	Standard deviation
SDHA	Succinate dehydrogenase complex subunit A
SDS	Sodium dodecyl sulfate
SDS-PAGE	Sodium dodecyl sulfate polyacrylamide gel electrophoresis
SCID	Severe combined immunodeficiency
SE	Standard error
SEM	Standard error of the mean
SF	Serum-free

SFM	Serum-free media
SHPS-1	SHP substrate 1
sMCAM	Soluble melanoma cell adhesion molecule
SPP1	Secreted phosphoprotein 1
SPP	Signal peptide peptidases
sRAGE	Soluble receptor for advanced glycation end products
SW	Swainsonine
TACE	Tumour necrosis factor-alpha converting enzyme
TC	Tissue culture
TCGA	The Cancer Genome Atlas
TE	Trypsin-Ethylenediaminetetraacetic acid
TEM	Trans-endothelial migration
TEMED	Tetramethylethylenediamine
TGF-α	Transforming growth factor-alpha
TGN	Trans-Golgi network
TIMP	Tissue inhibitor of metalloproteinase
TMD	Transmembrane domain
TME	Tumour microenvironment
TNF-α	Tumour necrosis factor-alpha
TOF	Time of flight
TP	Trifluoperazine dihydrochloride
Tris	Tris (Hydroxymethyl) Aminomethane
TX-100	Triton X-100
UV	Ultraviolet
VCAM	Vascular cell adhesion molecule
VEGF	Vascular endothelial growth factor

Wnt	Wingless
WRAMP	Wnt-receptor-actin-myosin-polarity
WT	Wild type
Zn^{2+}	Zinc

Table of Contents

List of Figures

List of Tables

Chapter 1

Introduction and Literature Review

1.1 Cancer progression and the tumour microenvironment

Throughout cancer progression, tumour cells modify and manipulate their surrounding microenvironment in order to survive and thrive. Although the complex interactions between tumour cells and the cellular and non-cellular components of the tumour microenvironment (TME) are not fully understood, it is apparent that stromal cells, the extracellular matrix (ECM), and soluble factors all impact tumour progression (Franco *et al.*, 2020).

Stromal cells encompass a large variety of cells that can be recruited to the tumour site in response to secreted factors (cytokines and chemokines), and include mesenchymal stem cells, immune cells and endothelial cells (Bussard *et al.*, 2016). Fibroblasts are also a major component of the TME and are collectively referred to as cancer associated fibroblasts (CAFs). These cells have diverse origins and enhance tumour growth by contributing to angiogenesis, immunosuppression, release of growth factors and cytokines, and remodelling of the ECM (Sahai *et al.*, 2020). Furthermore, both tumour and stromal cells secrete matrix-degrading enzymes that are critical for tumour cell invasion and metastasis (Castro-Castro *et al.*, 2015; Saad *et al.*, 2002); as remodelling of the ECM facilitates cancer cell migration and is associated with release of chemokines, growth factors and pro-angiogenic molecules (Balkwill *et al.*, 2012). Lastly, tumour and stromal cells also release suppressive factors (e.g. TGF-β, IL-10) that dampen the immune response (Dahmani & Delisle, 2018), thereby creating a niche that supports tumour growth, maintenance, and metastatic progression.

Evidently, complex interactions occur between the malignant and non-malignant components of the TME. These interactions may be facilitated either indirectly, such as through chemical signalling pathways, or via direct cell-cell communication, mediated by cell adhesion molecules (CAMs). CAMs are classified as either integrins, cadherins, selectins, or members of the immunoglobulin superfamily (IgSF). These are expressed on the surface of all cell types, are responsible for maintaining cell-cell and cell-matrix interactions and are crucial for the formation and

structural integrity of multicellular tissues (D'Arcy & Kiel, 2021). Importantly, changes in CAM expression profile are a hallmark of tumour initiation and progression.

Progression of cutaneous melanoma from the radial to vertical growth phase is characterised by progressive loss of E-cadherin, which mediates melanocyte-keratinocyte interactions and helps to regulate melanocyte proliferation (D'Arcy & Kiel, 2021). Meanwhile, expression of N-cadherin, αvβ3 integrin, and melanoma cell adhesion molecule (MCAM) on melanoma cells increases (McGary *et al.*, 2002). This switch in CAM expression reduces melanocyte-keratinocyte adhesion and facilitates the interaction of melanoma cells with each other, fibroblasts, endothelial cells and the ECM (Vandyck *et al.*, 2021), leading to invasion and intravasation into blood vasculature. Importantly, CAMs are also crucial for the initiation of metastatic growth of a tumour at secondary sites, where they allow tumour cells to adhere to and extravasate from blood vessels, followed by invasion of tissues distal to the primary site (Stoletov *et al.*, 2010). Evidently, CAM-mediated connections are important throughout tumour progression, allowing cells to maintain cell-cell contact, to interact with the matrix proteins that make up the scaffold of the tumour microenvironment, and to adhere to the blood vessel wall during extravasation. Beyond maintaining cell adhesions, CAMs conduct outside-in and inside-out signalling in response to binding other adhesion molecules or stromal elements or interacting with secreted factors within the intra-tumoural environment (Cavallaro & Dejana, 2011).

1.2 Melanoma is a cancer arising from melanocytes

Melanoma is an aggressive cancer that arises from melanin-producing cells called melanocytes. These cells originate from the neural crest and are predominantly located in the basal layer of the epidermis, but are also found in hair follicles, the meninges, and in the eye and ear (Mort *et al.*, 2015). Most frequently, melanoma arises from melanocytes of the skin (cutaneous melanoma) but can also develop from melanocytes in the eye (ocular melanoma) (Jovanovic *et al.*, 2013). For the sake of simplicity, the term "melanoma" will be used in this thesis in reference to the former, as it is the most common form of melanoma and is among the most

frequently diagnosed cancer types in Australia (Australian Institute of Health and Welfare, 2021b).

Global cancer data estimates there were 325 000 cases of cutaneous melanoma diagnosed in 2020 and 57 000 deaths. If these rates remain stable, it is estimated there will be 510 000 new cases and 96 000 deaths per year worldwide by 2040 (Arnold *et al.*, 2022). In Australia in 2021, cutaneous melanoma was one of the most frequently diagnosed cancer types, with a total of 16,878 cases and 1,315 deaths (Australian Institute of Health and Welfare, 2021a). The lifetime risk of being diagnosed with a melanoma in Australia has increased from 2.2% (1 in 46) in 1982, to 6.7% (1 in 22) in 2020; with the risk of death increasing from 0.4% to 0.7% over the same period (AIHW, 2021). Despite the high incidence, overall five-year survival rates for people diagnosed with cutaneous melanoma are over 90% (AIHW, 2021). This is primarily due to the detection of early-stage melanoma, which accounts for 78% of all melanoma diagnoses and has a 99.2% five-year survival rate. Five-year survival rates drop to 73.6%, 61.1% and 26.2% in people diagnosed with stage II, III and IV melanomas, respectively (National Cancer Control Indicators, 2019).

1.2.1 Melanoma staging

Following diagnosis, melanoma is staged to understand if and how far it has spread through the body, which informs prognosis and treatment. Melanoma is staged using the American Joint Committee on Cancer (AJCC) TNM system, which considers the depth and presence of ulceration of the primary lesion (tumour, T), whether the cancer has spread to nearby lymph nodes (nodes, N), and if the cancer has spread to distant lymph nodes and/or organs (metastasis, M) (Gershenwald *et al.*, 2017). In stage I melanoma, tumours are less than 1 mm thick (with or without ulceration) and are not associated with lymph node or distant metastasis. These tumours are treated by surgical excision, which is combined with sentinel lymph node biopsy if the tumour is ulcerated or greater than 0.8 mm thick (Davis *et al.*, 2019). Stage II melanoma includes primary lesions more than 1 mm thick (with or without ulceration); with no evidence of lymph node or distant metastasis (Gershenwald *et al.*, 2017).

Currently, patients with a risk of lymph node involvement undergo surgical excision of the primary tumour with 1-2 cm margins (depending on tumour thickness), plus sentinel lymph node biopsy (Curti & Faries, 2021). Patients who have sentinel node metastasis are categorised with stage III disease. Nodal observation (e.g. ultrasonography) rather than complete removal of surrounding lymph nodes is now recommended for these patients. This has reduced the number of patients undergoing invasive surgery and has not increased the risk of recurrence (Curti & Faries, 2021). Stage IV melanoma is when the cancer has spread to distant sites. Surgery may reduce tumour burden and relieve symptoms but is not curative and is accompanied by other treatments (Davis *et al.*, 2019).

1.2.2 Progression of cutaneous melanoma

During the early stages of melanoma development, tumours are restricted to the basal layer of the skin (stage I) and are generally treated by surgical excision (Davis *et al.*, 2019). The survival rates for these tumours are greater than 90%, however this decreases as tumour thickness increases (Lo *et al.*, 2018). Indeed, during the progression from stage I to stage II (tumour thickness >1-2 mm, +/- ulceration) (Gershenwald *et al.*, 2017), melanomas enter the vertical growth phase and begin to acquire metastatic capacity (Haqq *et al.*, 2005). Interestingly, certain melanoma-specific genes (*PLAB* and *L1CAM*) have been suggested to predict the likelihood of metastatic progression of melanoma, even in cases where tumour thickness is below 1 mm (Talantov *et al.*, 2005). As melanoma progresses and tumour thickness continues to increase, cells encroach the dermal layer of the skin. This is associated with increased risk of metastasis (Richetta *et al.*, 2018).

Stage III and stage IV melanomas are those that have spread- either to a local or distant lymph node, or to an organ. These tumours typically display a high mutational burden, increased proliferative capacity, resistance to apoptosis, and an ability to invade the basement membrane and migrate throughout the surrounding ECM (Rebecca *et al.*, 2020). Generally, these late-stage melanomas do not respond as well to therapeutic intervention and have a poorer prognosis. However, as addressed

in section 1.2.3, the therapeutic landscape for melanoma is changing and patient outcomes are improving (Jenkins & Fisher, 2021; Switzer *et al.*, 2022).

1.2.2.1 Genetic alterations in melanoma progression

Owing to their origin, transformed melanocytes (i.e. those that can progress to melanoma) display characteristics reminiscent of neural crest stem cells, including the ability to alter their gene expression and transition from an epithelial-like phenotype to a mesenchymal-like phenotype (Wessely *et al.*, 2021). Melanoma progression begins following alterations in key genes in melanocytes controlling cellular functions such as proliferation, apoptosis, and response to DNA damage (Bastian, 2014). Typically, these “driver mutations” lead to a gain of function in an oncogene. If this is followed by secondary loss of function mutations in tumour suppressor genes, melanocytes accumulate additional variants in growth and survival promoting genes (Bastian, 2014; Bertolotto, 2013). Following the acquisition of proliferative capacity, melanoma cells begin to move from the epidermis into the underlying dermis. Once in the dermis, it is widely believed tumour cells enter the lumen of blood and lymphatic vessels. Once in the vasculature, cancer cells are carried via the circulation and may then move across the vessel wall to establish distant metastases (Adler *et al.*, 2017).

Shain *et al.* (2018) explored the sequential accumulation of somatic mutations during melanoma progression by comparing precurser lesions, primary melanoma, and subsequent metastases. The earliest genetic changes (driver mutations) identified were in genes in the mitogen-activated protein kinase (MAPK) pathway, followed by telomerase upregulation; with both associated with enhanced cell proliferation (Table 1-1) (Shain *et al.*, 2018). Within the MAPK pathway, *BRAF* is the most commonly mutated gene, with variants found in 35-65% of melanomas (Motwani & Eccles, 2021). Activating mutations are also found in *NRAS* and Rac family small GTPase 1 (*RAC1*), in 20% and 6% of melanoma, respectively (Krauthammer *et al.*, 2015). The tumour suppressor gene *NF1*, a negative regulator of *NRAS* function, is inactivated in 12-30% of melanoma (Curtin *et al.*, 2005), while *TERT* mutations are found in 83% of melanoma (Hayward *et al.*, 2017) and typically develop after MAPK

pathway mutations (Shain & Bastian, 2016). Key gene mutations and changes in CAM profile (discussed briefly in Section 1.1) during melanoma progression are summarised in Figure 1-1.

Table 1-1 Early genetic changes driving melanoma progression

Pathway	Pathway alterations (% of melanomas)	Genes
MAPK	92%	*BRAF, NRAS, RAC1, NF1*
Telomerase	83%	*TERT*
Chromatin remodelling	38%	*ARID2, ARID1A, ARID1B*
Histone	48%	*HDAC9, SETD2, MLL2/3*
Cell Cycle	40%	*CDKN2A, CCND1, CDK4/6*
PI3K	56%	*PTEN, AKT1/2/3*
Methylation	19%	*IDH1/2, TET2*
TP53	37%	*TP53, CHEK1/2, ATM*
WNT	29%	*AXIN1/2, APC*
Receptor Tyrosine Kinase	49%	*ERB4, PDGRF*

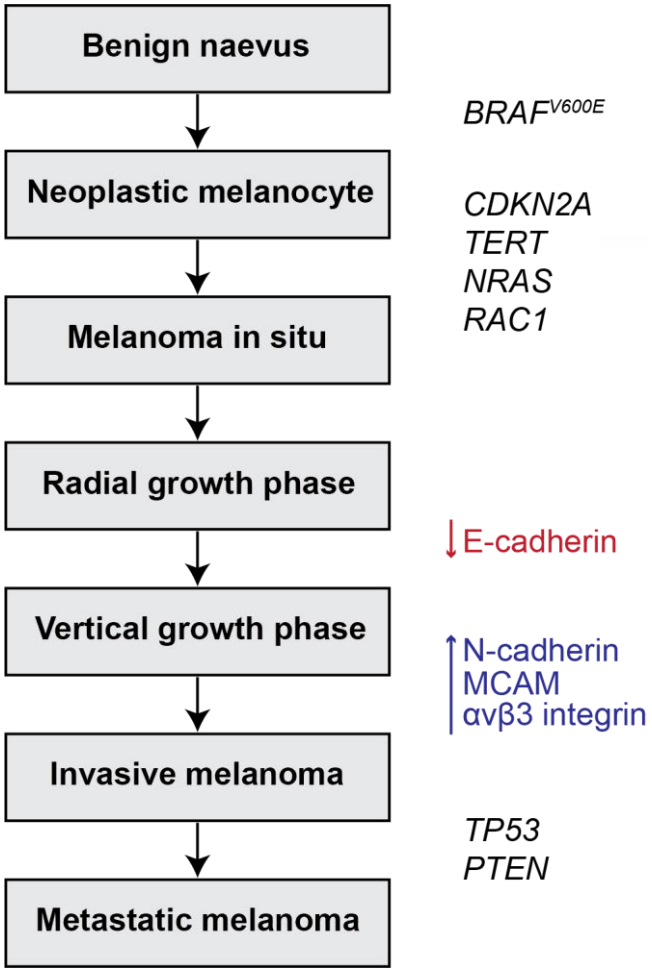

Figure 1-1 Simplistic overview of melanoma progression, key genetic driver mutations, and alterations in protein expression.

Various genetic mutations (italicised) are associated with the progression of melanoma from a benign naevus to a metastatic tumour. Alterations in the cell adhesion molecule profile (shown in red and blue) are also associated with progression towards a more aggressive phenotype.

Next, changes are seen in genes associated with chromatin remodelling, such as those that encode components of the human switch/sucrose non fermentable (SWI/SNF) chromatic remodelling complex, e.g. AT-rich interactive domain 1A, 1B and 2 (*ARID1A, ARID1B, ARID2*) and the polycomb repressive complex (*PRC2*) (Hayward *et al.*, 2017). In particular, *PCR2* activation is associated with the transition from a pre-cancerous lesion to melanoma (Shain & Bastian, 2016). Following this, mutations occur in genes that control the Gap 1 to Synthesis (G1/S) checkpoint in the cell cycle, and this is associated with the development of invasive potential (Shain & Bastian, 2016). The most commonly mutated gene is *CDKN2A,* which is also associated with familial melanoma (Potrony *et al.*, 2015). As

melanomas become thicker and more invasive, mutations accumulate in the tumour protein p53 (*TP53*) and phosphoinositide 3-kinase (PI3K) pathways (Shain & Bastian, 2016). Mutations in *TP53* and related genes are present in 37% of melanoma, while PI3K mutations are found in 56% of thicker melanomas. Of these, the majority (28–43%) are loss of function mutations in the phosphatase and tensin homolog gene (*PTEN*) (Motwani & Eccles, 2021).

The mutation burden in melanoma increases only slightly between melanoma *in situ* and those with invasive potential, suggesting that most mutations accumulate early in the disease process, consistent with a causative role of UV radiation (Shain & Bastian, 2016). Following the acquisition of invasive potential, the most common genetic changes are chromosomal copy number variations. The earliest changes are deletions in chromosome 9 and 10 followed by amplification of regions of chromosomes 1, 6, 7 and 8 (Shain & Bastian, 2016; Shteinman *et al.*, 2022).

1.2.3 Treatment of metastatic melanoma

From 1975 to 2011 the mainstay of treatment for metastatic melanoma was the chemotherapeutic agent dacarbazine, which had an objective response rate of 13-20%. Most tumour responses were partial, although a small number of complete, durable responses have been reported (Eggermont & Kirkwood, 2004). Since 2011, there has been a rapid evolution in treatment options, including targeted therapies and immune therapies. These are detailed below.

Targeted therapies include vemurafenib, dabrafenib, and encorafenib which act on the serine/threonine-protein kinase, B-Raf (BRAF) (Curti & Faries, 2021). These treatments may be used for the 50% of patients whose melanoma tumours contain an activating missense mutation (V600E, V600K) in the *BRAF* gene (Sanchez-Vega *et al.*, 2018; Schummer *et al.*, 2020). Initial response to these treatments is rapid, but progression-free survival is less than six months due to the development of resistance, which restores activity of the mitogen activated protein (MAP) kinase

signalling pathway (Curti & Faries, 2021). This can be addressed by combination therapy, where patients are treated with both BRAF and mitogen-activated protein kinase kinase (MEK1) inhibitors, which include trametinib, cobimetinib and binimetinib (Curti & Faries, 2021). There are currently three BRAF/MEK inhibitor combination therapies approved by the US Food and Drug Administration (FDA) for treatment of metastatic melanoma dabrafenib and trametinib, vemurafenib and cobimetinib, and encorafenib and binimetinib (Curti & Faries, 2021). All are associated with increased progression free survival (11-15 months) and overall survival (22 –34 months) compared to BRAF inhibitor monotherapy (Schummer *et al.*, 2020). However, patients will usually acquire resistance, and those with advanced BRAF-mutated melanoma often receive targeted therapy followed by immunotherapy (Curti & Faries, 2021).

Melanoma has historically been described as an immune-responsive tumour, based on evidence of spontaneous regression of the primary tumour in up to 5% of patients with metastatic disease, and the identification of vitiligo and the presence of tumour infiltration lymphocytes as favourable prognostic factors in melanoma patients (Huang & Zappasodi, 2022). However, the success of melanoma cell dissemination suggests that immune suppression or dysfunction offsets this immunogenicity (Huang & Zappasodi, 2022). In line with this, immunotherapy has transformed clinical outcomes in patients with metastatic melanoma (Curti & Faries, 2021).

Immunotherapy for melanoma includes monoclonal antibodies (mAbs) recognising cytotoxic T-lymphocyte antigen 4 (CTLA-4) and programmed death 1 (PD-1) protein (Curti & Faries, 2021; Davis *et al.*, 2019). These molecules are expressed on T cells and in a physiological environment are important in recognising “self” vs. “non-self” cells to prevent auto-immune reactions (Rotte, 2019). In the tumour microenvironment, melanoma cells upregulate the ligands of CTLA-4 and PD1 and thus escape immune recognition (Rotte, 2019). In simple terms, blockade of this interaction re-activates the immune system. Current standard of care for most patients with melanoma is now combination therapy using ipilimumab (anti-CTLA4 mAb) plus nivolumab (anti-PD1 mAb), which is associated with at 52% overall

survival at 5 years (Curti & Faries, 2021). Although survival is significantly increased compared to other treatments, few patients undergo complete remission (Curti & Faries, 2021). A new combination immunotherapy has recently been approved that combines nivolumab with relatlimab, which binds lymphocyte-activation gene 3 (*LAG-3*) (Tawbi *et al.*, 2022). Progression free survival at 12 months was 47% with this treatment, compared to 49% for ipilimumab-nivolumab in previous trials, suggesting relatlimab-nivolumab is a potential new treatment for melanoma patients (Tawbi *et al.*, 2022).

Side effects of these treatments can be significant, with 20% of patients experiencing immune-related adverse events including fatigue, rashes, lung, liver and gut inflammation and 3.5% of patients requiring hospitalisation (Kalinich *et al.*, 2021). Management of side-effects depends on both the body system affected and the severity of symptoms and includes immunosuppression and suspension of immunotherapy (Kalinich *et al.*, 2021; Schneider *et al.*, 2021). Despite these promising results, approximately 50% of patients with metastatic melanoma do not respond to immunotherapy and die of this disease. Recently, a model has been developed to predict response to immune therapy using routine clinical data, including the Eastern Cooperative Oncology Group Performance Status, presence/absence of liver and lung metastases, blood neutrophil-lymphocyte ratio and serum lactate dehydrogenase levels (Pires da Silva *et al.*, 2022). Predictive modelling can identify patients who are likely to benefit from immunotherapy, and just as importantly, those who are unlikely to and may be better directed to other therapies or clinical trials (Pires da Silva *et al.*, 2022).

1.3 Sequential proteolysis of transmembrane proteins in health and disease

Ectodomain shedding is a post-translational event involving protease-mediated cleavage of membrane-anchored proteins (Figure 1-2). Cleavage typically occurs at a membrane proximal region of the extracellular domain and leads to the release of a soluble protein (the “ectodomain”) into the extracellular space. Thus, ectodomain shedding converts membrane-anchored proteins into soluble factors that may

function independently of the full-length, membrane-bound proteins. Although recent data demonstrates that membrane shedding can occur in all organelles of the secretory and endocytic pathway (Lichtenthaler *et al.*, 2018), the focus of this review is on shedding from the plasma membrane.

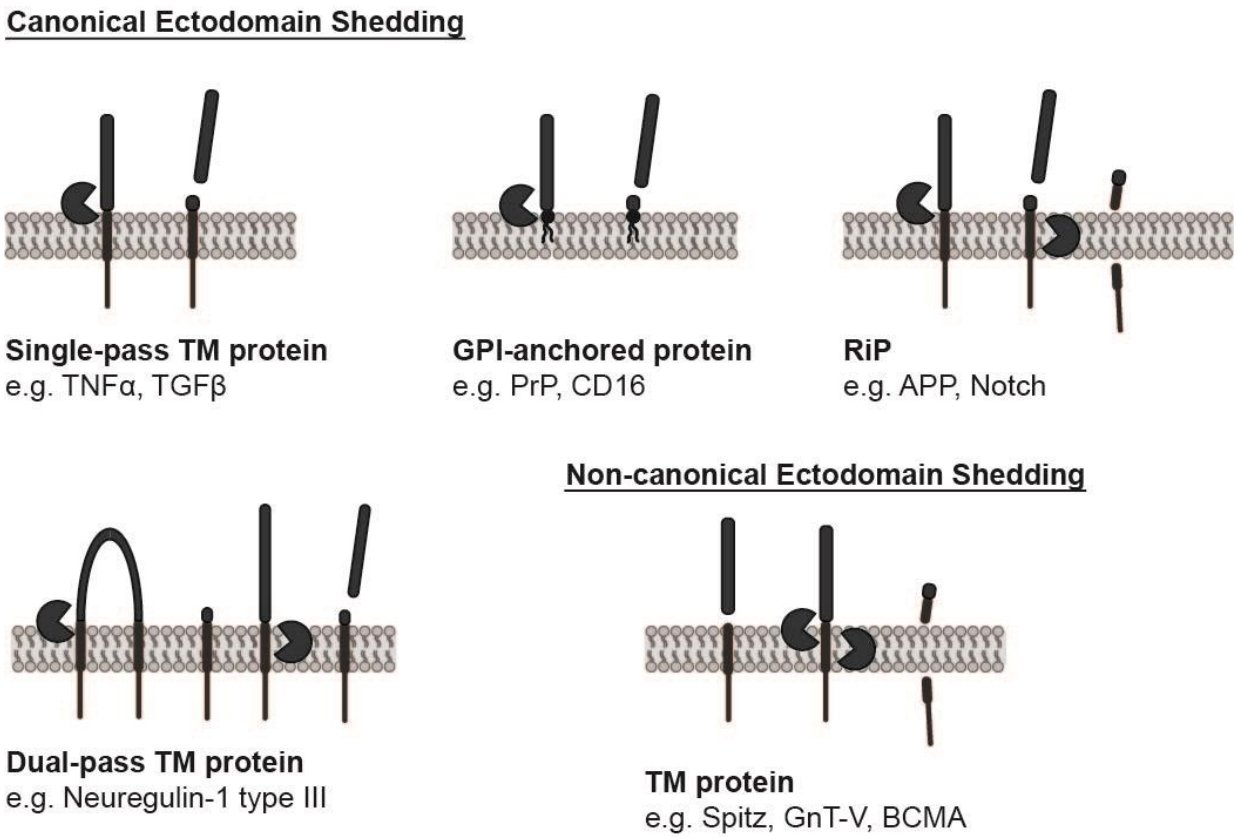

Figure 1-2 Sequential cleavage of type I transmembrane proteins

Membrane-bound proteins are susceptible to protease-mediated cleavage that leaves behind a remnant fragment that is often susceptible to further proteolytic processing. Adapted from Lichtenthaler *et al.* (2018).

A wide variety of cell surface proteins are susceptible to cleavage, including cytokines, growth factors, enzymes and cell adhesion molecules; and in many cases it is required for their biological activity (Hayashida *et al.*, 2010). Indeed, it has been shown that metalloproteinase-dependent ectodomain shedding is essential for activation of growth factors such as the epidermal growth factor (EGF) receptor ligands transforming growth factor-alpha (TGF-α), heparin binding EGF-like growth factor (HB-EGF), and amphiregulin (AR) (Jackson *et al.*, 2003; Sternlicht *et al.*, 2009). Similarly, tumour necrosis factor-alpha (TNF-α) (Bell *et al.*, 2007), interleukin

receptors (de Oca *et al.*, 2010), and granulocyte-macrophage colony-stimulating factor receptor alpha (GM-CSFRα) (Prevost *et al.*, 2002) are among the many receptors/ligands that undergo ectodomain shedding to produce biologically active molecules.

As well as generating novel signalling molecules, proteolytic cleavage of protein ectodomains is important for other functions, including the downregulation of cell surface ligand and receptor levels, and subsequent termination of downstream signalling pathways. For instance, cleavage of the transmembrane receptor RAGE (receptor for advanced glycation end products) generates soluble RAGE (sRAGE), which has been proposed to act as a decoy for RAGE ligands. More recently, RAGE ectodomain shedding has also been linked to cell migration through promotion of cell adhesion, spreading, and actin cytoskeleton reorganisation (Braley *et al.*, 2016).

Similarly, ectodomain shedding of several other cell surface proteins has been reported to promote cell migration, acting via a range of different mechanisms. This includes the ectodomain of L1 adhesion molecule (generated by ADAM10 cleavage), which promotes cell migration by interacting with, and signalling through, cell surface αvβ5 integrin in an autocrine and/or paracrine manner (Mechtersheimer *et al.*, 2001). Additionally, matrix metalloproteinase (MMP)-7-mediated shedding of E-cadherin in stomach cancer cells is associated with dissociation of E-cadherin/beta (β)-catenin complex and increased invasion *in vitro* (Lee *et al.*, 2007), and ectodomain shedding of SHPS-1 (SHP substrate-1), a transmembrane protein found on neurons and macrophages, has been shown to contribute to rearrangement of the cell cytoskeleton to promote cell migration (Ohnishi *et al.*, 2004).

Alternatively, shedding may contribute to cell motility simply by disrupting cell-matrix interactions. This has been demonstrated using rat neuroblastoma cells, where ectodomain shedding of the 140 kDa isoform of neural cell adhesion molecule (NCAM-140) promoted cell migration by decreasing cellular adhesion to ECM substrates, particularly fibronectin. Here, it was speculated that metalloproteinase-mediated cleavage of NCAM-140 promoted cell migration in an ERK1/2-MAPK

(extracellular signal related kinase 1/2-mitogen activated protein kinase) and β1 integrin-dependent manner. Indeed, treating cells with either GM6001 (a broad-spectrum metalloproteinase inhibitor) or U0126 (a MEK1/2 inhibitor), resulted in increased adhesion to fibronectin and decreased NCAM140-stimulated haptotactic cell migration, suggesting that MMP-mediated cleavage is involved in this process (Diestel *et al.*, 2005).

Importantly, ectodomain shedding can also be considered a precursor event to regulated intramembrane proteolysis (RIP). This processing involves sequential cleavage of the intracellular tail of transmembrane proteins within the plasma membrane and is mediated by a novel family of proteases that are collectively referred to as intramembrane cleaving proteases (iCLiPs) (Weihofen & Martoglio, 2003). Cleavage of transmembrane proteins by iCLiPs results in liberation of the cytoplasmic tail, which may then translocate to the nucleus to influence the transcription of target genes. This is true for molecules such as Notch (Struhl & Adachi, 1998), CD44 (Nagano & Saya, 2004; Okamoto *et al.*, 2001), and the amyloid precursor protein (APP)(von Rotz *et al.*, 2004). In the latter case, the APP intracellular domain (AICD) is believed to regulate the expression of more than 30 genes (Bukhari *et al.*, 2017). Alternatively, cleavage may promote disassembly of intracellular protein complexes and affect intracellular signalling events. Such is the case for E-cadherin, where cleavage interrupts the E-cadherin/β-catenin complex and releases β-catenin from the actin cytoskeleton (Marambaud *et al.*, 2002). Free cytoplasmic β-catenin is a key regulator of the Wnt signalling pathway, where it translocates into the nucleus and activates a subset of transcription factors, leading to changes in cell adhesion and migration (Tian *et al.*, 2011).

Evidently, ectodomain shedding plays a central role in maintaining many normal physiological processes. Meanwhile, aberrant shedding is frequently seen, and contributes to, pathologies such as cardiovascular (Fan *et al.*, 2016) and lung disease (Hayashida *et al.*, 2010), Alzheimer's disease (Lichtenthaler, 2006), schizophrenia (Hinkle *et al.*, 2006; Kalus *et al.*, 2006; Vawter *et al.*, 2001), and cancer, where release of soluble factors contributes to the formation/maintenance of

a “metastatic niche” (Miller *et al.*, 2017). Indeed, abnormal ectodomain shedding is a feature common to many types of cancer including melanoma, glioblastoma, lung cancer and breast cancer (Miller *et al.*, 2017), and the shed substrates may have oncogenic potential. Additionally, shedding of membrane-anchored proteins (such as vascular endothelial cadherin and vascular cell adhesion molecule 1) from the tumour vasculature has been speculated to contribute to neovascularisation and tumour cell extravasation (Fröhlich *et al.*, 2013). Understanding which proteins are shed in certain pathological conditions also has potential significance for developing a non-invasive screening process for disease biomarkers and/or monitoring treatment. Further, as ectodomain shedding is a complex event involving a number of intracellular regulatory proteins and membrane-associated proteases, understanding the regulation of this process may have important clinical significance for treatment of diseases that involve dysregulated shedding of membrane-bound proteins (Miller *et al.*, 2017).

1.3.1 Proteases are responsible for ectodomain shedding

Ectodomain shedding is an enzyme-driven process. Proteases are considered “canonical sheddases” if they cleave transmembrane proteins in the luminal juxtamembrane region, and “non-canonical sheddases” if they cleave within the transmembrane domain or at the membrane boundary (Lichtenthaler *et al.*, 2018). In addition, sheddases can be categorised as “full time”, if their primary role is ectodomain cleavage, or “part time”, if they primarily have non-shedding functions, but can act as sheddases for specific substrates. Unlike other proteases, sheddases do not cleave proteins at a clearly identified amino acid motif. Instead, they generally cleave substrates at a relatively fixed distance from the membrane (Lichtenthaler *et al.*, 2018). Thus, shedding is modulated by a wide range of factors, both protease and substrate-specific (see Section 1.4). Typically, members of the zinc $(Zn^{2})^{+}$-dependent family of proteases, including MMPs, A disintegrin and metalloproteinases (ADAMs), and membrane-type matrix metalloproteinases (MT-MMPs), are responsible for ectodomain shedding of membrane-anchored proteins and are classified as canonical sheddases. Indeed, a number of cases have demonstrated that broad spectrum inhibition of these proteases lowers the secretion of soluble proteins into cell culture media. In particular, ADAMs have a wide

repertoire of substrates, including CAMs such as L-selectin (Killock & Ivetić, 2010), N-cadherin (Reiss *et al.*, 2005), E-cadherin (Najy *et al.*, 2008b), and L1 adhesion molecule (Mechtersheimer *et al.*, 2001). Extracellular matrix proteins (e.g. laminins and collagens), Notch-1, and APP, among others, are also cleaved by ADAMs (Reiss & Saftig, 2009). Overall, regulated ADAM-mediated cleavage is essential for physiological and developmental processes, and dysregulation is associated with various pathological conditions.

MMPs are also frequently become overexpressed in diseases, and it is well known that MMP activity is upregulated in a range of cancers, making these proteases an appealing target for anti-cancer therapies (Cathcart *et al.*, 2015). In particular, overexpression of MMP2 and MMP9 is a common feature of many solid tumours (Roomi *et al.*, 2009), and is associated with metastatic progression of melanoma (Hofmann *et al.*, 2003; Zigler *et al.*, 2011), triple negative breast cancer (Mehner *et al.*, 2014), prostate (Xie *et al.*, 2016) and ovarian cancers (Hu *et al.*, 2012). MMP expression during the early stages of tumour dissemination allows tumour cells to remodel their surroundings through degradation of the ECM, facilitating tumour cell migration. Additionally, MMP activity has been indirectly linked to tumour progression through regulation of apoptosis, cell proliferation, and angiogenesis. These proteolytic-independent mechanisms by which MMPs contribute to tumour progression have been reviewed in more detail elsewhere (Kessenbrock *et al.*, 2010; Shay *et al.*, 2015). Importantly, MMPs are also involved in ectodomain shedding (Hayashida *et al.*, 2010). MMP7 in particular is a documented sheddase of TNF-α (Gearing *et al.*, 1994), HB-EGF (Kivisaari *et al.*, 2010), and E-cadherin (Lee *et al.*, 2007). The relevance of MMPs in cancer progression makes them an appealing target for anti-cancer therapies (Cathcart *et al.*, 2015), however despite showing promise in *in vitro* studies (Li *et al.*, 2020), MMP inhibitors have been largely unsuccessful in the clinic due to severe side effects and/or lack of tumour response to treatment (Bendell *et al.*, 2020; Verhulst *et al.*, 2022).

Further, the membrane-type MMPs (MT-MMPs), which are MMPs that are tethered to the cell membrane, also contribute to tumour progression and ectodomain

shedding. They are particularly important during the early stages of tumour invasion, directly cleaving a broad range of ECM substrates including fibronectin, vitronectin, and collagen (Itoh, 2015) to allow tumour cell migration. MT-MMPs can also activate certain MMPs, namely pro-MMP2 and pro-MMP13 (Knäuper *et al.*, 1996; Sato *et al.*, 1994). These MMPs display gelatinase and collagenase activity, respectively, and thereby further contribute to ECM degradation. Among the six MT-MMPs (MT1-, MT2-, MT3-, MT4-, MT5-, MT6-MMP), MT1-MMP (also known as MMP14) is the best characterised (Itoh, 2015), and is implicated in metastatic progression, being particularly important at invasive front of a tumour (Castro-Castro *et al.*, 2015). This is especially true for breast cancer cells (Artym *et al.*, 2006) and melanoma cells (Hofmann *et al.*, 2003), where MT1-MMP is concentrated at the invadopodia and drives proteolysis-dependent cell migration and invasion. It can also cleave CAMs to promote cell migration. This is true for MT1-MMP-mediated cleavage of Syndecan-1, which is associated with migration of HT1080 human fibrosarcoma cells (Endo *et al.*, 2003). In addition, proteolytic cleavage of αV integrin has been linked to adhesion and cell motility on vitronectin (Deryugina *et al.*, 2002), while MT1-MMP-mediated cleavage of CD44 appeared to be critical for stimulating migration of breast carcinoma and osteosarcoma cells (Kajita *et al.*, 2001). Similarly, MT2-MMP is implicated in carcinoma progression, where it has been linked to E-cadherin cleavage and epithelial-mesenchymal transition/transformation (EMT) (Liu *et al.*, 2016). While less is understood about the remaining MT-MMPs, it is evident that these proteases make a significant contribution towards disease progression (Itoh, 2015).

Finally, tissue inhibitors of metalloproteinases, or TIMPs, are important regulators of MMP activity, and can play an indirect role in ectodomain shedding by regulating the activity of the metalloproteinases. For example, TIMP3 inhibits ADAM10 and ADAM17, which blocks collagen-dependent shedding of discoidin domain receptor 1 (DDR1) in human embryonic kidney (HEK) cells (Slack *et al.*, 2006). TIMP3 has also been identified as an inhibitor of shedding of the interleukin-2 receptor (IL-2R)-β (de Oca *et al.*, 2010). A recent review discusses in more detail the complex role of TIMPs in regulating multiple proteolytic events that contribute to different stages of

cancer progression. In particular, overexpression of TIMP1 or loss of TIMP3 expression are consistently linked with cancer progression (Jackson *et al.*, 2016).

In addition to the metalloproteinases, a limited number of other unrelated proteases have been implicated in ectodomain shedding, namely the rhomboid-like 2 (RHBDL2) protease, a type of intramembrane serine protease. RHBDL2 has been recognised for its ability to cleave cell-surface proteins such as Spint-1, DDR1, interleukin-6 receptor (IL-6R), discoidin, CUB and LCCL domain containing protein 2 (CLCP1), and Neph1 in mammalian cells, contributing to the regulation of epithelial homeostasis (Johnson *et al.*, 2017). Further, exogenous factors have been studied extensively for their ability to promote the cleavage of transmembrane proteins. In particular, shedding can be stimulated *in vitro* by phorbol esters and calcium ionophores (Horiuchi *et al.*, 2007; Killock & Ivetić, 2010; Wong *et al.*, 2016). This is believed to be achieved, at least in part, through activation of ADAM10 and ADAM17, however the mechanisms have not yet been fully defined (Horiuchi *et al.*, 2007). Interestingly, ectodomain shedding can also occur under normal culture conditions, which has been attributed to the presence of endogenous factors in the serum, particularly lysophosphatidic acid (LPA) (Hirata *et al.*, 2001).

1.3.1.1 ADAMs are ectodomain sheddases

The ADAMs belong to the metzincin (Zn^{2+}-dependent) superfamily of metalloproteinases, which act on a range of substrates and are heavily implicated in ectodomain shedding (Reiss & Saftig, 2009). Among the 12 ADAMs that appear to function as sheddases in human cells, ADAM10 and ADAM17 are most commonly associated with both physiological and pathological shedding of membrane-bound proteins (see Table 1-2) (Weber & Saftig, 2012). ADAM17 was originally idenitifed as tumour necrosis factor-α converting enzyme (TACE), after it was named as the primary sheddases of pro-TNFα (Black *et al.*, 1997).

Table 1-2 A brief list of ADAMs and their substrates

ADAM	Substrate	Cell-type	Reference
ADAM8	Neural cell adhesion molecule CHL1	COS-7 cells	(Naus *et al.*, 2004)
ADAM9	proHB-EGF	African green monkey kidney Vero cells	(Izumi *et al.*, 1998)
ADAM10	Glycoprotein VI	Platelets	(Facey *et al.*, 2016)
	HER2	Breast cancer	(Liu *et al.*, 2006)
	N-cadherin	Fibroblasts, neuronal cells	(Reiss *et al.*, 2005)
	E-cadherin	Epithelial cells (keratinocytes, MEFs)	(Maretzky *et al.*, 2005)
	APP (α-secretase site)	HEK293 cells, SH-SY5Y (neuroblastoma) cells	(Hartmann *et al.*, 2002), (Kuhn *et al.*, 2010)
	L1-CAM	Melanoma cells	(Lee *et al.*, 2010b)
ADAM12	VE-cadherin; Tie-2	Vascular endothelial cells	(Fröhlich *et al.*, 2013)
	VCAM-1	Dermal fibroblasts Epithelial cells	(Garton *et al.*, 2003) (Fröhlich *et al.*, 2013)
ADAM15	E-cadherin N-cadherin Amphiregulin	MCF-7 breast cancer cells PC-3 prostate cancer cells Murine mammary organoids	(Najy *et al.*, 2008b) (Najy *et al.*, 2008a) (Sternlicht *et al.*, 2009)
ADAM17	VCAM-1	Murine stomach epithelial cells and dermal fibroblasts	(Garton *et al.*, 2003)
	L-selectin	Murine 300.19 pre-B cells and ADAM17$^{\Delta Zn/\Delta Zn}$ MEFs	(Killock & Ivetić, 2010)
	EGFR ligands: Amphiregulin (APR) TGFα; HB-EGF; APR	Mammary epithelial cells ADAM17$^{-/-}$ MEFs	(Sternlicht *et al.*, 2009) (Sahin *et al.*, 2004)
	TNFα	Neutrophils and macrophages	(Bell *et al.*, 2007)
ADAM19	β-type neuregulin	N1E115 neuroblasts, COS7 cells (cleavage at the golgi)	(Yokozeki *et al.*, 2007)
ADAM28	CD200	B-cell chronic lymphocytic leukameia	(Twito *et al.*, 2013)

ADAM10 and 17 share a similar structure consisting of an N-terminal signal sequence, pro-domain, catalytic domain and disintegrin domain, followed by a,cysteine rich region, transmembrane region, and cytoplasmic tail (Figure 1-3) (Kato *et al.*, 2018). Maturation of these proteins requires removal of the pro-domain by proprotein convertases such as furin in the trans-Golgi network (TGN). It has also been suggested these enzymes are packaged in lipid rafts in the TGN, facilitating spatial separation of enzyme from substrate during protein packaging and transport (Gooz, 2010).

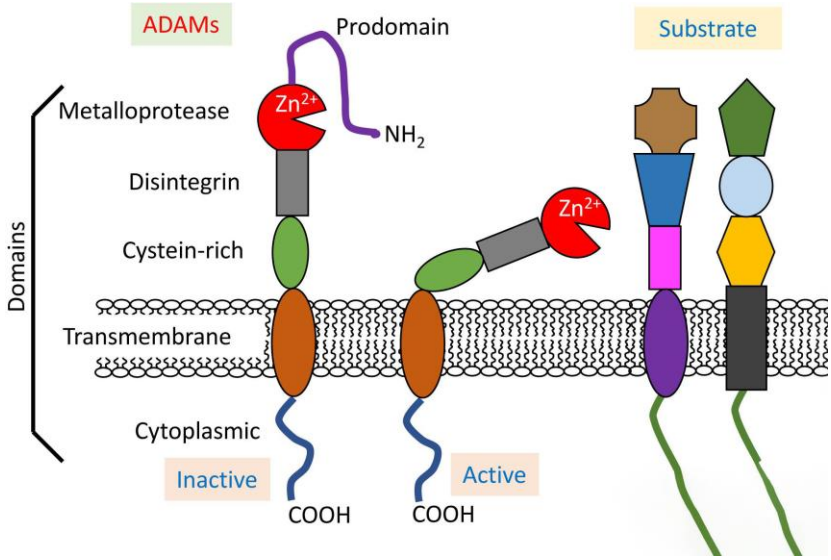

Figure 1-3 Schematic of ADAM10/ADAM 17 structure.

Removal of the pro-domain reveals the catalytically active metalloprotease domain. *Image credit: Kato et al. (2018)*.

ADAM10 and ADAM17 appear to play a central role in ectodomain shedding, and their importance has been scrutinised using mouse knockout models. In ADAM10-deficient mice, abnormal Notch-1 signalling affects the development of the central nervous system, somites, and cardiovascular system, leading to embryonic lethality at day 9.5 (Hartmann *et al.*, 2002). Meanwhile, ADAM17$^{-/-}$ mice are also non-viable, and this has been attributed to disruption of EGFR signalling (Peschon *et al.*, 1998b).

Cells derived from ADAM10- and ADAM17-deficient mice have further demonstrated the importance of these sheddases in physiology (Reiss & Saftig, 2009)).

Specifically, mouse embryonic fibroblasts (MEFs) derived from TACE$^{\Delta Zn/\Delta Zn}$ mice, which lack the Zn^{2+} binding domain required for activation of ADAM17, were used to demonstrate the importance of ADAM17 in ectodomain shedding of L-selectin. Here, cells from either wild-type or TACE$^{\Delta Zn/\Delta Zn}$ mice were transfected with L-selectin, and cell surface expression was measured in cells +/- treatment with Phorbol-12-myristate-13-acetate (PMA) or cantharidin to stimulate shedding. As expected, there was a significant reduction in shedding of L-selectin in cells from the knockout mice compared to WT mice (Killock & Ivetić, 2010). Fibroblasts from ADAM17-deficient mice were similarly used to demonstrate the role of ADAM17 in NCAM ectodomain shedding. In this instance, ADAM17-deficient fibroblasts expressing NCAM140 were transfected with ADAM17, which subsequently induced shedding of NCAM140 to produce a 110-kDa soluble ectodomain (Kalus *et al.*, 2006). In addition, cells from ADAM10-deficient mice have shown that ADAM10 is responsible for cleavage of substrates such as glycoprotein VI (Facey *et al.*, 2016), N-cadherin (Reiss *et al.*, 2005), and E-cadherin (Maretzky *et al.*, 2005). ADAM10 has also been identified as the α-secretase responsible for cleavage of APP, giving rise to a secreted version of APP that has a neuroprotective function (Kuhn *et al.*, 2010).

Increased ADAM activity is seen in several cancer types. For example, ADAM10 is elevated in metastatic melanoma (Lee *et al.*, 2010b) and has a pro-metastatic role in uveal melanoma (Gangemi *et al.*, 2014). ADAM10 expression has also been associated with breast cancer progression (Mullooly *et al.*, 2015), likely via increased HER2 shedding in breast cancer cells (Liu *et al.*, 2006). ADAM17 has also been studied in a number of model tumour systems (Hedemann *et al.*, 2018; Soto-Gamez *et al.*, 2020). Due to its role in activating EGFR ligands, it has been linked to cell proliferation, survival, invasion, and inflammation, which promote tumour progression. It is important to note that whilst increased ADAM expression in pathological conditions may account for increased shedding, the possibility also exists that proteolysis is regulated at the substrate level.

1.3.2 Intramembrane proteolysis by gamma secretase

In many cases, transmembrane proteins that undergo ectodomain shedding are also subject to further proteolysis of the intracellular domain. This sequential cleavage, termed regulated intramembrane proteolysis (RiP), typically occurs within the lipid bilayer, and is carried out by proteases collectively referred to as intramembrane cleaving proteases (iCliPs).

The predominant iCliP is γ-secretase, a multi-protein complex made up of four essential components: presenilin-1 or -2 (PS-1 and -2), nicastrin, anterior pharynx defective (Aph-1), and presenilin enhancer-2 (Pen-2) (Spasic & Annaert, 2008) (Figure 1-4). The presenilins are known as the catalytic components, while the remaining proteins are believed to be involved in docking of γ-secretase to the substrate (Shah *et al.*, 2005), formation and maturation of the γ-secretase complex (Chiang *et al.*, 2012), and promoting endoproteolysis of PS (Luo *et al.*, 2003), respectively. It is generally accepted that ectodomain shedding is an essential precursor event for RiP, and indeed studies have confirmed that nicastrin can sterically block the PS active site, thereby preventing substrates with large ectodomains from entering the γ-secretase complex (Bolduc *et al.*, 2016). However, substrates with naturally short ectodomains are susceptible to γ-secretase-mediated cleavage without prior processing by another protease (Laurent *et al.*, 2015).

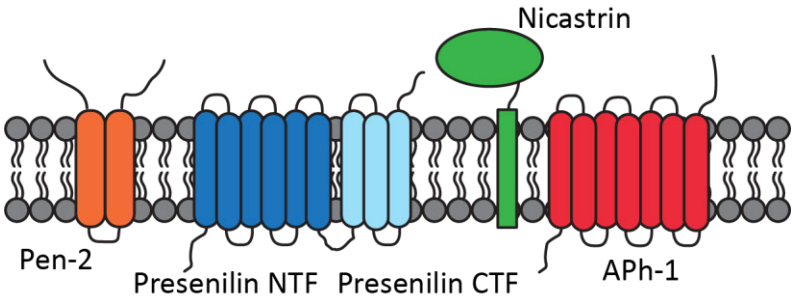

Figure 1-4 Schematic of the γ-secretase complex

γ-Secretase is a multi-subunit complex involved in the regulated proteolysis of type-I transmembrane proteins. Presenilin-1 and Presenilin-2 are the catalytic components of the γ-secretase complex. They undergo endoproteolysis by Presenilin-enhancer-2 (Pen-2), generating C-terminal and N-terminal fragments (CTF and NTF). Nicastrin is involved in docking substrates to γ-secretase and excluding large substrates. Anterior pharynx defective (Aph-1) participates in the maturation of γ-secretase.

In addition to γ-secretase, metalloproteinase site-1 and site-2 proteases (S1P and S2P, respectively) (Danyukova *et al.*, 2022), signal peptide peptidases (SPP) and SPP-like proteases (Mentrup *et al.*, 2020), and rhomboid proteases (Johnson *et al.*, 2017) are also recognised as iCliPs (Liu *et al.*, 2020). Together, these proteases share the responsibility of cleaving a broad array of substrates within the plane of the cell membrane. The overall consensus suggests that the proteolytic events orchestrated by iCliPs are responsible for the generation of soluble intracellular domains, which have important biological activity in a number of settings and appear to contribute to both physiological and pathological conditions (previously discussed in Section 1.3).

1.3.2.1 Presenilins and their relevance in cancer

Presenilin-1 (PS1) and presenilin-2 (PS2) are the highly homologous catalytic components of γ-secretase, encoded by the *PSEN1* and *PSEN2* genes, respectively. For these proteins to become catalytically active, full-length PS must undergo endoproteolytic processing as they become incorporated into the γ-secretase complex (Campbell *et al.*, 2003). This maturation step is facilitated by Pen-2, and ultimately produces an NTF and CTF (Luo *et al.*, 2003).

Structurally, mature PS proteins are multi-pass transmembrane proteins with an extracellular C-terminal domain and nine transmembrane domains (TMD) that are highly conserved between PS1 and PS2. Meanwhile, the intracellular N-terminal domain and cytosolic loop between TMD6 and TMD7 share little similarity (Sannerud *et al.*, 2016). In particular, the N terminus of PS2 contains an acidic dileucine sorting motif ([D/E]xxxL[L/I/M]). This motif is typically involved in endocytosis and trafficking of proteins from endosomes to the late endosome/lysosome (LE/lyso) (Pandey, 2009). In line with this, PS2 localises to lysosome-associated membrane protein (LAMP)-1-positive vesicles (Sannerud *et al.*, 2016), whereas PS1 is more widely distributed, being found in the perinuclear region and throughout the cytosol (Sannerud *et al.*, 2016; Takashima *et al.*, 1996). Moreover, domain switching experiments have confirmed the N-terminal region is responsible for directing PS2 to the late endosome/lysosome (Sannerud *et al.*, 2016).

PS1 is ubiquitously expressed and is considered a "tumour enhancer" in a number of cancers. Its expression is associated with lower survival rates in gastric cancer, contributing to migration and invasion of gastric cancer cells, and lymph node metastasis. Evidence suggests that it acts by dysregulating E-cadherin/β-catenin (Li *et al.*, 2016). *PSEN1* also contributes to enhancing chemosensitivity in bladder and gastric cancer, acting cooperatively with microRNA (miR)-193a-3p and miR-133a, respectively (Chen *et al.*, 2019a; Deng *et al.*, 2015). Further, in pancreatic cancer, increased expression of *PSEN1* (compared to non-cancerous tissue) was correlated with poor prognosis, while *PSEN2* expression was not (Jeon *et al.*, 2019). Interestingly, PS1 may be considered a favourable prognostic marker in breast cancer, where there was a significant association between low levels of expression of PS1 and poor survival (Peltonen *et al.*, 2013). It may also be favourable in oesophageal cancer, with research showing that downregulation of *PSEN1*, via miR-193a-3p, contributed to tumour resistance to radiation and chemotherapy (Meng *et al.*, 2016). The variances seen in different tumour types may be related to the origin of the tumour and the tissue-specific microenvironments (Li *et al.*, 2016).

The role of PS2 in cancer is less clear, however the association between PS2 and the Notch signalling pathway, which is associated with cancer progression, has linked deregulated PS2 expression to cancer progression. In breast cancer, two germline alterations in *PSEN2* (present in both primary tumour samples and in blood DNA) have been identified and may potentially contribute to malignancy. These alterations, (R62H and R71W) were associated with an increased rate of degradation of the full-length PS2 protein, which had downstream implications for Notch signalling in a *C. elegans* model. These alleles may also affect cell proliferation (To *et al.*, 2006). Furthermore, PS2 over-expression has been associated with regulation of reduced cell viability and increased apoptosis in neuronal cells, via activation of p53 and miR-34a (Li *et al.*, 2017).

Similar to PS1, PS2 can have opposing effects on cancer cells of different origin. In lung cancer, loss of PS2 expression has been linked to the development and growth of lung cancer cells. In particular, Yun *et al.* (2014) demonstrated that carcinogen-

induced lung cancer was more aggressive in PS2 knockout mice compared to WT mice. Here, loss of PS2 expression was associated with increased activity of the phospholipase A2 (iPLA2) motif of peroxiredoxin-6 (PRDX6). The authors suggest this enhanced iPLA2 activity may be linked to regulation of genes involved in cell proliferation, metastasis, and angiogenesis (Yun *et al.*, 2014). In contrast, in murine melanoma, *PSEN2* has been identified as a target of the MYC oncogene, such that increased *PSEN2* expression is linked to melanoma progression (Meliso *et al.*, 2017). Consistent with the murine data, microarray analyses using samples taken from human primary melanomas, benign nevi and healthy skin identified increased *PSEN2* expression in malignant melanomas compared to benign nevi (Haqq *et al.*, 2005; Talantov *et al.*, 2005). Analysis of a melanoma dataset from The Cancer Genome Atlas (TCGA) also found that patients whose tumours had high *PSEN2* expression had poorer overall survival compared to patients whose tumours had low *PSEN2*. Interestingly, *PSEN1* expression showed no relationship to survival in this dataset. Evidently, PS1 and PS2 have a relevant, yet controversial, role in tumorigenesis and tumour progression.

1.3.2.2 γ-secretase substrates and fate of the ICD

Owing to its relevance in Alzheimer's disease and Notch-signalling, γ-secretase has been well studied, and a diverse array of substrates are known to be cleaved by this complex, including Notch (Lee *et al.*, 2011), transmembrane glycoproteins such as E- and N-cadherin (Marambaud *et al.*, 2002; Uemura *et al.*, 2006), CD44 (Lammich *et al.*, 2002), nectins (Kim *et al.*, 2011), RAGE (Braley *et al.*, 2016; Zhang *et al.*, 2008a), and many more. These proteins share common features, including: a single pass transmembrane domain, a large ectodomain that can mediate cell adhesion, and a C-terminal domain that has intracellular signalling capabilities (Haapasalo & Kovacs, 2011).

Among the many γ-secretase substrates, APP remains the most well characterised and has been referred to as the "prototype RiP substrate". APP is constitutively cleaved at the N-terminus by either an α-secretase (ADAMs) or β-secretase (BACE1) to yield a membrane-tethered C-terminal fragment (C83 and C99,

respectively), as well as a soluble ectodomain. These proteolytic events are followed by cleavage of the APP C-terminal fragments by γ-secretase, giving rise to either a small P3 peptide (if C83 is cleaved) or the secreted amyloid beta (Aβ) peptide (following C99 cleavage) (Nhan *et al.*, 2015). This occurs at the ε-cleavage site and is followed by sequential truncation of the TMD fragment (Güner & Lichtenthaler, 2020). Finally, cleavage by γ-secretase gives rise to the APP intracellular domain (AICD), which is capable of translocating to the nucleus to regulate gene expression (von Rotz *et al.*, 2004).

Similar to APP, Notch also undergoes ectodomain shedding prior to γ-secretase-mediated cleavage and release of the intracellular domain. Here, ligand binding to Notch first initiates the signal transduction pathway, resulting in α-secretase mediated cleavage of the Notch ectodomain (by ADAM17), followed by intramembrane cleavage to generate the functional Notch intracellular domain (NICD). The NICD is then able to translocate to the nucleus where it binds the CSL (CBF1, Suppressor of Hairless, Lag-1) transcription factor and the transcriptional co-activator Mastermind, forming an activation complex that regulates the transcription of Notch target genes (Borggrefe *et al.*, 2016; Schroeter *et al.*, 1998; Tamura *et al.*, 1995).

Whilst many proteins undergoing RiP are involved in transcription regulation through nuclear translocation of the ICD, the E-cadherin C-terminal fragment (CTF-2) does not accumulate in the nucleus following its liberation from the cell membrane (Lal & Caplan, 2011). Rather, the evidence points towards it acting as a cytosolic effector that regulates cellular processes through β-catenin. The proposed mechanism involves PS1/γ-secretase mediated release of CTF-2, leading to dissociation of E-cadherin-β-catenin complexes and subsequent solubilisation of β-catenin. Ultimately, this promotes disassembly of cadherin-based adhesion junctions (Marambaud *et al.*, 2002). Meanwhile, other ICDs released after γ-secretase cleavage are simply degraded.

1.3.3 Transmembrane proteins can be released into the extracellular space via exosomes

Most studies on the ectodomain shedding of transmembrane proteins report that cleavage is a cell surface event. However, the presence of soluble ectodomains and metalloproteinases within cell-derived vesicles, particularly exosomes, suggests that shedding can also occur with intracellular compartments (Gutwein *et al.*, 2003; Stoeck *et al.*, 2006). Exosomes are small (30-100 nm) vesicles formed by the inward budding of LE/multi-vesicular body (MVB) membranes. They are a means for intercellular communication and typically contain an array of proteins, lipids, messenger RNAs (mRNA) and miRNAs that contribute to normal biological processes (Rashed *et al.*, 2017). Importantly, there are striking differences in the contents released by tumorigenic cells compared to non-transformed cells, which has been highlighted in a recent study comparing the contents of exosomes from pancreatic cancer cells to that of pancreatic endothelial cells. Here, exosomes released from tumour cells were enriched for proteins involved in metastatic niche formation and hallmarks of tumour progression such as proliferation, invasion and metastasis (Emmanouilidi *et al.*, 2019).

Additional studies have highlighted the presence of soluble ectodomains, as well as their sheddases, within exosomes secreted from tumour cells. Typically, this cleavage event is believed to occur following endocytosis from the cell surface. In the case of L1 adhesion molecule, this protein is subject to intracellular proteolytic processing following endocytosis from the cell surface. Soluble L1 is then released in exosomes and apoptotic vesicles that can be detected in the ascites from ovarian carcinoma patients (Gutwein *et al.*, 2005; Stoeck *et al.*, 2006). In addition, cleavage products from CD44 have been detected within exosomes released from ovarian carcinoma cells and ascites, along with ADAM10 and ADAM17 (Stoeck *et al.*, 2006). Interestingly, ADAM17 has been shown to undergo internalisation from the cell surface, followed by redistribution to exosomes when endothelial cells with were activated by lipopolysaccharide treatment. This led to release of mature ADAM17 via exosomes, which was capable of cleaving substrates on the surface of distant cells (Groth *et al.*, 2016).

1.4 Regulation of ectodomain shedding

Proteolysis of cell membrane proteins is critical to physiological cell signalling and functioning and must therefore be tightly regulated. Regulatory mechanisms include trafficking, abundance and co-localisation of sheddase and substrate; post-translational modifications of both sheddase and substrate, modulation by membrane lipids, and the presence of activators and inhibitors of shedding, such as tissue inhibitors of metalloproteinases (TIMPs) (Lichtenthaler *et al.*, 2018). These are discussed more broadly elsewhere (Hayashida *et al.*, 2010; Lichtenthaler *et al.*, 2018). In this thesis, the discussion will be restricted to substrate-specific regulatory mechanisms. Specifically, glycosylation (Goth *et al.*, 2015; Shirakabe *et al.*, 2017) and palmitoylation (Ebsen *et al.*, 2015) of the extracellular domain, and phosphorylation of the intracellular domain (Dang *et al.*, 2013) will be discussed. In addition, protein-protein interactions that can either stabilise or promote shedding will be described (Deng *et al.*, 2011; Lambert *et al.*, 2008; Rzeniewicz *et al.*, 2015).

1.4.1 Structure of the membrane-proximal ectodomain

Recent data suggests that negatively charged amino acids in the external juxtamembrane (”stalk”) region of transmembrane proteins may contribute to regulation of ectodomain shedding. Two splice variants of activated leukocyte cell adhesion molecule (ALCAM) were found to have different susceptibilities to ADAM-17 mediated cleavage, due to the inclusion of a 39 bp (13 amino acid) alternate exon containing a large number of negatively charged amino acids (Iwagishi *et al.*, 2020). The isoform containing the alternate exon was resistant to shedding, and the introduction of this string of negatively charged amino acids into the “shedding susceptible” isoform of activated leukocyte (AL)CAM conferred protection against shedding. Similarly, negatively charged amino acids in the stalk region of Erb-B2 receptor tyrosine kinase 4 (ERBB4) were also associated with resistance to shedding (Iwagishi *et al.*, 2020). In addition, shedding of the interleukin-6 (IL-6) receptor was influenced by a single nucleotide change, which caused an aspartic acid to alanine substitution (Riethmueller *et al.*, 2017).

Additional structural features that influence ectodomain shedding include domain accessibility, helical conformation, and glycosylation. For shedding to occur, the juxtamembrane domain must be accessible and not within a globular domain, whilst some substrates, such as APP, require a helical conformation to enable shedding (Lichtenthaler & Meinl, 2020).

1.4.2 Post-translational modifications affect ectodomain cleavage

Typically, post-translational modifications provide stability and structure to proteins (Amore *et al.*, 2017; Bann *et al.*, 2000), control protein localisation (Janes *et al.*, 2009), or alter protein conformation (Janes *et al.*, 2009; Rzeniewicz *et al.*, 2015). Often, these modifications are altered in disease states, in a way that disrupts normal protein functioning.

1.4.2.1 Glycosylation

Although no defined consensus sequence has been identified within proteins that are cleaved by ADAMs, a number of studies have noted that O-glycosylation (Figure 1-5) is a common feature of ADAM cleavage sites located at the extracellular juxtamembrane region of target substrates. Consequently, it has been proposed that susceptibility to ADAM-mediated shedding may be influenced by protein glycosylation (Goth *et al.*, 2015; Shirakabe *et al.*, 2017).

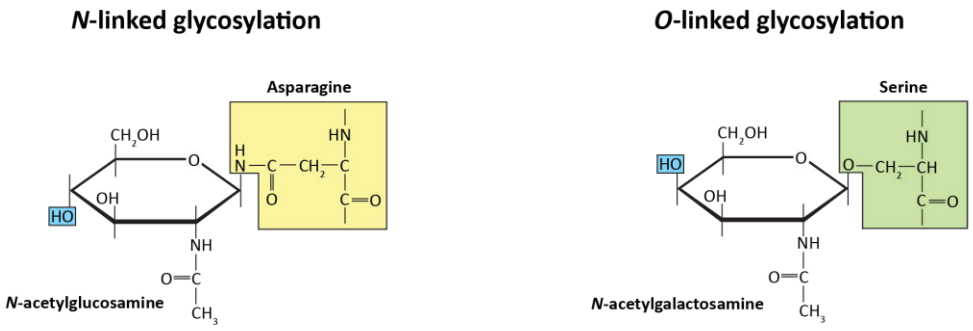

Figure 1-5 O-glycosylation vs. N-glycosylation

Glycosylation is a post-translational modification involving the addition of glycan molecules (e.g. N-acetylglucosamine) to the side chain of an amino acid. N-linked glycosylation refers to the addition of glycans to the amino group of asparagine (yellow box), occurring in the ER. O-linked glycosylation occurs when monosaccharides bind to the hydroxyl group of either serine or threonine (green box), which occurs in the ER, golgi, cytosol, and nucleus (adapted from website: PremierBiosoft.com).

Goth *et al.* (2015) investigated the potential of O-glycosylation to affect ADAM17 cleavage in 25 membrane proteins with known cleavage sites in the juxtamembrane region, and putative O-glycosylation sites (serine or threonine residues) within four amino acid residues of the cleavage site. In at least half of the proteins investigated, shedding was regulated to some extent by O-glycosylation and in most cases, it resulted in resistance to proteolysis (Goth *et al.*, 2015). Interestingly, detailed analysis of TNF-α (which is cleaved by multiple ADAMs) found that glycosylation of Ser80 offered partial protection to cleavage by ADAM9, -10 and -17, but completely abrogated processing by ADAM12. Potentially, glycosylation at different amino acid residues (Goth *et al.*, 2015), which is mediated by different N-acetylgalactosamine transferase (GalNAc-T) isoforms (Nielsen *et al.*, 2022), may affect substrate cleavage by specific ADAM proteases. Overall, this level of co-regulatory control provides an enormous capacity to fine tune efficiency and selectivity of sheddase activity.

In addition, as glycosylation is dysregulated in a number of pathological conditions (Reily *et al.*, 2019) it is likely it may affect ectodomain cleavage in disease processes. For instance, APP is subject to both O- and N-glycosylation as part of its post-translational processing. Both O- and N-glycosylation has been linked with appropriate trafficking of APP to and from the cell membrane (Akasaka-Manya &

Manya, 2020), while O-glycosylation has also been implicated in shedding of APP (Liu *et al.*, 2017). Enhanced O-glycosylation of APP was associated with decreased production of Aβ proteins and increased soluble APP; with this difference believed to be due to the decreased susceptibility of APP to cleavage, rather than a change in secretase activity (Akasaka-Manya *et al.*, 2016).

Similar to O-glycosylation, N-glycosylation has been suggested to increase protein stability (Lee *et al.*, 2015), and therefore may also be involved in regulating ectodomain shedding. This is supported by studies exploring the effects of N-glycosylation inhibitors, including tunicamcin and swainsonine (SW), on the generation of soluble proteins (Kim & Jung, 2012; Yang *et al.*, 2015). Yang *et al*. (2015) demonstrated this when investigating the role of N-glycosylation on the distribution and proteolytic processing of the transmembrane protein, CDCP1 (CUB-domain-containing protein 1). Upon treatment with tunicamycin, prostate cancer cells displayed predominantly intracellular localisation of CDCP1 (i.e. loss of surface expression). Whilst they did not directly measure the effects of tunicamycin on ectodomain shedding, they demonstrated that tunicamycin treatment affected protein stability and increased the susceptibility to proteolysis (Yang *et al.*, 2015). Further, matriptase 2, a hepatic serine protease, has several N-glycosylation sites, and the presence of glycans at specific sites within the ectodomain is essential for its activation (Jiang *et al.*, 2014). When mutations were introduced at these sites, the protein was expressed on the cell surface but ectodomain cleavage and subsequent activation of this protease was impaired (Jiang *et al.*, 2014).

Altered protein glycosylation has long been associated with oncogenic transformation (Kobata & Amano, 2005; Stowell *et al.*, 2015), although the contribution of cancer-associated glycosylation changes to ectodomain cleavage are not well documented. However, it seems reasonable that the profound changes seen during cancer progression are likely to affect ectodomain cleavage. It is also likely that changes in ectodomain processing may contribute to changes in cell-cell and cell-matrix interactions, signalling, and metastasis. Indeed, a review of Notch glycosylation in cancer describes that Notch receptors with modified glycans may

undergo unusual cleavage in intracellular vesicles to release the NICD fragment, and truncated Notch receptors that reach the plasma membrane cannot interact with ligands, which in turn may contribute to tumour development and progression (Pakkiriswami *et al.*, 2016).

1.4.2.2 Phosphorylation

Protein tyrosine kinases (PTK) have been identified as positive regulators of ectodomain shedding. This has been highlighted with the use of inhibitors such as pervanadate, which targets protein tyrosine phosphatases and enhances shedding of proteins including NCAM (Hinkle *et al.*, 2006), L1 adhesion molecule (Mechtersheimer *et al.*, 2001), and the HER2 ectodomain (Codony-Servat *et al.*, 1999). Tyrosine kinase activity is also required for stimulated shedding of syndecan-1 and -4, including shedding in response to PMA and cellular stress-inducers (e.g. ceramide, and hyper-osmotic conditions) (Fitzgerald *et al.*, 2000). Importantly, phosphorylation of substrates, which can be induced by interaction with its ligand/receptor, can also alter protein conformation to allow proteases to access the cleavage site (Janes *et al.*, 2009).

1.4.2.3 Palmitoylation

S-palmitoylation is a form of reversible post-translational modification involving the addition of a 16-carbon fatty acid chain (palmitic acid) to peptide residues via a thioester bond. This modification typically involves cysteine residues, however palmitoylation has also been described for serine and threonine (O-palmitoylation) (Deschenes, 2013)), glycine (Kleuss & Krause, 2003) and lysine residues (N-palmitoylation; (Hackett *et al.*, 1994)). The addition of palmitic acid is catalysed by a group of enzymes belonging to the family of DHHC (Asp-His-His-Cys) motif-containing palmitoyltransferases (Korycka *et al.*, 2012), and is reversed by acyl protein thioesterases (APTs) which catalyse the hydrolysis of thioester bonds (Won *et al.*, 2018). Though palmitoylation is relatively transient, it is nonetheless important for regulating the function of many proteins, and there is evidence to suggest that cleavage of certain transmembrane proteins is influenced by palmitoylation status.

For example, S-Palmitoylation of APP, which occurs at Cys186 and Cys187 (located in the N-terminus) targeted APP to lipid rafts, where it was susceptible to BACE1-mediated cleavage, leading to increased detection of palmitoylated sAPP-β. Meanwhile, mutation of Cys^{186} and Cys^{187} residues led to retention of APP in the ER, accompanied by reduced production of APP-CTF and sAPP (Bhattacharyya *et al.*, 2013).

1.4.3 Protein dimerisation and conformational changes

In some cases, substrate dimerisation has been shown to be required for shedding. Hartmann *et al.* (2015) found that CD44 and neuregulin (NRG1) cleavage by ADAM17 depends on 1) substrate homodimerisation and 2) specific modification of the ICD (Hartmann *et al.*, 2015). In addition, they suggest that sheddases such as ADAM17 may be associated with substrates even when proteolysis is not occurring. This means that when substrates are made "cleavage competent" through dimerisation and/or protein modifications, cleavage can occur rapidly and in an on/off fashion.

In the model proposed by Hartmann *et al*. (2015), an ectodomain interaction (e.g., ligand binding) may stimulate or stabilize dimerisation, and this is followed by the binding of an intracellular binding partner or ICD modification. This change to the ICD stimulates a switch from a restrictive to a permissive configuration, and allows ectodomain cleavage (Hartmann *et al.*, 2015). A similar model has been described for Notch, where Notch and ADAM10 are associated in a "steady state" environment, but cleavage does not occur until ligand binding (Meloty-Kapella *et al.*, 2012). Notch-ligand binding stimulates endocytosis and "pulls" on the Notch ectodomain to produce a permissive structure, enabling ADAM10 mediated cleavage to occur (Meloty-Kapella *et al.*, 2012).

1.3.2.3 Intracellular binding partners

Interactions between the cytoplasmic tail of substrates and intracellular proteins appear to be particularly important in regulating ectodomain shedding by altering the

accessibility of proteases to their substrates. To date, CaM and moesin appear to be major players in this process and can bind competitively within the juxtamembrane region of transmembrane proteins to either inhibit or promote ectodomain shedding, respectively (Rzeniewicz *et al.*, 2015). Similar to calmodulin, Rab5 appears to be a negative regulator of ectodomain shedding, with GDP and GTP bound Rab5 acting as a "molecular switch" for inhibiting or promoting ectodomain shedding of Syndecan-1 (Hayashida *et al.*, 2008).

1.4.4 Calmodulin negatively regulates ectodomain shedding

Calmodulin is a ubiquitous eukaryotic calcium-binding protein encoded by three genes- *CALM1, CALM2,* and *CALM3*. It interacts with a diverse array of intracellular proteins to modulate their function (Berchtold & Villalobo, 2014; Tidow & Nissen, 2013), and is responsible for many of the second messenger effects of Ca^{2+}. Mechanistically, this involves the formation of a Ca^{2+}/CaM complex, which subsequently alters the conformation of CaM and allows it to interact with its target enzymes. Among the diverse array of target enzymes, CaM-dependent kinases (CAMK) are the best characterised, and are known to modulate numerous signalling pathways, including those involved in regulation of lipid metabolism (Nishizawa *et al.*, 1988), initiation of apoptosis (Wright *et al.*, 1997) and inflammation (Ainscough *et al.*, 2015; Zhang *et al.*, 2011).

The binding affinity of a protein for CaM can be predicted based on certain features of the peptide sequence, and there are at least two databases available that assist with the identification of potential calmodulin recognition sites (Mruk *et al.*, 2014; Yap *et al.*, 2000). However, the functional importance of CaM binding can only be confirmed through experimental processes. CaM has been shown to bind to a number of transmembrane proteins, including angiotensin-converting enzyme 2 (ACE2) (Lai *et al.*, 2009; Lambert *et al.*, 2008), L-selectin (Gifford *et al.*, 2012), and platelet endothelial cell adhesion molecule-1 (PECAM-1) (Wong *et al.*, 2004), where it is involved in regulating ectodomain shedding. Studies suggest that CaM interacts within the intracellular juxtamembrane region of transmembrane proteins,

altering/stabilising the protein conformation in such a way that it can render the protein resistant to ectodomain shedding (Deng *et al.*, 2011; Lambert *et al.*, 2008).

1.4.4.1 L-selectin and shedding is regulated by CaM binding

L-selectin is involved in leukocyte tethering and rolling on the surface of endothelial cells. Upon cell activation, it has been shown to undergo proteolytic cleavage at a membrane proximal region (Kahn *et al.*, 1994; Migaki *et al.*, 1995). This has been widely reported and in neutrophils can be stimulated by exposure to inflammatory stimuli, mechanical stimuli, exposure to low density lipoprotein, receptor clustering, or osmotic stress (Ivetic, 2018). In human leukocytes undergoing transendothelial migration, it has been shown that L-selectin shedding is regulated by CaM, such that dissociation of CaM resulted in cleavage from the cell surface (Rzeniewicz *et al.*, 2015). Conversely, in resting cells/non-transmigrated areas of monocytes, CaM is bound constitutively to the juxtamembrane region of the cytoplasmic tail of L-selectin, where it acts to protect the molecule against proteolytic cleavage (Rzeniewicz *et al.*, 2015).

Although the exact mechanisms by which CaM negatively regulates ectodomain shedding of L-selectin remain unclear, it has been proposed that activation of CaM leads to a conformational change that alters its binding affinity for L-selectin, and that CaM dissociation may make proteins more amenable to ectodomain shedding by uncovering a cleavage site (Gifford *et al.*, 2012). Pharmacological inhibition of CaM has also been shown to increased ectodomain shedding of L-selectin (Kahn *et al.*, 1998), as well as a variety of other cell surface molecules (Kalus *et al.*, 2006; Kalus *et al.*, 2003; Lambert *et al.*, 2008). Further, increased shedding of L-selectin was induced by a mutation at Ser367, which mimicked L-selectin phosphorylation and hindered CaM binding (Rzeniewicz *et al.*, 2015). Together, these studies highlight an important role for CaM in L-selectin ectodomain shedding.

1.4.4.2 Phosphatidylserine interaction with L-selectin affects CaM binding

While shedding of L-selectin appears to be regulated by its interaction with CaM, it is important to note that some studies provide evidence that CaM does not bind directly to L-selectin. Deng *et al*. (2011) created an artificial cell bilayer to study the interactions between full-length CaM and L-selectin-derived peptides. Interestingly, negatively charged phospahtidylserine lipids appeared to associate with the basic-rich juxtamembrane region of L-selectin, thereby blocking interactions with CaM (Deng *et al.*, 2011). This data suggests that the membrane bilayer may influence interactions between CaM and L-selectin, thus adding another layer of complexity to the CaM hypothesis for ectodomain shedding. These findings were contradicted by Gifford et al, where CaM was predicted to have a compact conformation, allowing it to bind directly with an L-selectin-15-mer peptide, LSEL*15* (Gifford *et al.*, 2012). To resolve this discrepancy, Deng *et al.* (2013b) conducted a further study into the mechanisms underlying CaM-mediated L-selectin shedding. Here, the structure of CaM in association with L-selectin was assessed within a lipid bilayer, where it was found to have an extended conformation under these conditions (Deng *et al.*, 2013b). This provides further evidence that CaM may not interact directly with L-selectin under biological conditions. Further investigation revealed that the actin-binding protein, moesin, may have a role in mediating L-selectin-CaM interactions (Deng *et al.*, 2013a).

1.4.5 Moesin is an actin-binding protein that promotes cell migration and may enhance ectodomain shedding

Moesin is a member of the Ezrin-Radixin-Moesin (ERM) complex of proteins, which are predominantly known for their role in linking transmembrane proteins to the actin cytoskeleton. This not only maintains cell shape, but also helps to regulate signal transduction pathways, particularly those involving RhoA (Kawaguchi *et al.*, 2017; Louvet-Vallée, 2000). Collectively, the ERMs are involved in a number of cellular processes, including T cell activation and IL-2 production, PKC signalling, and apoptosis (Neisch & Fehon, 2011). Independently, moesin appears to be critical for maintaining epithelial cell morphology (Speck *et al.*, 2003), and has been shown to

contribute to the formation of the mitotic spindle in *Drosophila* embryos (Vilmos *et al.*, 2016). Further, moesin has been implicated in collective cell migration, cooperating with Rab11 in *Drosophila* oocytes to promote cell-cell communication and collective migration (Ramel *et al.*, 2013).

Additionally, moesin has been reported to contribute to the regulation of ectodomain shedding. In the case of L-selectin, it has been shown to bind within the cytoplasmic juxtamembrane region in a PKC-dependent manner and appears to promote ectodomain shedding. Mutating the ERM domain of L-selectin led to impaired shedding and was associated with reduced tethering of leukocytes to endothelial cells (Ivetic *et al.*, 2004). Rzeniewicz *et al.* (2015) also performed functional studies to investigate the effect of L-selectin shedding on monocyte transendothelial migration (TEM), demonstrating that preventing L-selectin shedding through pharmacological or genetic inhibition, led to enhanced pseudopod formation and accentuated cell spreading. This was also correlated with decreased cell migration. Further investigation revealed that L-selectin-ERM interactions may be important for the formation of membrane protrusions during the early stages of TEM, which was partly attributed to phosphorylation of L-selectin at Ser367 (allowing L-selectin to “peel away” from the inner leaflet of the cell membrane). Later during TEM, however, phosphorylation at Ser364 was proposed to promote preferential binding of L-selectin to phosphatidylserine in the plasma membrane, thereby blocking CaM binding and enhancing its ectodomain shedding (Rzeniewicz *et al.*, 2015).

Together, these findings suggest that CaM and moesin may bind non-competitively to L-selectin to regulate its shedding, in a manner that is at least partly influenced by lipids in the cell membrane. It has also been proposed that CaM and moesin can interact directly, and that they may form a heterotrimeric complex with L-selectin to regulate the rolling and arrest of leukocytes in the bloodstream (Killock *et al.*, 2009). Deng *et al*. (2013a) have similarly demonstrated the formation of a moesin-L-selectin-CaM ternary complex. Here, phospholipid liposomes were used to mimic the cell membrane, and binding of moesin and CaM to the L-selectin cytoplasmic tail was assessed. While the presence of phosphatidylserine seemingly abrogated any

direct interactions between CaM and L-selectin, it appeared to enhance moesin binding, which subsequently exposed the basic-rich region of the cytoplasmic tail of L-selectin, allowing CaM to bind (Deng *et al.*, 2013a). Interestingly, this coincides with findings by Riess *et al.* (2017), who identified the plasma membrane as an unexpected regulator of ectodomain shedding (Reiss & Bhakdi, 2017). Ultimately, these studies indicate that together, CaM and moesin play critical and complementary roles in regulating ectodomain shedding of L-selectin. Whether this occurs for other transmembrane proteins requires further exploration.

1.5 Immunoglobulin superfamily of cell adhesion molecules

Cell adhesion molecules are categorised as either cadherins, integrins, selectins, or immunoglobulin-like proteins, based on both their structural and functional features. Members of the immunoglobulin superfamily of cell adhesion molecules are probably the most diverse group of cell adhesion molecules and are classified based on their possession of at least one Ig-like domain in the extracellular region (Homrich *et al.*, 2016). Functionally, these cell adhesion molecules are well known for their role in mediating cell adhesion and migration. Some examples include NCAM (neural cell adhesion molecule), which participates in neuronal growth and migration (Kleene *et al.*, 2010), and PECAM-1, which is expressed on vascular endothelial cells, regulates endothelial cell permeability through cell-cell contacts (Albelda *et al.*, 1991). It is also implicated in leukocyte transmigration (Muller *et al.*, 1993). Similarly, vascular cell adhesion molecule-1 (VCAM-1) is also expressed on endothelial cells and, under inflammatory conditions, promotes transendothelial migration of leukocytes (Reglero-Real *et al.*, 2016).

In the context of disease, members of the IgSF have been shown to contribute to tumour metastasis. For example, L1 cell adhesion molecule is abnormally expressed on breast cancer cells, where it is associated with metastatic progression (Wu *et al.*, 2018). In particular, the soluble ectodomain of L1 has been linked to increased cell adhesion and transmigration of metastatic breast cancer cell lines, where it may act as a chemotactic signal (Li & Galileo, 2010). It may also act as a prognostic marker for primary breast cancer patients (Wu *et al.*, 2018). Similarly, melanoma cell

adhesion molecule (MCAM) is abnormally expressed on melanoma cells, where it appears to have a multifaceted role in promoting tumour progression. Indeed, MCAM is known to modulate cell migration and invasion, and can alter several apoptotic proteins to mediate cell survival, proliferation, and tumour angiogenesis (Stalin *et al.*, 2016). This strongly implicates the molecule in tumour progression and suggests that MCAM may serve as a predictive biomarker for metastasis and poor prognosis (Naik, 2021; Pearl *et al.*, 2008).

1.6 Melanoma cell adhesion molecule

Melanoma cell adhesion molecule (MCAM/CD146/S-Endo/MUC18) is a transmembrane glycoprotein that is conserved between species (Vainio *et al.*, 1996; Yang *et al.*, 2001). Structurally, it has an extracellular domain, a transmembrane domain, and an intracellular domain. The immunoglobulin-like extracellular domain contains three constant regions and two variable regions, and these can be N-glycosylated at eight potential glycosylation sites (Figure 1-6). This increases the molecular weight of the protein from ~72 kDa to ~110-118 kDa (Bardin *et al.*, 1998). The intracellular domain interacts with proteins of the cell cytoskeleton to promote cell migration (Dye *et al.*, 2009; Luo *et al.*, 2012) and is also involved in intracellular signalling pathways (Anfosso *et al.*, 2001).

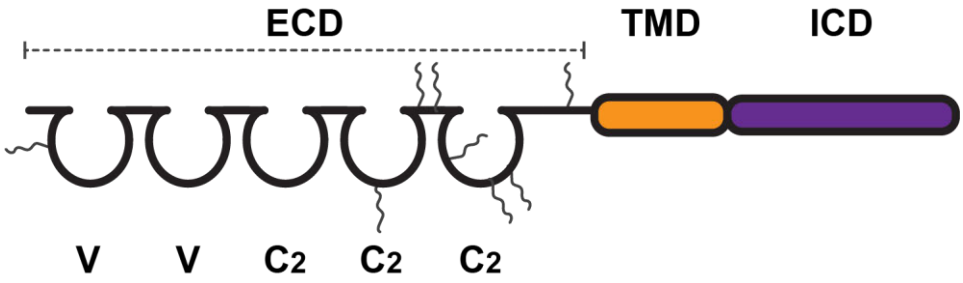

Figure 1-6 Schematic of MCAM protein structure.

MCAM is member of the immunoglobulin (Ig) superfamily of cell adhesion molecules. Its extracellular domain (ECD) has two variable (V) Ig domains and three constant (C) Ig domains and is highly glycosylated. It also has a transmembrane domain (TMD) and intracellular domain (ICD).

MCAM was originally identified on melanoma cells, where it was recognised as marker of melanoma progression (Lehmann *et al.*, 1987). It has since been associated with a number of other malignancies, including malignant rhabdoid tumour (Nodomi *et al.*, 2016a), hepatocellular carcinoma (Jiang *et al.*, 2016), epithelial ovarian cancer (Aldovini *et al.*, 2006), and triple-negative breast cancer (Zeng *et al.*, 2012). Typically, its expression has a negative impact on tumour outcome and is associated with epithelia-mesenchymal transition (Nodomi *et al.*, 2016; Zeng *et al.*, 2012), enhanced invasion (Jiang *et al.*, 2016; Nodomi *et al.*, 2016), and resistance to apoptosis (Zeng *et al.*, 2012). In addition to tumour cells, MCAM is widely expressed in embryonic tissue (Wang & Yan, 2013) but is only expressed by select cell types in adult tissue. This includes mesenchymal stem cells and vascular smooth muscle cells (Espagnolle *et al.*, 2014), vascular endothelial cells (Bardin *et al.*, 1998), and blood mononuclear cells (Elshal *et al.*, 2005), where it is implicated in processes such as angiogenesis (Mills *et al.*, 2002b) and T cell recruitment (Guezguez *et al.*, 2007). More recently, MCAM has been recognised to play a role in chondrogenic and myogenic differentiation, where its expression has been linked to initiation of cell polarity (Moreno-Fortuny *et al.*, 2017).

1.6.1 MCAM ligands in tumour and non-tumour cells

The ability for MCAM to exhibit an array of effects on both transformed and non-transformed cells, including proliferation, migration, angiogenesis, and resistance to apoptosis (Wang & Yan, 2013), could be linked to its ability to bind a number of different ligands that are responsible for mediating various downstream signalling pathways. In vascular endothelial cells, MCAM binds to vascular endothelial growth factor receptor 2 (VEGFR-2) and is involved in VEGF-induced phosphorylation of VEGFR-2 and activation of AKT/p38 MAPK/NF-κβ signalling. This ultimately promotes tumour angiogenesis by enhancing endothelial cell migration and microvascular tube formation (Jiang *et al.*, 2012). Netrin-1 has also been uncovered as a novel ligand for MCAM, responsible for inducing MCAM dimerisation and phosphorylation of VEGFR2, ERK1/2, and p38, ultimately leading to endothelial cell activation and angiogenesis (Tu *et al.*, 2015). In addition to promoting angiogenesis by acting on vascular endothelial cells, MCAM is also important for controlling cell morphogenesis during development; by acting as a receptor for fibroblast growth

factor 4 (FGF4), MCAM contributes to the co-ordination of apical-basal polarity (Gao *et al.*, 2017).

There is also a growing list of ligands that bind to MCAM on tumour cells, including Laminin-411 and -421 (Ishikawa *et al.*, 2014), Galectin-3 (Colomb *et al.*, 2017), S100A8/9 (Ruma *et al.*, 2016), and Wnt5a (Wang *et al.*, 2020). It is important to note here that whilst MCAM has been proposed to mediate homophilic (MCAM-MCAM) interactions (Guezguez *et al.*, 2007), the evidence strongly points towards MCAM medicating cell-cell interactions through a heterophilic ligand (Bardin *et al.*, 2009; Johnson *et al.*, 1997; Shih *et al.*, 1997). A summary of known MCAM ligands is given in Table 1-3.

Table 1-3 Extracellular ligands that bind MCAM

Ligand	Cells	Function/s	Reference
VEGFR-2	Vascular endothelial cells	Promotes tumour angiogenesis	(Jiang *et al.*, 2012)
VEGF-C	Lymphatic endothelial cells	Stimulates lymphangiogenesis	(Yan *et al.*, 2017)
Netrin-1	Vascular endothelial cells	Promotes angiogenesis (endothelial cell proliferation, migration and tube formation)	(Tu *et al.*, 2015)
FGF4	HEK293 cells; zebrafish embryos; *Xenopus* embryos	Co-ordinates apical-basal polarity in chemotaxing cells	(Gao *et al.*, 2017)
Wnt5a	Melanoma cells	Regulation of cell polarity and directional migration	(Witze *et al.*, 2008)
Wnt1	Skin fibroblasts	Proliferation of fibrobalsts, expression of genes promoting fibrosis, ECM production	(Zhang *et al.*, 2018)
Galectin-3	Vascular endothelial cells	Secretion of cytokines that promote tumour metastasis	(Colomb *et al.*, 2017)
Galectin-1	Endothelial cells	Protectes endothelial cells against Galectin-1-induced apoptosis	(Jouve *et al.*, 2013)
Laminin-411	Vascular endothelial cells	Facilitates TH17 entry into the CNS	(Flanagan *et al.*, 2012)
	Melanoma cells	Enhances tumour cell migration	(Ishikawa *et al.*, 2014)
Laminin-421	Melanoma cells	Promotes tumour cell migration	(Ishikawa *et al.*, 2014)
S100A8/9	Melanoma cells	Enhances adhesion to ECM, promotes cell proliferation, activates NFκB# and ROS*	(Ruma *et al.*, 2016)
Matriptase	Murine brain endothelial cells	Maintains cell-cell contact between endothelial cells and neural stem cells	(Tung & Lee, 2017)

*ROS= reactive oxygen species
NFκB= Nuclear factor kappa-light-chain-enhancer of activated B cells

1.6.2 The relevance of MCAM in tumour progression

Following the initial identification of MCAM in melanoma (Lehmann *et al.*, 1987), its role in tumour progression was confirmed by Xie *et al.* (1997), who showed that enforced expression of MCAM enhance the metastatic capabilities of melanoma cells *in vitro*. Specifically, MCAM expression was associated with increased homotypic adhesion, enhanced adhesion to human endothelial cell and decreased adhesion to an extracellular matrix protein and promoted invasion through matrigel-coated filters (Xie *et al.*, 1997). The effects of MCAM expression on melanoma cells have also been studied *in vivo*. In BALB/c-nude mice, enforced expression of MCAM in SB2 melanoma cells led to increased tumorigenicity and metastatic capacity (Xie *et al.*, 1997), whereas in severe combined immunodeficiency (SCID) mice, MCAM transfected SK-2 and XP44 melanoma cells did not display the same level of enhanced metastatic capacity, and failed to produce larger or more aggressive tumours compared to non-transfected cells (Schlagbauer-Wadl *et al.*, 1999). Similarly, in a syngeneic CH3 mouse model using murine MCAM-expressing melanoma cells, tumorigenesis was minimally affected by enforced MCAM expression, however cells displayed augmented motility and invasiveness *in vitro* (Wu *et al.*, 2008). Collectively, these results show that MCAM can increase the malignant potential of some melanoma cells and suggest that certain cell-intrinsic factors may influence the overall outcome of MCAM overexpression. However, it should not be discounted that the immune status of the host may have also contributed towards these differences.

MCAM expression has also been associated with several other malignancies, including malignant rhabdoid tumour (Nodomi *et al.*, 2016a), hepatocellular carcinoma (Jiang *et al.*, 2016), epithelial ovarian cancer (Aldovini *et al.*, 2006), and triple-negative breast cancer (Zeng *et al.*, 2012). Here, expression also appears to have a negative association with tumour outcome.

Evidently, its relevance in tumour progression makes MCAM is an attractive therapeutic target. However, the physiological expression of MCAM (described above) presents a challenge for the development of anti-tumour therapies targeting

MCAM. While there have been several MCAM-specific antibodies developed (outlined in Table 1-4), their therapeutic use is limited due to the risk of undesirable effects on healthy cells. However, an improved understanding of the differences between physiological and pathological isoforms of a protein (e.g. in terms of post-translational modifications such as glycosylation) (Díaz-Fernández *et al.*, 2018) opens up the possibility of developing tumour specific antibodies. To this end, a monoclonal antibody specific for MCAM expressed on tumour cells has been investigated recently and has shown success in reducing the growth of MCAM-positive tumours in mice, while avoiding deleterious effects on non-transformed cells (Nollet *et al.*, 2017). Further, an antibody specifically targeting sMCAM and not binding to membrane-bound, full-length MCAM, has shown promising results both *in vitro* and *in vivo* (Stalin *et al.*, 2016; Stalin *et al.*, 2020).

Table 1-4 Therapeutic MCAM antibodies

	Target	*In vitro* effects	*In vivo* effects	Reference
ABX-MA1	MCAM-ECD	Disrupted homotypic interactions and inhibited MMP2 activity in melanoma cells	Impaired tumour growth and experimental lung metastasis in mice	(Mills *et al.*, 2002a)
AA98	MCAM-ECD	Impaired proliferation and migration of HUVECs*	Reduced growth and vascularity of tumours (pancreatic cancer, hepatocellular carcinoma, leiomyocarcinoma) in mice	(Yan *et al.*, 2003)
M2J-1	sMCAM	Decreased proliferation, induced apoptosis and senescence of cancer cells;	Reduced tumour growth (pancreatic), decreased tumour vascularisation and increased apoptosis in mice	(Stalin *et al.*, 2016)
		Decreased proliferation of HUVECs* Blocked EMT-related proteins and coagulation-related proteins	Decreased tumour growth, reduced metastatic spread of melanoma and ovarian cancer cells, acted on EMT, CSC and coagulation pathways	(Stalin *et al.*, 2020)
tsCD146 mAb	MCAM-ECD	Decreased proliferation and increased apoptosis of melanoma and pancreatic cancer cell lines; No effect on endothelial cell lines	Decreased size of melanoma in NOD/SCID mice, decreased size of pancreatic tumours in nude mice.	(Nollet *et al.*, 2017)

**HUVECs= Human vascular endothelial cells*

1.6.3 MCAM genomic structure and transcriptional regulation

In humans, MCAM is encoded by an ~14 kilobase (kb) gene located on chromosome 11q23.3. The MCAM transcript is 3.3 kb and contains 16 exons that code for the full-

length transmembrane protein (Lehmann *et al.*, 1989; Sers *et al.*, 1993). There are five immunoglobulin (Ig)-like regions that make up the extracellular domain of MCAM. Four of these five Ig-like regions are encoded by two exons, with the remaining one encoded by three exons (Sers *et al.*, 1993). Exons 14 -16 code for the transmembrane and cytoplasmic domains. Alternative splicing of exon 15 leads to expression of long (MCAM-l) and short (MCAM-sh) isoforms (Sers *et al.*, 1993). Typically, MCAM-l is expressed by melanoma cells (Dye *et al.*, 2009), while endothelial cells express both MCAM-l and MCAM-sh (Kebir *et al.*, 2010). How alternative splicing of MCAM in melanoma cells is regulated in order to favour expression of one isoform over the other is unclear but could be related to aberrant splicing that is common in malignant cells (Sciarrillo *et al.*, 2020), or to lineage-specific differences.

The 5' regulatory region of *MCAM* is devoid of TATA- and CAAT-boxes, and possesses a single transcription start site/initiation region. The core promoter region lies between -106 to +22 base pairs (bp) and contains four putative recognition motifs for the SP-1 transcription factor, two for AP-2, and a binding motif for cAMP response element (Mintz-Weber & Johnson, 2000; Sers *et al.*, 1993). Each of these transcription factors has been identified to contribute to the regulation of MCAM expression in tumour cells, including glioma, colon carcinoma, and melanoma (Mintz-Weber & Johnson, 2000). Interestingly, the homeodomain transcription factor MEIS1, was identified as a potential transcriptional regulator of MCAM in pancreatic cancer cells (von Burstin *et al.*, 2017). Genome wide expression analysis confirmed MCAM overexpression in highly motile pancreatic cancer cells and reported that MES1 interacted with the MCAM enhancer region, within a MEIS1 consensus site 113 kb upstream of the MCAM transcription start site (von Burstin *et al.*, 2017). Collectively, these studies highlight the complexity of understanding the regulation of *MCAM* gene expression. Furthermore, epigenetic mechanisms have also been proposed to regulate MCAM expression in prostate cancer cells (Dudzik *et al.*, 2019b) and breast cancer cells (Dudzik *et al.*, 2019a). Each of the aforementioned studies found that expression of MCAM - at both the mRNA and protein level - was increased in response to treatment with the demethylating agent, 5-aza-2-deoxycytidine. Interestingly, in breast cancer cells, hypermethylation of CpG islands

in the promoter region of MCAM was reported (Dudzik *et al.*, 2019a), but this was not observed in prostate cancer cells (Dudzik *et al.*, 2019b). Based on these studies, it is possible that MCAM protein expression in cancer cells is also subject to epigenetic regulation, but further studies are required.

1.6.4 Expression of MCAM and its role in migration and intracellular signalling

As mentioned above, two membrane-associated isoforms of MCAM exist due to alternative splicing of exon 15, which differ only in the cytoplasmic tail. MCAM-sh (603 amino acids) has a short cytoplasmic tail, which possesses a PKC phosphorylation site and a PDZ domain, while MCAM-l isoform (646 amino acids) contains two PKC phosphorylation sites, as well as an endocytosis signal sequence within its cytoplasmic tail (Figure 1-7) (Stalin *et al.*, 2017). Both isoforms of MCAM possess a single transmembrane domain, and an extracellular domain consisting of five Ig-like domains (V-V-C2-C2-C2) and eight putative glycosylation sites in the membrane proximal region. The full-length molecule is subject to a number of post-translational modifications, including N-glycosylation, which gives rise to the mature glycoprotein with a molecular weight ranging from approximately 110-118 kDa (Bardin *et al.*, 1998). Further, MCAM is susceptible to proteolytic cleavage and shedding of the extracellular domain, generating a third, soluble isoform (~100 kDa). This was first identified in endothelial cells (Bardin *et al.*, 1998), but has also been described in tumour cells, including melanoma (Stalin *et al.*, 2016).

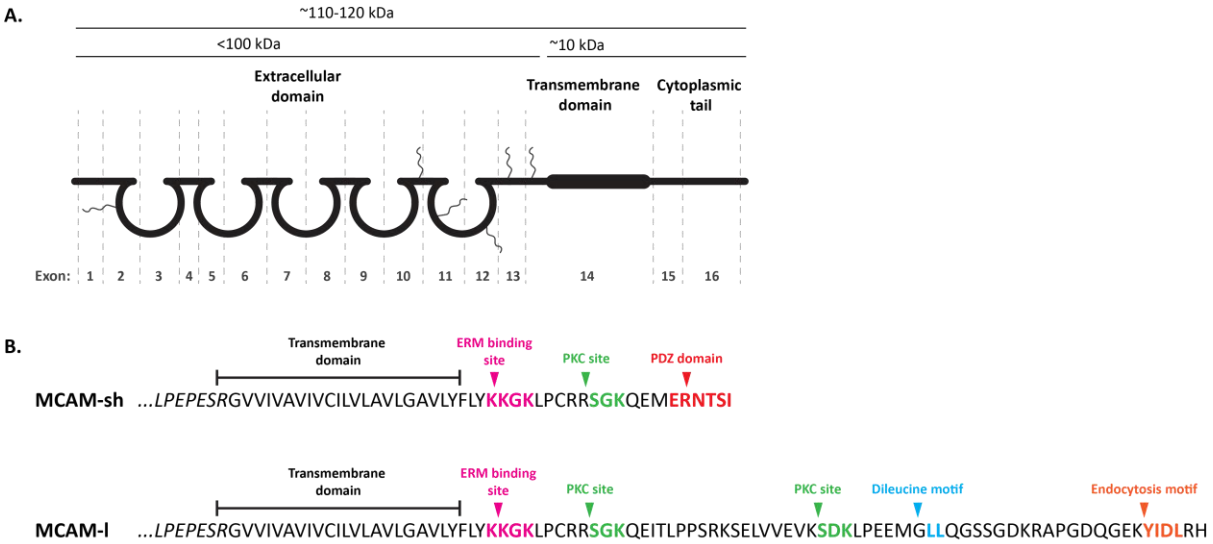

Figure 1-7 Structure and protein sequence of MCAM.

Full-length MCAM is comprised of an extracellular domain that contains up to eight potential glycosylation sites, a transmembrane domain, and cytoplasmic tail. MCAM can undergo alternative splicing to produce either the long (MCAM-l) or short (MCAM-sh) isoforms (A). Differences in the peptide sequences of MCAM-l and MCAM-s are shown. Both isoforms contain the KKGK motif (ERM binding site) and a PKC site. MCAM-sh also contains a PDZ domain. The MCAM-l sequence contains an additional PKC site, as well as a di-leucine (LL) and tyrosine (YIDL) endocytosis motif (B).

1.6.4.1 Localisation and interactions of MCAM with the cell cytoskeleton

The two membrane-bound isoforms of MCAM display different localisations within the cell and appear functionally distinct. In endothelial cells MCAM-sh is targeted to the apical cell surface in a confluent monolayer and appears to promote adhesion, migration and proliferation (Kebir *et al.*, 2010). Meanwhile, MCAM-l is located basolaterally, where it influences trans-endothelial permeability (Kebir *et al.*, 2010). Similarly, in MDCK (canine kidney) cells transfected with either MCAM-l or MCAM-sh, MCAM-l was directed to the basolateral membrane, while MCAM-sh was targeted to the apical surface (Guezguez *et al.*, 2006). Evidently, cell-specific differences also exist. In tumour cells, particularly in melanoma, it is predominantly the long isoform that is expressed (Dye *et al.*, 2009). In these cells, MCAM is found at the cell surface (Zhang *et al.*, 2008b), and also displays strong perinuclear localisation (Dye *et al.*, 2009), which is consistent with the hypothesis that MCAM can undergo trafficking to the ER following endocytosis (Witze *et al.*, 2013).

Meanwhile in migrating cells, MCAM is redistributed, and has been reported to localise at the trailing edge of melanoma cells (distal to the Golgi apparatus) in response to Wnt5a treatment. This was associated with membrane retraction and cell migration (Witze *et al.*, 2008).

Early studies also implicated MCAM in dissemination and metastatic progression of other tumour cells. MCAM has been shown to promote migration and invasion of triple negative breast cancer cells by inducing stem cell-like properties and, acting via the Slug transcription factor, can regulate EMT in cancer cells (Zeng *et al.*, 2012). In melanoma cells, enforced expression of MCAM leads to increased migration across matrigel-coated filters (Xie *et al.*, 1997), while MCAM knockout in host mice can reduce the hematogenous dissemination of subcutaneous melanoma (Jouve *et al.*, 2015). This impact of MCAM on melanoma cell motility is achieved, at least in part, by its indirect interactions with the cell cytoskeleton (Bardin *et al.*, 2001), which are mediated by cytoskeletal adaptor proteins, including moesin (Luo *et al.*, 2012) and hShroom1 (Dye *et al.*, 2009). Importantly, a putative PKC phosphorylation site in the cytoplasmic tail of MCAM-l has also been shown to be necessary for MCAM interactions with the cell cytoskeleton, promoting microvilli formation in an NK cell line (Guezguez *et al.*, 2007).

1.6.4.2 Extracellular ligands and intracellular signalling

MCAM forms dimers in both endothelial and melanoma cell lines (Bu *et al.*, 2007), and is an important mediator of cell-cell adhesion through homotypic interactions (Johnson *et al.*, 1997). Further, MCAM displays heterophilic interactions with a number of ligands. This was first described for the avian homologue of MCAM, known as gicerin, which was shown to interact with neurite outgrowth factor (NOF; an ECM protein) (Taira *et al.*, 1994; Taniura *et al.*, 1991).

More recently, Laminin-411 (Flanagan *et al.*, 2012), Galectin-1 and Galectin-3 (Colomb *et al.*, 2017; Jouve *et al.*, 2013), have been shown to interact with the extracellular domain of MCAM. These interactions can initiate outside-in signalling

cascades, promoting T-cell mediated inflammation in the CNS, regulating apoptosis of endothelial cells, increasing the secretion of pro-metastatic cytokines, and promoting angiogenesis, respectively (Colomb *et al.*, 2017; Flanagan *et al.*, 2012; Jouve *et al.*, 2013). Additionally, MCAM plays an important role in the regulation of cell morphogenesis during development by acting as a receptor for fibroblast growth factor 4 (FGF4), which allows it to participate in the coordination of apical-basal polarity (Gao *et al.*, 2017).

MCAM is also a co-receptor for VEGF-A (with VEGF-R2) (Jiang *et al.*, 2012) and platelet-derived growth factor (PDGF)-β (with PDGFR-β) (Chen *et al.*, 2018) in endothelial cells. MCAM-s forms a heterodimer with VEGFR-2 and is associated with VEGF-induced phosphorylation of VEGFR-2 and activation of protein kinase B (AKT)/p38 MAPK/nuclear factor kappa-light-chain-enhancer of activated B cells (NF-κB) signalling. This ultimately promotes tumour angiogenesis by enhancing endothelial cell migration and microvascular formation (Jiang *et al.*, 2012). Recently, netrin-1 was also uncovered as a novel ligand for MCAM (Tu *et al.*, 2015). Netrin-1 induced MCAM dimerisation, leading to phosphorylation of VEGFR2, ERK1/2, and p38, which promoted endothelial cell activation and angiogenesis (Tu *et al.*, 2015). These receptor/co-receptor properties of MCAM allow it to elicit various functions following ligand binding, including angiogenesis, lymphangiogenesis, migration, cell polarisation, and changes in vasculature integrity (Wang *et al.*, 2020).

A number of studies have also reported on the involvement of MCAM in intracellular signalling pathways. In endothelial cells, MCAM engagement (using an anti-MCAM monoclonal antibody) resulted in downstream phosphorylation of a number of intracellular proteins (Anfosso *et al.*, 1998). In particular, proto-oncogene tyrosine kinase (FYN), focal adhesion kinase (FAK), and paxillin were activated in response to MCAM-induced tyrosine phosphorylation, and promoted cytoskeletal reorganisation (Anfosso *et al.*, 2001). MCAM is also important for FAK activation in response to vascular endothelial growth factor (VEGF) stimulation, since MCAM deficiency (in lung microvascular endothelial cells derived from CD146

knockout mice) led to decreased FAK activation following VEGF treatment, and decreased transendothelial migration of murine melanoma cells (Jouve *et al.*, 2015).

Further, AKT has been shown to mediate both inside-out and outside-in signalling pathways involving MCAM in melanoma cells (Li *et al.*, 2003). Here, MCAM expression was associated with increased AKT activity and subsequent increased cell survival, coinciding with inactivation (phosphorylation) of pro-apoptotic proteins such as BAD. Overexpression of AKT was also shown to concurrently increase MCAM expression, suggesting that a reciprocal regulation loop may occur between MCAM and AKT (Li *et al.*, 2003).

More recently, MCAM has been identified as a component of the “Wnt-receptor-actin-myosin-polarity" (WRAMP) structure, which contributes to cell polarity and directional cell migration (Witze *et al.*, 2008). Witze and colleagues suggest that Wnt5a stimulation of melanoma cells stimulates MCAM endocytosis and trafficking via early and then late endosomes from the leading edge to the rear of the cell. At the rear of the cell, MCAM forms part of the WRAMP structure with actin and myosin and a range of cytoskeletal linker and focal adhesion proteins including Filamin-A, Talin-1, and Kindlin-3 and the IQ Motif Containing GTPase Activating Protein 1 (IQGAP1). IQGAP is believed to link MCAM to the actin cytoskeleton within the WRAMP. Lastly, cortical endoplasmic reticulum (ER) is also recruited, which leads to localised Ca^{2+} release followed by rear membrane retraction and directional cell migration (Witze *et al.*, 2013; Witze *et al.*, 2008). The WRAMP structure can also rapidly disassemble, before re-assembling in a new location. In this way, the WRAMP can rapidly control changes in direction in cell migration (Connacher *et al.*, 2017).

The Wnt5a (wingless family member 5a)-mediated recruitment of cell surface MCAM to the WRAMP appears to be mediated by de-palmitoylation of Cys590 in the MCAM cytoplasmic tail (Wang *et al.*, 2015). Palmitoylation is the attachment of fatty acids (e.g., palmitic acid) to cysteine residues of proteins and helps tether proteins to the cell membrane. This process is reversible and facilitates the movement of proteins to

and from membranes (Conibear & Davis, 2010). Mutation of Cys590 to a glycine appeared to stabilise MCAM at the cell membrane and inhibited movement of MCAM into the WRAMP (Wang *et al.*, 2015). It is possible that palmitoylation/ depalmitoylation of MCAM at least partially regulates the stability of MCAM in the cell membrane, and this may affect whether it is available to undergo ectodomain cleavage. However, this is yet to be investigated.

Interestingly, MCAM signalling can also act at the nuclear level to regulate gene transcription. This has been exemplified in melanoma cells, where MCAM was shown to regulate Inhibitor of DNA binding-1 (Id-1) at the transcriptional level by downregulating the activity of activating transcription factor 3 (ATF3). This led to increased activity of Id-1, which promoted transcription of MMP-2 (Figure 1-8) (Zigler *et al.*, 2011). In addition, in vascular endothelial cells the intracellular domain of MCAM-sh can translocate to the nucleus in response to recombinant soluble MCAM (rsMCAM) treatment, which is associated with up-regulation of anti-apoptotic proteins such as Bcl-xl and pro-caspase-3 (Stalin *et al.*, 2016a). Similarly, in tumour cells sMCAM is able to modulate expression of a number of proteins involved in cell growth and survival (Stalin *et al.*, 2016), and EMT (Stalin *et al.*, 2020). Interestingly, treatment of vascular endothelial cells with conditioned medium derived from the MCAM-expressing melanoma cell line, A375, resulted in redistribution of NFκB from the cytosol to the nucleus, which was abrogated when the MCAM-binding antibody, AA98, was added to the conditioned medium as a decoy receptor (Bu *et al.*, 2007). This hints at MCAM having a further regulatory role through the NFκB pathway. Overall, the research described here highlights the versatility of MCAM as an adhesion molecule, ligand receptor, transcriptional regulator, and signalling molecule, in both endothelial and melanoma cells.

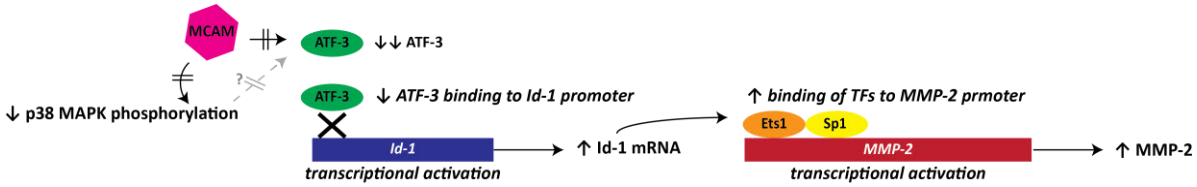

Figure 1-8 MCAM regulates the activity of MMP-2

MCAM regulates the expression of ATF3 and Id-1 transcription factors, which has downstream effects on MMP-2 activity. Expression of MCAM downregulates ATF3, and thereby reduces ATF3 binding to the Id-1 promoter. This promotes transcription of Id-1. Increased levels of Id-1 enhance the binding of two transcription factors- Est1 and Sp1- to the MMP-2 promoter, leading to transcriptional activation of MMP-2 in MCAM-expressing cells. MCAM expression is also linked to decreased phosphorylation of p38 MAPK. P38 MAPK is capable of inducing members of the ATF/CREB family of transcription factors, which includes ATF3.

1.6.5 MCAM ectodomain shedding

The soluble form of MCAM is a product of ectodomain shedding that was first described in human umbilical vein endothelial cells (HUVECs), which were shown to produce a soluble, 100 kDa fragment of MCAM that could be detected in both cell culture media and in the blood of healthy donors (Bardin *et al.*, 1998). A number of other cell types have since been shown to release sMCAM, including monocytes, where MCAM shedding has been associated with enhanced monocyte transmigration (in response to TNF-α) (Bardin *et al.*, 2009).

sMCAM is also associated with inflammatory conditions, for example it was found at increased levels in patients with chronic renal failure (Bardin *et al.*, 2003), it appears to correlate with atherosclerosis plaque inflammation and instability (Qian *et al.*, 2014), and it may have a role in inflammatory bowel diseases (Bardin *et al.*, 2006). sMCAM is also produced in chronic obstructive pulmonary disease (COPD), where it is associated with decreased cell surface expression of full-length MCAM, and concurrent increases in the permeability of pulmonary endothelial cells (Adelheid *et al.*, 2013).

Further, sMCAM has potential diagnostic and/or prognostic value in liver disease (Nomikou *et al.*, 2015) and cancers such as non-small cell lung cancer (Ilie *et al.*, 2014) and multiple myeloma (Wrobel *et al.*, 2006). Malignant cells, including

pancreatic and colon tumour cells, melanoma, and tumours cells derived from the prostate, brain, and adrenals, have also been shown to cleave MCAM (Stalin *et al.*, 2016), and there is evidence linking this to tumour progression and poor prognosis (Stalin *et al.*, 2020).

As discussed in section 1.6.3, MCAM undergoes alternative splicing at exon 15 to produce MCAM-sh. Two intronic poly-A signals are also present in the pre-mRNA after transcription of genomic MCAM - one of which is located in exon 14 and interrupts the cytoplasmic tail after 14 amino acids (Sers *et al.*, 1993). Importantly, the presence of intronic poly-A signals can lead to novel transcript variants. Alternate splicing of the chicken homologue of MCAM (HEMCAM) has been reported to produce three mRNA transcripts encoding long and short transmembrane isoforms, as well as a soluble form of HEMCAM (Vainio *et al.*, 1996).

Interestingly, two novel variants believed to encode sMCAM were recently identified in endothelial cells via RNA sequencing (Nollet *et al.*, 2022). One novel variant retained intron 10 (I10-sCD146), whilst the other retained introns 5 and 13 (I5-13-sMCAM). I10-sMCAM is hypothesized to produce a protein comprising the first three and a half Ig like domains of MCAM, followed by 55 amino acids of novel sequence; while I5-13-sMCAM lacks the first two Ig domains (and instead contains novel sequence), and retains the next three Ig domains. Nollet *et al*. (2022) report that these variants may account for up to 25% of sMCAM produced by endothelial cells, with I10-sMCAM. The remaining 75% of sMCAM was associated with ectodomain cleavage of MCAM-sh and MCAM-l (Nollet *et al.*, 2022).

1.6.5.1 MCAM shedding in endothelial cells

MCAM is an important component of endothelial cell junctions and is functionally involved in maintaining cell-cell cohesion and regulating paracellular permeability (Bardin *et al.*, 2001). Shedding of MCAM may also contribute to vascular permeability, since treating $CD146^{-/-}$ cells with sMCAM was associated with increased vascular permeability in response to VEGF stimulation (mediated via FAK

phosphorylation) (Jouve *et al.*, 2015). Further to this, sMCAM is able to promote angiogenesis; at the molecular level, exposure of endothelial progenitor cells to sMCAM led to up-regulation of genes associated with angiogenesis, including VEGFR2, MMP-2, eNOS and uPA (Harhouri *et al.*, 2010), as well as increased expression of the anti-apoptotic proteins Bcl-xL and pro-caspase-3, and down-regulation of anti-apoptotic proteins such as cathepsin D, FADD, caspase 10, cystatin A, and pro-casapse-4 (Stalin *et al.*, 2013). Meanwhile at the physiological level, sMCAM is associated with increased vascularisation and blood perfusion, which has been studied in mice with hind-limb ischemia (Stalin *et al.*, 2016a).

Importantly, these events have been found to be mediated through the novel sMCAM binding partner, angiomotin (Stalin *et al.*, 2016a). The p80 isoform of angiomotin (Amot p80) forms part of a 'signalosome complex' consisting of sMCAM, MCAM-sh, VEGFR1 and VEGFR2, an MMP/ADAM, and presinilin-1. Here, it was proposed that binding of sMCAM to Amot p80 facilitated MMP-mediated cleavage and release of the soluble MCAM extracellular domain, followed by shedding of the intracellular domain by presinilin-1 (Stalin *et al.*, 2016a). In this model, the cleaved intracellular domain of MCAM then interacted with a transcription factor (CSL) at the nucleus to induce gene transcription, while the cleaved ectodomain (sMCAM) further amplified the mechanisms in a positive feedback manner (Stalin *et al.*, 2016a). It is important to note that this was only seen for the short isoform of MCAM; MCAM-l was seen to behave differently, and its function was not affected by sMCAM under these experimental conditions (Stalin *et al.*, 2016a).

1.6.5.2 Soluble MCAM has a role in tumour progression

In contrast to vascular endothelial cells, little is known about sMCAM signalling in melanoma. In a study investigating the targeted inhibition of sMCAM with a monoclonal antibody, Stalin *et al.* (2016) reported that sMCAM could induce the proliferation and survival of MCAM-positive tumour cells, acting through Amot p80. Further, mRNA expression of certain pro-angiogenic and pro-invasive factors, including Angiopoietin-2, IL-8, VEGFR2, Amot p80, and MMP9, was upregulated in both melanoma cells and pancreatic tumour cells in response to recombinant

sMCAM treatment (Stalin *et al.*, 2016). Using an antibody array, it was also shown that sMCAM regulated proteins involved in cell survival, cell cycle, and cell stress and was able to protect tumour cells from apoptosis and reduce cellular senescence, possibly through induction of Bcl-xL and sirtuin-1, which act as anti-apoptotic and anti-senescence factors, respectively (Stalin *et al.*, 2016).

Importantly, sMCAM promoted tumour growth *in vivo*, and was linked to increased endothelial cell proliferation and tumour vascularisation; this was reduced when mice were treated with a monoclonal antibody specifically targeting sMCAM (M2J-1 mAb), and not cell-associated MCAM (Stalin *et al.*, 2016). A recent study using the sMCAM-targeted M2J-1 mAb found that sMCAM is associated with increased metastatic dissemination of both melanoma and ovarian carcinoma cells, and that this can be traced back to the effect of sMCAM on EMT, cancer stem cell (CSC) generation, and a procoagulant state (Stalin *et al.*, 2020). Specifically, treatment of tumour-bearing mice with M2J-1 resulted in decreased tumour mass and reduced number and size of metastases, and RNA expression profiling showed increased expression of tumour-suppressor genes and pro-metastatic genes, and reduced expression of proto-oncogenes (e.g. KRAS, SPP1), EMT-related genes (e.g. Snail, Fibronectin1), as well as CSC and pro-coagulation mRNAs (Stalin *et al.*, 2020). Collectively, the studies described above indicate that sMCAM may have a profound role in melanoma progression but harnessing this for therapeutic benefit will require a greater understanding of how MCAM shedding occurs in melanoma cells.

1.6.6 Proteolysis of the MCAM-ICD

Proteolytic processing of MCAM does not appear to be restricted to the extracellular region, with some evidence to suggest that the molecule undergoes intramembrane proteolysis. This was exemplified by the presence of a small intracellular domain fragment detected within cells following treatment with recombinant sMCAM, which indicates that MCAM undergoes cleavage to release the ICD from the cell membrane (Stalin *et al.*, 2016a). Further, the presence of a valine-rich site within the TMD of MCAM may act as a substrate for γ-secretase activity, and reports that treatment with γ-secretase inhibitors reduce the translocation of MCAM-ICD to the

perinuclear region (Stalin *et al.*, 2016a) support the hypothesis that it is involved in the intramembrane proteolysis of MCAM, at least in endothelial cells.

1.7 Conclusion

Ectodomain shedding is an essential physiological process that broadens the function of many membrane-anchored proteins, including cytokines, growth factors, and adhesion molecules. In other cases, cleavage of the ectodomain is necessary for protein activation. Importantly, soluble ectodomains are, in many cases, biologically active molecules with distinct functions. Further, shedding may be considered a necessary precursor event for intramembrane proteolysis, whereby the regulated cleavage and intracellular release of a protein transmembrane domain and/or cytoplasmic domain only occurs in the absence of the large extracellular domain. Since intramembrane proteolysis releases an intracellular fragment that is capable of regulating gene transcription and modulating intracellular signalling pathways, shedding not only causes downregulation at the cell surface, it can also lead to termination (or activation) of intracellular signalling events.

Overall, ectodomain shedding has important biological significance, allowing mammalian cells to respond to environmental and physiological changes, and dysregulated shedding is often associated with pathological conditions such as cancer, as well as neurological and cardiovascular diseases. In melanoma, sMCAM may be a biomarker for melanoma progression, and it holds potential as a therapeutic target. However, in order to target this molecule therapeutically, further validation of its role in tumour progression is needed. This includes understanding how sMCAM shedding occurs and is regulated in melanoma cells.

1.8 Project aims

The overall aim of this project was to gain insight into the shedding of MCAM from melanoma cells, including cleavage of the ectodomain and proteolysis of the intracellular domain. The specific aims were:

Aim 1: determine whether MCAM is shed from melanoma cells and can be detected in the cell culture media

Aim 2: identify the protease/s involved in MCAM proteolysis, including ectodomain shedding and regulated intramembrane proteolysis

Aim 3: investigate the intracellular mechanisms regulating MCAM cleavage (e.g., calmodulin, moesin, palmitoylation)

Chapter 2

Materials and Methods

2.1 Molecular methods

2.1.1 Reagents

Luria broth (LB) and LB agar

One litre (L) of LB was prepared by dissolving 10 g NaCl (BIODB0483), 5 g yeast extract (BIOG096) (both from Astral Scientific, NSW, Australia) and 10 g Bacto ™ tryptone (211705, ThermoFisher Scientific, Waltham, MA) in ddH_2O. The broth was sterilised by autoclaving. LB-Agar was prepared as above, with the addition of 1.5 g agar (BIOFB0010, Astral Scientific) prior to autoclaving.

Antibiotics

Ampicillin (A9518, Sigma-Aldrich, Merck, Darmstadt, Germany) was prepared as a 100 mg/mL stock by dissolving in 50% ethanol (EtOH; 459844, Sigma-Aldrich) and storing at -20^{o}C. It was used at a working concentration of 50-100 µg/mL.

2.1.2 Plasmids

pcDNA3-Delta(Pro-MP)ADAM10-HA (Addgene plasmid 65107), pcDNA3-Delta(Pro-MP)ADAM17-HA (Addgene plasmid 65221), pcDNA3-ADAM10-HA (Addgene plasmid 65106) and pcDNA3-ADAM17-HA (Addgene plasmid 65105) were a gift from Axel Ullrich (Gschwind *et al.*, 2003). These plasmids are tagged with the haemagglutinin (HA) peptide. pSpCas9(BB)-2A-GFP (Addgene plasmid 48138) was a gift from Feng Zhang (Ran *et al.*, 2013). All were purchased from Addgene (Watertown, MA). The pCDNA3.1-MCAM plasmid was provided by Dr Stéphane Karlen. Full-length MCAM-l was inserted into the MCS of pCDNA3.1 (-), between the *NotI* and *XbaI* restriction sites (Dye, 2007).

2.1.3 Plasmid expansion, purification, and validation

Chemically competent XL10 Gold *Escherichia coli* (*E.coli)* cells (provided by Dr Carl Mousley, Curtin University) were transformed with plasmid DNA (heat shock at 42^{o}C for 45s), then plated on a LB-Agar plate with ampicillin and incubated overnight (O/N) at 37^{o}C. Single colonies were selected and expanded in LB with ampicillin,

incubating O/N at 37^{o}C with rotational shaking at 220 rpm. Glycerol stocks were prepared by gently mixing 100 µl culture and 900 µl of 10% sterile glycerol (BIOGB0232, Astral Scientific) and storing at -80^{o}C.

Plasmid DNA was isolated using the Bioline Isolate II Plasmid Mini Kit (BIO-52056, Bioline, Meridian Biosciences, London, UK) according to the manufacturer's instructions. Briefly, this involved resuspension, alkaline lysis and neutralisation of bacterial pellets, followed by column-based purification. Purified plasmid DNA was eluted in molecular grade H_2O. Concentration and purity were measured on the NanoDrop (Thermo Fisher Scientific) and plasmid size confirmed by agarose gel electrophoresis. Samples were stored at -20^{o}C.

Prior to use in any downstream applications, sequencing was performed to confirm that the correct plasmid had been isolated (0). Sequencing was undertaken by the Australian Genome Research Facility (AGRF, Melbourne, Australia). Primer sequences for sequencing reactions are shown in Table 2-1.

Table 2-1 Sequencing primers

Construct	Primer name	Primer sequence (5`- 3`)
pcDNA-ADAM 10 and 17	ADAM-HA_F	CACTGCTTACTGGCTTATCG
	ADAM-HA_R	TGGCAACTAGAAGGCACAG
pCDNA3.1-MCAM	CMV_F	CGCAAATGGGCGGTAGGCGTG
	BGH_R	GGGTCAAGGAAGGCACG
	MCAM 500_F	GGTCGCTACCTGTGTAGGGAG
	MCAM 880_F	GCAGAACCCCAGCACCAGG
	MCAM 1270_F	CCAGCATACCCGGCCTGAACCG
	MCAM Tail_F	GACAGGTGTTGAATGCACGG
pSpCas9(BB)-2A-GFP	pSPCas9_F	CAAGGCTGTTAGAGAGATAATTGGA

Once correct sequences were confirmed, cultures containing the correct plasmid were expanded by inoculating 3 mL of LB-Ampicillin with cultures from a glycerol stock, and incubating O/N at 37ºC with shaking. This culture was further expanded by taking 1 mL of the bacterial prep and incubating it in 100 mL of LB-Amp O/N at 37ºC with shaking. Plasmid DNA was extracted the following day, using the NucleoBond Xtra Midi EF kit (740420.50, Machery-Nagel, Duren, Germany). DNA was eluted in molecular grade H_2O, and concentration and purity were measured on the NanoDrop and plasmid size confirmed by agarose gel electrophoresis. Samples were diluted to 1000 µg/mL, if necessary, and used for transient transfections. Purified plasmid DNA was stored at -20ºC.

2.2 Cell culture and maintenance

2.2.1 Cell lines

Table 2-2 summarises the cell lines used in this study. The MCAM negative SB2 melanoma cell line was provided by Dr Stéphane Karlen (Dermatologicla Clinic, Inselspital, Berne, Switzerland). These cells were derived from a primary melanoma and do not express MCAM. SB2 cells were previously transfected to stably express either wild-type MCAM (SB2 14.1) or mutant MCAM. These mutants are referred to as SB2LP and SB2YG and contain mutations in the dileucine motif and tyrosine motif, respectively. The point mutations introduced into the MCAM sequence to produce these mutants are described in Figure 1-7 The A2058 cell line was obtained from European Collection of Cell Culture (91100402, ECACC, Porton Down, UK). The MM96L, SK-Mel-28 and MM253 cell lines were provided by Professor Peter G. Parsons (Queensland Institute of Medical Research). HUV-EC-C cells, a human umbilical vein/vascular endothelial cell line, were purchased from the American Type Culture Collection (CLR-1730, lot 58469351, ATCC, Manassas, VA). Most melanoma cell lines available to purchase are derived from metastatic sites (Table 2.2). The SB2 cell line (as a primary, MCAM negative cell line) was modified to express high levels of MCAM in our laboratory for a previous research project. This modified cell line (SB2 14.1) was used in this project because preliminary data indicated it consistently produced sMCAM.

PS-1 and PS-2 knockout (KO) HEK293 cells with PS-1 and/or PS-2 knockout (KO) were a kind gift from Ms Melissa Eccles (Curtin University). Immunoblot confirmation of PS KO in these cells was confirmed by Ms Eccles. PS-1 and PS-2 KO versions of MM253 melanoma cells lines were generated using CRISPR/Cas-9. This is fully described in Section 5.2.4.

All cell lines were confirmed to be Mycoplasma negative. Testing was performed routinely on cell culture supernatants and/or cell pellets. STR profiling was also performed on cell lines used to confirm cell line authenticity. STR profiling of cells

agreed with published profiles, where these were available for comparison (Chapter 1).

Table 2-2 Cell lines used

	Cell line	Origin/Source	Notes	BRAF status	Base media
Melanoma	**A2058**	Metastatic site – lymph node	MCAM positive, unmodified	$BRAF^{V600E}$	RPMI
	MM96L	Metastatic site – lymph node	MCAM positive, unmodified	$BRAF^{V600E}$	RPMI
	MM253	Metastatic site – lymph node	MCAM positive, unmodified	$BRAF^{V600E}$	RPMI
	MM253 PS1 KO	Metastatic site – lymph node	CRISPR mediated PS1 KO	$BRAF^{V600E}$	RPMI
	MM253 PS2 KO	Metastatic site – lymph node	CRISPR mediated PS2 KO	$BRAF^{V600E}$	RPMI
	SB2	Primary melanoma	MCAM negative	WT	DMEM
	SB2 14.1	Derived from SB2	MCAM positive WT	WT	DMEM
	SB2 LP	Derived from SB2	MCAM positive, AA623 MT	WT	DMEM
	SB2 YG	Derived from SB2	MCAM positive, AA641 MT	WT	DMEM
	SkMel28	Metastatic site-lymph node	MCAM positive, unmodified	$BRAF^{V600E}$	RPMI
Other	**HEK293T**	Kidney	Unmodified	N/A	DMEM
	HEK293 PS KO*	Kidney	CRISPR mediated PS1/PS2 KO	N/A	DMEM
	HUV-EC-C	Endothelial cells	MCAM positive, unmodified	N/A	M199

2.2.2 Tissue culture reagents

Basic tissue culture media, additives and plasticware

Dulbecco's Minimum Essential Medium (DMEM; 11965118), Roswell Park Memorial Institute 1640 (RPMI; 21870092), Medium 199 (M199; 11150059), 1 M Hepes (15630080), 200 mM L-glutamine (25030081) and 100 mM sodium pyruvate (NaPyr; 11360070) were all from Gibco (Thermo Fisher Scientific). Foetal bovine serum (FBS) was purchased from Serana (Bunbury, Australia). Tissue culture plasticware (flasks and plate) were from Nunc (Thermo Fisher Scientific).

Complete media

DMEM and RPMI used for maintenance of melanoma cell lines were supplemented with 10 mM HEPES, 2 mM L-glutamine, 1 mM NaPyr, and 10% FBS. Serum-free media (SFM) was prepared as above, excluding FBS. For stably transfected SB2 cell lines, 0.5-1.0 mg/mL G418 disulfate salt solution (G8168, Sigma-Aldrich) was also added to the culture media to maintain selection for MCAM-expressing cells. HUV-EC-Cs were maintained in M199 containing 20% FBS, 10 mM Hepes, 100 mM L-glutamine, endothelial cell growth supplement (ECGS, 30 µg/mL, E0760, Sigma-Aldrich) and Heparin (0.1 mg/mL, Celsus Laboratories, Cincinnati, OH).

Freeze media

For routine freezing of cells, the following recipe was used: 50% complete media, 40% FBS and 10% dimethyl sulfoxide (DMSO; D2650, Sigma-Aldrich).

2.2.3 Cell harvesting and counting

2.2.3.1 Using a Coulter Counter

All cell lines were passaged routinely every 2-3 days. When cells were 70-80% confluent, media was removed from the flask and monolayers were washed with 3 mL PBS (Thermo Fisher Scientific). Adherent cells were removed from the tissue culture plastic by incubating at 37^{o}C in the presence of 0.5 mL 0.05% Trypsin-Ethylenediaminetetraacetic acid (TE; 25300062, ThermoFisher). After 3-5 minutes

(min), detached cells were recovered in 3 mL complete media, and 100-200 µL was taken for counting. Cells were diluted in 10 mL isotonic solution (PathWest, Perth, Australia) and counted using the Coulter CZ1 cell counter (Beckman Coulter®, Brea, CA), with the following size parameters: SB2 cell lines: 10-18 uM; A2058: 12-19 µM; MM96L: 12-21 µM, MM253: 16-23 µM, HEK293 WT and double knockout (dKO): 12-19 µM. Three cell counts were taken, and the cell concentration was calculated as follows (Equation 2-1). SB2 cell lines were plated at 40-70 x 10^4 cells per 25 cm^2. A2058 and MM253 cells were plated at 20-40 x 10^4 cells per 25 cm^2 for 2-3 days, and MM96L cells were plated at 10-15 x 10^4 cells per 25 cm^2 for 2-3 days. All HEK293 cell lines were plated at 20-40 x 10^4 cells per 25 cm^2 and grown for 2-3 days. Each cell line was grown at 37^{o}C in a humidified incubator with 5% carbon dioxide (CO_2).

Equation 2-1:

cells/mL= average cell # x dilution factor x 2

2.2.3.2 Using a Haemocytometer

For HUV-EC-C cells, subculture was performed when cells were 70-80% confluent (3-4 times per week). Cells were harvested using either 0.05% TE or 2.5mM EDTA containing a 1/50 dilution of stock TE. Detached cells were collected in culture medium (minus growth factors and heparin) and pelleted. The cell pellet was resuspended in normal growth medium and cell number was obtained using a haemocytometer. This approach was chosen for obtaining accurate cell counts as the Coulter CZ1 cell counter does not account for the large size variability of the HUV-EC-C cells. Briefly, an aliquot of the cell suspension was diluted 1:1 in 0.4% trypan blue (15250061, ThermoFisher) and 10 µL was ejected into the counting chamber of the haemocytometer. The number of cells in each of the four corner grids was counted (Figure 2-1) and averaged, and the cell concentration was calculated, as per Equation 2-2. HUV-EC-Cs were plated at 0.7-1 x 10^4 cells per 25 cm^2.

Equation 2-2:

cells/mL = average cell # x 10^4 x 2 (trypan blue dilution) x cell dilution factor

Figure 2-1 Haemocytometer grid layout

The number of cells in each corner square (1-4) was counted and averaged. Cells on the outer edges (solid black line) were included in the cell count, while cells on the inner edges (dotted black line) of each corner square were excluded. (Image adapted from http://www.microbehunter.com/the-hemocytometer-counting-chamber/).

2.2.4 Freezing and thawing cells

Cells were harvested and counted, as above, then pelleted at 200 g for 5 min. The supernatant was carefully removed and the cell pellet resuspended in freeze media at 2 x 10^6 cells/mL, and 0.5 mL was transferred to each cryovial (1 x 10^6 cells per vial). Vials were placed in a “Mr Frosty” freezing container and placed at -80^{o}C for at least 24 hours before being transferred to liquid nitrogen for long-term storage. DMSO was from Sigma-Aldrich and cryovials from Greiner Bio-One (Nürtingen, Germany).

To thaw cells, cryovials were rapidly warmed by immersing in a 37^{o}C water bath. An additional 0.5 mL pre-warmed complete media was gently added to the vial and cells were then transferred to a tissue culture flask. Media (4 mL) was slowly added to the flask in a dropwise manner with gentle mixing. Cells were incubated at 37^{o}C until adhered and spread on the TC plastic. The media (which contained residual DMSO from the freeze media) was removed and replaced with fresh culture media. Alternatively, thawed cells were transferred to a 10 mL tube containing warm media and centrifuged at 330 g for 5 min. Media containing DMSO was discarded, and the cell pellet resuspended in fresh media and transferred to a cell culture flask.

2.2.5 Transient transfection

HEK293 cell lines

HEK293 WT and HEK293 PS1/2 dKO cells were plated on Poly-D-Lysine-coated TC plastic to aid cell adhesion. Briefly, the bottom of a 12-well plate was coated with 5 µg/mL of Poly-D-lysine (A3890401, ThermoFisher) O/N at 37^{o}C. The surface was washed once with sterile ddH_2O and twice with sterile PBS. Cells were then plated at 5 x 10^4 cells/well and allowed to adhere O/N in a tissue culture incubator. The following morning, transient transfections were performed using 1 µg pcDNA3.1-MCAM plasmid and 3 µl Lipofectamine™ 3000 (L3000015, ThermoFisher) per well, according to the manufacturer's instructions (Figure 2-2).

Melanoma cell lines

A2058, MM253 and SB2 14.1 melanoma cells were transiently transfected to overexpress either ADAM10-HA or ADAM17-HA, as well as their DN counterparts, which lack the pro- and MP-domains required for proteolytic cleavage of substrates (ProMP-ADAM10-HA and ProMP-ADAM17-HA) (Section 2.1.2). Cells were seeded in either a 24-well plate or a 12-well plate and incubated at 37^{o}C with 5% CO_2 O/N. When immunofluorescence (I.F) was to be performed, the cells were seeded onto collagen-coated coverslips instead of TC plastic (Section 2.8.3). The following morning, cells were transfected using Lipofectamine™ 3000 (Invitrogen), according to the manufacturer's instructions. 0.5-1 µg of DNA was used per well, along with 1-2 µL Lipofectamine (24 vs. 12 well plate).

Figure 2-2 Transient transfection protocol with Lipofectamine™ 3000

Cells were seeded on day 0 and transfected the following morning. Two concentrations of Lipofectamine were prepared in OptiMEM and vortexed. DNA was diluted in OptiMEM and mixed with P3000 reagent, then combined with Lipofectamine and incubated for 10 min at RT. The DNA-lipid complexed were added dropwise to the cell culture media and incubated for at least 24 hours before sample collection. Image sourced from https://tools.thermofisher.com/content/sfs/manuals/lipofectamine3000_protocol.pdf

2.3 Collection of cell culture medium for secreted proteins

Experiments were carried out in a 24 well tissue culture plate, unless otherwise described. Cells were plated and grown in complete media O/N, at a sufficient density to reach ~70% confluence at the time of collection. Immediately prior to changing media, cell monolayers were rinsed with either SFM or PBS to remove serum proteins. Cells were then incubated in either DMEM/RPMI SFM, DMEM/RMPI + 10% FBS, DMEM/RPMI + 2% FBS, or DMEM/RPMI + 1% bovine serum albumin (BSA), unless otherwise stated. All media was supplemented with 10 mM HEPES, 2 mM L-glutamine, and 1 mM NaPyr. Where heat-inactivated serum was required, an aliquot of FBS was heated to 56^{o}C in a water bath and incubated for 30 min, then cooled prior to use. Once fresh media was added, cells were cultured for a further

~24 hours, then media and lysates were collected for further processing and analysis.

Media was harvested and subject to sequential centrifugation to pellet dead cells and debris (330 g for 5 min, then ~15,600 g for 15 min, at 4^{o}C). Supernatants were recovered and concentrated approximately 10-fold using a SpeedVac (Savant, Thermo Fisher Scientific). In some cases, this was performed in the presence of 1x cOmplete^{TM} EDTA-free protease inhibitors (CPI; 469313200, Roche, Basel, Switzerland). However, the presence or absence of these inhibitors did not appear to affect MCAM protein stability. Concentrated media was either stored at -20^{o}C or used immediately for SDS-PAGE.

2.4 Preparation of whole cell lysates

Cell monolayers were rinsed once with PBS, then cells were detached from tissue culture plastic by incubating with 2.5 mM EDTA/PBS. For SB2 cell lines, 0.05% trypsin was diluted 1/50 in 2.5 mM EDTA/PBS to aid cell detachment. Detached cells were collected in ice cold PBS and pelleted at 330 g for 5 min, washed again with ice cold PBS and pelleted. The cell pellet was resuspended in lysis buffer (1% NP40 in PBS) containing CPI. Lysis was carried out on ice for 30 min, and lysates were centrifuged at ~15,600 g for 15 min, at 4^{o}C. Supernatants were recovered and either used immediately or stored at -20^{o}C.

2.5 Experimental conditions for stimulating and inhibiting shedding

2.5.1 Reagents

Calcium ionophore

Ionomycin calcium salt from *Streptomyces conglobatus* (I0634, Sigma-Aldrich) was supplied as a sterile 1 mM stock solution in DMSO. Aliquots were stored at -20^{o}C. Serial dilutions were prepared in culture media for testing (final concentrations 0-10 µM). DMSO (diluted 1/100) in culture media was used as a vehicle control. A

range of treatment times and conditions were tested, and cell culture supernatants and lysates were collected and processed for Immunoblot.

PMA

Phorbol 12-myristate 13-acetate (PMA; P8139, Sigma-Aldrich) was prepared as a 2 mg/mL stock solution in DMSO, which was stored at -20ºC, protected from light. Working solutions were prepared by diluting PMA 1/100 (20,000 ng/mL) in culture media, and serial dilutions were performed to test concentrations ranging from 0-200 ng/mL. DMSO was used as a vehicle control. Prior to treating with PMA, cells were serum-starved for 2 hours. Cells were then incubated with PMA at 37ºC for either 2 hours or 16 hours. Next, media and lysates were harvested to analyse the effect of PMA on ectodomain shedding.

For I.F. analysis, cells were plated on collagen-coated coverslips (Section 2.8.3) and grown to <70% confluence. They were then treated with 0-100 ng/mL PMA under serum-free conditions for 16 hours. Cells were fixed, permeabilised, and stained for the MCAM-CTF (Section 2.8.4). Alternatively, cells plated on fibronectin-coated coverslips were treated with 100 µM PMA for 1-2 hours to activate cells. Treated cells were fixed, permeabilised, and immunofluorescently labelled for focal adhesions and actin filaments.

Metalloproteinase inhibitors

The broad-spectrum metalloproteinase inhibitor GM6001 (M5939, Sigma-Aldrich) was solubilised in DMSO. Aliquots of the 10 mM stock solution were stored at -20ºC until needed. Thawed solutions were serially diluted in reduced serum media (2% FBS) for experimental use (0-100 µM). 1% DMSO in culture media was used to represent the unstimulated control. Cells were treated O/N and samples were collected the following morning.

MMP inhibitor I (444250, Calbiochem, Merck) was prepared to a 2 mM stock solution in sterile ddH_2O and stored at -20ºC for up to one month. A working solution was

prepared by diluting the stock solution in SFM and serial dilutions were performed to test a range of concentrations (0-500 µM). MMP inhibitor III (444264, Calbiochem) was solubilised in DMSO as a 2 mM solution. This was then further diluted to a 1 mM stock solution, and aliquots were stored at -20ºC. Before use, MMP inhibitor III was diluted 1/1000 to generate a 1 µM working solution. This was used to prepare serial dilutions for testing the effects of different concentrations (0-500 nM) of inhibitor on ectodomain shedding. DMSO only or water only was used as an untreated/vehicle control as appropriate. These were diluted in SFM using the same dilution factor as the highest concentration of inhibitor. Cells were treated for 2 hours at 37ºC and media and lysates were collected and processed.

Swainsonine

Swainsonine (SW; 16860, Sapphire BioScience, NSW, Australia) was prepared to 1 mg/mL in DMSO and stored at -20ºC. Cells were plated and allowed to adhere and spread for ~3 hours. Media was removed and replaced with media containing SW. A range of concentrations were tested (0, 0.25, 0.5, 0.75 and 1 µg/mL) to determine an effective concentration for experimental use. After ~48 hours in culture, samples were collected, as above. Lysates were subject to Immunoblot analysis to confirm impaired glycosylation based on reduced protein molecular weight, while media was compared between treated and untreated samples to determine whether impaired glycosylation interfered with MCAM ectodomain shedding.

2-bromohexadecanoic acid

2-bromohexadecanoic acid (2-BP; 21604, Sigma-Aldrich) was prepared as a 5 M stock solution in DMSO and stored at -80ºC (long-term) or -20ºC (short-term). A working stock of 50 mM was prepared by diluting 2-BP in DMSO. Concentrations ranging from 0-250 µM were prepared in normal culture media, and SB2 14.1 and A2058 melanoma cells were treated for ~24 hours at 37ºC.

Trifluoperazine dihydrochloride

A 100 mM stock solution of trifluoperazine dihydrochloride (TP; T6062, Sigma-Aldrich) was prepared in DMSO and stored at -20ºC. Working solutions ranging from 10-500 µM were prepared by serial dilution. The 500 µM working solution required rapid mixing to avoid precipitation of TP. SB2 14.1 melanoma cells at >70% confluence were incubated with TP at 37ºC for 2-3 hours to test its ability to inhibit CaM.

γ-secretase inhibitors

The broad-spectrum γ-secretase inhibitor *N*-[*N*-(3,5-difluorophenacetyl)-L-alanyl]-(*S*)-phenylglycine t-butyl ester (DAPT; GSI-IX, LY-374973, S2215; Selleckchem, Houston, TX) was kindly provided by A/Prof Giuseppe Verdile and Melissa Eccles. The 5 mM stock solution of DAPT was diluted directly in culture media and used at concentrations ranging from 0-50 µM. In all cases, DMSO was used as a vehicle control. Cells were treated with inhibitors O/N, and lysates were collected the following day (16 - 24 hour timepoints).

I.F. analysis was also performed on cells plated on collagen-coated coverslips. Briefly, cells were grown to <70%, then treated with 0-20 µM DAPT for 16 hours. Cells were then fixed, permeabilised, and immunofluorescently labelled for MCAM-CTF (Section 2.8.4).

2.5.2 Treatment procedures

Cells were seeded in either a 6-, 12- or 24-well plate, as required, and allowed to adhere O/N (unless otherwise stated). Prior to treatment, media was removed, and monolayers were rinsed with warm SFM. The shedding stimulators/inhibitors were diluted in SFM or reduced serum media (2% FBS), as required, and added directly to the cells. Cells were incubated at 37ºC and media and lysates were collected at specific time-points. Samples were prepared for SDS-PAGE (Sections 2.3, 2.4, and 2.7).

2.6 MCAM synthesis studies

Cycloheximide (CHX; C7698) was purchased from Sigma-Aldrich. A 50 mg/mL stock solution was prepared by solubilising CHX in 70% EtOH under sterile conditions. The stock solution was stored at -20^{o}C. A pilot experiment was performed to test the concentrations and time points necessary for inhibiting protein synthesis. SB2 14.1 cells were grown to 70% confluence and then serum-starved for two hours in SFM. A working solution of CHX was then prepared at 5,000 µg/mL, by diluting the stock solution in normal culture media. Further dilutions were performed to generate a range of concentrations for testing (50-200 µg/mL). For the vehicle control, 70% EtOH was diluted 1/1250. 1 mL of media containing CHX or vehicle was added to each well, and cells were incubated for 2-24 hours. Lysates were collected at each time-point (2, 4, 6 and 24 hours) and protein concentration was determined by bicinchoninic acid assay (BCA). MCAM expression was assessed by Immunoblot (Sections 2.3, 2.4, and 2.7).

2.7 SDS-PAGE and immunoblotting

2.7.1 Reagents and buffers

Lysis buffer

Cells were lysed using ice-cold 1% NP40 in PBS. 1x cOmplete^{TM} EDTA-free protease inhibitor cocktail was added immediately before use.

SDS-PAGE running buffer

10x Tris-glycine-SDS running buffer containing 250 mM Tris-base (T1503) 1.92 M glycine (G7126) and 1% SDS (L4509), all from Sigma-Aldrich, was prepared in ddH_2O. The pH was adjusted to 8.3 using concentrated HCl. The stock was diluted 1/10 to prepare a 1x Tris-glycine-SDS running buffer for electrophoresis.

SDS loading buffer

5x SDS sample loading buffer contained 250 mM Tris-HCl (pH 6.8), 10% SDS (w/v), 50% glycerol (v/v), and 0.5% Bromophenol blue (w/v)(Cat: B0126), all from Sigma-Aldrich.

Blotting buffer

10x blotting buffer (250 mM Tris-base, 2 M glycine) was prepared to 1 L in ddH_2O. Concentrated HCl was used to adjust to pH 8.3. A 1x blotting buffer solution was prepared by diluting 200 mL 10x blotting buffer in 400 mL methanol (179337, Sigma-Aldrich) and 1400 mL ddH_2O.

Phosphate buffered saline (PBS)

Non-sterile 1x PBS, pH 7.4, was prepared from PBS tablets (09-2051, Astral Scientific) dissolved in ddH_2O (1 tablet per 100 mL). 10x PBS (pH 7.4) was prepared containing 1.37 M NaCl (S9888), 0.02 M KCl (P3911), 0.10 M Na_2HPO_4, (S9763) and 0.02 M KH_2PO_4 (P0662) (all from Sigma-Aldrich) and diluted 1/10 in ddH_2O to make a 1x working solution (pH 7.4).

PBS/Tween-20 wash buffer

0.1% (v/v) Tween-20 (P1379, Sigma-Aldrich) was mixed with 1 x PBS.

SDS-PAGE resolving and stacking gel

Resolving/running gels were prepared to the appropriate percentage (Table 2-3). Immediately prior to pouring the gel, 0.1% (v/v) ammonium persulfate (APS; BIOAB0072, Astral Scientific) and 0.02% (v/v) Tetramethylethylenediamine (TEMED; BIOTB0508, Astral Scientific) were added. Gels were cast in a Hoefer mini gel caster (Hoefer, Holliston, MA) between two glass plates separated by a 2 mm spacer. A gap of ~2 cm was left at the top of the plates, which was overlaid with ddH_2O. Gels were allowed to polymerise at room temperature.

Table 2-3 Reagent measurements for different percentage running gels

	10%	**12%**	**15%**
1 M Tris (pH 8.8)	5 mL	5 mL	5 mL
29:1 Acrylamide/Bis-acrylamide (1610156, BioRad Laboratories, Hercules, CA)	3.4 mL	4 mL	5 mL
10% SDS	100 µL	100 µL	100 µL
ddH_2O	1.65 mL	0.90 mL	-

A 5% stacking gel was prepared by combining acrylamide/bis-acrylamide (29:1), 125 mM Tris-HCl (pH6.8), 0.1% (v/v) SDS and ddH_2O to a final volume of 3 mL per gel. Just prior to pouring, 0.1% (v/v) APS and 0.02% (v/v) TEMED were added and mixed. The stacking gel was poured on top of the running gel (after removing water overlay) and wells were made using a 10-well casting comb. The stacking gel was left to polymerise at RT while samples were prepared.

Coomassie Blue

Coomassie Blue protein stain was prepared as follows: 40% (v/v) methanol, 10% (v/v) acetic acid (A6283, Sigma-Aldrich), 0.5% (w/v) Coomassie Blue Coomassie R-250 dye (161-0400, BioRad Laboratories) in ddH_2O.

De-staining solution

De-staining solution comprised 40% (v/v) methanol and 10% (v/v) acetic acid in ddH_2O.

Stripping solution

Stripping solution contained 1.5% glycine (w/v), 0.1% SDS (w/v), 1% Tween-20 (v/v) in ddH_2O. The solution was adjusted to pH 2.2 with HCl.

2.7.2 BCA and sample preparation

Protein concentration was determined using the bicinchoninic acid assay (BCA) (23225, Thermo Fisher Scientific), as per manufacturer's instructions. A linear regression was applied to the BSA standards (ranging from 2 mg/mL to 0.05 mg/mL) and used to calculate total protein concentration of the tested lysates. Samples were adjusted to the same total protein concentration by diluting in lysis buffer. Where media was collected in parallel with lysates, it was diluted in the same manner. For SDS-PAGE, samples were routinely prepared as follows: 20 µL sample mixed with 5 µL 5x SDS loading buffer and boiled for 5 min at 90^{o}C using a thermocycler.

2.7.3 SDS-PAGE

For cell lysates and concentrated media, ~18 µL of sample was loaded in each well of the SDS-poylacrylamide gel. Pre-stained Protein Ladder (10-245 kDa, ab116028, Abcam, Cambridge, United Kingdom) was used as a reference for protein size. The total protein concentration in lysates was measured by BCA as above, and an equal amount of protein for each sample were loaded on the gel. Protein quantity was usually 10 µg. In some instances, the capacity to load protein was limited to less than 10 µg because the samples were collected from a 24-well plate (surface area 2 cm^{2}). This was due to availability and expense of inhibitor treatments. Proteins were separated by electrophoresing at 25 milliamps (mAmp) per gel, under non-reducing conditions. Following separation, proteins were transferred to an Immobilon-P polyvinylidene difluoride (PVDF) membrane (IPVH00010, Millipore, Sigma-Aldrich), or the gel was stained with Coomassie Blue.

2.7.4 Protein transfer

Proteins were electrotransferred from the SDS-polyacrylamide gel to a PVDF membrane. Membranes were first activated in 100% methanol, then equilibrated in 1x blotting buffer before use. A wet blotting transfer system (Hoeffer) was used, running at 200 mAmp for 1 hour at RT. After electrotransfer, membranes were blocked in 5% skim milk powder (Diploma, Anchor Foods) (w/v) in PBS/0.1% Tween-20 for 1 hour at RT, or 4^{o}C O/N. In some cases, membranes were air dried or fixed

with 1% paraformaldehyde (PFA; Section 2.8.1) and rehydrated in methanol prior to blocking. This was to help cross-link smaller proteins to the membrane.

Equal loading was confirmed using Revert700® (LI-COR Biosciences, Lincoln NE). This is a total protein stain that can be used as an alternative to housekeeping proteins for protein quantification by immunoblot (Kirshner & Gibbs, 2018). Before blocking, membranes were rinsed with ddH_2O then incubated with 1 mL Revert700® for 5 min. Membranes were briefly rinsed twice with wash solution (6.7% (v/v) glacial acetic acid, 30% (v/v) methanol in ddH_2O), followed by ddH_2O. Membranes were then imaging using the IR680 nM channel on the ChemiDoc (BioRad Laboratories). Alternatively, membranes were probed for β-tubulin (Table 2-4) or were stained with Coomassie Blue at the end of the experiment to confirm equal protein loading. This is described below.

2.7.5 Immunoblot

After blocking, primary antibody was diluted in 5% skim milk powder (w/v) in 1x PBS with 0.1% Tween-20 (v/v) (PBS/Tween-20) and added directly to the membranes and incubated for 1 h at RT, or O/N at 4^{o}C. Prior to secondary antibody incubation, membranes were rinsed thoroughly 3 x 5 min using PBS/Tween-20 to remove unbound antibody. Secondary antibodies were diluted in 5% skim milk-PBS/Tween-20 and incubated at RT for 45 min to 1 hour. Membranes were again washed 3 x 5 min with PBS/Tween-20, followed by three washes with PBS only. Membranes were developed using Clarity or Clarity Max ECL western blotting reagents (1705060 or 1705062, BioRad) for 5 min, and protein bands were visualised using the ChemiDoc Imaging System (BioRad). Any subsequent antibody incubations on the same membrane were performed (as above) after additional washes and blocking in 5% skim milk powder in PBS/Tween-20. All antibodies and dilutions used are listed in Table 2-4.

Table 2-4 Primary antibodies

Antigen	Reactivity	Clone	Species, isotype	Application^	Manufacturer/ Supplier, Cat. #
Moesin	Mouse, Rat, Human	Monoclonal EP1863Y	Rabbit	IF (1 µg/mL) WB (1/5000)	Abcam ab52490
CD146 (CTF)	Mouse, Rat, Human	Monoclonal EPR3208	Rabbit IgG	IF (0.25 µg/mL) WB (1/2000)	Abcam ab75769
CD146 (ECD)	Human	Monoclonal CC9	Mouse IgG2a	IF (1 µg/mL) WB (1 µg/mL) FC (10 µg/mL) Co-IP (500 µg/mL)	In-house[$]
Calmodulin	Mouse, Rat, Human	Monoclonal EP799Y	Rabbit IgG	IF (1 µg/mL) WB (1/1000)	Abcam ab45689
MMP14	Mouse, Rat, Human	Monoclonal EP1264Y	Rabbit IgG	IF (1 µg/mL) WB (1/2500)	Abcam ab51074
Golgin97	Mouse, Human, Other	Monoclonal CDF4	Mouse IgG1	IF (1 µg/mL)	Molecular Probes A21270
LAMP1	Hamster, Human, Primate, Rat	Monoclonal H4A3	Mouse IgG1	IF (0.5 µg/mL)	DSHB*
LAMP2	Human	Monoclonal H4B4	Mouse IgG1	IF (1 µg/mL)	DSHB*
Vinculin	Mouse, Rat, Human, Other	Monoclonal	Mouse IgG1	IF (1/400)	Sigma-Aldrich V9131
Phalloidin-iFluor 488	N/A	N/A	N/A	IF (1/2000)	Abcam ab176753
P-paxillin Tyr118	Mouse, Rat, Human, Other	Polyclonal	Rabbit	IF (1/50)	Cell Signalling Technology 2541
Presinilin-1 (NTF)	Human	Monoclonal, NT1	Mouse IgG1	WB (1 µg/mL)	BioLegend 823404

Presinilin-2 (NTF)	Human	Polyclonal	Rabbit	WB (1/1000)	In-house[#]
Presinilin-2 (NTF)	Human	Monoclonal	Mouse IgG1	WB (1/1000)	BioLegend *814204
APP	Mouse, Rat, Human	Monoclonal C1/6.1	Mouse IgG1	WB (1/1000)	BioLegend 802801
ADAM10	Human	Polyclonal	Rabbit IgG	WB (1/1000)	Cell Signalling Technology 14194
ADAM17	Human	Polyclonal	Rabbit IgG	WB (1/1000)	Cell Signalling Technology 6978
Calnexin	Human	Monoclonal W17077C	Rat IgG2a$_K$		BioLegend 699402
HA-Alexa Fluor 488	N/A	Monoclonal 16B12	Mouse IgG1		BioLegend 901509
β-tubulin	Mouse, Rat, Human, Other	Monoclonal E7	Mouse IgG1	WB (0.6 µg/mL)	DSHB
GAPDH	Human Mouse Rat Other	Monoclonal (D16H11)	Rabbit IgG	WB (1/1000)	Cell Signalling Technology 5174

^ IF (immunofluorescence); WB (Western blot); FC (flow cytometry); Co-IP (co-immunoprecipitation)

[$] CC9 anti-MCAM antibody hybridoma was courtesy of Dr. Andrew Zannettino, University of Adelaide

* DSHB (Developmental Studies Hybridoma Bank)

PS2 affinity purified antibody was courtesy of Professor Paul E Fraser, University of Toronto

2.7.6 Coomassie Blue staining

Staining method for SDS-polyacrylamide gels

After protein separation was complete, the gel was incubated in Coomassie Blue solution for at least 1 h at RT, with rocking. The stain was then removed, and the gel

rinsed with ddH_2O. The gel was incubated with de-stain solution on a rocking platform, changing the solution as needed, until distinct protein bands were visible and there was minimal background. Gels were imaged using the ChemiDoc Imaging System (BioRad).

Staining method for PVDF membranes

When required, PVDF membranes were stained with Coomassie blue. Following immunoblot visualisation, membranes were rinsed with ddH_2O then incubated with Coomassie Blue solution for 1-2 h. The stain solution was then removed, and membranes rinsed with ddH_2O. De-stain solution was added and incubated on a rocking platform, changing the solution as required until distinct protein bands were visible and there was minimal background. Imaging was then performed, as above, to capture the staining of total protein within the membrane.

2.7.7 Membrane stripping

Membranes that required stripping after imaging were washed 3 x 5 min with PBS/Tween-20, followed by thorough rinsing with PBS only. Stripping solution was then added to the membrane and incubated, with gentle agitation/rocking, for 30-60 min at RT. Membranes were washed again, as described above, then blocked and probed, as per section 2.7.5.

2.7.8 Quantification of protein expression via immunoblot

Analysis was performed using Image Lab 6.0.1 (BioRad). First, total protein signal was measured from Revert700®-stained membranes. Lanes were automatically detected and the lane area was adjusted manually, if necessary. The “adjusted total lane volume” of each sample was determined by subtracting the background signal to give the total protein signal. A normalisation factor was calculated by dividing the signal from the sample of interest, by the signal from the control sample. Membranes probed with antibody were analysed using a similar method, except following lane detection, protein bands of interest were selected, and the sensitivity was adjusted

using the rolling ball method. The “adjusted total protein signal” was then calculated by subtracting the background signal.

The adjusted total protein signal for the protein of interest was multiplied by the normalisation factor calculated from the total protein stain, to derive “normalised protein expression”. To calculate the fold-change of protein expression in a sample relative to a control, the normalised protein expression of the sample of interest was divided by the normalised protein expression of the control sample. Results were then plotted using GraphPad Prism (GraphPad Software, San Diego, CA) and presented as either a dot plot or as a histogram representing the mean values from 2-3 biological or technical replicates (+/- standard deviation).

2.8 Immunofluorescent staining

2.8.1 Reagents and materials

Etching solution

15 g NaOH pellets were dissolved in a solution containing 90 mL of absolute EtOH and 60 mL ddH_2O.

HEPES buffered saline (HBS)

10 mM Hepes, 1 mM $CaCl_2$ and 1mM $MgCl_2$ were added to 150 mM NaCl and pH adjusted to 7.0 using 1M HCl. The buffer was filter sterilised and stored at 4^{o}C.

4% (w/v) paraformaldehyde

Paraformaldehyde (PFA) was prepared by dissolving 2.4 g PFA powder in 50 mL HBS in a dark water bath set to 55^{o}C. Once the powder had dissolved, the pH was adjusted to 7.4 using 1M NaOH and the solution was successively passed through 0.45 µM and 0.2 µM syringe filters to sterilise. The solution was kept sterile and stored at 4^{o}C for one month.

0.1% Triton X-100 (TX-100)

Triton X-100 (Sigma-Aldrich) was diluted in sterile HBS to prepare 0.1% (v/v) Triton X-100 solution and stored at 4ºC.

Blocking buffer

Blocking solution consisted of 1% (v/v) BSA (Hyclone) and 10% (v/v) goat serum (Gibco, Thermo Fisher Scientific), diluted in HBS.

Antibody diluent

Antibodies were diluted in a solution of HBS and 2% (v/v) goat serum.

2.8.2 Etched glass coverslips

Coverslips were immersed in etching solution (Section 2.8.1) and incubated for at least one hour at RT, with gentle agitation. Coverslips were washed thoroughly with dH_2O, followed by ddH_2O, then air dried O/N. Prior to use, coverslips were cleaned with 70% EtOH and UV sterilised for 30 minutes.

2.8.3 Matrix coating coverslips

To aid cell adhesion, sterile (etched) coverslips were coated with 1 µg/cm^2 calf type I collagen (Sigma-Aldrich) for 2 hours at 37ºC, or at 4ºC O/N. Alternatively, when experiments were aimed at detecting focal adhesions, cells were plated on fibronectin-coated coverslips (2 µg/cm^2; Sigma-Aldrich).

2.8.4 Fixing, permeabilising, blocking and staining

Coverslips were rinsed three times with warm HBS before incubating with 4% PFA for 15 min in the dark to fix cells. Coverslips were rinsed a further three times with HBS, then cells were permeabilised for 3-5 minutes at 4ºC, using cold 0.1% TX-100. Cells were rinsed three times with HBS, then either kept in HBS at 4ºC for short-term

storage or incubated in blocking buffer either at RT for 1 h, or O/N at 4ºC. Alternatively, where described, cells were fixed and permeabilised with ice cold methanol: acetone (50:50) at -20ºC for 5 min, then blocked as above.

After blocking, cells were labelled with primary antibody for 1 h at RT (list of primary antibodies and isotype control antibodies are given in Table 2-4 and Table 2-5, respectively). Unbound antibody was removed by washing coverslips with HBS for 3 x 5 min with gentle agitation. Secondary antibody (Table 2-6) was then added and incubated at RT for 45 min to 1 h. Coverslips were then washed, as above. If a second target protein was to be investigated, additional primary and secondary antibody incubation steps were performed, as described above. Depending on the experiment, antibodies were either diluted in blocking solution or antibody diluent. Nuclei were stained using 4′,6-diamidino-2-phenylindole (DAPI; 1 µg/mL, diluted in HBS), by incubating for 10-15 minutes at RT before washing and mounting onto glass coverslips using VectaShield (Cat: H-1900-10, Vectorlabs, Burlingame, CA). Finally, coverslips were dried and sealed with nail varnish, then imaged using a Nikon A1 confocal microscope (Nikon, Tokyo, Japan). Samples were stored at 4ºC, protected from light.

Table 2-5 Isotype control antibodies

Isotype control	**Manufacturer/supplier** **Cat. #**
Mouse IgG_1	Zymed (Thermo Fisher Scientific) 02-6100
Mouse IgG_{2a}	Zymed (Thermo Fisher Scientific) 02-6200
Rabbit IgG	Abcam ab172730

Table 2-6 Secondary antibodies

Antibody name	Reactivity	Conjugate	Application	Manufacturer/ supplier, Cat. #
Goat anti-mouse Ig	Mouse Ig	HRP	WB (1/2000)	Dako, Agilent^ P0447
Goat anti-rabbit Ig	Rabbit Ig	HRP	WB (1/2000)	Dako, Agilent P0448
Goat anti-mouse IgG	Mouse IgG (H + L)	AlexaFluor555	IF (1/400)	ThermoFIsher A32727
Goat anti-rabbit IgG	Rabbit IgG (H + L)	AlexaFluor488	IF (1/400)	ThermoFisher A32723
Goat anti-mouse Ig	Mouse Ig	FITC	FC (1/40)	Dako, Aligent F0479
Goat anti-mouse IgG	Mouse IgG (H + L)	Alexa Fluor647	FC (1/4000)	Abcam Ab150115

^ Santa Clara, CA

2.8.5 Wound-healing assays

For 2D migration experiments, cells were grown to confluence on collagen-coated coverslips. A P1000 pipette tip was used to make two parallel wounds in the monolayer. Detached cells were removed by gently rinsing monolayers with warm media at least three times, and fresh media added to the wells. Cells were then grown in normal culture media for approximately 24 hours, allowing enough time for cells to migrate into the wound. Fixation, permeabilisation, blocking, and staining steps were carried out as described above.

2.9 Flow cytometry

2.9.1 Reagents and materials

Flow wash buffer

1 mM EDTA was added to PBS containing 0.25% (w/v) BSA.

Antibody diluent

Antibodies were diluted in PBS containing 0.1% (v/v) BSA.

Permeabilization solution

Flow wash buffer was supplemented with 0.2% Saponin (Sigma-Aldrich)

Paraformaldehyde

4% PFA (Section 2.8.1) was diluted in flow wash buffer to a final concentration of 1%.

2.9.2 Harvesting and labelling cells

Harvesting and counting cells

Cells were grown to 70-80% confluence (usually this was 2 days following passage), then media was removed, and the monolayer was rinsed with PBS, followed by 2.5 mM EDTA. Cells were detached from the TC plastic by incubating at 37^{o}C in the presence of 2.5 mM EDTA. For cells that were more difficult to detach (e.g. the SB2 cell series), a 1/50 dilution of TE was added. Cold media was then used to collect the de-adhered cells, which were pelleted by centrifugation at 4^{o}C (~200 g for 5 min). Cell pellets were washed twice with ice cold PBS. Where possible, a cell count was performed between the first and second wash. All further steps were performed on ice.

Labelling surface proteins

Cells were resuspended in a volume of PBS/0.5% BSA to yield between ~330-1000 x 10^4 cells/mL (or 10-30 x 10^4 cells/30 µL), and 30 µL of suspension was added to each flow cytometry tube (i.e. 10-30 x 10^4 cells/tube). Alternatively, for samples harvested from a 12-well plate, cells were harvested and added directly to flow cytometry tubes, washed, then stained. Primary antibody was added directly to the tube and cells were incubated on ice for 30 min. Unbound antibody was removed by washing with 3 mL ice-cold flow wash buffer, and cells were pelleted (~200 g for 5 min at 4^{o}C). The cell pellet was resuspended and incubated with 50 µL of diluted secondary antibody for 30 min, on ice, then washed as above.

If live/dead labelling was performed, cells were next washed once with flow wash buffer, followed by PBS only, then incubated for 10 min on ice with 100µL Zombie NIR (BioLegend, San Diego, CA). The Zombie NIR dilution used was determined via titration and was cell type-specific but in most cases was ~1/2000. Next, cells were washed with flow wash buffer. Cell pellets were resuspended in flow wash buffer containing 1% PFA, and then analysed on the Attune NxT flow cytometer (Thermo Fisher Scientific).

Labelling intracellular proteins

After washing, cells were resuspended in 1% paraformaldehyde and incubated on ice for a minimum of 15 minutes. Following fixation, the cells were pelleted, washed once with PBS, and resuspended flow wash buffer containing 0.2% saponin. Cells were permeabilised on ice for 10 minutes, then pelleted. Meanwhile, the antibody (HA-Alexa Fluor488) was diluted 1/1000 in PBS/0.5% BSA/0.2% saponin. Cells were then resuspended with diluted antibody and incubated on ice for 30 min, in the dark. Flow wash buffer containing 0.2% saponin was used to wash cells. Cell pellets were resuspended in flow wash buffer and 1% PFA. Samples were then analysed on the Attune NxT flow cytometer.

2.10 Gelatin zymography

2.10.1 Gels and buffers

Gelatin gels

1 mg/mL of gelatin (type A from porcine skin, Sigma-Aldrich) was dissolved in 4.8 mL of ddH_2O at 65°C for ~15 min. Once cooled, gelatin was mixed with 9.9 mL Acrylamide-Bis (29:1), 15 mL of 1M Tris (pH 8.8), and 300 µL of 10% SDS. Immediately prior to pouring the gel, 60 µL TEMED and 300 µL APS was added.

5x non-reducing SDS-glycerol loading buffer

5x SDS loading buffer contained 4% (v/v) SDS, 20% (v/v) glycerol, 0.01% (w/v) bromophenol blue, and 125 mM Tris-HCl (pH 8.8) in ddH_2O (all from Sigma-Aldrich).

Zymography wash buffer

2.5 % (v/v) TritonX-100, 50 mM Tris-HCl (pH 7.5), 5 mM $CaCl_2$, 1 µM $ZnCl_2$ (all from Sigma-Aldrich) were prepared in ddH_2O.

Zymography incubation buffer

The incubation buffer contained 1% TX-100, 50 mM Tris-HCl (pH 7.5), 5 mM $CaCl_2$ and 1 µM $ZnCl_2$ in ddH_2O.

Zymography gel staining solution

A solution containing 40% (v/v) methanol, 10% (v/v) acetic acid, and 0.5% Coomassie Blue (w/v) in ddH_2O was used to stain gelatin-containing gels.

De-staining solution

Gels were incubated with 40% (v/v) methanol and 10% (v/v) acetic acid in ddH_2O to de-stain the gel.

2.10.2 Gelatin gel pouring and running

The Hoeffer SE400 gel apparatus was assembled (15 x 18 cm glass plates with 1 mm spacers) and the gelatin gel was poured until ~2-3 cm away from the top of the glass plate. It was overlaid with ddH_2O and allowed to polymerise for 1 hour. A 5% stacking gel was prepared, as described above (adjusting the volumes of the reagents accordingly). A 15-well comb was inserted, and the gel was set for 1 hour. After removing the comb, each well was washed and filled with running buffer.

Gelatinase activity of MMP-2 and MMP-9 in melanoma cells was measured in serum-free medium removed from cells following an O/N incubation. Cells were seeded at equal cell numbers in the wells of a 24 well plate, the morning before the O/N incubation. Harvested media was subject to sequential centrifugation to remove cellular debris (330 g for 5 min, then ~15,600 g for 15 min at 4^{o}C). If samples were not used immediately, they were stored at -20^{o}C.

Samples (100 µL) were mixed with 20 µL 5x non-reducing SDS-glycerol loading buffer and the entire sample loaded directly onto the gel, without boiling. Empty wells were loaded with 1x loading buffer to ensure even running of the gel. The gel was transferred to the running tank and the upper and lower running tanks were assembled and filled with cold 1x SDS-PAGE running buffer. Gels were run O/N in the cold room, at a constant of 15 mAmps.

The gel was trimmed, then washed for 15 min in Zymography wash buffer, with rocking. The wash buffer was refreshed and incubated for a further 1 hour (minimum). The gel was then washed 5x with ddH_2O before incubating with zymography incubation buffer at 37^{o}C, O/N, with rocking. Incubation buffer was removed, and staining solution added. The gel was rocked on a rocking platform at room temp for a minimum of 1 hour, until the gel was stained blue. After rinsing with ddH_2O, de-stain solution was added and replaced, as needed, until clear bands (depicting gelatinase activity) were visible. The gel was them imaged using the Coomassie gel protocol on a ChemiDoc (BioRad Laboratories).

2.11 Pull-down/binding experiments with MCAM-ICD

2.11.1 Protein production

Plasmids containing the MCAM-l cytoplasmic tail (aa584-646, Figure 1-7) in the pCDNA3.1 vector were kindly provided by Dr Stéphane Karlen. The tail was previously inserted into the glutathione S-transferase (GST)-expressing vector pGex-4T-1 (Amersham, GE Healthcare, Chicago IL) via BamHI/NotI restriction digest in our laboratory. Thus, pGex-MCAM-T expresses a GST-MCAM-T fusion protein. pGex.4T, which lacks an insert (pGex-empty), and will produce GST alone, was used as a negative control.

BL21 (DE3) *E.coli* cells contain the lambda DE3 phage encoding T7 RNA polymerase under the control of a lacUV5 promoter and were provide by Dr Carl Mousley. These cells were used for isopropyl ß-D-1-thiogalactopyranoside (IPTG) induced expression of pGex-MCAM-T and pGex-empty.

BL21 (DE3) *E.coli* cells were transformed with pGex-MCAM-T or pGex-empty and grown on LB-Agar plates with 100 µg/mL ampicillin. Single colonies were selected and expanded in 100 mL of LB media, shaking at 220 rpm at 37^{o}C until the optical density at 600 nm was between 0.6-1.0 (as determined by spectrophotometer). Protein expression was induced by adding 0.5 mM IPTG (Sigma-Aldrich) to the culture and incubating for a further 3-4 hours. Cells were then pelleted at 3,300 g for 5 min at 4^{o}C) and stored at -20^{o}C. Protein purification was performed by first lysing the cells, then incubating with GST beads. Briefly, cells pellets were thawed on ice, then resuspended in ice-cold PBS and centrifuged. Cells were washed once more in cold PBS before resuspending in 1 mL lysis buffer (PBS, 5 mM Dithiothreitol (DTT), 100 ug/mL Lysozyme, 1x CPI)(DTT and Lysozyme from Sigma-- and incubating on ice for 20 min. Next, samples were sonicated for 20 pulses at 80V. Each pulse was 10 seconds (10 s) “on”, followed by 20 s “off”. Samples were allowed to sit on ice to cool, then sonication was repeated. Lysates were passed through an 18G and then a 23G needle to sheer DNA. Triton X-100 (1% v/v) was added to the lysates and the solution incubated for 30 min at 4^{o}C with end-over-end mixing. Debris was pelleted

by centrifugation at 3,300 g for 15 min, 4ºC, and supernatant was incubated with pre-washed glutathione-sepharose beads (Sigma-Aldrich) with end-over-end mixing at 4ºC to bind GST-tagged proteins (i.e. MCAM-T).

2.11.2 Cell lysate preparation and pull-down for immunoblot analysis

Pull-down experiments were used to determine whether the purified GST-MCAM-T protein would pull-down proteins from melanoma cell lysates that are known to interact with the MCAM. Beads were pelleted and washed, then incubated with whole cell lysates collected from the SB2 14.1 melanoma cell line. Samples were mixed end-over-end at 4ºC, O/N, then beads were pelleted and washed with HBS to remove unbound protein. Proteins interacting with the beads were eluted by resuspending in SDS-loading buffer and boiling for 5 min at 90ºC. Samples were then run on an SDS-PAGE gel and processed as described for immunoblot analysis.

2.11.3 Mass spectrometry

Beads from pull down experiments as described above were pelleted, washed three times with ice-cold PBS, and treated with 10 mM L-glutathione in Tris (pH 8.0) for 10 min on a rocking platform to release bound proteins. The beads were pelleted by gentle centrifugation and supernatants were recovered and incubated with acetone at -20ºC to precipitate the proteins. Precipitated proteins were recovered by centrifugation and acetone was evaporated by air-drying at RT. Samples were stored at -20ºC until ready for further processing and analysis at Proteomics International, Harry Perkins Institute of Medical Research, Perth, Western Australia. Samples were analysed by electrospray ionisation mass spectrometry using the Shimadzu Prominence nano HPLC system (Shimadzu, Kyoto, Japan) coupled to a 5600 TripleTOF mass spectrometer (Sciex, Framingham, MA).

2.12 RNA extraction, cDNA synthesis and qPCR

2.12.1 RNA extraction

Cell pellets were collected for RNA extraction and stored at -20ºC until needed. Briefly, cells were harvested according to standard protocol, then washed 3x with PBS (centrifuging at ~200 g for 5 min to pellet cells) and stored at -20ºC. To extract RNA, cells were first thawed, then lysed in 1 mL TRI Reagent (T9424, Sigma-Aldrich) in a 1.5 mL tube. After a 5 min incubation at RT, 0.2 mL chloroform (C2432, Sigma-Aldrich) was added, and tubes were mixed by vigorously shaking for 15 s. This was followed by a 15 min incubation at RT, before centrifuging samples at 12,000 x g for 15 min, 4ºC, to separate into three phases: an aqueous phase containing RNA (top), an interphase containing DNA (middle), and organic phase containing protein (bottom). The aqueous phase was carefully transferred to a fresh tube, avoiding contamination with the interphase, and washed with 1 mL isopropanol (Sigma-Aldrich). Tubes were centrifuged at 12,000 x g for 30 min, 4ºC, with the RNA precipitate forming a small pellet at the bottom/side of the tube. This pellet was resuspended in 1 mL 75% EtOH to wash, and centrifuged at 7,500 x g for 10 min, 4ºC. After removing the EtOH, pellets were left to air dry, before resuspending in Baxter H_2O and storing at -20ºC (short-term) or -80ºC (long-term). RNA quality and quantity were measured on a NanoDrop and by running an aliquot on an agarose gel to confirm the presence of RNA in the sample (that is, by confirming the presence of ribosomal RNA).

2.12.2 cDNA synthesis

The Tetro cDNA synthesis kit (BIO-65043, Bioline) was used to prepare cDNA for downstream applications. Each reaction contained: 1 µg total RNA, 1 µL Oligo (dT), 1 µL 10mM dNTP mix, 3 µL 5 x RT Buffer, 1 µL RiboSafe RNase Inhibitor, 1 µL Reverse Transcriptase (200 u/µL) and DEPC-treated water to a final reaction volume up to 15 µL. Samples were mixed by gentle pipetting and incubated at 45°C for 30 min, followed by 5 min at 85ºC, after which they were immediately transferred to ice. Samples were stored at -20ºC or -80ºC until needed.

2.12.3 Quantitative PCR (qPCR)

The following primers (Table 2-7) were used for qPCR experiments:

Table 2-7 Primer sequences used in qPCR reactions

	Forward (5`- 3`)	**Reverse (5`- 3`)**
MCAM-l	CGCTGTCCTCTATTTCCTCTAT	CAACTACAAGTTCGCTCTTACG
MCAM-sh	CGCTGTCCTCTATTTCCTCTAT	TTTCTCTCCATCTCCTGCTTC
MCAM-t	ATCGCTGCTGAGTGAACCACAG	CTACTCTCTGCCTCACAGGTCA
MCAM l10	GGCAGAGGAAGAGACAACCA	TTGGGGTGACCTGGTCTCTA
MCAM l5,13	GGACATCTAGACGGTGCTC	ACAAATGCAAGCTGGAAACC
PSEN1	GCAGTATCCTCGCTGGTGAAGA	CAGGCTATGGTTGTGTTCCAGTC
PSEN2	GCTGTTTGTGCCTGTCACTCTG	TGTGTCCTCAGTGAATGGCGTG
ADAM10	GAGGAGTGTACGTGTGCCAGTT	GACCACTGAAGTGCCTACTCCA
ADAM17	AACAGCGACTGCACGTTGAAGG	CTGTGCAGTAGGACACGCCTTT
CALM1	AACAGAAGCTGAATTGCAGGA	AATTCGGGGAAGTCAATGG
CALM2	ATGGCTGACCAACTGACTGA	CAGTTCCAATTCCTTTGTTG
CALM3	AACCTTGATCCCCGTGCT	AGGCCTCCTTGAACTCTGC
CASC3	GGACTTGAGCAAGATGTGGCAC	AAACTGAGGTGGAGGTCCTGCT
RPS2	CGATGACTGCTACACCTCAGC	CTCCTGATAGGGAGACTTGGTG
ACTAB	TCCCTGGAGAAGAGCTACG	GTAGTTTGGATGCCACA
TBP	CCCGAAACGCCGAATATAATCC	AATCAGTGCCGTGGTTAGTG
GAPDH	AAGGGATTTGGTCGTATTGGGC	AGGGATGATGTTCTGGAGAGC
SDHA	TGGCATTACGACACCGTG	GCCTGCCGTGGTTAGTG

Abbreviations: MCAM-l - MCAM long, MCAM-s – MCAM short, MCAM-t – MCAM total, I10-CD146 – MCAM isoform, intron 10 variant ; I5-13-CD146 – MCAM isoform, intron variant 5/13 variant; PSEN-1/PS-2 – presenilin-1/2; ADAM10/17 - a disintegrin and metalloproteinase 10/17, CALM1/2/3 - calmodulin 1/ 2/3, CASC3 –cancer susceptibility candidate 3, RPS2 ribosomal protein S2, ACTAB - beta actin; TBP - TATA-binding protein, GAPDH - glyceraldehyde 3-phosphate dehydrogenase; SDHA - succinate dehydrogenase complex subunit A.

Primer sequences for MCAM-l, MCAM-s and MCAM-t were designed in-house, primer sequences for I10-CD146 and I5-13-CD146 were from Nollet et al. (2022), and primer sequences for PSEN1, PSEN2, ADAM10 and ADAM17 were obtained from Origene (Rockville MD). Primer sequences for CALM 1,2 and 3 were from Esteras *et al.* (2012). ASC3 and RPS2 primer sequences were from Origene; based on data from Christensen et al. (2020), who found these two genes to be the most stable of 24 genes tested across four independent melanoma cell lines and eight additional subclones. ACTA-B, TBP, GAPDH and SDHA primer sequences were from PrimerBank (Wang *et al.*, 2011) and have previously been identified as potential control genes. All primers were ordered from Sigma Aldrich.

A master mix was prepared for each primer set (Table 2-8), vortexed, and 14 µL was transferred to each well of a 96-well PCR microplate. The cDNA was thawed and diluted 1/2, then 1 µL was added to each well.

Table 2-8 qPCR reaction set-up

	Volume per sample
2x SensiFAST SYBR® No-ROX mix (BIO-98005, Bioline)	7.5 µL
10 µM forward primer	0.5 µL
10 µM reverse primer	0.5 µL
ddH_2O	5.5 µL

A BioRad CFX Connect Real Time system was used to perform the qPCR reaction. Samples were first denatured for 2 min at 95^{o}C, then the following cycling conditions were used: 95^{o}C for 5 s, 60^{o}C for 10 s, 72^{o}C for 30-60 s; for 40 cycles. A melt curve was generated at the end of the run, by incubating at 95^{o}C for 10 min, 58^{o}C for 5 s, and 95^{o}C for 50 s; to confirm the amplification of a single product.

Primer efficiency was assessed using serial dilutions of pooled cDNA (neat, 1/10, 1/50, 1/000, 1/200) and plotting the Ct value of the dilutions against a log scale of the dilution factor, then using the slope of the line to determine efficiency using Equation 2-3 (see Appendix E for efficiency calculations). All primer efficiencies were between 85 – 110% (optimal range 90 – 110%).

Equation 2-3

Primer efficiency= (10(-1/slope)-1) x 100

Analysis was performed on the Cq values, using the ΔΔCt method (Kannan, 2016). The geometric mean of the control genes was calculated for each sample and these Ct values were subtracted from those of the gene of interest, generating the delta (Δ)Ct value. The cell line used as a control differed in different assays and will be identified for each experiment through the thesis. The ΔΔCt value was then calculated by subtracting the ΔCt value of the control cells from the ΔCt values of each test cell line. The fold change in gene expression was then solved using by calculating $2^{-\Delta\Delta Ct}$. GraphPad Prism was used for statistical analysis and qPCR data analysed using the non-parametric Kruskal-Wallis followed by the post-hoc Dunn's multiple comparisons test. A $p \leq 0.05$ was considered statistically significant.

2.13 Nuclear extraction

Cells at ~80-90% confluence were harvested using 2.5 mM EDTA (with TE diluted 1/50 for more adherent cells). Detached cells were collected in ice-cold PBS and pelleted. An additional wash in PBS was performed, and cells were counted. The total number of cells was determined, and cell pellet was either stored at -20^{o}C or

resuspended in hypotonic buffer (20 mM Tris-HCl, pH 7.4; 10 mM NaCl; 3 mM $MgCl_2$) with gentle pipetting, at 1 x 10^7 cells/mL for immediate use. The suspension was incubated for 15 min on ice, allowing the cells to swell. NP40 was then added to the solution to a concentration of 2% (v/v) and vortexed for 10 s on the maximum setting. To confirm that cells were lysed, a small volume of cells was taken before and after the addition of NP40 and viewed under a microscope. Intact cells appeared as a nucleus surrounded by a halo of cytoplasm, which was not apparent in lysed cells.

After vortexing, homogenate was centrifuged at 860 g for 10 min, at 4^{o}C. The supernatant containing cytoplasmic proteins was collected in a clean tube. The pelleted material was resuspended in Cell Extraction Buffer supplemented with 1 mM Phenylmethylsulfonyl fluoride (PMSF) (both from Thermo Fisher Scientific) and 1x CPI immediately prior to use. The suspension was incubated for 30 min on ice, vortexing rapidly every 10 min. Debris was pelleted by centrifuging at ~15,600 g for 15 min, at 4^{o}C. The supernatant containing nuclear proteins was collected in a clean tube. Samples were stored at -20^{o}C (short-term) or -80^{o}C (long-term), until needed. Samples were subject to analysis via immunoblotting, as per the standard protocol described above (Section 2.7).

2.14 Protein sequencing by MS/MS

Up to 20 µg total protein was prepared for SDS-polyacrylamide gel separation by incubating cell lysates with 5X SDS loading buffer at 90^{o}C for 5 min. The sample was loaded onto a 15% SDS-polyacrylamide gel (see section 2.7.1), which was poured using a wide comb to allow a larger volume of sample-loading. Proteins were separated by electrophoresis and the gel stained with Coomassie blue. Following the de-stain procedure, gel bands between ~10-20 kDa were excised and delivered to Proteomics International (samples provided at ambient temperature). Below are the method details provided by Proteomics International.

Protein samples were trypsin digested and peptides extracted according to standard techniques (Bringans *et al.*, 2008). Peptides were analysed by electrospray ionisation mass spectrometry using the Shimadzu Prominence nano HPLC system (Shimadzu) coupled to a 5600 TripleTOF mass spectrometer (Sciex). Tryptic peptides were loaded onto an Agilent Zorbax 300SB-C18, 3.5 µm (Agilent Technologies) and separated with a linear gradient of water/acetonitrile/0.1% formic acid (v/v). Spectra were analysed to identify proteins of interest using Mascot sequence matching software (Matrix Science, London UK) with UniProt database.

2.15 Statistics

Statistical analysis was performed using GraphPad Prism. For qRT-PCR data, the non-parametric Kruskal-Wallis test was used to determine if there was a statistically significant difference between the medians of the delta CT values of all cell lines tested (Yuan *et al.*, 2006). If the Kruskal-Wallis analysis revealed a statistically significant result, a post-hoc Dunn's Multiple Comparison Test was performed, which compared the delta CT values of each cell line to every other cell line, to determine which groups were different. A correction for multiple comparisons was also applied to the Dunn's test, to produce a multiplicity adjusted p value (Motulsky, 2023). Similarly, the non-parametric Kruskal-Wallis test was used to determine whether the median differences in protein expression were statistically significant when samples were compared to a control. The adjusted p value was calculated using the post-hoc Dunn's Multiple Comparison Test, as described above.

Chapter 3

MCAM and its isoforms: expression, localisation and function

3.1 Introduction

MCAM has been labelled an attractive target for cancer therapy. It is neo-expressed in a number of solid tumours, including melanoma, epithelial ovarian carcinoma, and prostate, breast, and pancreatic cancer (Zhu *et al.*, 2015), where it has been shown to regulate cell motility and invasiveness (Wu *et al.*, 2001; Zabouo *et al.*, 2009), and is associated with advanced tumour stage (Aldovini *et al.*, 2006). However, the physiological relevance of this molecule, particularly in maintaining vascular homeostasis (Bardin *et al.*, 2001; Roostalu *et al.*, 2018; Yan *et al.*, 2003), has largely hindered the development of MCAM-specific therapies for clinical use in cancer treatment. Indeed, whilst a number of therapeutic anti-MCAM antibodies have been tested in melanoma (Table 1-4), their success has largely been limited to pre-clinical models (Mills *et al.*, 2002a; Nollet *et al.*, 2017; Yan *et al.*, 2003). This highlights the need to focus on developing novel therapeutic strategies that specifically target tumour expressed MCAM, thus avoiding potential deleterious effects of anti-MCAM therapies on normal tissues.

sMCAM, the product of ectodomain shedding of full-length MCAM, has been shown to have both autocrine and paracrine effects on tumour cells and endothelial cells, respectively (Stalin *et al.*, 2016), and has been identified as a possible target to overcome the limitations of other MCAM-targeted therapies. The development of an sMCAM-specific neutralising antibody has shown promise in both *in vitro* and *in vivo* models, where it inhibits proliferation of both tumour cells and tumour vascular endothelial cells, without binding to MCAM on the cell surface (Stalin *et al.*, 2016). In addition, recent data suggests that blocking sMCAM with a neutralising antibody reduces metastasis of MCAM positive melanoma and ovarian cancer cells, but not MCAM negative colon cancer cells, in a nude mouse model (Stalin *et al.*, 2020). These data indicate the importance of further investigation into understanding the mechanism and relevance of sMCAM in melanoma progression.

To date, most studies investigating sMCAM and MCAM ectodomain shedding have used vascular endothelial cells. The first study to demonstrate the generation of a soluble isoform of MCAM was performed in human vascular endothelial cells, where

sMCAM was detected in the cell culture media (Bardin *et al.*, 1998). Further research has elaborated the mechanisms involved in MCAM ectodomain shedding. In microvascular lung endothelial cells, calcium influx was shown to promote ectodomain shedding, and MMPs (more specifically, MMP3) were clearly implicated in the proteolytic cleavage of MCAM from the cell surface (Boneberg *et al.*, 2009). More recent work performed by Stalin *et al.* (Stalin *et al.*, 2016a) confirmed the role of MMPs in MCAM shedding in endothelial cells, and further indicated that MCAM undergoes sequential cleavage of the ECD and ICD, the latter of which appeared to be mediated by PS-1. Importantly, this study also highlighted the different effects that recombinant sMCAM (rsMCAM) had on MCAM-l and MCAM-sh. MCAM-sh responded to rsMCAM and was responsible for the many downstream effects of sMCAM binding, such as transcription of genes involved in cell survival and angiogenesis, while MCAM-l was not (Stalin *et al.*, 2016a). This is particularly interesting in the context of melanoma cells, which have previously been shown to preferentially express MCAM-l (Dye *et al.*, 2009).

In contrast, comparatively little is known of the cellular processes involved in MCAM cleavage in melanoma cells. It has been shown that sMCAM has pro-survival and anti-apoptotic effects on melanoma cells and can act on endothelial cells to support tumour growth and vascularisation (Stalin *et al.*, 2016). However, it is still unclear how sMCAM is generated in melanoma cells, or how its production is regulated. This creates a barrier for understanding how ectodomain shedding of MCAM may be exploited for therapeutic benefit in melanoma and other MCAM positive cancers which express MCAM-l. As such, we aimed to investigate the proteolytic processing of MCAM in melanoma cell lines, with an initial focus on demonstrating the localisation of both full-length MCAM and the cleavage products (i.e. MCAM-CTF) (Figure 3-1). The generation of cleavage fragments (sMCAM and MCAM-CTF) under stimulated and non-stimulated conditions was also investigated.

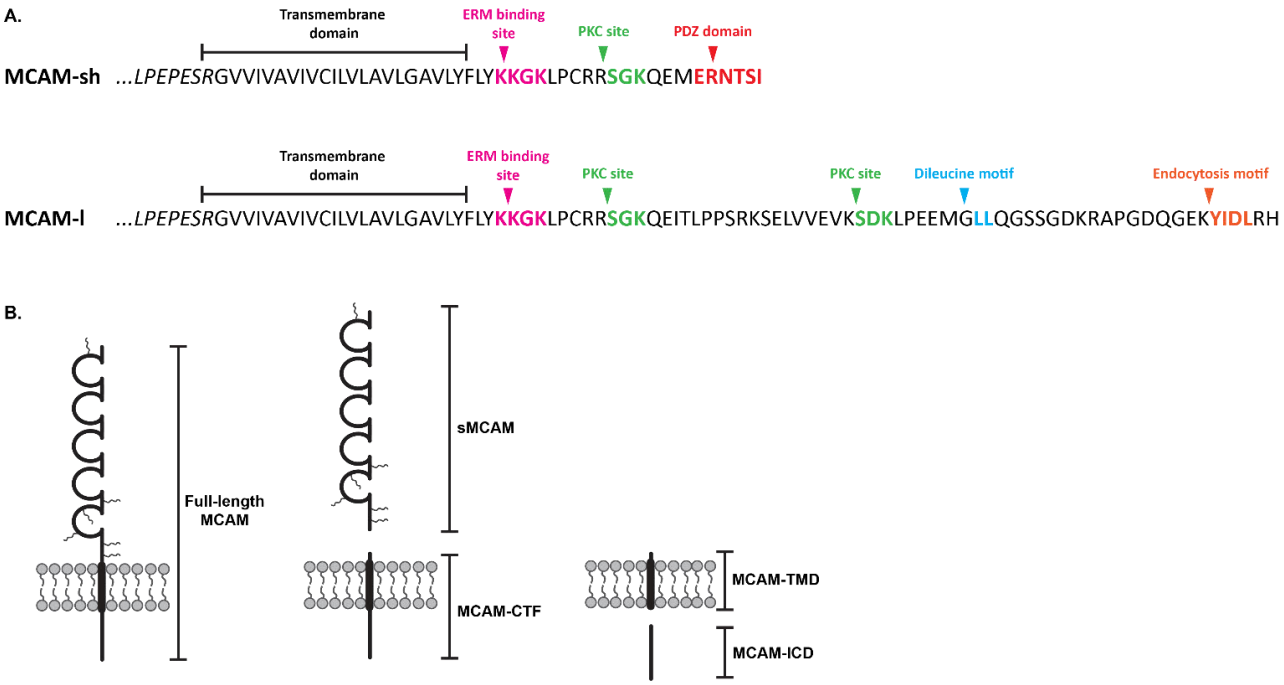

Figure 3-1 Sequence comparison of the MCAM-CTF and MCAM proteolytic processing.

The long and short isoforms of MCAM (MCAM-l and MCAM-sh) differ only within the intracellular domain (A). These differences may be involved in regulating ectodomain shedding and RiP of MCAM. The proteolytic processing of MCAM involves cleavage of the extracellular domain to generate a soluble protein (sMCAM) and C-terminal fragment (MCAM-CTF). The MCAM-CTF comprises the transmembrane domain (TMD) and cytoplasmic/intracellular domain (MCAM-ICD), which are also susceptible to proteolytic cleavage (B).

Approach: the main experimental details are provided in Chapter 2. Briefly, we began by confirming the expression of MCAM isoforms (MCAM-l and MCAM-sh) in melanoma cell lines via qPCR, comparing expression to human vascular endothelial cells (HUV-EC-Es) which are known to express both isoforms. Expression of MCAM was also shown at the protein level, using immunoblot to demonstrate the ability to distinguish between sMCAM, full-length MCAM, and MCAM-CTF in various melanoma cell lines. The main cell lines of interest were the natural MCAM expressors, A2058, MM253, and MM96L, and the SB2 cell lines transfected to overexpress WT MCAM (SB2 14.1) or mutant (MT) MCAM (tyrosine motif mutant, SB2YG 3.1.2; di-leucine motif mutant, SB2LP #5.13). Cells expressing MT MCAM were included in this study as previous data suggested MT MCAM was associated with different subcellular localisation and enhanced migration, compared to WT MCAM; and we hypothesized this may be due, in part, to differential proteolytic

cleavage. Expression was confirmed under a variety of conditions. The localisation of full-length MCAM and the MCAM-CTF was investigated using immunofluorescent staining and confocal microscopy, to identify the compartmental localisation of the MCAM-CTF. Various chemical factors, which have been well established as stimulators of ectodomain shedding, were then used in an attempt to promote/up-regulate the shedding of MCAM from the cell surface.

3.2 Materials and Methods

The main experimental details are provided in Chapter 2, with supplementary or additional information described below.

3.2.1 Cell lines

Various melanoma cell lines were used, including SB2, SB2 14.1, SB2 LP, SB2 YG, MM253, MM96L, SkMel28 and A2058. In addition, HUV-EC-Cs were used as a control for qPCR. The origin and maintenance of these cells is outlined in Table 2-2 and Section 2.2.

3.2.2 RNA extraction, cDNA synthesis and qPCR

Gene expression of MCAM-sh, MCAM-l and other splice variants (Nollet *et al.*, 2022) were compared in various cell lines using qPCR. Briefly, cell pellets were collected from sub-confluent cultures and RNA was extracted using TRI Reagent, as described. cDNA synthesis was then performed using the Tetro cDNA synthesis kit (BioLine), as per the manufacturer's instructions. qPCR reactions were set up using 2 x SensiFAST SYBR® No-ROX mix (Bioline). For more details, please refer to Section 2.1.3.

3.2.3 SDS-PAGE and immunoblot

Cells were seeded in a 24 well plate and grown to >70% confluence. Media was then removed, and cells were rinsed with PBS or SFM before adding either SFM, or media containing 2% heat-inactivated serum (HIS), 2% FBS, or 10% to the

respective wells. Cells were incubated for ~24 hours, then media and lysates were collected. Cell culture media was centrifuged to pellet any debris, first at 330 g for 5 min, followed by ~15,600 g at 4^{o}C for 15 min. Supernatants were collected and concentrated ~10-fold by SpeedVac. Cell pellets were collected by harvesting adherent cells with 2.5 mM EDTA (containing a 1/50 dilution TE for more adherent cell lines such as the SB2 cell series) and collecting detached cells in normal culture media. Cells were pelleted and washed 3x with cold-PBS and were then lysed by incubating for 30 min on ice in lysis buffer (1% NP40 in PBS with CPI). Debris was pelleted by centrifuging at ~15,600 g for 15 min at 4^{o}C and supernatants were collected.

Total protein concentration was measured by BCA, and samples were adjusted to the same concentration. Media samples were diluted in the same way as the corresponding lysate, to adjust for variability in cell number and protein content between samples. Samples were mixed with loading buffer and denatured by boiling for 5 min at 95^{o}C under non-reducing conditions, then loaded onto a 15% SDS-polyacrylamide gel. Proteins were separated by electrophoresing at 25 mAmp per gel. Separated proteins were then transferred to Methanol-activated PVDF membrane using a wet transfer system. After ~1 hour at 200 mAmp, membranes were removed and, if necessary, were air-dried at room temp to help fix the smaller proteins to the membrane. They were then rehydrated in methanol and rinsed. If total protein staining was performed, membranes were stained with Revert700, as described in section 2.7.4. Blocking was performed by incubating membranes in 5% skim milk powder in PBS/0.1% Tween-20 (PBST) either at RT for 1 hour, or O/N at 4^{o}C. To detect MCAM-ECD in the lysates and media, CC9 mAb was diluted 1/1000 in blocking solution. To detect MCAM in the cell lysates, CD146-ICD mAb was diluted 1/2500. This antibody is specific for the ICD of MCAM-l. Primary antibodies were incubated for 1 hour at RT, or O/N at 4^{o}C. Membranes were washed 3 x 5 min with PBST, then secondary antibodies (anti-mouse or anti-rabbit HRP, Dako, each at 1/2000) were prepared and incubated for 1 hour at RT. Unbound antibody was removed by washing membranes with PBST, as described above. This was followed by 3 x 3 min washes with PBS only. Membranes were then developed and imaged

with chemiluminescence. Further information on the antibodies used in this thesis are shown in Table 2-4, Table 2-5, and Table 2-6.

3.2.4 Immunofluorescence staining and confocal microscopy

Cells were seeded onto collagen-coated, etched glass coverslips in a 24-well plate, and were grown to 100% confluence. A scratch wound was then performed. Briefly, two parallel scratches were made in the monolayer using a P1000 pipette tip. Each well was gently rinsed with warm SFM to remove debris, then normal culture media was returned to each well and cells were incubated at 37ºC with 5% CO_2 for ~24 hours, allowing cells to migrate into the wound. Prior to fixing, wells were rinsed with warm HBS (37ºC) to remove traces of serum proteins. Warm 4% PFA was added, and cells were fixed for 15 min in the dark. PFA was then removed, and wells were rinsed thrice with HBS, followed by the addition of 0.1% TX-100 for 3-5 min to permeabilise the cells. After washing 3 times with HBS, blocking solution (1% BSA, 10% goat serum in HBS) was added and left O/N at 4ºC. The following day, cells were stained with the necessary primary and secondary antibodies (Table 2-4, Table 2-5, and Table 2-6), as described. After staining was complete, nuclei were labelled with DAPI, and then coverslips were mounted onto glass slides using VectaSield (Vectorlabs). Once set, clear nail varnish was used to seal the edges, and samples were stored at 4ºC until imaging was performed. Coverslips were gently cleaned with 70% EtOH prior to imaging on the Nikon confocal microscope, using the 60X water immersion objective (unless otherwise stated).

3.2.5 Treating cells with chemical stimulants

For further information regarding the reagents described below, please refer to Section 2.5.

PMA

Melanoma cells were grown to ~70% confluence and treated with PMA under serum-free conditions. Prior to treating with PMA, monolayers were rinsed with SFM to remove any trace of serum proteins, then cells were serum-starved for 2 hours at

37ºC. A working stock of PMA was prepared to 2 µg/mL, then serial dilutions were performed, giving a range of concentrations (0-200 ng/mL) for treatment. DMSO was used as the vehicle control. Cells were incubated at 37ºC with 5% CO_2 for ~2 hours. Cell morphology of treated cells was compared to vehicle control-treated cells to confirm an activated phenotype, then both media and whole cell lysates were collected for immunoblot analysis. Alternatively, for determining effects of PMA on focal adhesion formation and the cell cytoskeleton, or for analysing the effects on MCAM-CTF distribution, cells were grown on fibronectin- or collagen-coated coverslips, respectively. Cells were treated with 0-100 ng/mL PMA O/N (~16 hours), before fixing and permeabilising for IF analysis.

Ionomycin

Cells were grown to 70% confluence, then treated with ionomycin under serum-free/low serum conditions. A 1 mM stock solution was serially diluted and used at concentrations ranging from 0-4 µM, and cells were incubated in the presence of ionomycin (or vehicle control) for 2-16 hours. Samples were then collected for I.F. analysis of immunoblot, as described.

Cyclohexamide

Cyclohexamide (CHX) is an inhibitor of protein translation elongation (Schneider-Poetsch *et al.*, 2010), and was used to explore MCAM protein synthesis in SB2 14.1 cells. The concentration and duration of treatment is very dependent on the protein of interest and the cell type; therefore, a range of concentrations were tested, and whole cell lysates were collected at varying time points in order to gauge the optimal treatment conditions for inhibiting protein synthesis.

Cells were seeded on TC plastic and grown to 70% confluence. Prior to treatment, media was removed, and monolayers rinsed with PBS to remove and remnants of FBS. Cells were serum-starved by incubating in SFM for 2 hours prior to treatment. A 5,000 µg/mL working solution of CHX was prepared in 70% EtOH, then serially diluted in culture media. Concentrations ranging from 25-200 µg/mL were tested, and

70% EtOH was diluted (1/1250) and used as a vehicle control. Cells were incubated in the presence of CHX for 2-24 hours, with cell lysates being collected at 2, 4, 6 and 24-hour time-points. A BCA assay was performed to measure total protein concentrations and immunoblot was performed to confirm inhibition of MCAM synthesis.

3.2.6 Nuclear extraction

SB2 14.1 cells were grown to ~80-90% confluence and then harvested using 2.5 mM EDTA and 1/50 TE. Detached cells were collected in ice-cold PBS and pelleted. An additional wash in PBS was performed, and cells were counted. The total number of cells was determined, and cells were resuspended in hypotonic buffer at 1 x 10^7 cells/mL. The suspension was incubated for 15 min on ice, before adding 2% NP40. Tubes were vortexed for 10 s, then homogenate was centrifuged at 860 g for 10 min, at 4^{o}C. The supernatant containing cytoplasmic proteins was collected, whilst the pelleted material was resuspended in Cell Extraction Buffer, supplemented with 1 mM phenylmethylsulfonyl fluoride (PMSF) and 1x CPI prior to use. The suspension was incubated for 30 min on ice, vortexing rapidly every 10 min. Debris was pelleted by centrifuging at ~15,600 g for 15 min, at 4^{o}C. The supernatant containing nuclear proteins was collected in a clean tube. Samples were stored at -20^{o}C (short-term) or -80^{o}C (long-term), until needed. Samples were subject to analysis via immunoblot, as described.

3.3 Results

Ectodomain shedding of MCAM in endothelial cells is relatively well characterised, and studies have confirmed that it is predominantly the short isoform of MCAM that is implicated in the autocrine and paracrine effects of sMCAM in these cells. Meanwhile, MCAM-l appears to have a less potent role in enhancing the survival and angiogenic properties of endothelial cells in response to sMCAM (Stalin *et al.*, 2016a). Interestingly, it has been shown that melanoma cells express mainly the long isoform of MCAM, with negligible amounts of MCAM-sh detected (Dye *et al.*, 2009). The significance of this in the context of ectodomain shedding remains unclear. As expression of each membrane-bound MCAM isoform has not yet been

quantitatively analysed in melanoma cells, we first aimed to measure the expression of MCAM-sh and MCAM-l in a number of melanoma cell lines, relative to a human umbilical vein vascular endothelial cell line (HUV-EC-C).

3.3.1 MCAM-sh and MCAM-l expression in melanoma cells

Using this approach, we confirmed the expression of both isoforms of MCAM in HUV-EC-Cs, consistent with previous literature (Kebir *et al.*, 2010). As these data were generated using different primer pairs (using a common F primer, different R primers) we cannot directly compare the levels of *MCAM-l* and *MCAM-sh* in HUV-EC-C. However, efficiency assays indicate the *MCAM-l* and *MCAM-sh* amplification reactions had similar efficiencies (103% vs. 101%; see Appendix E); and the raw Cq values suggest that MCAM-sh was expressed at slightly higher levels compared to MCAM-l in sub-confluent HUV-EC-Cs. The expression of *MCAM-sh* and *MCAM-l* in melanoma cells was then compared to these amplicons in HUV-EC-Cs (Figure 3-2A).

Overall, *MCAM-l* was expressed at similar levels in melanoma cell lines compared to HUV-EC-C. A2058, MM96L and SkMel28 showed a slightly higher expression while MM253 a lower expression (~2/3 fold, ~0.5 fold, respectively). The MCAM negative/low cells lines, SB2 and Colo239F had very low levels of *MCAM-l* transcripts (0.02-fold compared to HUV-EC-C). The difference between the level of *MCAM-l* in HUV-EC-Cs vs Colo239F reached statistical significance ($p<0.05$) according to a non-parametric Kruskal-Wallis test with Dunn's multiple comparisons correction. SB2 14.1 (which was modified to express MCAM-l) showed similar *MCAM-l* expression levels to HUV-EC-Cs. All melanoma cell lines showed low levels of *MCAM-sh*, with the highest expressers (A2058, MM96L and SkMel28) showing ~0.1/0.15-fold expression compared to HUV-EC-C. SB2, SB2 14.1 and Colo239F expressed negligible levels of *MCAM-sh*, with the Colo238F cells expressing significantly less *MCAM-sh* ($p<0.05$; Figure 3-2B).

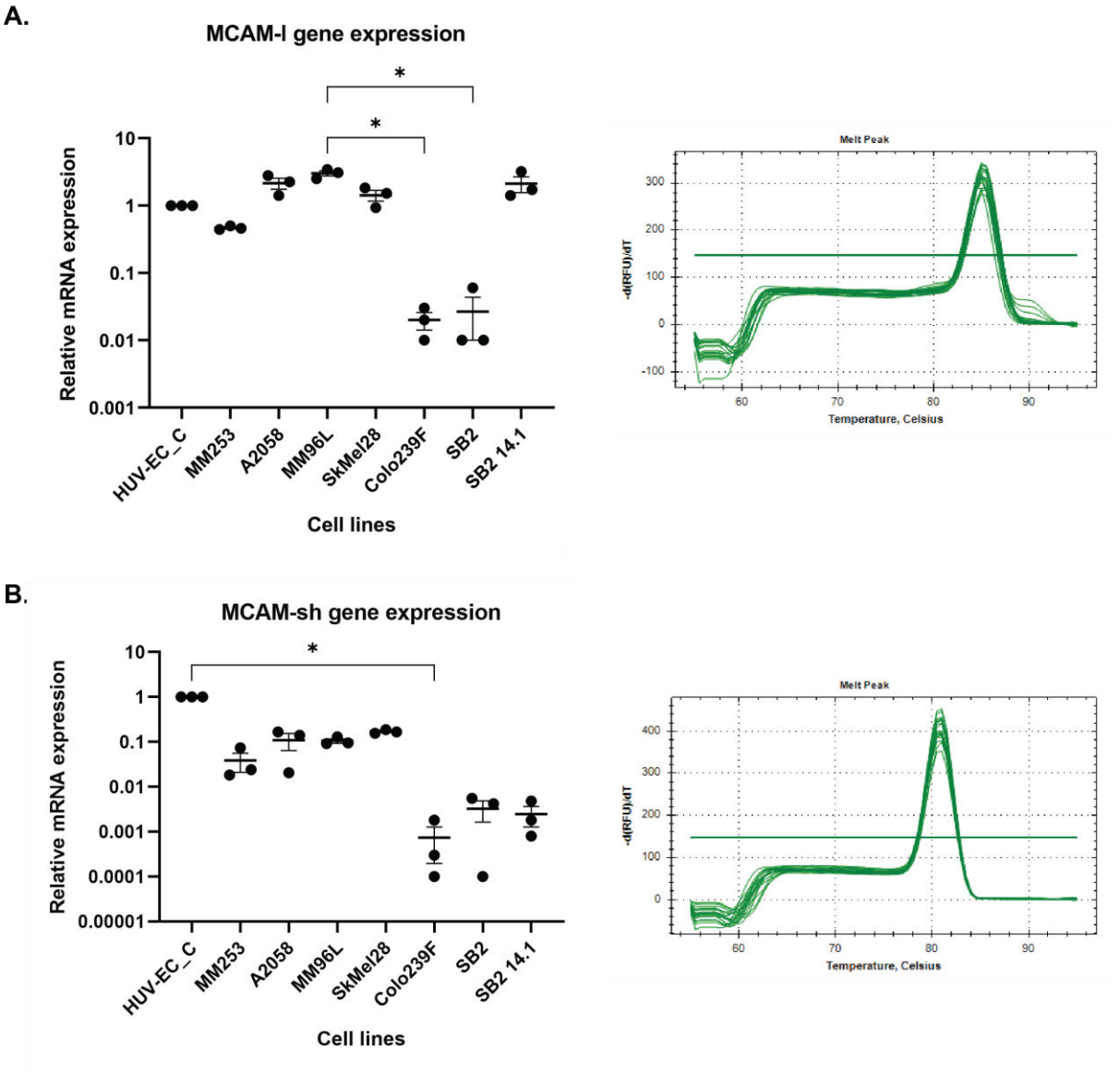

Figure 3-2 *MCAM-l* and *MCAM-s* expression in melanoma cells.

MCAM-l (A) and *MCAM-sh* (B) were amplified in HUV-EC-C and melanoma cells and fold changes calculated using the 2 (-ΔΔCT) method, using the reference genes CASC3 and RPS2, and HUV-EC-C as the reference cell line for each amplicon (n=3, mean and SEM are shown). The melt curve associated with each amplicon is shown on the right and indicates the presence of a single amplification product. MCAM-expressing melanoma cells showed similar expression of *MCAM-l* compared to HUV-EC-C, but reduced *MCAM-sh* expression, although this was not statistically significant. Low expression of *MCAM-l* and *MCAM-sh* was confirmed in melanoma cells described as MCAM negative. Colo239F and SB2 cells showed significantly less *MCAM-l* expression compared to MM96L cells (*p<0.05) and Colo239F cells also had significantly less *MCAM-sh* expression compared to HUV-EC-C (*p<0.05)

Nollet *et al.* (2022) recently reported two novel MCAM splice variants (I10-sMCAM and I5-13 sMCAM) which encode the ECD for MCAM only and would be expected to produce sMCAM. Using the oligo sequences provided in the publication, we also

explored the presence of these transcripts in HUV-EC-C and melanoma cells. We were unable to quantify I5-13 sMCAM, as amplicons were present in very few samples and Cq values were all > 40 cycles. Low levels of I10-sMCAM were detectable in HUV-EC-Cs and some melanoma cell lines. However, all Cq values were >35 cycles, approximately 10 cycles after the MCAM-l amplicon was quantifiable (Figure 3-3). Statistical analyses using a non-parametric Kruskal-Wallis test with Dunn's multiple comparisons correction found no significant difference in expression of I10-sMCAM between any of the cell lines tested.

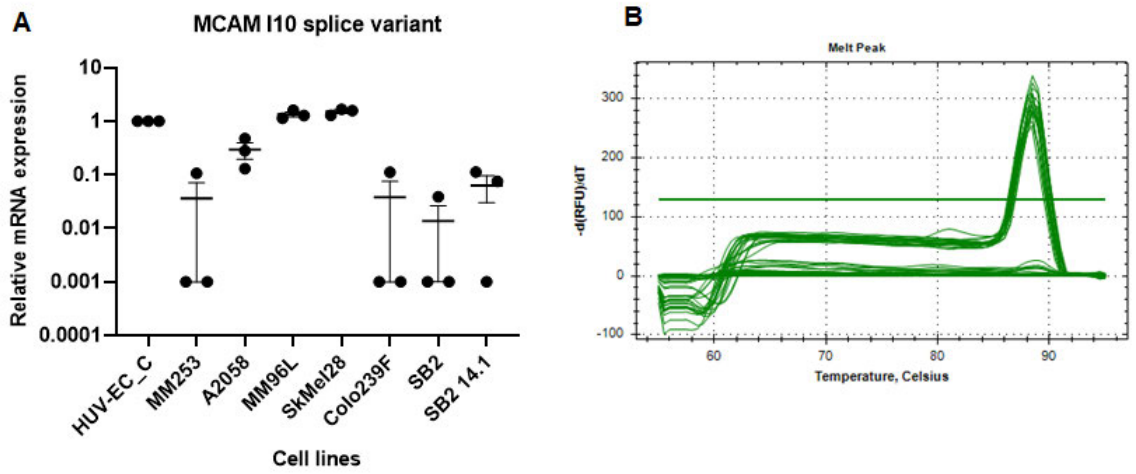

Figure 3-3 MCAM ECD splice variants in melanoma cells

I10-sMCAM was amplified in HUV-EC-C and melanoma cells and fold changes calculated using the 2 (-ΔΔ*CT)* method, using the reference genes *CASC3* and *RPS2*, and HUV-EC-C as the reference cell line for each amplicon (mean and SEM are shown) (A). Melt curve analysis confirms the presence of a single amplification product for *I10-sMCAM*, in those samples that did amplify (B). Samples that did not amplify show a flat amplification curve and were assigned a Cq of 45 (equating to 0.001 relative expression) for the purposes of graphing relative mRNA expression. However, statistical analyses found no significant difference in expression of I10-sMCAM between any of the cell lines.

3.3.2 MCAM ectodomain shedding under basal conditions

Immunoblot analysis was next used to confirm the expression of MCAM at the protein level. An antibody directed against the MCAM-ECD (CC9 mAb) was used to detect full-length MCAM and sMCAM, while an antibody directed against the ICD (MCAM-CTF mAb) detected both full-length MCAM and the MCAM-CTF (Figure 3-4A). Shedding of MCAM from melanoma cell lines was tested under a variety of conditions over a period of 24 hours, including in the absence of serum (SFM), in the

presence of 2% or 10% FBS, and in the presence of 10% heat-inactivated serum (10% HIS). Interestingly, cells cultured in 2% FBS showed the greatest levels of MCAM ectodomain shedding, as demonstrated by the increased amount of sMCAM in concentrated cell culture media (Figure 3-4B). This was consistent in the SB2 cell lines expressing MCAM-l (both WT and MT protein) but inconclusive in the A2058 cells, which have a lower baseline expression of MCAM compared to the stably transfected SB2 cell lines. Similarly, MM96L and MM253 cells expressed lower levels of MCAM at the protein and mRNA level and thus, were not included in this initial screen.

The levels of full-length MCAM, MCAM-CTF and sMCAM were measured at the protein level by immunoblot. Antibodies directed against either the ECD or CTF were used to distinguish between these three forms of MCAM (Figure 3-4A). During initial studies, the cleavage of MCAM by cells cultured in either SFM, or in the presence of 2% FBS, 10% FBS, or 10% HIS was investigated. Consistently, cells cultured in the presence of 2% FBS maintained the highest amount of sMCAM in the culture media, relative to the other conditions tested (Appendix F). Consequently, 2% FBS was used for further experiments to verify MCAM shedding/cleavage in a larger panel of melanoma cell lines (Figure 3-4B). sMCAM signal was quantified and graphed. As there is no standard factor to normalise expression, data represents the absolute sMCAM signal. Full-length MCAM and MCAM-CTF were normalised based on Revert700 total protein signal and graphed. A non-parametric Kruskal-Wallis test was used to compare MCAM positive cells to MCAM-negative SB2 melanoma cell lines. Only SB2 14.1 and MM253 cells released significantly more sMCAM ($p<0.05$). A small amount of sMCAM was released by MM96L and A2058 cells.

The levels of full-length MCAM and MCAM-CTF did not correlate with the amount of sMCAM in the media, such that increased sMCAM was not associated with significant increases in MCAM-CTF or decreases in full-length protein. For example, MM96L and A2058 appeared to produce low amounts of sMCAM, although full length MCAM and MCAM-CTF were readily detected in cell lysates of these cell lines. The amount of full-length MCAM and MCAM-CTF was significantly higher in

A2058 and SB2 14,1 cells compared to the MCAM-negative SB2 cells ($p<0.05$). While Western blot analyses may not be sensitive enough to detect subtle changes in protein levels, it does allow for a reliable distinction between sMCAM, full-length MCAM, and the MCAM-CTF only (Figure 3-4C), whereas other techniques, such as enzyme-linked immunosorbent assay (ELISA), do not.

The MCAM-CTF may be further cleaved at the transmembrane domain, producing a small ~7 kDa fragment representing the MCAM-ICD, which we hypothesised may be detectable in samples separated on a Tris-Tricine gel. Tris-Tricine gels have superior resolution of proteins < 30 kDa compared to Tris-Glycine (Schägger & von Jagow, 1987). However, there was no evidence of a cleaved MCAM-ICD within melanoma cell lysates (Appendix G).

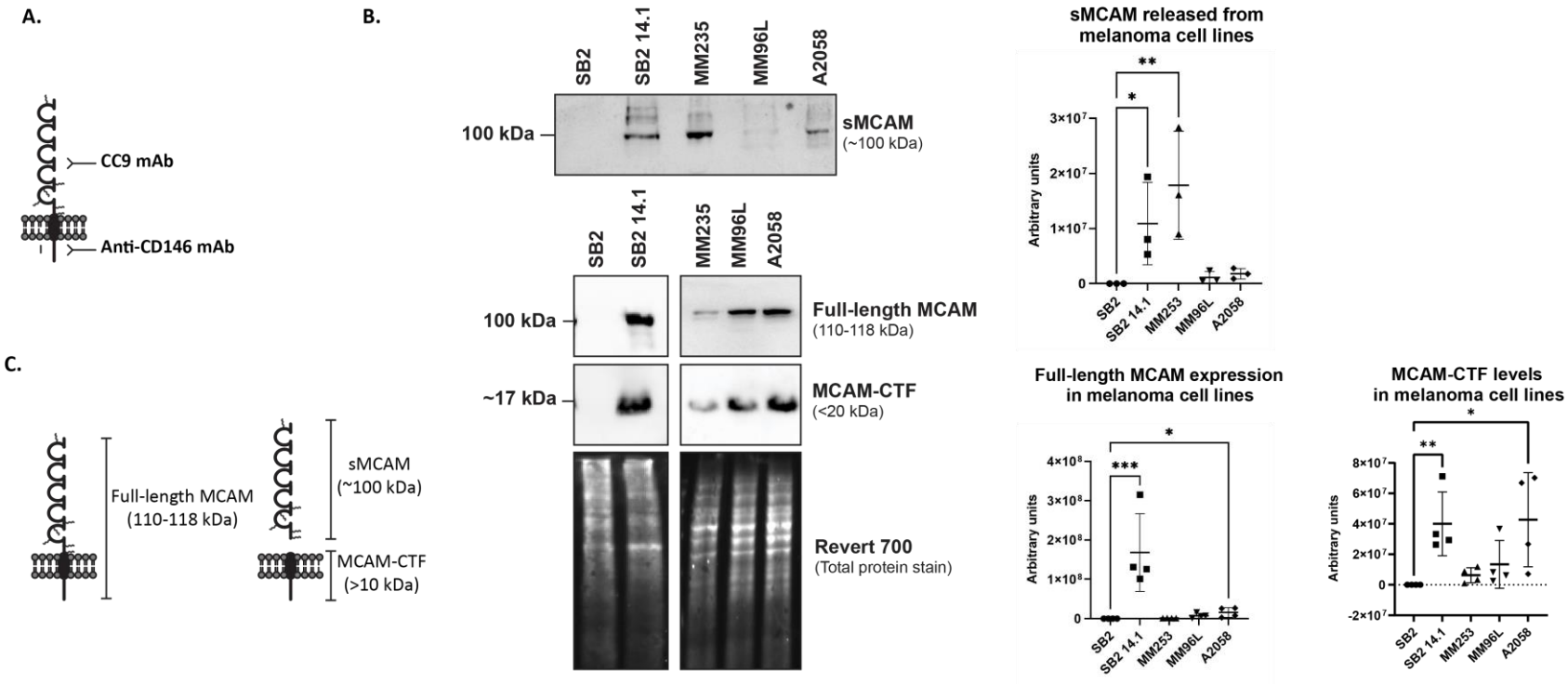

Figure 3-4 MCAM shedding detected in melanoma cell lysates and media.

The soluble ectodomain of MCAM was detected in cell culture media using an antibody directed against the extracellular domain, while full-length MCAM and the cleaved intracellular tail were measured using an antibody that recognises the intracellular tail of MCAM (A). Four melanoma cell lines known to express MCAM were assayed with SB2 cells (MCAM negative) used as a negative control. sMCAM was clearly detected in SFM harvested from SB2 14.1 and MM253 melanoma cells, at a significantly higher level compared to SB2 cells (*p<0.05, **p<0.01). A lessor amount of sMCAM was identified in SFM from MM96L and A2058 cells (not statistically significant) (B). Full-length MCAM was present in lysates of all MCAM-expressing cell lines (~110 kDa), along with a smaller fragment corresponding to the C-terminal fragment (CTF) of MCAM-l (~10-12 kDa). Both SB2 14.1 and A2058 expressed significantly higher levels of FL and MCAM-CTF (*p<0.05, **p<0.01), ***p<0.001) (B). The part of the protein that each detected fragment corresponds to is outlined (C). The western blots represent a single experiment, whilst the quantification represents n=3 independent experiments for sMCAM and n=4 for full length MCAM and MCAM-CTF. The mean and SD are shown.

3.3.3 Localisation of full-length MCAM and the MCAM-CTF under basal conditions

Immunofluorescent labelling was then used to investigate the localisation of both full-length MCAM and the MCAM-CTF in melanoma cells undergoing 2D migration over a collagen matrix. Directional migration was achieved using a wound-healing assay. This approach was chosen as previous data in the laboratory indicates cells in routine culture display variable polarity and random cell movement. By encouraging directional migration, we aimed to reduce variability in the assay.

In migrating cells, full-length MCAM was found predominantly at the cell periphery, with a polarised distribution towards the leading edge (Figure 3-5).This was seen with both the MCAM-CTF mAb (green) and CC9 mAb (red), and co-localisation was confirmed in an overlaid/merged image (yellow/orange). Our lab has previously confirmed the expression of full-length MCAM on the cell surface using flow cytometry (not shown), thus MCAM localised at the cell periphery likely represents MCAM expressed on the cell surface. The MCAM-CTF mAb also detected a pool of MCAM-l CTF only. This was located in the juxtanuclear region of migrating SB2 14.1 and SB2 LP cells. Interestingly, this intracellular staining pattern was less obvious in SB2 YG cells, which express MCAM with a mutation in the tyrosine motif. Rather, MCAM-CTF staining in these cells was primarily restricted to the cell surface, with minimal perinuclear staining, which could indicate that the CTF in SB2 YG may be processed in a different manner (Figure 3-5A).

In the MM96L and A2058 melanoma cell lines MCAM had a similar expression pattern, whereby full-length MCAM localised at the plasma membrane, with a small amount of staining in the perinuclear region of some cells, corresponding to the MCAM-CTF (Figure 3-5B). This is consistent with immunoblot data, which demonstrated a minimal amount of MCAM-CTF in the whole cell lysates collected from these cell lines. Interestingly, MM253 melanoma cells displayed a different staining pattern of the MCAM-CTF, with evidence of this fragment localising to the nucleus/nuclear membrane. Taken together, this suggests that the processing of the MCAM-CTF may be regulated in a cell-specific manner. Further, overexpression of

MCAM in the MCAM-negative SB2 melanoma cells may interfere with the rate at which the CTF is processed after ectodomain shedding. This phenomenon may be advantageous for understanding how and where MCAM-CTF processing occurs.

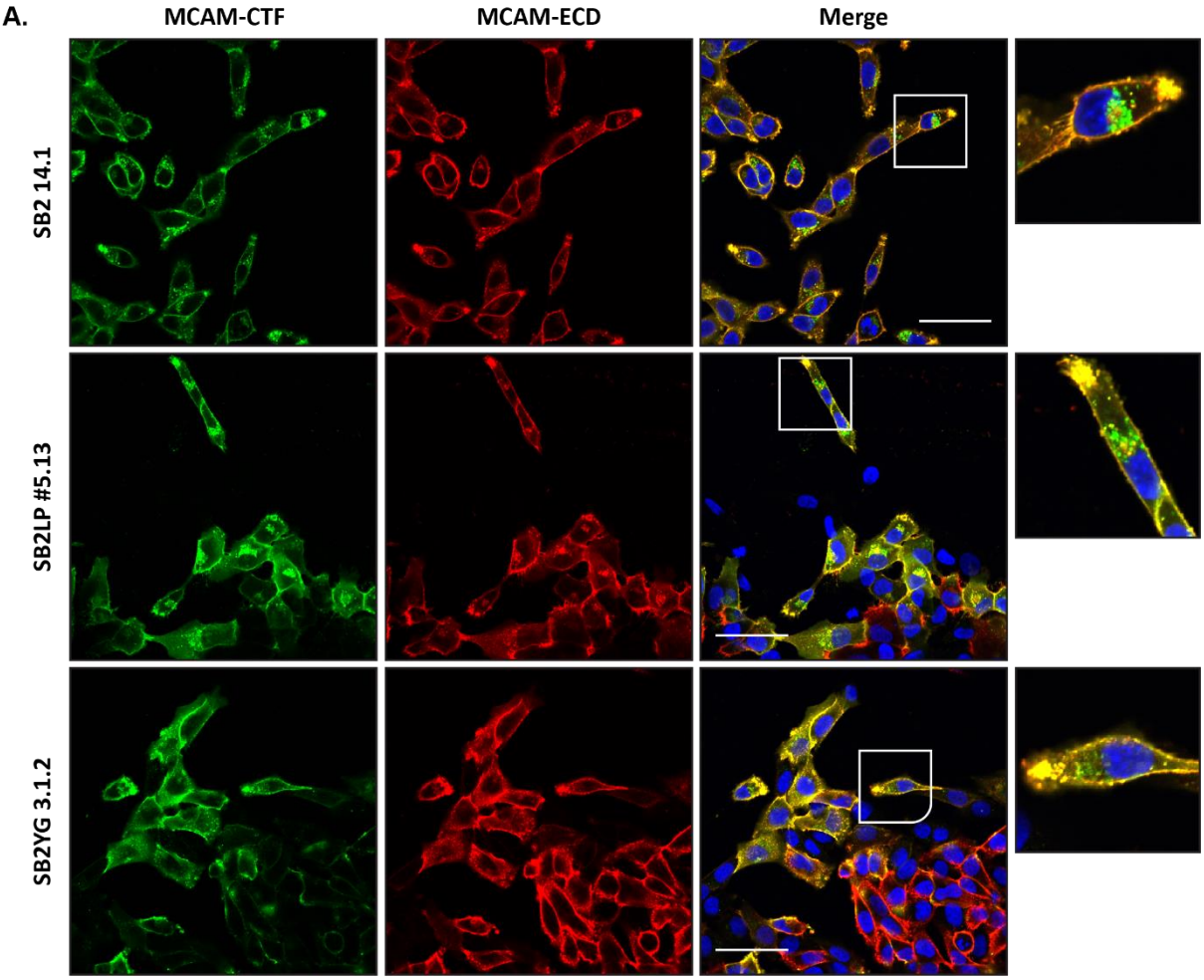

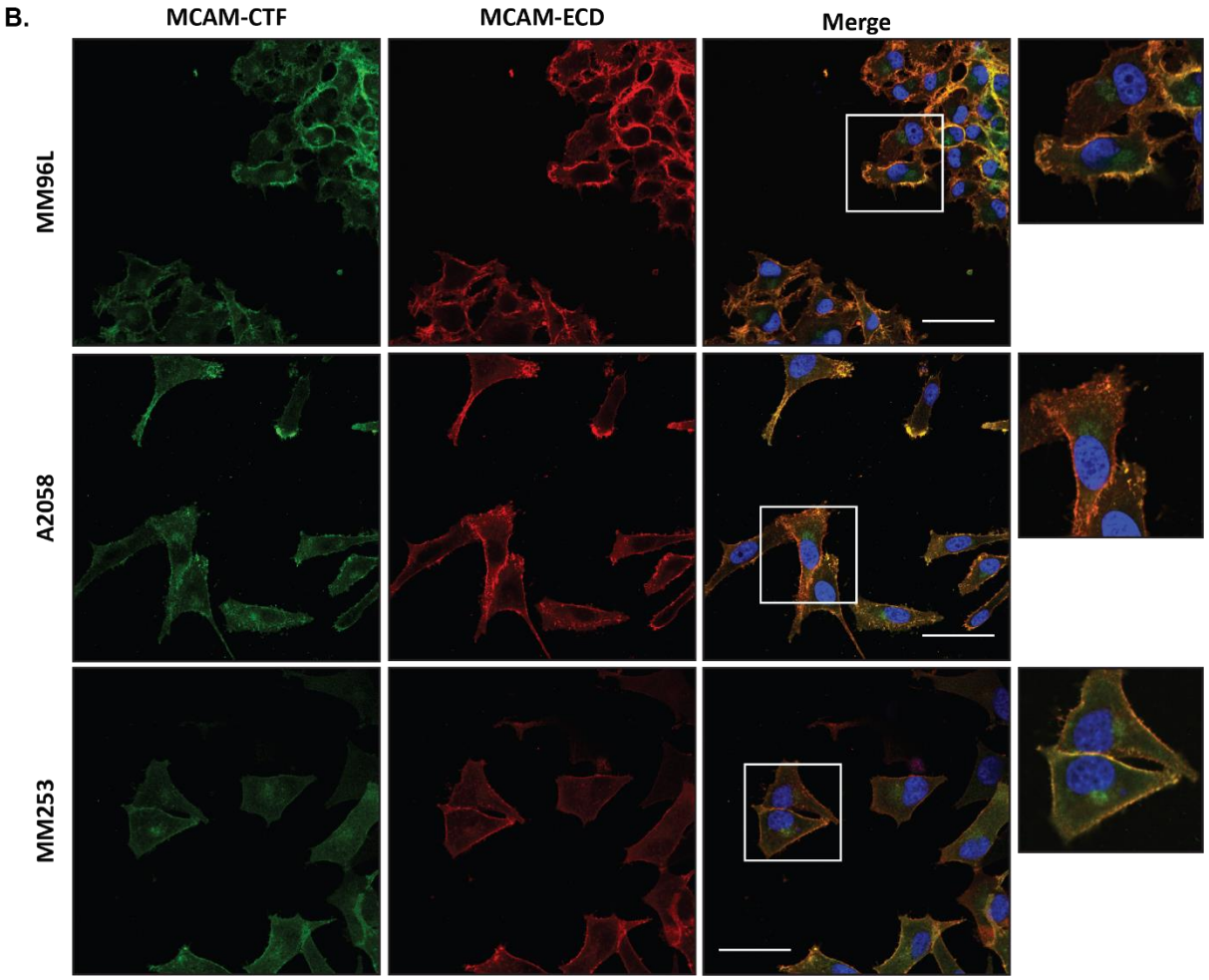

Figure 3-5 An antibody against the ICD of MCAM detects full-length protein at the cell surface, and a perinuclear CTF.

Melanoma cells migrating over a 2D collagen matrix were immunostained for MCAM, using one antibody against the extracellular domain of MCAM (CC9 mAb; red), and a second anti-MCAM antibody that recognises the intracellular domain of MCAM-I (MCAM-CTF mAb; green) (n=2). All cell lines showed a similar staining pattern for full-length, membrane-bound MCAM (yellow/orange, due to the overlap of CC9 and MCAM-CTF antibody staining). The MCAM-CTF mAb also detected a perinuclear pool of protein that did not stain positive with the CC9 mAb, indicating the presence of cleaved MCAM in a perinuclear location. This was visible in both (A) (B) transfected melanoma cells (SB2 cell series) and (B) native MCAM-expressing melanoma cells (MM96L, A2058 MM253). Scale bars in merged image are 50 µm. Boxed areas in merged images are shown at higher magnification in the inserted images on the right (n=2).

To further investigate the cell compartment in which the MCAM-CTF was located, cells were co-stained with markers for the Golgi complex, the endoplasmic reticulum (ER), or the lysosomal/late endosomal (Lyso/LE) compartments. All experiments were performed on migrating cells following a scratch wound assay. Firstly, Golgin97 was used to investigate the localisation of MCAM-CTF in relation to the Golgi

membrane. Typically, Golgin97 showed concentrated staining within the juxtanuclear region, however there was no co-localisation with the MCAM-CTF (Figure 3-6A), suggesting that the CTF may be contained within another intracellular compartment.

In line with this, other reports suggest that the MCAM-CTF could be located within the ER (Witze *et al.*, 2013). To investigate this, cells were co-stained with calnexin, a chaperone protein found in the membrane of the ER. Calnexin staining revealed ER networks throughout the cell, with strong perinuclear staining, however, the MCAM-CTF did not show specific localisation to the ER (Figure 3-6B). Of note in this experiment, however, was the differences in calnexin staining between each cell line. Whilst all melanoma cells tested here showed strong staining for calnexin around the nucleus, MM253 cells had the least intense staining pattern overall, with the most concentrated staining around the nucleus, and punctate staining throughout the cytoplasm. Interestingly, SB2 14.1 cells appeared most similar to the MM253 cells. In contrast, the other cell lines- including SB2LP and SB2YG, typically displayed an abundance of calnexin-positive ER networks throughout the cytoplasm.

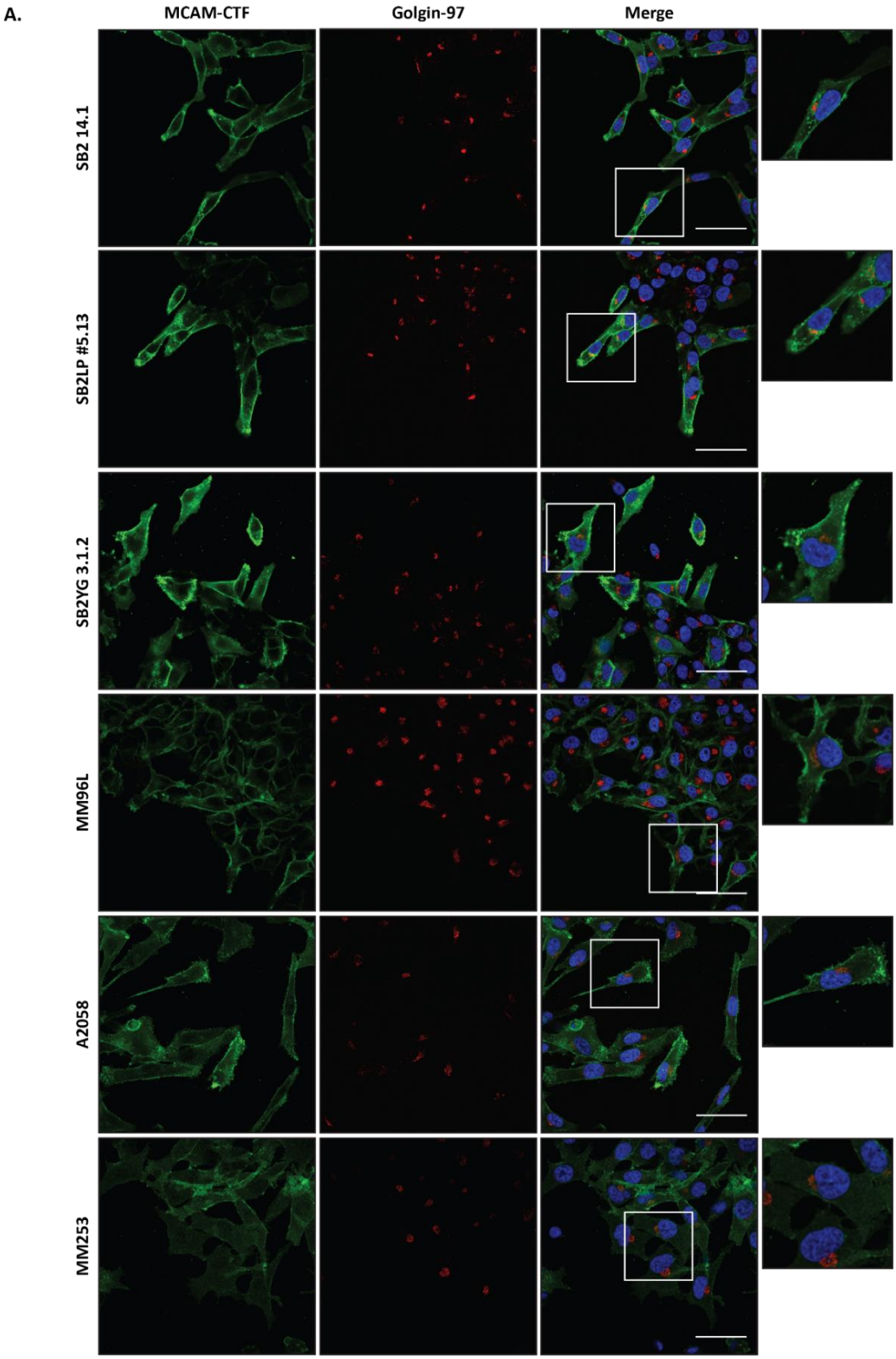
A.
MCAM-CTF
Golgin-97
Merge
SB2 14.1
SB2LP #5.13
SB2YG 3.1.2
MM96L
A2058
MM253

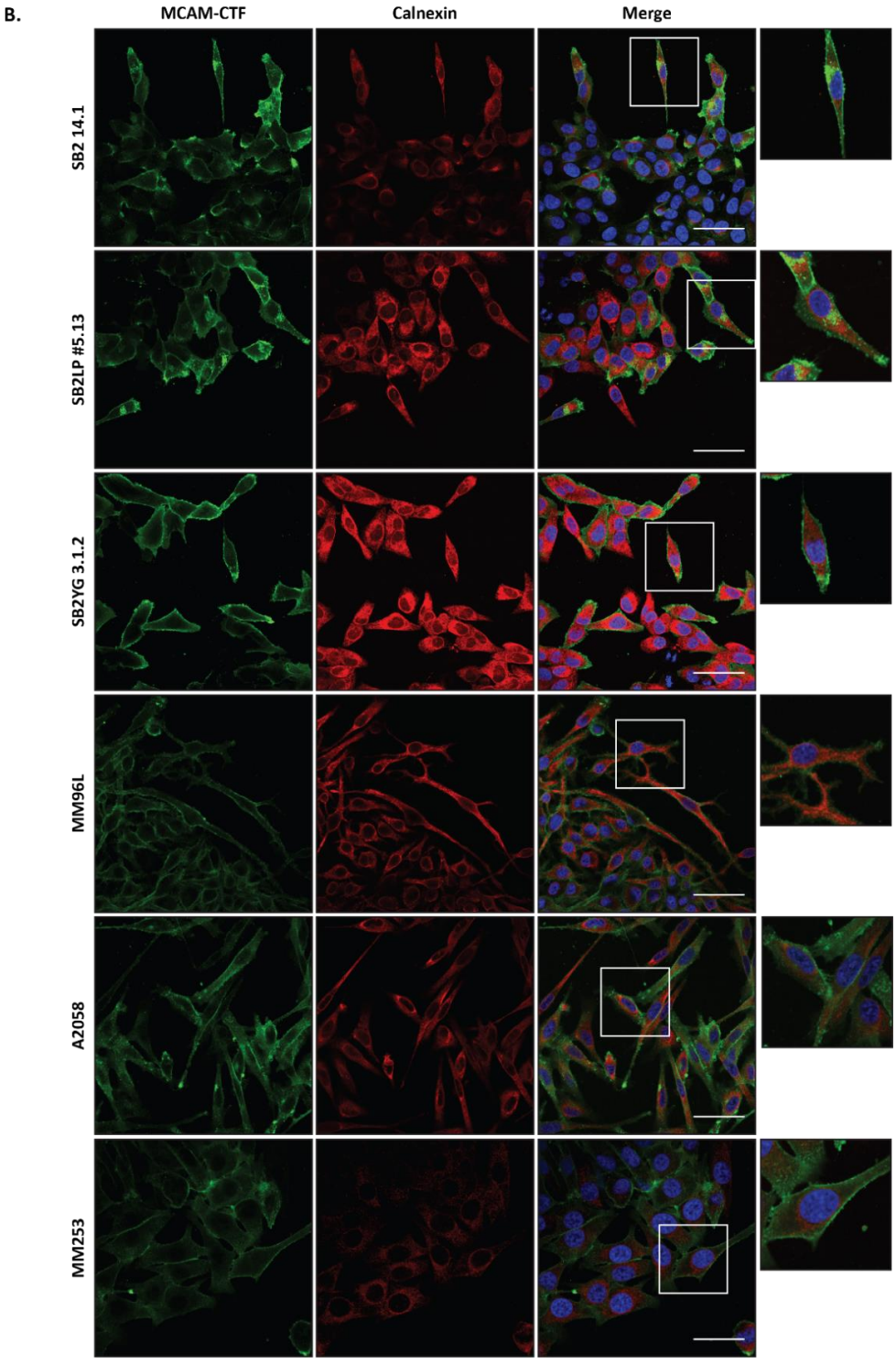

Figure 3-6 MCAM-CTF does not localise with the Golgi or ER.

Co-localisation between the MCAM-CTF and the Golgi apparatus (A) or ER (B) was investigated in migrating cells (n=3). There was little evidence of the MCAM-CTF localising with Golgin97 in SB2 14.1, SB2 YG or A2058 cells. Some co-localisation was apparent in SB2 LP cells. Similarly, there was little overlap between the MCAM-CTF and Calnexin, consistent with the fragment being a product of ectodomain shedding, rather than protein synthesis. Scale bars in merged image are 50 µm. Boxed areas in merged images are shown at higher magnification in the inserted images on the right.

The localisation of the MCAM-CTF in a compartment other than the Golgi or ER suggests that the fragment is not generated during protein synthesis. To support this hypothesis, cells were treated with CHX to inhibit protein synthesis, however preliminary experiments suggested that MCAM has a long half-life (>24 hours), and cells did not survive long enough to measurably deplete MCAM protein levels (data not shown).

Further investigation revealed that the MCAM-CTF fragment co-localised with LAMP2, a marker of the late endosome/lysosome (Figure 3-7). LAMP2-positive structures were distributed throughout the cytoplasm but were concentrated within the juxtanuclear region. There was clear co-localisation between LAMP2 and the juxtanuclear pool of MCAM-CTF in SB2 14.1 and SB2 LP#5.13 cells, however as mentioned above, the SB2YG 3.1.2 cells lack the clear intracellular pool of MCAM-CTF in the majority of cells, and therefore did not show co-localisation with LAMP2 (Figure 3-7A). In the native MCAM-expressing cell lines, the MCAM-CTF also co-localised with LAMP2 in the juxtanuclear region, however it was noted that co-localisation was less prominent in the MM253 cell line (Figure 3-7B).

Collectively, findings thus far suggest that: 1) MCAM is constitutively cleaved from the cell surface, and 2) the remnant fragment (MCAM-CTF) is internalised and often localises to late endosomes and/or lysosomes.

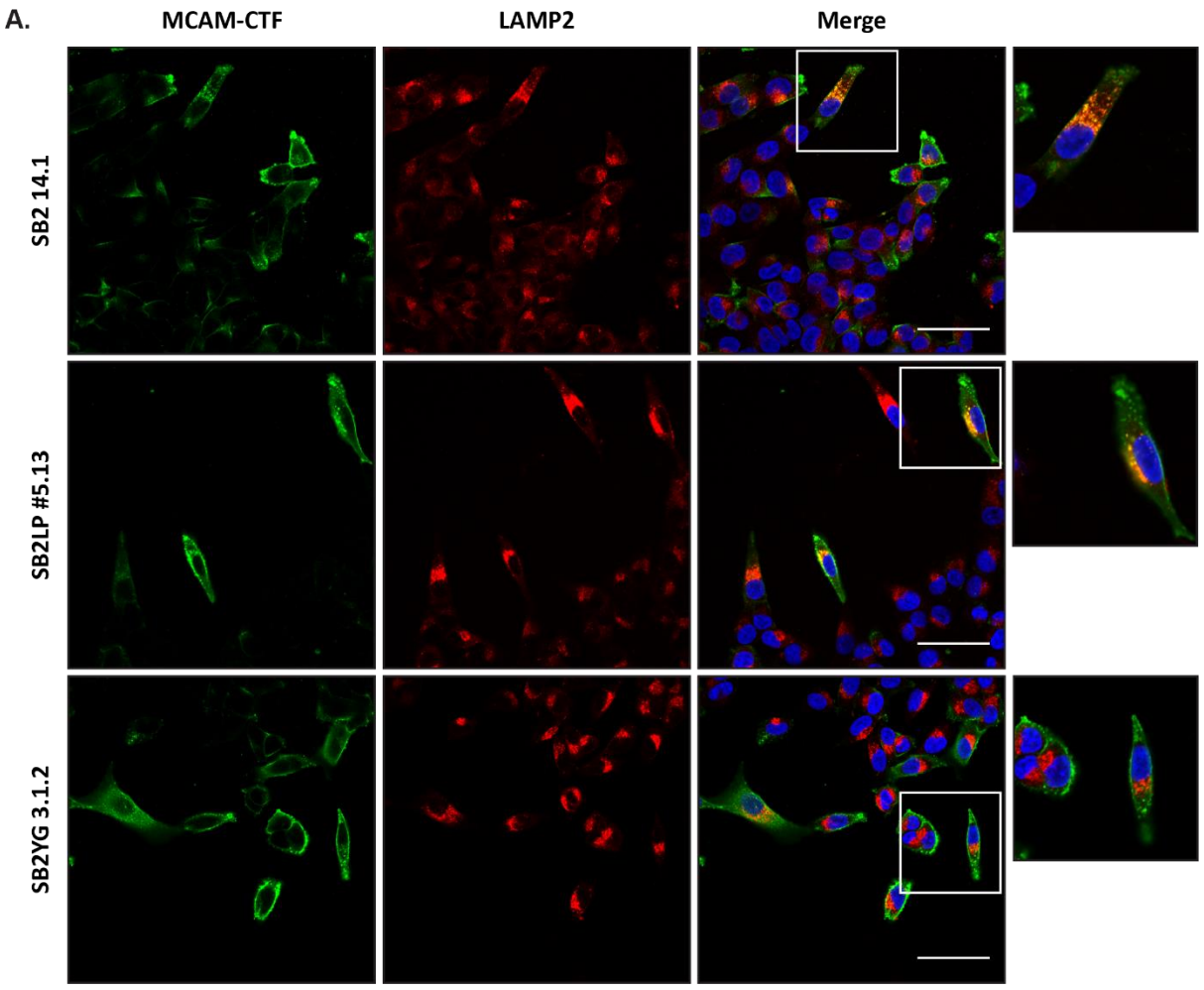
A.
MCAM-CTF
LAMP2
Merge
SB2 14.1
SB2LP #5.13
SB2YG 3.1.2

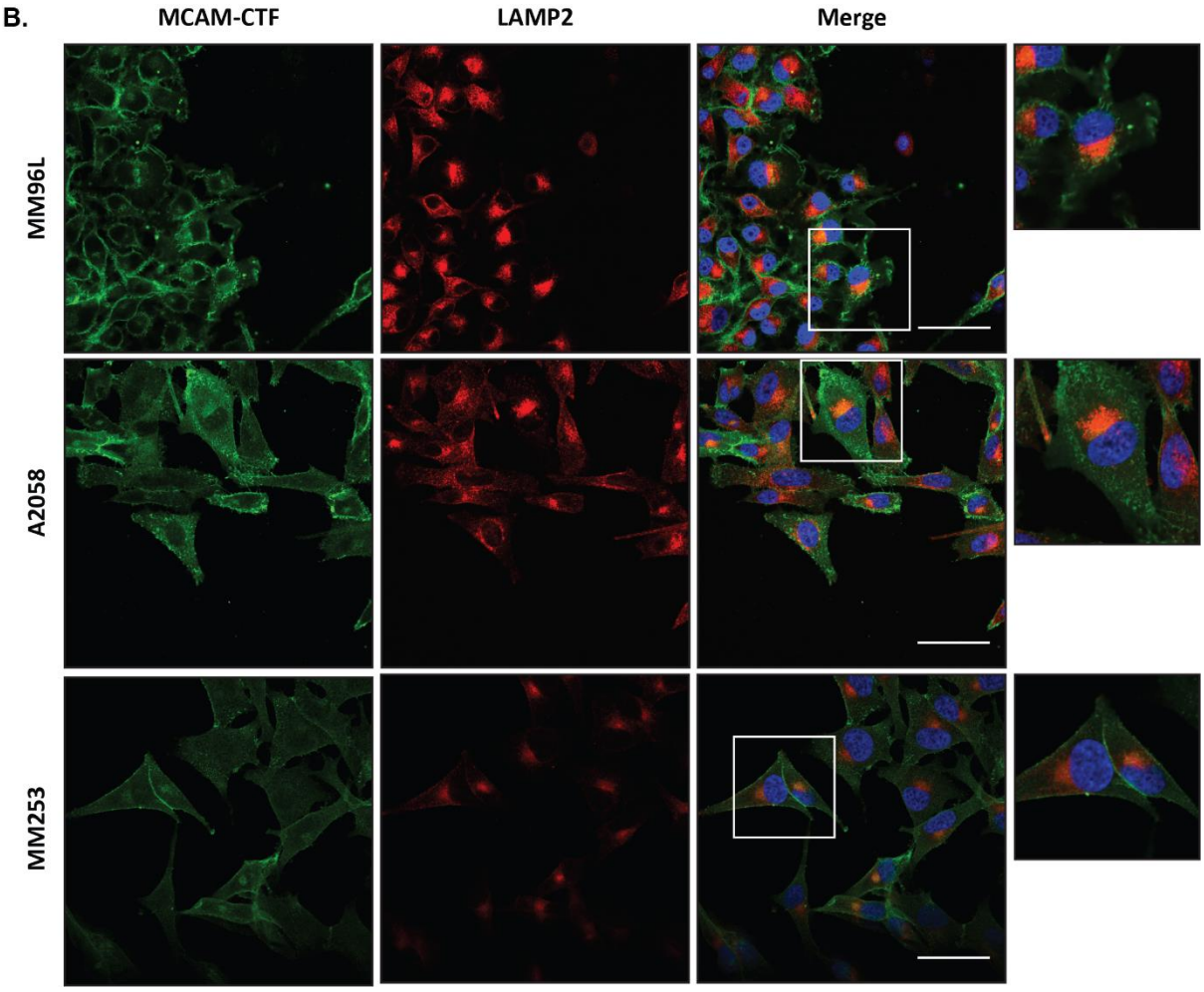

Figure 3-7 Co-localisation between MCAM-CTF and late endosome/lysosomes in the juxtanuclear region of migrating melanoma cells.

Migrating melanoma cells were labelled with antibodies directed against LAMP2 and the MCAM-CTF, in order to determine whether the MCAM-CTF may be targeted to these organelles following ectodomain shedding (n=3). There was a considerable amount of overlap in the staining for each of the target proteins, which was consistent between MCAM-overexpressing SB2 cell lines (excluding the SB2 YG) (A), and the native MCAM-expressing melanoma cell lines (excluding MM253 cells) (B). Scale bars in merged image are 50 µm. Boxed areas in merged images are shown at higher magnification in the inserted images on the right.

3.3.4 Nuclear localisation of MCAM-CTF in melanoma cells

Previously, the ICD of MCAM-sh has been shown to localise in the perinuclear region of endothelial cells and can undergo rapid translocation to the nucleus following stimulation with recombinant sCD146 (Stalin *et al.*, 2016a). To address the possibility that the CTF of MCAM-l may undergo further processing to generate an ICD fragment that can translocate to the nucleus, where it could act as a transcriptional regulator, nuclear extraction was performed on SB2 14.1 whole cell

lysates. These cells were chosen because they reliably produce detectable amounts of MCAM-CTF and they express only MCAM-l, because they are a transfected cell line.

In our hands, the selected nuclear extraction protocol was unsuccessful in separating nuclear and cytoplasmic proteins, evident from the presence of β-tubulin in the nuclear extract (Figure 3-8A). Due to limited access to alternative methods for nuclear extraction, this procedure was not pursued further. Alternatively, immunofluorescent staining was utilised to investigate the potential nuclear localisation of the MCAM-CTF/ICD, which consistently demonstrated that the MCAM-CTF/ICD was not present within the nucleus of these cells under non-stimulated conditions.

3.3.5 Localisation of full length MCAM and the MCAM-CTF following stimulation

To determine whether stimulation of cells affected MCAM localisation or could induce nuclear translocation of the MCAM-CTF/MCAM-ICD, SB2 14.1 cells were grown to ~70% confluence on collagen-coated coverslips and treated O/N with either ionomycin or PMA, then immunofluorescently labelled for MCAM. Overall, there was no evidence of nuclear translocation following stimulation. Cells treated with ionomycin showed more punctate staining, however the MCAM-CTF was still predominantly located in the juxtanuclear region (Figure 3-8B). Similarly, cells treated with PMA showed morphological changes consistent with cell activation, but MCAM remained strongly localised to the cell membrane and the juxtanuclear region.

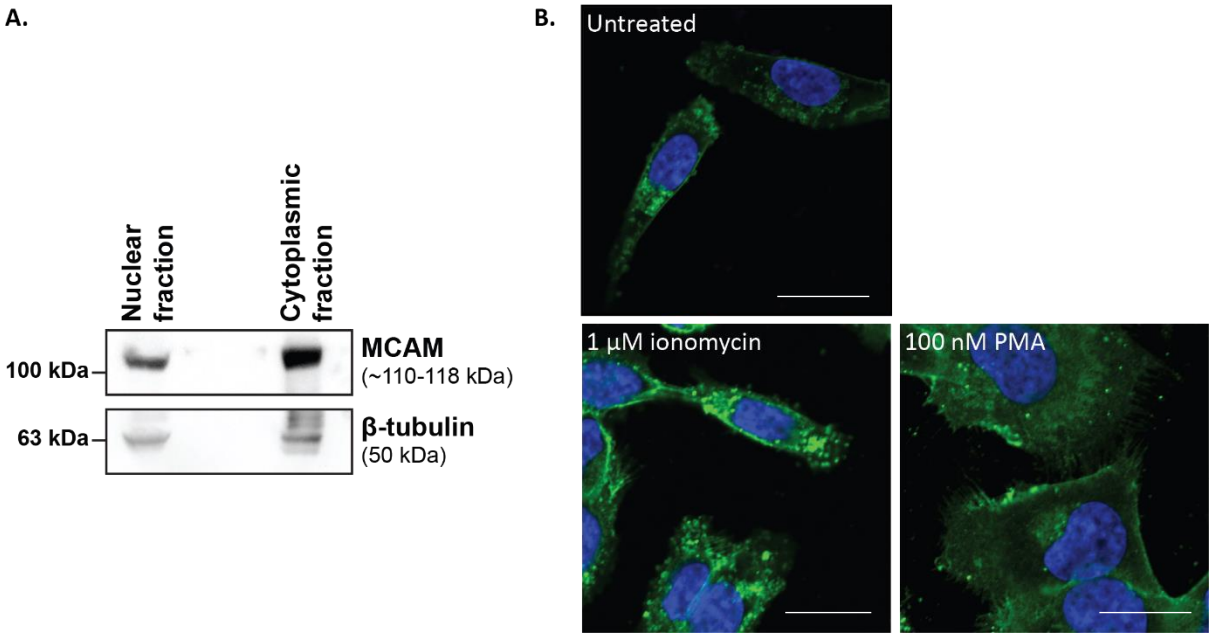

Figure 3-8 Nuclear translocation of the MCAM-CTF was not detected in SB2 14.1 melanoma cells.

A nuclear extraction protocol from ThermoFisher Scientific was optimised for use in SB214.1 cells, with the aim to separate nuclear and cytoplasmic fractions of MCAM-expressing melanoma cells. Full-length MCAM was consistently detected in the nuclear extract, along with β-tubulin. This indicates that this method was not effective in removing cytoplasmic proteins from the non-cytoplasmic fractions (n=2) (A). Immunofluorescent imaging showed perinuclear localisation of the MCAM-CTF. Cells were treated with non-toxic doses of either ionomycin or PMA for 16 hours at 37ºC, then stained for MCAM. The distribution of the MCAM-CTF appeared to become more punctate in cells treated with ionomycin; and cell shape changed following PMA treatment (lower images); compared to untreated cells (upper image). However, the MCAM-CTF was not detected in the nucleus under any conditions (n=3) (B). Scale bars are 25 µm.

3.3.6 MCAM ectodomain shedding following stimulation

We hypothesised that stimulating shedding of MCAM would allow us to further investigate its regulation; and whether ectodomain shedding contributes to the intracellular accumulation of MCAM-CTF. Previous studies have shown that phorbol esters (e.g. PMA) can be used to stimulate PKC-dependent ectodomain shedding, while calcium ionophores (e.g. ionomycin) are used to increase intracellular Ca^{2+} (Dedkova *et al.*, 2000), and are associated with ectodomain shedding of other cell surface proteins. Here, we tested increasing concentrations of both ionomycin and PMA for their ability to induce MCAM shedding in melanoma cell lines.

Short-term treatment of cells with low concentrations of ionomycin (e.g. 3.5 μM) did not induce ectodomain shedding of MCAM in SB2 14.1 melanoma cells. Whilst there were detectable levels of MCAM in the cell culture media harvested from the cells treated with higher concentrations of ionomycin (e.g. 4 μM), the molecular weight of the protein was not consistent with sMCAM. Furthermore, the level of full-length MCAM in the whole cell lysate was reduced, and β-tubulin was absent in the corresponding lysates samples. In addition, the melanoma cells began to detach from the plastic and displayed nuclear shrinkage (Figure 3-9A). Together, this is suggestive of cell death and indicates that the MCAM detected in the media is likely full-length MCAM released by dead/dying cells, rather than by ectodomain cleavage. To explore whether the sensitivity to ionomycin was specific to the SB2 14.1 cell line, A2058 and MM96L melanoma cells were also treated with the same conditions. Here, 4 μM ionomycin also appeared to be toxic to these cells (data not shown) and this line of enquiry was not pursued.

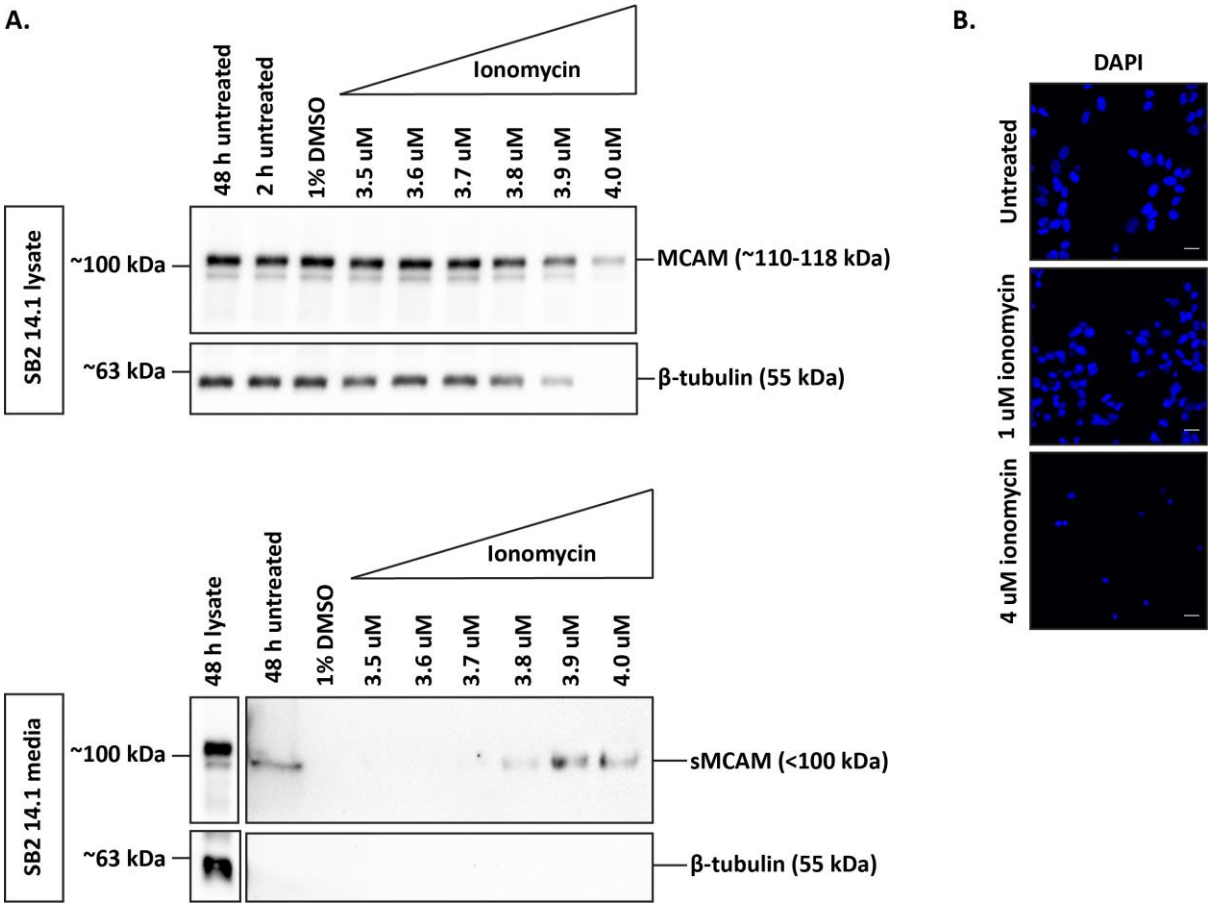

Figure 3-9 High concentrations of ionomycin were toxic to cells.

MCAM ectodomain shedding in response to ionomycin was tested in SB2 14.1 melanoma cells. Cells were treated with ionomycin for two hours, with concentrations ranging from 0-4 µM (n=2) Lysates and concentrated media were run on a Western blot. There was a reduction in the amount of full-length MCAM in the lysates, along with a loss of β-tubulin expression. This corresponded with an increase in MCAM in the media. This is suggestive of apoptosis (A). DAPI staining of cells treated with ionomycin also indicated that cells are undergoing apoptosis after short-term exposure (1 hour). The nuclei were condensed, particularly in cells treated with 4µM ionomycin, which is a hallmark feature of cells undergoing apoptosis (B). Scale bars in images are 50 µm.

In contrast, melanoma cells treated with PMA displayed morphological changes consistent with activation, including the acquisition of a spindle-like morphology in A2058 and MM253 cells. In SB2 14.1 cells, morphological changes included rounding of the cell body and shortening of cell projections (Figure 3-10), which likely coincides with activation of PKC (Vääräniemi *et al.*, 1997). Such changes were first noticeable within 30 min of treating melanoma cells with 50 and 100 ng/mL PMA, and were still evident up to 16 hours later, indicating the long-lasting effects of PMA on these cells.

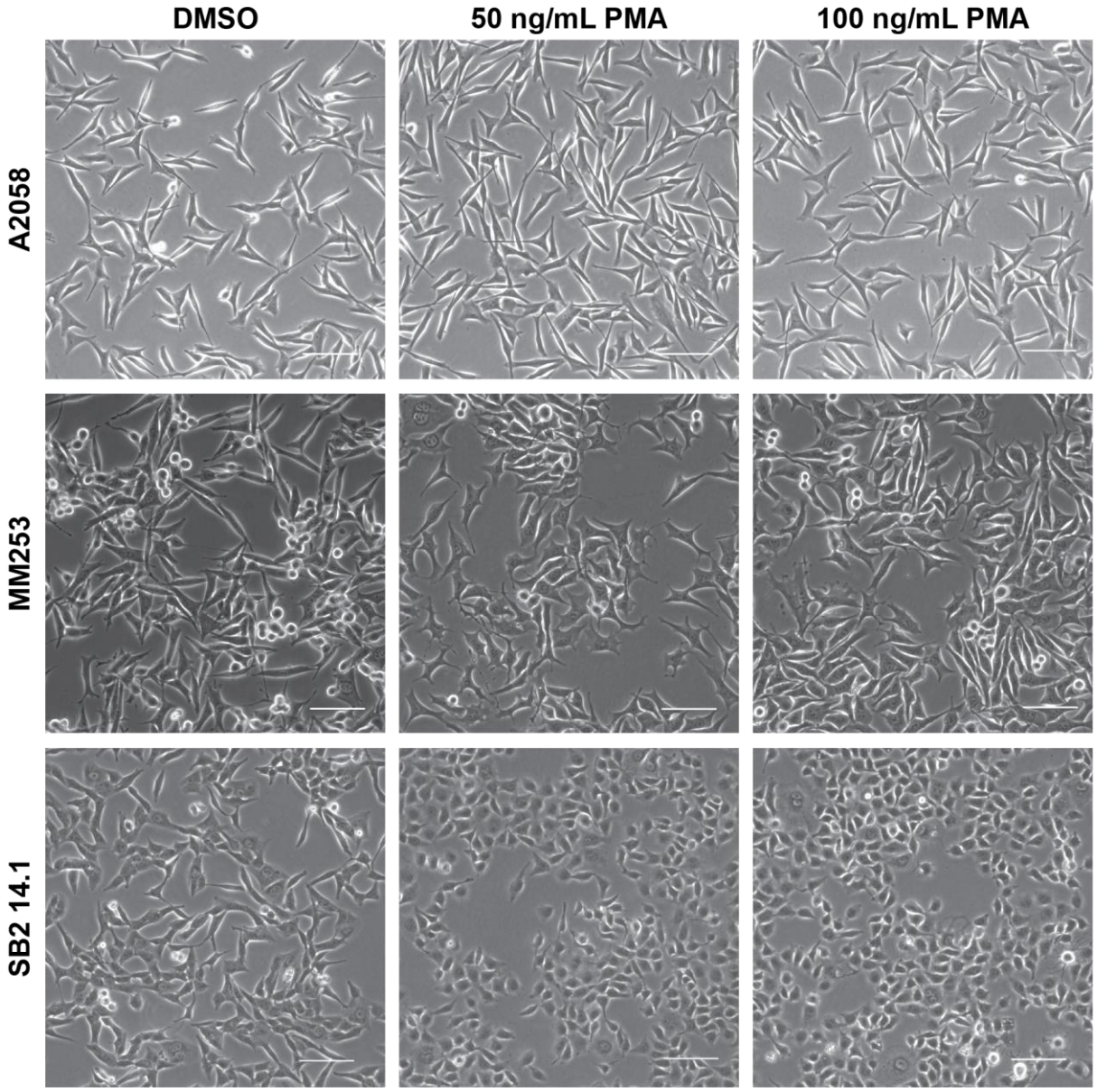

Figure 3-10 PMA-treated cell morphology indicative of activated phenotype.

Melanoma cells were grown to sub-confluence on tissue culture plastic. After serum-starving for 2-hours, cells were treated with DMSO or PMA under SF-conditions for 2 hours, then imaged (n=3). Changes in cell morphology were observed in MM253 and SB2 14.1 melanoma cells, where treated cells appeared to have a lower cytoplasm:nuclear ratio and rounding of the cell body. In contrast, A2058 cells maintained a similar physical appearance, with no apparent differences between DMSO vs. PMA-treated cell morphology. Scale bars in images are 100 µm.

Immunofluorescent labelling of cells with the MCAM-CTF-specific antibody demonstrated the effects of PMA treatment on MCAM-CTF expression/localisation. In A2058 cells (Figure 3-11i), the effects of PMA of the localisation of MCAM-CTF were minimal. Although the localisation of MCAM at the cell surface may have been

reduced in PMA-treated cells, there did not appear to be a corresponding increase in intracellular MCAM-CTF. In contrast, the effects of PMA on the localisation of MCAM-CTF in MM253 (Figure 3-11ii) and SB2 14.1 (Figure 3-11iii) were clearer, with a distinct increase in perinuclear MCAM-CTF compared to DMSO-treated cells. Interestingly, localisation at the cell surface did not appear to be affected.

To determine whether PMA-induced activation of melanoma cells coincided with increased sMCAM production and increased intracellular MCAM-CTF, media and whole cell lysates were collected from melanoma cells that had been serum-starved and then treated with 0-100 ng/mL PMA (under SF conditions) for ~2 hours. There was no sMCAM detected in concentrated cell culture media after short-term exposure to PMA, but there was a slight increase in the amount of MCAM-CTF in the lysate (data not shown).

Since I.F data was collected on cells that were stimulated with PMA for ~16 hours, a longer treatment period was then tested. However, there was still no sMCAM detected in the cell culture media after 16 hours (data not shown), despite a trend towards an increase in the amount of MCAM-CTF (relative to total protein, measured by Revert700) in PMA-treated cells compared to DMSO-treated cells (Figure 3-12). In particular, cells treated with 50 μM PMA showed accumulation of MCAM-CTF, but interestingly this decreased in cells treated with 100 μM PMA. In MM253 cells, the relative amount of MCAM-CTF was even slightly lower in cells treated with 100 μM PMA compared to untreated cells. Despite the inability to detect changes in sMCAM in the media, this data indicates that ectodomain shedding may still be occurring, as measured by the MCAM-CTF cleavage product.

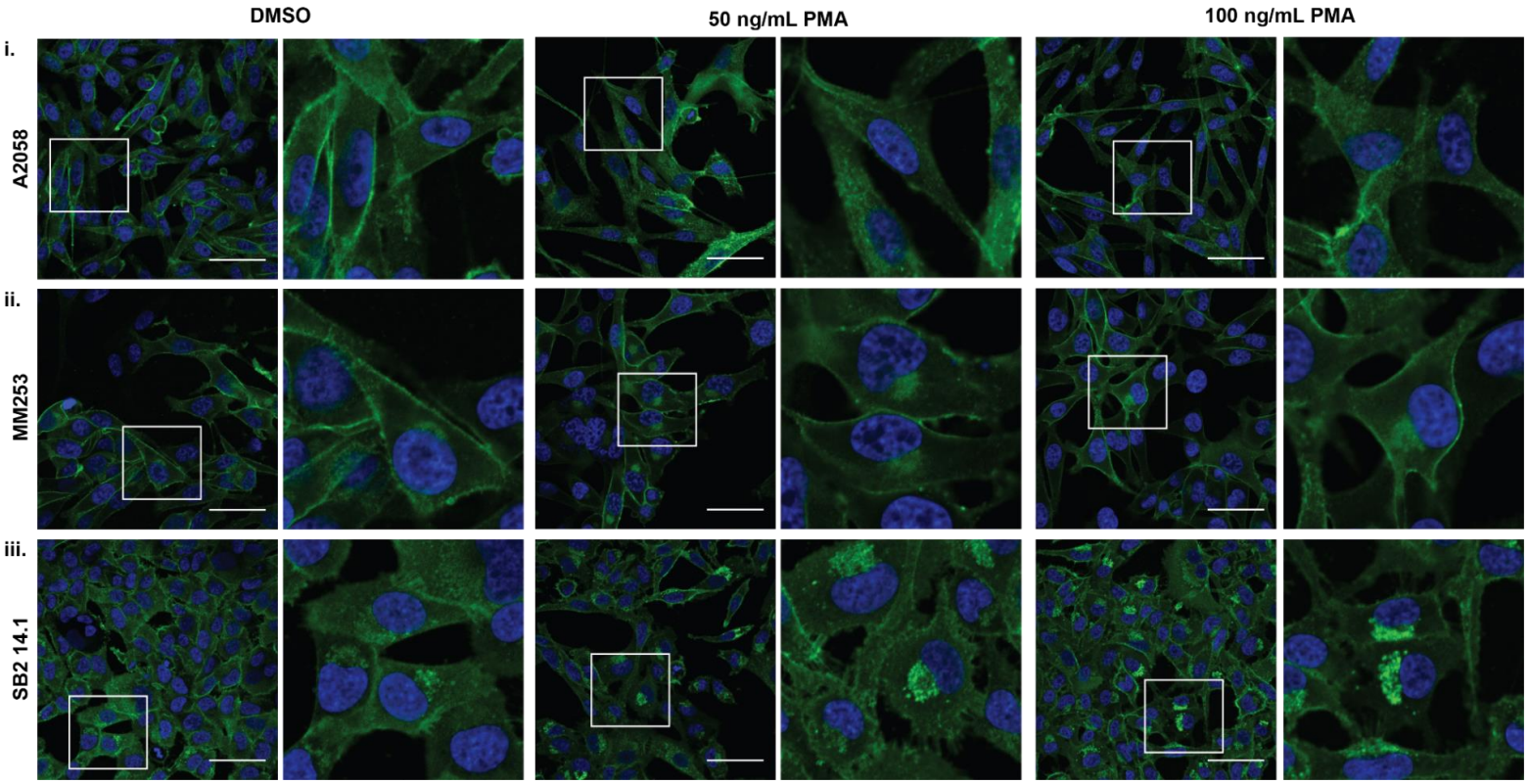

Figure 3-11 Localisation of the MCAM-CTF altered in PMA-treated melanoma cells.

Melanoma cells were grown on collagen-coated coverslips for two days, before treating with 50 ng/mL PMA or DMSO overnight for 16 hours (in SFM). Cells were fixed and labelled for the MCAM-CTF using I.F staining techniques (n=4), then visualised using confocal microscopy (60x objective magnification). In A2058 melanoma cells (i), intracellular MCAM-CTF appeared to be more punctate in PMA-treated cells, while in DMSO-treated cells, there was more prominent staining at the cell surface. MM253 cells (ii) appeared to have an increased accumulation of intracellular MCMA-CTF in PMA-treated cells, which localised in the perinuclear region. Changes in the amount/localisation of MCAM-CTF in PMA-treated SB2 14.1 cells (iii) were less subtle, with a clear increase in MCAM-CTF in the perinuclear region of PMA-treated cells compared to DMSO-treated cells. Scale bars in images are 50 µm. Boxed areas in are shown at higher magnification on the right of each image.

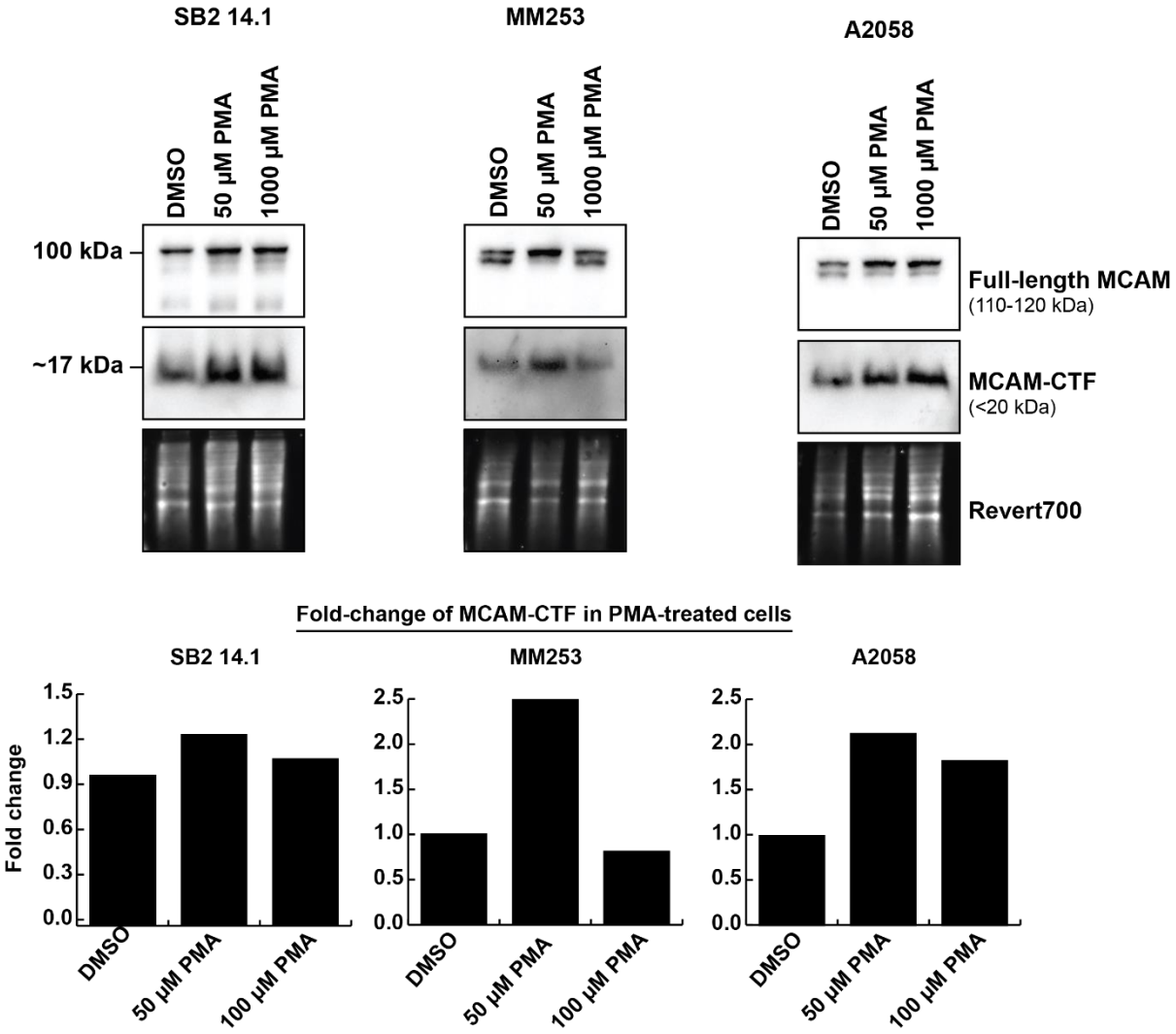

Figure 3-12 PMA treatment may stimulate cleavage of MCAM in melanoma cells

Cells were treated with DMSO (vehicle) or PMA for ~16 hours under serum-free conditions (n=2). The amount of full-length MCAM and MCAM-CTF in whole cell lysates was measured by immunoblot. Consistently, treatment with 50 µM PMA resulted in an increase in MCAM-CTF levels compared to both DMSO only and 100 µM PMA.

3.4 Discussion

sMCAM is generated by endothelial cells and tumour cells, and interacts with the transmembrane protein, angiomotin, to mediate a number of downstream signalling processes, including activation of pathways that promote cell survival, resistance to apoptosis, and angiogenesis (Stalin *et al.*, 2013; Stalin *et al.*, 2016). To date, most publications assessing the release of sMCAM *in vitro* have used ELISA to provide evidence for MCAM shedding. Whilst this method is appropriate for accurate

quantification of soluble protein levels, it is inherently flawed by its inability to distinguishing between the MCAM ectodomain versus the full-length protein.

In contrast, we used an immunoblot approach. This allowed us to definitively distinguish between the two isoforms based on the size of the band detected. In the whole cell lysates, a band of ~110-120 kDa was detected, corresponding to the full-length, glycosylated protein. Meanwhile, in the concentrated cell culture media, CC9 mAb detected a protein band measuring ~100 kDa, which coincides with the expected size of the MCAM ectodomain. The presence of a <20 kDa “remnant fragment” (referred to as the MCAM-CTF) within whole cell lysates that was recognised by an antibody specific for the MCAM-l-CTF (which consists of the TMD and ICD) and is a further indication that full-length MCAM undergoes proteolytic cleavage in melanoma cell lines (Stalin *et al.*, 2016).

The fate and potential functional relevance of the MCAM-CTF following ectodomain shedding in melanoma cells has not yet been investigated, however in endothelial cells, the MCAM-CTF has been shown to be internalised and undergoes further cleavage, most likely mediated by PS1 (Stalin *et al.*, 2016a). Interestingly, researchers showed here that whilst the ICD of both MCAM-sh and MCAM-l were present within the perinuclear region of endothelial cells under basal conditions, only the ICD of MCAM-sh underwent nuclear translocation, and only after cells were treated with rsMCAM. This was associated with interaction with transcription factors (namely CSL), promoting transcription of target genes (Stalin *et al.*, 2016a). Due to limited availability of commercially produced antibodies against the MCAM-CTF, we were unable to investigate the potential involvement of the MCAM-sh CTF in melanoma cells. However, an antibody targeted to the CTF of MCAM-l, binding somewhere between the di-leucine motif (aa623-624) and the tyrosine motif (aa641-644) was readily available and allowed us to focus on understanding the cleavage of MCAM-l in melanoma cells.

Our focus on the cleavage of MCAM-l was informed by our data that MCAM-l is expressed at higher levels in melanoma than MCAM-sh, consistent with previous

reports (Karlen & Braathen, 1999). Although it is not possible to directly compare levels of MCAM-l and MCAM-sh (as our amplification reactions used a different oligo combination) our data suggests that, under basal conditions, HUV-EC-C express MCAM-l and MCAM-s at similar levels, consistent with previous reports (Kebir *et al.*, 2010). In our hands, MCAM-expressing melanoma cells showed similar levels of MCAM-l and reduced levels of MCAM-sh, relative to HUV-EC-C, under non-stimulated conditions.

A very recent paper indicated that endothelial cells may also produce splice variants that encode only the ectodomain of MCAM and estimated these variants may contribute ~ 25% of sMCAM under stimulated conditions (Nollet *et al.*, 2022). We were able to amplify only one variant in our samples and it appeared to be present at a much lower level than MCAM-l and MCAM-s (again, with the caveat that direct quantification is not possible from our experiments). These data are consistent with Nollet *et al.* (2022), who performed absolute quantification, as opposed to our relative quantification.

Taken together, we are confident that melanoma cells express predominantly MCAM-l, and that the majority of sMCAM produced by melanoma cells is from cleavage of MCAM-l, rather than cleavage of MCAM-sh or expression of alternate transcripts encoding sMCAM. Further, the MCAM-negative SB2 cell lines were stably transfected with MCAM-l only, providing us with a tool to study and understand the relevance of MCAM-l alone.

The presence of a perinuclear pool of MCAM-CTF that co-localised with LAMP1 and LAMP2 suggested that MCAM is a potential substrate of the intramembrane cleaving protease, PS-2. PS-2 is one of the catalytic components of γ-secretase that cleaves proteins following ectodomain shedding, and it has been shown to localise mainly within the late endosome/lysosome (LE/Lys) (Sannerud *et al.*, 2016). To investigate whether the MCAM-CTF in melanoma cells underwent further cleavage to generate an MCAM-ICD, whole cell lysates were run on a tris-tricine gel, which resolves proteins of a lower molecular weight. Whilst there were no detectable levels of

MCAM-ICD found in whole-cell lysates collected from cells grown under normal culture conditions, we hypothesised that the MCAM-ICD was potentially enriched within the nucleus.

Thus, a nuclear extraction protocol was performed in SB2 14.1 melanoma cells. In our hands, however, this experiment was unable to successfully separate cytoplasmic and membranous proteins, such as β-tubulin and full-length MCAM, from the nuclear fraction. Hence this approach was not suitable for investigating whether the MCAM-ICD was present in the nucleus. In the future, alternative approaches such as sucrose density fractionation or commercially available kits will be considered when attempting to isolate nuclear proteins from whole cell lysates. Previously, I.F has been used to demonstrate the localisation of the MCAM-CTF within the nucleus of endothelial cells (Stalin *et al.*, 2016a), however in our hands, IF data did not show strong evidence of nuclear translocation of the MCAM-ICD under basal or stimulated conditions. Interestingly, MM253 melanoma cells appeared to express the MCAM-CTF in the outer nuclear region, but we were unable to find definitive evidence of nuclear translocation of MCAM.

The inability to detect the MCAM-ICD in most cases may be due to this fragment being short-lived and therefore difficult to detect in specific cell lines. This is not uncommon for ICD fragments, as they are unstable and can undergo rapid lysosomal degradation (Wu *et al.*, 2017). Further, the persistence of the MCAM-CTF within melanoma cells, and its co-localisation with markers of the LE/lysosome in all cell lines tested, may suggest that the MCAM-CTF and/or the MCAM-ICD is targeted for lysosomal degradation.

It is important to note, however, that the role of LE/lysosome goes beyond that of waste removal. As previously mentioned, the lysosome is the site of PS-2 mediated cleavage of substrates such as APP-CTF, generating the AICD (Sannerud *et al.*, 2016). Typically, the fate of protein fragments that have undergone γ-secretase/PS-mediated cleavage involves translocation to the nucleus, where the ICD fragment plays a role in transcription regulation. However, studies have confirmed that

lysosomes are also capable of fusing with the plasma membrane to release exosomes into the extracellular space. This may be cell- or substrate-specific, since ectodomain shedding/CTF cleavage products for CD44 and L1 have been detected in exosomes, and the mechanism proposed for this involved endocytosis and trafficking through the early endosome (EE) to LE to multivesicular bodies (MVB) to membrane fusion (Stoeck *et al.*, 2006). Interestingly, in endothelial cells, Stalin et al. (2016) used co-IP to demonstrate that MCAM-sh formed a complex that contained PS1 but not PS2 (Stalin *et al.*, 2016a). The localisation of MCAM in relation to the PSs has not previously been reported and as such, it would be of interest in the future to investigate the localisation of PS1 and PS2 relative to MCAM, as this may shed light on whether the MCAM-CTF localised within the LE/lysosome compartment is susceptible to PS-mediated cleavage.

Evidently, consecutive cleavage of transmembrane proteins, which encompasses ectodomain shedding and RiP, is a complex process and studying it *in vitro* has a number of limitations. In particular, culturing cells in the presence of FBS exposes them to exogenous factors that could affect the cleavage/processing of transmembrane proteins. In the current study, sMCAM was only generated in the presence of FBS, which indicates that a factor present in the serum could be responsible for MCAM shedding. A similar phenomenon has been reported for SHP substrate-1(SHPS-1)(Ohnishi *et al.*, 2004) and ProHB-EGF (Hirata *et al.*, 2001). In the case of the latter, it was found that lysophosphatidic acid (LPA) present in FBS was required for generation of the soluble protein in the cell culture media (Hirata *et al.*, 2001). Interestingly, ADAM17 (but not ADAM10) has been reported to respond to LPA stimulation, which resulted in increased ectodomain shedding of TGFα (Le Gall *et al.*, 2010).

To overcome the limitations introduced by the use of FBS in the cell culture media, chemical factors are often used, either to stimulate or inhibit cleavage events under serum-free conditions. Commonly used factors for stimulating ectodomain shedding include calcium ionophores and PMA, which promote Ca^{2+}- and PKC-induced shedding, respectively (Hayashida *et al.*, 2010). Both ionomycin and PMA have

previously been reported to induce shedding of MCAM from endothelial cells (Boneberg *et al.*, 2009), where HMVEC-L cells treated with 0.3-30 μM ionomycin for two hours displayed increased levels of sMCAM in the cell culture media, as measured by ELISA. In this instance, ionomycin was selected for its ability to promote intracellular calcium influx, which has been observed when MCAM on endothelial cells is cross-linked by an anti-MCAM antibody, proposed to be analogous to activation of endothelial cells following CD146 engagement by its ligand (Anfosso *et al.*, 2001). In HMVEC-L cells, a concentration of 10 μM was shown to promote the most shedding, while cells treated with the higher concentration (30 μM) released less sMCAM. This was proposed to be due to the toxicity of ionomycin at higher concentrations (Boneberg *et al.*, 2009).

In our hands, however, even comparatively low concentrations of ionomycin (≤4 μM) induced cellular toxicity, which was evident by cells detaching from the collagen-coated glass coverslips and TC plastic. In addition, nuclear shrinkage was observed by IF staining and β-tubulin expression was also reduced/absent in some treated cell lysate samples. Lastly, the release of full-length MCAM into the cell culture media was suggestive of cell death. The degradation of cell cytoskeletal elements, including tubulin, has previously been linked to the early stages of apoptosis in murine cerebellar neurons (Ortega & Morán, 2011). Since ionomycin promotes calcium influx, we hypothesized that melanoma cells may be undergoing calcium-induced apoptosis. This was not confirmed experimentally due to time constraints, however in future investigations it may be beneficial to confirm if cells are undergoing apoptosis. Nuclear fragmentation could be assessed using a TUNEL assay kit, while Annexin V staining followed by flow cytometry will detect if phosphatidylserine has translocated to the outside of the plasma membrane (an early step in apoptosis) (Plesca *et al.*, 2008).

In cells that do not respond to ionomycin, activation of a PKC-dependent pathway is more likely to induce ectodomain shedding. PMA has been widely used in this instance and is known to induce shedding through PKC-dependent activation of ADAM17 (Endres *et al.*, 2003). Whilst ADAM17 has not specifically been named as a

sheddase of MCAM, PMA treatment was shown to promote a slight increase in sMCAM released from endothelial cells (Boneberg *et al.*, 2009). In addition, PMA treatment has been reported to promote dissociation of CaM and association of moesin with the ICD of trasmembrane proteins, which renders them susceptible to cleavage by sheddases (Ivetic *et al.*, 2004). In our hands, melanoma cells treated with PMA (0-200 μM) showed changes in cell morphology, including the shortening of stress fibres, which may be caused by PMA-induced PKCα-mediated phosphorylation of vinculin (Ziegler *et al.*, 2002), and increased formation of focal adhesions. The effects of PMA on MCAM-CTF localisation were investigated in SB2 14.1, MM253 and A2058 melanoma cells using I.F. Whilst full-length MCAM remained localised to the cell surface and MCAM-CTF remained concentrated within the perinuclear region, the amount of intracellular MCAM-CTF was increased. This was especially clear in SB2 14.1 melanoma cells and was also apparent in MM253 cells. Although A2058 cells did not show such a striking increase in perinuclear MCAM-CTF, it appeared that MCAM-CTF in treated cells was perhaps more focal, whereas the intracellular MCAM-CTF in DMSO-treated cells was punctate. The differences seen between different cell lines may relate back to their basal MCAM expression levels or may be related to some other cell-intrinsic properties.

Interestingly, immunoblot data was not completely consistent with I.F. data. In particular, immunoblot testing demonstrated an increase in MCAM-CTF in A2058 cells, despite this not being clearly seen in I.F. data. Similarly, MCAM-CTF in whole cell lysates collected from PMA- and DMSO-treated SB2 14.1 cells indicated that MCAM-CTF increase only slightly in the PMA-treated cells vs. DMSO controls, despite visual observations (using I.F.) that PMA-treatment greatly enhanced the accumulation of MCAM-CTF in the perinuclear region. Overall, these results suggests that further optimisation of experimental conditions may be required to understand how shedding of MCAM in melanoma cells is regulated. Indeed, the inability to induce PMA-stimulated sMCAM production under SF conditions, despite an increase in detectable MCAM-CTF, warrants further investigation and experimental optimisation. In particular, the effect of pervanadate could be explored. Pervanadate is a protein tyrosine phosphatase inhibitor and has been associated with ectodomain cleavage of proteins resistant to PMA-induced cleavage

(Schlöndorff *et al.*, 2001). The identification of a compound capable of stimulating MCAM-l shedding, without affecting cell viability, would significantly enhance our ability to explore the role of sMCAM in melanoma.

3.5 Conclusion

Three isoforms of MCAM have been identified between endothelial cells and melanoma cells, including two transmembrane isoforms (MCAM-l and MCAM-sh), and a soluble isoform. sMCAM has been shown to be produced by alternate splicing and ectodomain shedding in endothelial cells. At present, the production of sMCAM in melanoma cells has not been clearly defined, however data from endothelial cells suggests that MCAM undergoes sequential cleavage events including ectodomain shedding, mediated by MMPs and/or ADAMs, followed by regulated intramembrane processing, mediated by γ-secretase.

In our hands, MCAM was readily cleaved from melanoma cells that were cultured in the presence of FBS, producing a soluble ectodomain and a perinuclear pool of MCAM-CTF. Importantly, since these experiments were performed in the presence of FBS, it could not be ruled out that an external factor (i.e. bovine MMPs or ADAMs) may be responsible for producing sMCAM in cell culture media, although there is also evidence to suggest that LPA in FBS may stimulate endogenous cellular proteases.

To overcome the potential involvement of external factors, cells were stimulated with PMA and ionomycin under serum-free conditions. Both PMA and ionomycin are known to induce ectodomain shedding of many other transmembrane proteins. In our hands, treatment with PMA under serum-free conditions promoted cell activation, evident by a change in cell morphology. In addition, PMA appeared to promote accumulation of the MCAM-CTF in the perinuclear region, which suggested that ectodomain shedding was also increased and immunoblot confirmed that MCAM-CTF was increased in PMA-treated cells. However, there was no evidence of

increased sMCAM in the cell culture media. Conversely, treatment with ionomycin led to apoptotic cell death, and was therefore not investigated further.

Since the MCAM-CTF was present in the perinuclear region, and co-localised with markers of the LE/lyso, we suspect that the MCAM-CTF either has no functional significance and is targeted for degradation; or is subject to further proteolytic processing by γ-secretase (specifically, PS-2), followed by translocation of the MCAM-ICD to the nucleus. Although we did not find conclusive evidence of nuclear translocation of an MCAM-ICD fragment, investigations in the following chapters aimed to clarify whether the MCAM-CTF is a substrate of γ-secretase.

Chapter 4
Metalloproteinase-mediated cleavage of the MCAM ectodomain

4.1 Introduction

Most type-I transmembrane proteins are believed to undergo ectodomain shedding to release soluble proteins into the extracellular space (Hartmann *et al.*, 2013), however alternative splicing can also lead to the production of soluble isoforms of transmembrane proteins (Xing *et al.*, 2003). The avian homologue of MCAM (HEMCAM/gicerin), which is a type-I transmembrane glycoprotein, exists as multiple isoforms, including a soluble protein that was originally shown to be a product of alternative splicing (Vainio *et al.*, 1996). In contrast, in HUVEC and HMVEC-L cells, sMCAM was shown to be generated by MMP-mediated ectodomain shedding (Bardin *et al.*, 2009; Boneberg *et al.*, 2009). Importantly, it has recently been demonstrated that the long and short isoforms of MCAM expressed by endothelial cells are cleaved by ADAM10 and ADAM17, respectively, giving rise to sMCAM. In addition, two novel splice variants were identified in these cells, with evidence supporting that these also give rise to sMCAM (Nollet *et al.*, 2022).

Meanwhile in human melanoma cells, it has not yet been established which mechanism leads to the production of sMCAM, despite evidence that both melanoma and non-melanoma cancer cell lines release varying levels of sMCAM into cell culture media under normal/non-stimulated conditions (Stalin *et al.*, 2016). Further, studies have assessed the effects of recombinant sMCAM on tumour cells and/or the tumour microenvironment (Stalin *et al.*, 2013; Stalin *et al.*, 2016; Stalin *et al.*, 2020), without acknowledging the source of endogenous sMCAM.

Data presented in Chapter 3 suggests that sMCAM is generated by melanoma cells under basal (non-stimulated) conditions; with sMCAM detected in the media, and MCAM-CTF present in late endosomes/lysosomes within the cells. Analyses of MCAM transcripts revealed that melanoma cells express primarily MCAM-l, and there is low expression of MCAM-sh or the novel sMCAM transcripts recently described by Nollet *et al.* (2022). Taken together, these data suggest that most (if not all) of sMCAM released by melanoma cells, is due to ectodomain cleavage.

Importantly, ectodomain shedding of other members of the IgSF of CAMs have been investigated in melanoma, and studies have identified ADAM10 and ADAM17 as key players in ectodomain shedding of these molecules. For example, ADAM17 is implicated in the cleavage of ALCAM, ICAM-1, L1-CAM, NCAM, and VCAM-1 (Singh *et al.*, 2005; Zunke & Rose-John, 2017). ADAM10 is also involved in ectodomain shedding of L1-CAM and other CAMs from the surface of melanoma cells, which is believed to contribute to tumour progression (Lee *et al.*, 2010b). Membrane type MMPs have also been implicated in ectodomain shedding of integrins and cadherins. In particular, MMP14 (MT1-MMP) is involved in shedding of syndecan-1, αV integrin and CD44; with all of these cleavage events associated with enhanced motility and migration (Deryugina *et al.*, 2002; Endo *et al.*, 2003; Kajita *et al.*, 2001).

Finally, it is also possible that secreted MMPs contribute to cleavage of membrane proteins, although these proteases are better known for their role in the degradation of matrix components (Quintero-Fabián *et al.*, 2019). Of interest in melanoma are MMP2 and MMP9, which were first associated with melanoma progression two decades ago (Hofmann *et al.*, 2000). MMP9, in particular, has been associated with rapid progression and poor outcome in melanoma patients (Nikkola *et al.*, 2005). Although there is limited data in melanoma, MMP9 is associated with cleavage of N-cadherin from smooth muscle cells and syndecan-9 from chondrocytes (Bollmann *et al.*, 2019; Dwivedi *et al.*, 2009). In addition, MMP2 is associated with β1 integrin cleavage in colon cancer cells, leading to decreased cell adhesion and enhanced cell migration (Kryczka *et al.*, 2012). Adding to the complexity is that MMP2 is activated at the cell surface via its interaction with MT-MMPs. The interaction between MMP2 and MT1-MMP (MMP14) has been extensively studied, but MMP2 can also be activated by MT-MMPs 3, 5 and 6 (Visse & Nagase, 2003).

A number of studies have described the upregulation of ADAM10, ADAM17, MMP2 and MMP9 in metastatic melanoma (Cireap & Narita, 2013; Lee *et al.*, 2010b; Stalin *et al.*, 2016; Zigler *et al.*, 2011), and have reported on the relevance of MMP14 in the melanoma microenvironment (Pach *et al.*, 2021). This suggests that these sheddases may play a role in MCAM cleavage in melanoma cells. Overall, the

relevance of sMCAM in melanoma progression, including its ability to 1) promote proliferation and dissemination of melanoma cells (Stalin *et al.*, 2020), and 2) support tumour angiogenesis through paracrine effects on vascular endothelial cells (Stalin *et al.*, 2016), warrants further investigation into how sMCAM is generated and how its production may be regulated.

Approach: Gelatin zymography was first used to compare MMP activity in melanoma cell lines and confirmed robust MMP2 activity in MCAM-expressing cells. Since SB2 14.1 cells readily secrete sMCAM into the cell culture media, the broad-spectrum MMP inhibitor, GM6001, was used to determine whether sMCAM is a product of MMPs/ADAM-mediated cleavage in melanoma cells. Targeted MMP inhibitors were also tested but experiments were confounded by the requirement for FBS in the cell culture media of cells releasing sMCAM. As an alternative approach, A2058 and MM253 melanoma cells were transiently transfected with ADAM10 and ADAM17 WT and dominant-negative plasmids, and the effects on surface MCAM expression were used as an indirect measure of ectodomain shedding. The presence of endogenous MT1-MMP, ADAM-10 and ADAM-17 in a range of melanoma cells was also confirmed by immunoblot and/or qPCR.

4.2 Materials and methods

4.2.1 Gelatin zymography for measurement of MMP activity

Melanoma cells were grown in a 6-well plate until ~70% confluent. Media was removed and cell monolayers were rinsed three times with SFM to remove any traces of FBS. 1.25 mL of SFM was then added to each well and cells were incubated for an additional 24 hours at 37^{o}C, 5% CO_2. The following day, media was collected and centrifuged at ~200 g for 5 min, then stored at -20^{o}C. Meanwhile, cell monolayers were rinsed with PBS and detached from the TC plastic with 2.5mM EDTA. Detached cells were collected in media and counted. Cells were then pelleted and washed three times with ice-cold PBS, then stored at -20^{o}C.

On the day of the zymography experiment, media samples were thawed on ice and centrifuged at ~15,600 g for15 min at 4ºC. Media volumes were adjusted based on cell number, then mixed with 5x non-reducing SDS-glycerol loading buffer and loaded directly onto an SDS-polyacrylamide gel containing 1mg/mL gelatin (Section 2.10). The gel was run until proteins were adequately separated (e.g., 15 mA, O/N at 4ºC), then the gel was successively incubated in wash buffer, incubation buffer, Coomassie blue staining solution, and then de-stain solution, (Section 2.10.2). The gel was imaged, and MMP2 and MMP9 activity measured based on degradation of the gelatin embedded in the gel.

Whole cell lysates were prepared from cell pellets collected from the above-mentioned samples. Briefly, cell pellets were thawed and resuspended in 1% NP40 lysis buffer containing 1X CPI. Cells were lysed on ice for 30 min, then centrifuged at ~15,600 g for 15 min at 4ºC, to remove debris. A BCA was performed, and total protein was adjusted such that equal amounts of protein were loaded onto each gel. Samples were prepared for immunoblot, as detailed in Section 2.7. Following electrotransfer, membranes were incubated with Revert700 and total protein was measured. Levels of MMP14 protein expression were measured, following the standard immunoblot protocol.

4.2.2 Broad spectrum inhibitors of cleavage at the cell surface

GM6001 is a broad-spectrum inhibitor of MMPs and ADAMs (Rawlings *et al.*, 2017). This was first used to determine the relevance of MMPs and ADAMs in MCAM ectodomain shedding. SB2 14.1 cells, which readily secrete sMCAM, were treated with a range of concentrations of GM6001 over short- and long-term experiments, using reduced-serum conditions. At the end of the treatment window, media was collected and successively centrifuged (330 g for 5 min, followed by ~15,600 g for 15 min at 4ºC) to remove debris. It was then concentrated ~10-fold by evaporation (Speedvac) prior to analysis via immunoblot. Cells were harvested concurrently, and total protein concentration was determined by BCA protein assay. Total protein concentration was adjusted such that all samples were at the same concentration

prior to loading onto an SDS-polyacrylamide gel. Concentrated media samples were subject to the same dilutions as the lysates, in order to maintain consistency. Following protein separation on an SDS-polyacrylamide gel, proteins were electro-transferred to methanol-activated PVDF membranes, blocked, and probed for MCAM.

4.2.3 Expression of HA-tagged ADAM10 and ADAM17 variants in melanoma cells

Transient transfection protocol

Since ADAM10 and ADAM17 are major sheddases of transmembrane proteins, we investigated the potential role of these proteases in MCAM shedding by overexpressing HA (haemagglutinin)-tagged either wild-type (WT) or dominant negative (DN) ADAM10 and ADAM17 (Figure 4-1). For this, a transient transfection approach was chosen, using plasmids obtained from Addgene (Gschwind *et al.*, 2003). Briefly, these plasmids contained sequences encoding either WT ADAM10 or ADAM17, inserted into the pcDNA3 expression vector with a HA tag (pcDNA3-ADAM10-HA and pcDNA3-ADAM17-HA; Appendix H-i andAppendix H-ii, respectively). Additionally, DN variants were obtained from Addgene and consisted of truncated ADAM10 and ADAM17 sequences, which lacked the regions coding for the pro-domain and metalloproteinase domain, inserted in the pCDNA3 vector (pcDNA3-Delta(ProMP)-ADAM10-HA and pcDNA3-Delta(ProMP)-ADAM17-HA; Appendix H-iii and Appendix H-iv, respectively). Prior to transfecting cells, sequencing was performed to confirm that the plasmids contained the expected ADAM10/17 sequences (see Appendix A).

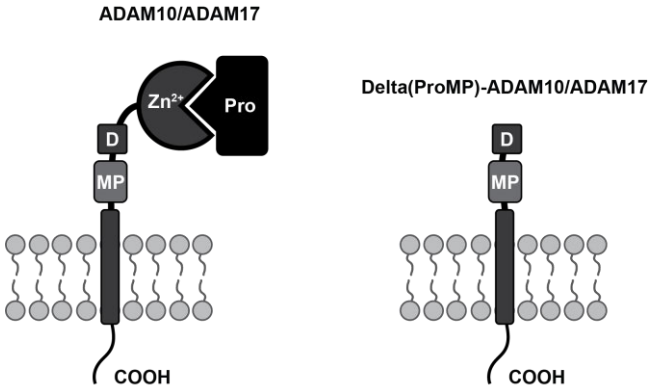

Pro: prodomain
Zn^{2+}: metalloproteinase domain
D: disintegrin domain
MP: membrane proximal (cysteine-rich) domain

Figure 4-1 Structure of ADAM10 and ADAM17

ADAM10 and ADAM17 are single-pass transmembrane proteins consisting of a metalloproteinase (Zn^{2+}) domain, a prodomain (Pro), a disintegrin domain, and a membrane-proximal (MP), cysteine-rich domain. The Zn^{2+} domain is responsible for proteolytic cleavage but is inactive until the prodomain is removed by endoproteolytic processing. Removal of the sequence encoding the Zn^{2+} and Pro domains generates dominant negative variants of ADAM10 or ADAM17, which are proteolytically inactive and therefore unable to cleave their target substrates.

A2058 melanoma cells were plated at a density of 5 x 10^4 or 10 x 10^4 cells/well in a 24 or 12 well plate, respectively. MM253 cells were plated at 2.3 X 10^4 or 4.6 x 10^4 cells/well in a 24 or 12 well plate, respectively. For immunofluorescence studies, cells were seeded onto collagen-coated coverslips. After culturing O/N, cells at ~70-80% confluence were transfected using Lipofectamine™ 3000, using the optimised volumes and concentrations outlined in Table 4-1. Briefly, DNA and P3000 reagent were diluted in OptiMEM and vortexed. Lipofectamine™ 3000 was diluted separately in OptiMEM, then combined with the DNA and P3000 mixture. After mixing well the DNA, P3000 and Lipofectamine™ 3000, DNA-lipid complexes were allowed to form by incubating at RT for 10 min. Immediately prior to transfection, cell culture media was replaced, and DNA-lipid complexes were added to each well in a dropwise manner.

Table 4-1 Reagent volumes for transient transfection of melanoma cells with ADAM10/17 constructs (per well of 12, 24 well plates)

	A2058 melanoma cells		MM253 melanoma cells		SB2 14.1 melanoma cells	
	12-well plate	24-well plate	12-well plate	24-well plate	12-well plate	24-well plate
DNA	1 µg	0.5 µg	2 µg	0.5 µg	1 µg	0.5 µg
P3000	2 µL	1 µL	4 µL	2 µL	2 µL	1 µL
OptiMEM	50 µL	25 µL	50 µL	25 µL	50 µL	25 µL
Lipofectamine™ 3000	2 µL	1 µL	2 µL	1 µL	3 µL	1.5 µL
OptiMEM	50 µL	25 µL	50 µL	25 µL	50 µL	25 µL
Volume of complex added to each well	100 µL	50 µL	100 µL	50 µL	100 µL	50 µL

4.2.4 Investigation of ADAM localisation in transfected cells

Cells (A2058 or MM253) were plated on collagen-coated coverslips in a 24-well plate. Once adhered, the cells were transiently transfected, as described above (Section 4.2.3). After ~24 hours cells were fixed with 4% paraformaldehyde and permeabilised with 0.1% TX-100, then blocked in 1% BSA/10% goat serum in HBS for 1 h at RT, or O/N at 4^{o}C, and immunofluorescently labelled. Cells were stained using an AlexaFluor488-conjugated α-haemagglutinin (HA) antibody, and the CC9 mAb against the MCAM ectodomain. As both antibodies were raised in mouse and the secondary antibody was not isotype-specific, staining was performed sequentially as follows: cells were incubated with CC9 mAb for 1 hour at RT, followed by α-mouse IgG-AlexaFluor555 for 45 min at RT, then α-HA-AlexaFluor488 for 1 hour at RT. After labelling the nuclei with DAPI, coverslips were mounted onto glass slides, sealed with varnish, and imaged on the Nikon A1 confocal microscope.

Staining was also performed using the AlexaFluor488-conjugated α-HA antibody, followed by αCD146-CTF, as per the standard protocol (all detailed in Section 2.8.4).

4.3 Results

4.3.1 MMP activity in melanoma cell supernatants

Upregulated MMP2 and MMP9 activity is characteristic of invasive tumours and can be measured *in vitro* using gelatin zymography. Interestingly, MCAM has been shown to positively regulate MMP2 activity via Id-1 and ATF3 (Zigler *et al.*, 2011). In our hands, however, there was little difference in MMP2 gelatinase activity observed in supernatants collected from MCAM positive vs. MCAM negative cells (Figure 4-2). Due to the lack of an internal standard, accurate quantification of MMP activity was not possible. In addition, we consistently observed evidence of pro-MMP2 activity in lanes that did not contain sample, suggesting that there was spillage between wells. In all samples it was also apparent that pro-MMP2 was present in saturating concentrations, with a much smaller amount of MMP2 observed (68 vs. 62 kDa, respectively). MMP2 also formed a dimer, represented by a high molecular weight band (~120 kDa).

A band representing pro-MMP9 was present in SFM from all SB2 cell lines (both MCAM positive and negative) but was absent from the native MCAM-expressing cell lines. Instead, MM96L and MM253 displayed higher levels of MMP9 activity, while A2058 cells had no detectable gelatinocytic activity, other than pro-MMP2. As the ~60 kDa active form of MMP14 has been recognised as an activator of MMP2 activity (Lehti *et al.*, 1998), MMP14 protein expression was measured in the corresponding whole cell lysates taken from cells cultured in SFM. However, there was no apparent relationship between the level of MMP14 protein expression and the gelatinocytic activity of MMP2. Interestingly, there was a trend toward an increased amount of MMP14 protein found in cells that express higher levels of MCAM (e.g. compare SB2 14.1 vs. SB2; and MM96L vs. MM253). This difference was not statistically significant according to a non-parametrix Kruskal Wallis test (Figure 4-3).

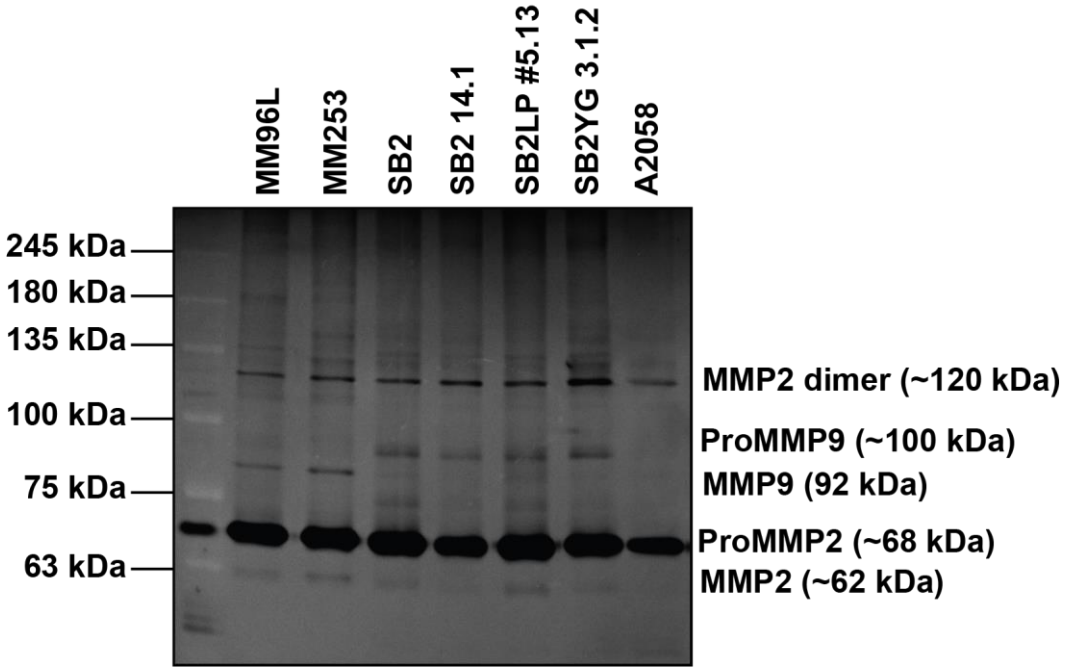

Figure 4-2 Gelatinocytic activity of MMP-2 and MMP-9 in melanoma cell supernatants.

Melanoma cells were grown to ~70% confluence, then normal culture media was replaced with SFM. Cells were cultured in SFM for a further 24 hours, before culture media and lysates were collected. Gelatin zymography was performed on SFM that was normalised based on cell number. All cell lines showed the presence of an MMP2 dimer (~120 kDa). MM96L and MM253 melanoma cells had low levels of Pro-MMP9 activity (~100 kDa) and higher levels of MMP9 activity (~92 kDa). Conversely, the SB2 cell lines had a minimal amount of active MMP9 activity but a higher amount of Pro-MMP9 activity. A2058 melanoma cells had comparably little ProMMP9 or MMP9 activity. All cell lines showed a large amount of Pro-MMP2, and all samples had a low but measurable amount of active MMP2, excluding A2058 cells which showed little-to-no MMP2 activity. The image has been inverted and the exposure adjusted to more clearly demonstrate the gelatinocytic activities. This experiment was undertaken n=3 times, and a representative image is shown.

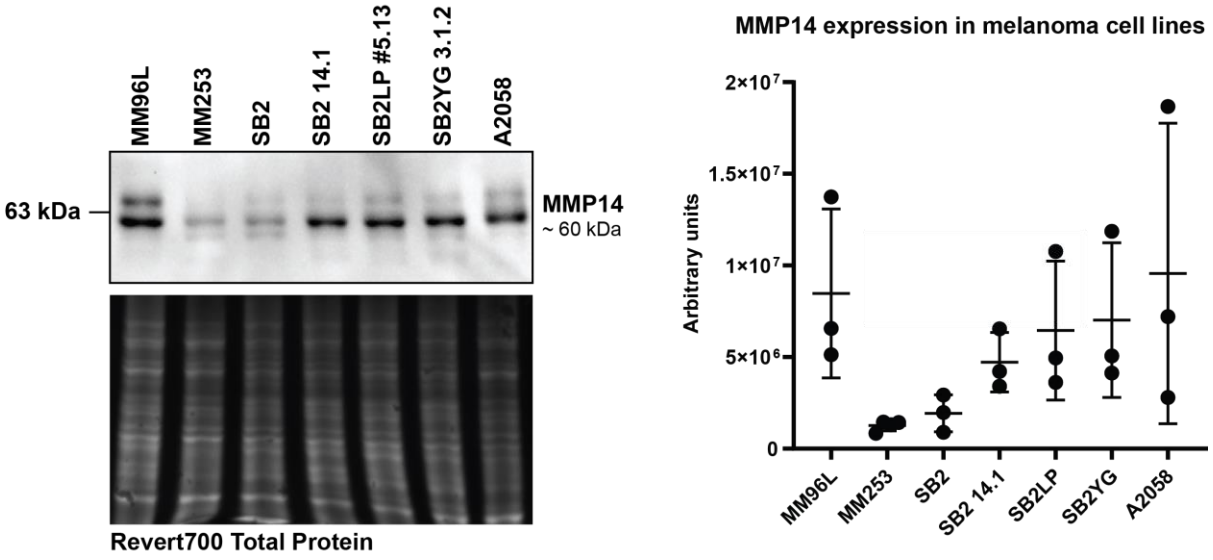

Figure 4-3 Expression of MMP14 in melanoma cell lysates.

Whole cell lysates were collected after 24 hours in SFM, and expression of MMP14 was compared between different melanoma cell lines. A distinct band of ~60 kDa, representing active MMP14, was present in all samples, but was notably lower in the MM253 melanoma cells, and the MCAM-negative SB2 cells. A band of slightly higher molecular weight is likely the inactive precursor of MMP14. This was also present in all samples. The lower image depicts total protein staining on the PVDF membrane prior to blocking and antibody incubation, as measured using Revert700 total protein stain. MMP14 was normalisaed to total protein and plotted on a graph (n=3; error bars reprepsen mean +/- SD). No significant difference in MMP14 epxression between each cell line was found ($p>0.05$).

4.3.2 Broad-spectrum inhibition of MMPs

To gain insight into whether MMPs can cleave the MCAM ectodomain in melanoma cells, a broad-spectrum metalloproteinase inhibitor, GM6001, was used. This inhibitor targets both MMPs and ADAMs. SB2 14.1 cells were selected for this experiment as sMCAM is readily detectable in cell culture media collected from these cells. Treatment with increasing concentrations of GM6001 resulted in reduced amounts of sMCAM in the cell culture supernatants compared to vehicle control, even in the presence of 2% FBS. In particular, the lowest tested concentration of GM6001 (10 µM) showed a noticeable decrease in the absolute amount of sMCAM compared to the vehicle control (0 µM) (Figure 4-4A). Importantly, there were no changes in cell morphology following treatment with 10 µM GM6001 (Figure 4-4B), suggesting that treated cells were not adversely affected by this concentration of the inhibitor.

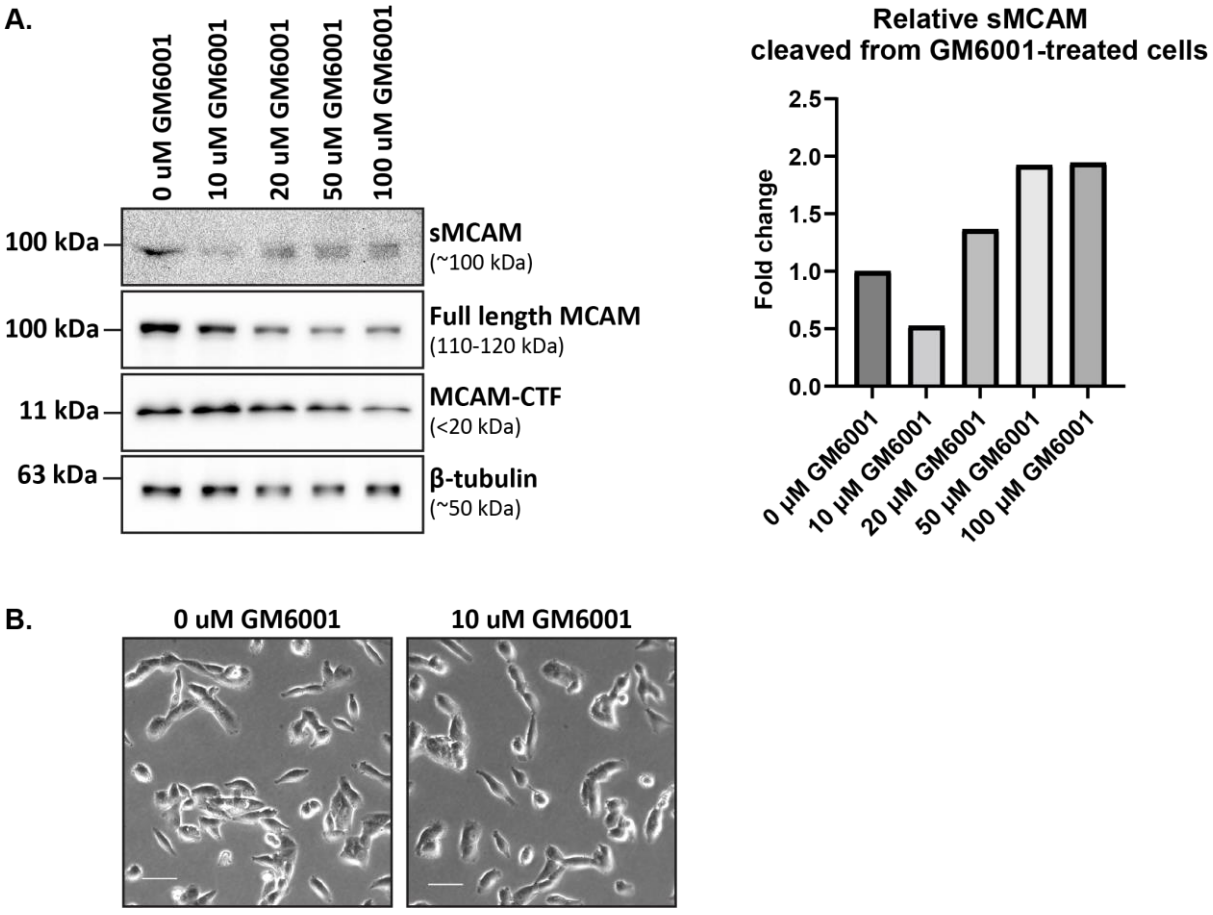

Figure 4-4 Broad-spectrum MMP inhibitor decreases sMCAM production in melanoma cells.

SB2 14.1 cells were grown overnight, then treated with increasing concentrations of GM6001 (or DMSO, vehicle) in media containing 2% FBS. After two hours, media and lysates were collected, processed, and analysed by Western blot (n=2, mean fold-change is shown). sMCAM was detected in the media, but at lower levels in GM6001-treated cells compared to DMSO-treated cells. Full-length MCAM and MCAM-CTF levels appeared to decrease slightly with increasing GM6001 concentrations (A). Short-term treatment was not associated with any changes in cell morphology (B) (scale bar= 50 μM)

To investigate the potential involvement of specific MMPs in MCAM cleavage, melanoma cells were treated with a range of concentrations of targeted MMP inhibitors, including ones that have been shown to inhibit sMCAM generation in endothelial cells (Boneberg *et al.*, 2009). The SB2 14.1 melanoma cell line was used for these treatments as these cells shed comparatively large amounts of sMCAM when cultured in the presence of FBS. Cells were treated with increasing concentrations both MMP inhibitor I and MMP inhibitor III (Figure 4-5A) in media containing 2% FBS, which was necessary as shedding does not occur under SF conditions, and we were unable to use common pharmacological stimuli such as

PMA or calcium ionophore, as these caused significant cell death (as described in Chapter 3). There was some indication of reduced sMCAM in cells treated with MMP Inhibitor I at 1000 µM, although this was not consistently observed. For MMP Inhibitor III, there were no changes in sMCAM levels in treated vs. untreated cells (Figure 4-5B). However, the presence of FBS in the cell culture medium may have affected the activity of these inhibitors.

A.

	Targets	IC_{50}
MMP inhibitor I $C_{23}H_{34}N_6O_6$	MMP-1	1.0 µM
	MMP-3	150 µM
	MMP-8	1.0 µM
	MMP-9	30 µM
MMP inhibitor III ($C_{19}H_{29}N_3O_4$)	MMP-1	7.4 nM
	MMP-2	2.3 nM
	MMP-3	135 nM
	MMP-7	10-100 nM
	MMP-13	1-10 nM

B.

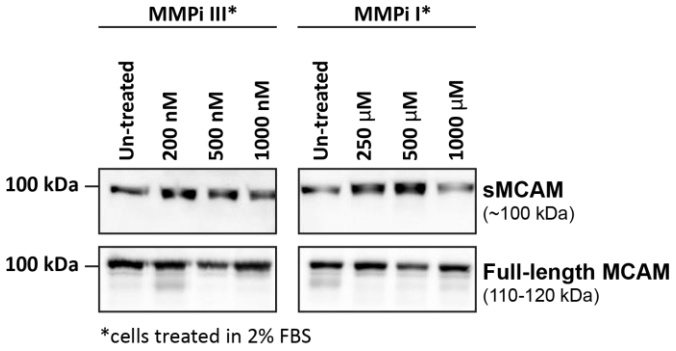

Figure 4-5 MMP-targeted inhibitors did not prevent generation of sMCAM.

SB2 14.1 melanoma cells were treated with inhibitors that target an array of MMPs (A). Media was collected and concentrated, whole cell lysates were prepared, and samples were analysed by immunoblot (n=2). The presence of sMCAM was confirmed in all samples, with no clear reduction in the amount of sMCAM generated by treated compared to control cells, except for MMP inhibitor I at 1000 µM. In addition, full-length MCAM levels were not significantly different in treated vs. control cells (B).

Taken together, these data indicate that the protease responsible for cleaving MCAM is GM6001-sensitive and is unlikely to be an MMP, suggesting ADAM10 and ADAM17 as likely candidates. Accordingly, we next investigated the expression of these specific metalloproteinases in melanoma cell lines.

4.3.3 Expression of ADAM10 and ADAM17 in melanoma cell lines

ADAM10 and ADAM17 are necessary for normal development (Hartmann *et al.*, 2002; Peschon *et al.*, 1998a), but are also frequently implicated in diseases such as cancer, where they aberrantly cleave substrates that contribute to tumour progression (Cheng *et al.*, 2021; Hedemann *et al.*, 2018; Lee *et al.*, 2010b). Expression of ADAM10 and ADAM17 was assessed in melanoma cell lines by

immunoblot and qPCR, to determine whether there was any potential correlation with MCAM ectodomain shedding. ADAM10 protein was detected in all cell lines tested and was present as a precursor (~100 kDa) and an active form (~70 kDa). Both forms were highly expressed in MM96L cells relative to MM253, A2058, SB2 and SB2 14.1 (Figure 4-6A). In contrast, ADAM17 expression was lowest in MM96L cells, and was highest in MM253 cells. Both SB2 and SB2 14.1 cells had a similar level of ADAM17 expression, which was lower than MM253 cells but higher than A2058 and MM96L cells (Figure 4-6B). Statistical analyses were performed but found no significant difference in ADAM10 or ADAM17 expression in any of the cell lines tested (non-parametric Kruskal-Wallis test with Dunn's multiple comparisons correction). Differences in glycosylation may account for the slight variation in molecular weight of ADAM10 (precursor) and ADAM17 between each of the cell lines (Chavaroche *et al.*, 2014), which is important to acknowledge because glycosylation of ADAMs is believed to be required for their proteolytic activity (Escrevente *et al.*, 2008).

In general, mRNA expression correlated with protein expression data, except for ADAM17 expression in MM96L and MM253 cells. Whereas ADAM17 protein expression was clearly increased in MM253 cells, this was not reflected at the mRNA level. Meanwhile, MM69Ls expressed the lowest amount of ADAM17 protein in all cell lines tested, while *ADAM17* mRNA in the same cells was appeared to be increased compared to other melanoma cells, although this was not statistically significant according to non-parametric Kruskal-Wallis test with Dunn's multiple comparisons correction (Figure 4-6C and Figure 4-6D).

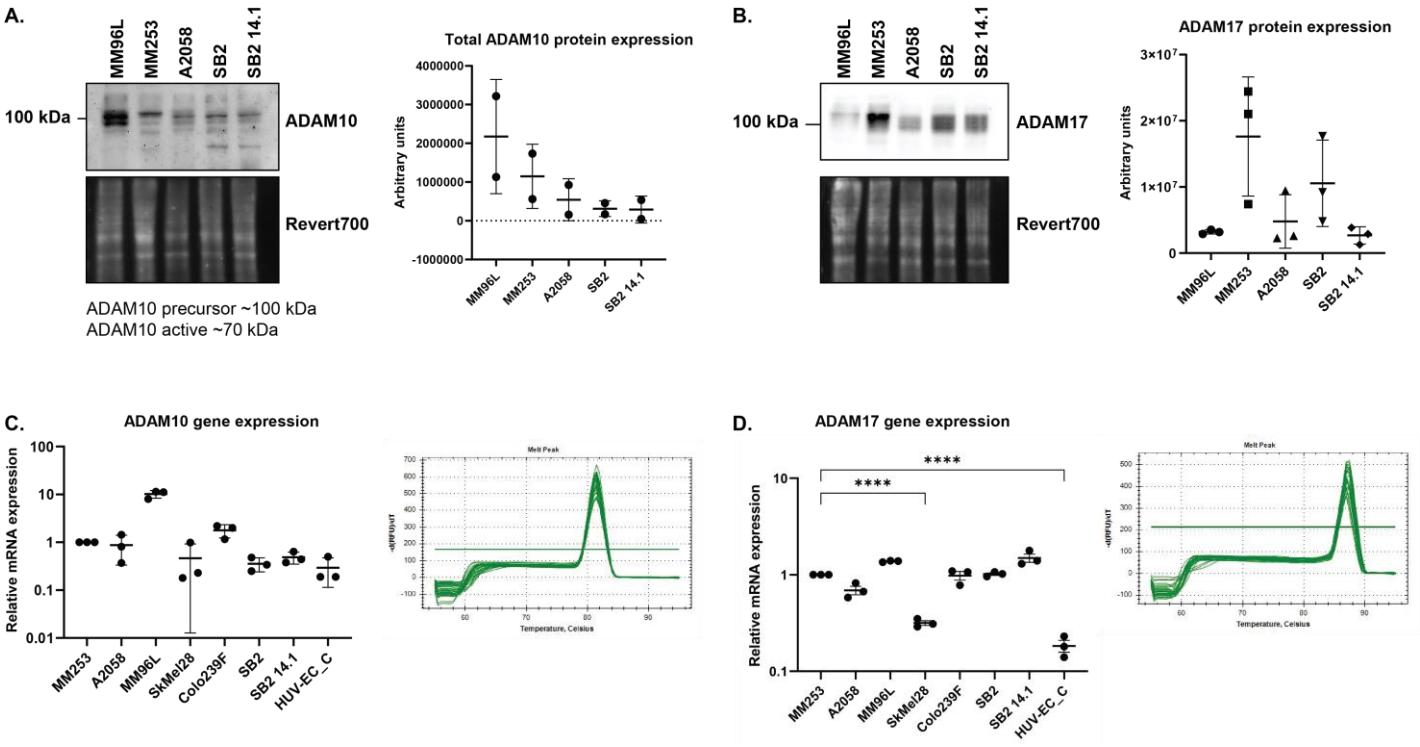

Figure 4-6 ADAM10 and ADAM17 expression in melanoma cell lines

Protein levels of ADAM10 and ADAM17 were assessed in five melanoma cell lines cultured under normal conditions (n=2 and n=3, respectively). Revert700 was used to confirm that similar levels of total protein had been loaded. ADAM10 was present as a precursor and mature form in all cell lines and was highly expressed in MM96L cells. The remaining cells expressed comparably less ADAM10 (A). Expression of ADAM17 was lowest in MM96L cells, highest in MM253 cells, with moderate levels in A2058, SB2 and SB2 14.1 cells. However, there were no statistically significant differences in ADAM10 or 17 protein expression between any cell lines (B). Gene expression analysis by qPCR found no statistically significant differences in *ADAM10* expression between the melanoma and non-melanoma HUV-EC-Cs (n=3, mean and SEM are shown), although there appears to be a trend towards increased expression of *ADAM10* in MM96L cells (C). *ADAM17* expression was lower in the non-melanoma HUV-EC-Cs and SkMel28 melanoma cells, compared to MM253 melanoma cells (n=3, mean and SEM are shown, ****p<0.0001)(D). Melt curves for each reaction are shown on the bottom row, indicating the presence of a single amplicon.

Overall, the relative expression of ADAM10 and ADAM17 did not appear to be directly associated with the amount of sMCAM generated by ectodomain shedding, and a more targeted approach would be required to determine the relevance of ADAMs in MCAM cleavage.

Therefore, we aimed to investigate whether overexpression of ADAM10 or ADAM17 influenced MCAM shedding. For this, plasmids containing either WT or DN variants of ADAM10 and ADAM17 were transiently transfected into A2058, MM253 and SB2 14.1 melanoma cells to force over-expression of these sheddases. We hypothesized that overexpression of WT ADAM10 and/or ADAM17 would lead to enhanced cleavage of MCAM and increased levels of sMCAM in the cell culture media. Unfortunately, transfection efficiency in A2058 and MM253 cells was low (~10%), while the viability of SB2 14.1 cells was affected by transfection with ADAM10 and ADAM17 plasmids (both WT and DN) and could not be used for this set of experiments. Due to the low transfection efficiency, and apparent cell death that occurred in the first 24 hours post-transfection, it was not feasible to attempt to detect changes in levels of sMCAM in the media following transfection. As an alternative, we attempted to measure MCAM-CTF levels by immunoblot, and flow cytometry was used in attempt to compare cell surface levels of MCAM in transfected vs. untransfected cells (data not shown). However, these approaches were unsuccessful due to the limited number of transiently transfected cells in these experiments. In the immunoblot experiments, we were unable to consistently detect full length MCAM or MCAM-CTF due to low cell numbers and protein concentration. The flow cytometry approach involved permeabilisation of cells to enable intracellular staining of the MCAM-CTF and HA-tagged ADAM10 or ADAM17. This method requires cell multiple centriguation steps, meaning very few cells remained at the end of the procedure. The cost of reagents for transient tranfection also limited our ability to scale these experiments up.

Despite these limitations, it was possible to investigate the localisation of the ADAMs- albeit from an exogenous source- relative to MCAM, using I.F. These experiments examined the localisation of the HA-tagged ADAM10 and ADAM17

proteins in A2058 and MM253 melanoma cell lines. As shown in Figure 4-7A, the MCAM-CTF antibody labelled both surface and intracellular MCAM. In both A2058 and MM253 cells, the amount of MCAM-CTF within the juxtanuclear region was similar in transfected vs. untransfected cells. There was, however, an accumulation of ADAM10-HA observed in transfected MM253 cells, which co-localised with MCAM-CTF. There was some co-localisation of ADAM10-HA and MCAM-CTF close to the cell surface in both cell lines, however there was also an apparent reduction in ADAM10-HA expression towards the cell periphery and particularly within cell protrusions (Figure 4-7A). ADAM17-HA displayed a similar staining pattern, with strong expression in the nuclear region where it overlapped with DAPI. It was also diffusely expressed throughout the cytoplasm, with much lower expression towards the periphery. There was also localisation of ADAM17-HA and MCAM-CTF at the cell periphery, represented as punctate peripheral accumulations (Figure 4-7B). Staining of cells transfected with DN variants is shown in Appendix I.

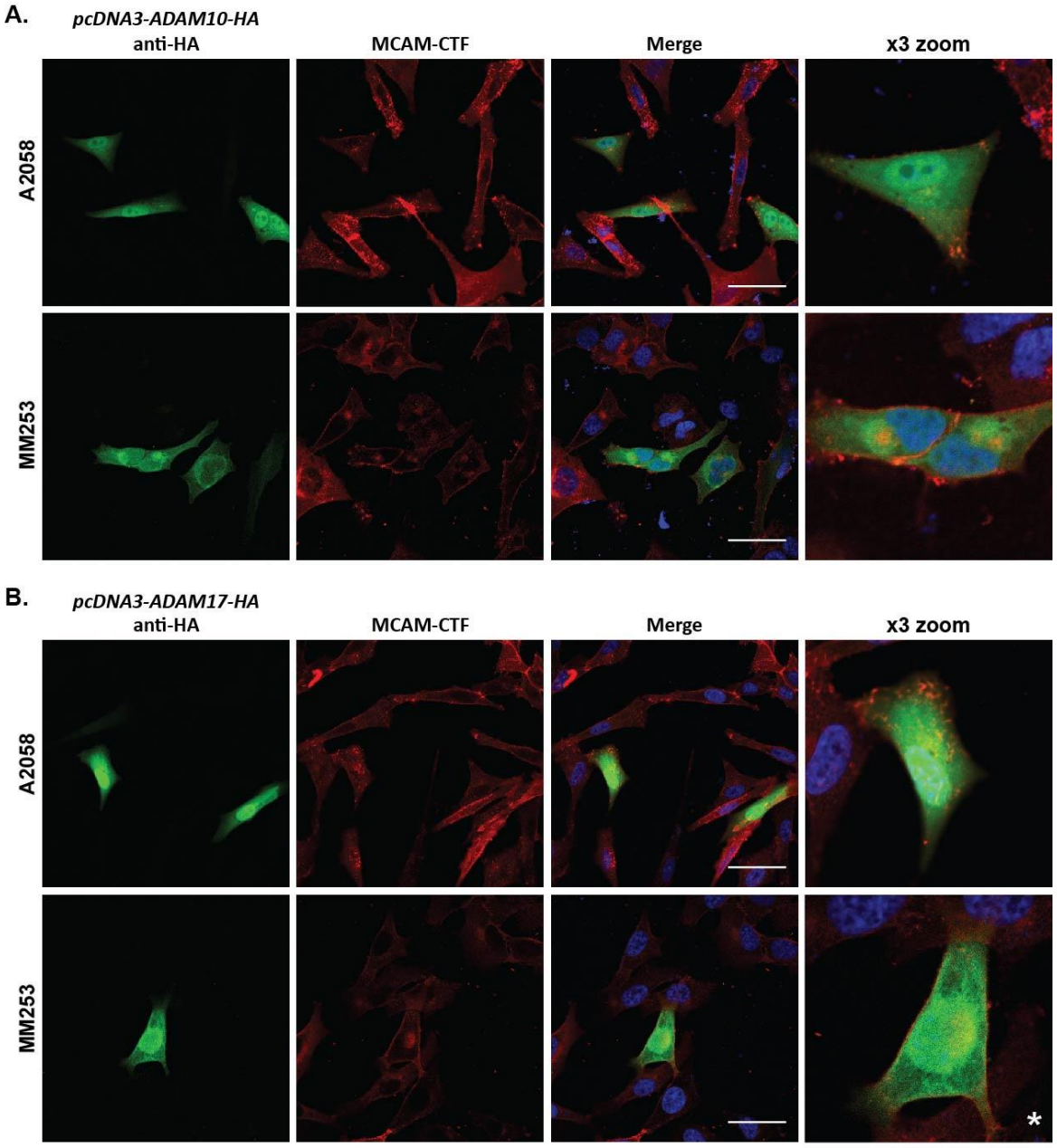

Figure 4-7 Localisation of HA-tagged ADAMs in transiently transfected A2058 melanoma cells.

HA-tagged ADAM10 and ADAM17 were overexpressed in melanoma cells by transient transfection, and their localisation in relation to MCAM was observed by I.F. staining. (A) ADAM10-HA was highly concentrated within the nuclear region, where it overlapped with DAPI staining. There was some co-localisation with the MCAM-CTF throughout the cytoplasm, particularly within the juxtanuclear region of MM253 cells, as well as at the cell periphery in both cell lines. (B) ADAM17-HA was similarly concentrated within the nucleus, along with diffuse staining throughout the cytoplasm. MCAM-CTF accumulated in the juxtanuclear region of some transfected cells, where it overlapped with cytoplasmic ADAM17-HA. Co-localisation was also evident at the cell surface, particularly in MM253 cells. The scale bar in the merged image is 50 µM, **denotes a single image that was magnified digitally.*

4.4 Discussion

Proteases responsible for ectodomain shedding encompass several membrane-bound enzymes that have both physiological and pathological relevance. MMPs and ADAMs are the two main types of ectodomain sheddases. In particular, ADAM17 has been reported to cleave more than 80 substrates (Calligaris *et al.*, 2021), and ADAM10 was linked with ~40 transmembrane substrates in a screen conducted in neurons (Kuhn *et al.*, 2016). The role of MMPs in transmembrane protein cleavage is less clear, but there are some key examples, such as MMP7, which can cleave E-cadherin (Lee *et al.*, 2007) and N-cadherin (Williams *et al.*, 2010). In addition, (Boneberg *et al.*, 2009) reported that MMP3 may be responsible for MMP-mediated shedding of MCAM in endothelial cells (Boneberg *et al.*, 2009). Recently, ADAM17 has also been linked to cleavage of MCAM in endothelial cells (Nollet *et al.*, 2022).

Expression/activity of select MMPs and ADAMs was investigated in three native MCAM-expressing cell lines, as well as three cell lines overexpressing WT and mutant MCAM, and their MCAM negative parental cell line. Despite previous reports of MCAM promoting activation of MMP2 (Zigler *et al.*, 2011), we saw no convincing evidence of enhanced MMP2 activity in any of the MCAM-expressing cells compared to the MCAM negative SB2 cells. There was, however, robust expression of MMP14 (MT1-MMP) protein, which is responsible for MMP2 activation (Nagase, 1998), in five of the six MCAM-positive cell lines tested, suggesting that MCAM-expressing cells may at least have the capacity to increase MMP2 activation. Although gelatin zymography, as used in this thesis, can distinguish between the pro- and active forms of MM2 and MMP, in our hands it was limited by sample spill over between wells. To further explore MMP-2 expression in melanoma cells, additional methods including enzyme-linked immunosorbent assays and fluorogenic peptide enzyme assays could be explored (Merino *et al.*, 2021).

MCAM expression has also been shown to reciprocally regulate MMP9 in melanoma cells, with Stalin *et al.* (2016) demonstrating that treating cells with rsMCAM led to increased MMP9 mRNA expression. Further, MCAM has been shown to be required for upregulation of MMP9 genes in endothelial cells in response to secretions from

hepatocarcinoma cells (Zheng *et al.*, 2009). Interestingly, MMP9 and pro-MMP9 activity was strikingly different in SB2 cell lines (both MCAM positive and negative) compared to the native MCAM-expressing cell lines. As with other MMPs, pro-MMP9 is secreted as a latent enzyme that is activated within the extracellular space (Van Wart & Birkedal-Hansen, 1990). A number of proteases have been suggested to cleave the pro-domain of MMP9, namely serine proteases (Ra & Parks, 2007) and Cathepsin K (Christensen & Shastri, 2015), however the lack of an established regulatory factor makes it difficult to understand how/why activation of MMP9 is enhanced in MM253 and MM96L compared to SB2 and A2058 cells. Importantly, tissue inhibitors of metalloproteinases (TIMPs) play an integral role in regulating the activity of other metalloproteinases and are often implicated in tumour progression. In particular, elevated TIMP1 expression and reduced TIMP3 expression have been consistently associated with cancer progression and poor patient outcome (Jackson *et al.*, 2016). It is worth noting, however, that TIMPs do not only regulate MMPs and they may contribute to metastatic change in other ways. For example, TIMP1 interacts with CD63 and β1 integrin and activates intracellular signalling pathways associated with resistance to anoikis (Toricelli *et al.*, 2013). TIMP expression has not been explored in the present study, but their relevance should not be discounted in future studies.

The lack of evidence that MMP2, MMP9 and MMP14 have a role in MCAM cleavage lead us to consider the role of ADAM10 and 17. Expression of both ADAM10 and ADAM17 was confirmed via immunoblot, which identified an apparent inverse relationship between the expression of these proteins in a panel of melanoma cells. Most strikingly, MM96L melanoma cells had the highest expression of ADAM10 and lowest expression of ADAM17 relative to all other cell lines tested, while MM253 cells had the highest expression of ADAM17 and moderate expression of ADAM10. A2058, SB2 and SB2 14.1 cells each had moderate expression levels of ADAM10 and ADAM17.qPCR data was largely consistent with protein expression data. Since we were only interested in the link between ADAM expression and MCAM shedding, we did not explore any other factors associated with such differences in ADAM expression between each melanoma cell line.

However, it is important to acknowledge that ADAM10 expression is upregulated in melanoma where it has been linked to cell proliferation and release of soluble L1-CAM, promoting tumour progression (Lee *et al.*, 2010b). Meanwhile, *ADAM17* gene expression is upregulated in melanoma and is associated with tumour stage and correlated with the release of soluble TNF-α (Cireap & Narita, 2013). Further, ADAM expression can also have a significant impact on the success of certain treatments, including contributing to resistance to anti-PD-L1 immunotherapy (Orme *et al.*, 2020).

Having confirmed that melanoma cells expressed these sheddases, we proceeded to inhibition studies using the broad spectrum MMP/ADAM inhibitor, GM6001. SB2 14.1 melanoma cells were chosen for this experiment because they produced measurable levels of sMCAM in 2 hours, under non-stimulated conditions. The short time frame was required to maximise activity of the GM6001. In our hands, GM6001-treated cells released less sMCAM into the media than cells treated with vehicle control only. These data, taken together with the fact that MMP specific inhibitors did not affect shedding, supports the hypothesis that ADAMs are involved in MCAM ectodomain shedding. However, as GM6001 did not completely inhibit sMCAM production, this may hint that the generation of sMCAM is not fully dependent on ectodomain shedding. Similar results were recently seen by Nollet *et al.* (2022), who found that a fraction of sMCAM released from endothelial cells was “GM6001-insensitive”, which they hypothesised was produced by alternative splicing of the MCAM transcript. However, it is important to note that our experiments were performed under low-serum conditions, while in most instances, GM6001 treatment is performed under serum-free conditions, with or without the use of a stimulator of ectodomain shedding (Diestel *et al.*, 2005; Golubkov & Strongin, 2012; Sanderson *et al.*, 2008). The presence of a low percentage of serum in the media presents some challenges to interpreting our results, as it may reduce the inhibitory potential of GM6001.

Interestingly, the use of serum in these experiments may also have acted asa physiological stimulus of shedding. Physiological stimuli of ADAM17 (but not ADAM-

10) include lysophosphatidic acid (LPA), thrombin, TNF-α, and EGF (Le Gall *et al.*, 2010). Interestingly, a number of these (e.g. LPA and thrombin) are likely to be present in FBS. This may suggest that ADAM17 is a potential candidate, given that we required the presence of 2% FBS to consistently detect cleavage. We could explore the effect of these individual stimuli on MCAM cleavage to strengthen the evidence for ADAM17, and/or use an ADAM10-specific inhibitor under these serum-containing conditions.

To further investigate the role of ADAM10 and 17 in MCAM shedding and overcome the modest rates of shedding achieved in the absence of a chemical stimulus, we attempted transient transfection to induce ADAM10 and ADAM17 overexpression. Unfortunately, this approach was unsuccessful, as the transfection efficiency was too low for it to be feasible to explore levels of sMCAM in tissue culture media. Further optimisation of this experimental design, including the use of empty vector controls/HA-tagged plasmid, will be necessary for future studies. Due to time constraints, we were unable to perform optimisation prior to submission of this thesis. We did, however, investigate the cellular location of ADAM10 and 17 relative to MCAM using I.F, Localisation between MCAM and the ADAMs was observed, particularly with ADAM10. Additional studies will be required to investigate the distribution of endogenous ADAMs in melanoma cells, as we only stained for the presence of exogenous (HA-tagged) proteins. Importantly, however, the expression pattern of ADAM17-HA appeared to be in line with previous reports, where it was localised mainly intracellularly with limited expression on the cell surface (Groth *et al.*, 2016). Interestingly, it is typically the active form of ADAM17 that is expressed at the cell surface, whilst the inactive zymogen is distributed intracellularly (Schlöndorff *et al.*, 2000). Whilst the nuclear localisation of ADAM17 has not been widely reported, nuclear positivity for ADAM10 in melanoma cells has been noted in tumour tissue samples taken from both primary and metastatic lesions (Lee *et al.*, 2010b).

4.5 Conclusions

Despite the expanse of research into the biological function of sMCAM, including its contribution towards the metastatic progression of melanoma, little is understood

about the processing of MCAM to generate the soluble isoform in melanoma cells. By understanding how sMCAM is produced by melanoma cells, including where and how cleavage takes place, and how it is regulated, it may be possible to downplay the contribution of MCAM in tumour progression. Thus far, it appears that production of sMCAM from melanoma cells occurs in a metalloproteinase-dependent manner. In particular, cleavage of MCAM in response to PMA treatment- measured indirectly through the increased production of MCAM-CTF-suggests that ADAM17 may be involved in the cleavage of MCAM. Our inability to detect sMCAM except in the presence of serum also supports a role of ADAM17 in MCAM cleavage, as serum constituents (such as LPA) have been identified as physiological stimuli of ADAM17 but not ADAM10. Additionally, the upregulation of ADAM17 that occurs in melanoma cells, and that was observed in most melanoma cells investigated here, further supports the hypothesis that ADAM17 may be involved in MCAM cleavage. However, it is also possible that other proteases may be involved in the cleavage of MCAM, or that MCAM is cleaved by more than one protease. This has previously been reported for the cleavage of Nectin, which is a substrate for both ADAM10 and ADAM17 (Buchanan *et al.*, 2017). Indeed, the dysregulated expression of multiple metalloproteinases in melanoma cells could contribute many potential sheddases to cleave transmembrane proteins, including MCAM, and contribute to tumour progression.

Chapter 5

Intramembrane proteolysis of the C-terminal fragment of MCAM in melanoma cells

5.1 Introduction

Beyond generating soluble proteins, ectodomain shedding is also important for producing membrane-localised protein fragments, which often undergo subsequent regulated intramembrane proteolysis (RiP) to produce bioactive molecules. This event is typically mediated by proteases such as PS1 and PS2, which are the catalytic components of the γ-secretase complex and are known to cleave the remnant CTF of transmembrane proteins, liberating the ICD (McCarthy *et al.*, 2017; Selkoe & Wolfe, 2007). This has been particularly well summarised for both APP and Notch, where the extracellular domain initially undergoes ADAM-mediated cleavage to release the soluble ectodomain, followed by cleavage of the CTF by γ-secretase to release the intracellular domain (AICD or NICD, respectively) (Güner & Lichtenthaler, 2020).

The AICD is produced by both the amyloidogenic and non-amyloidogenic processing of APP. It likely forms dimers or oligomers with other intracellular proteins, mainly regulated by its phosphorylation status, allowing it to be involved in multiple pathways that regulate processes such as cytoskeletal dynamics and cell migration, and apoptosis (Chakrabarti & Mukhopadhyay, 2012; Müller *et al.*, 2008). In addition, the AICD may also act as a transcriptional regulator by translocating to the nucleus (von Rotz *et al.*, 2004), although views on this are controversial due to the AICD being very short-lived (Bukhari *et al.*, 2017). Transcriptional regulation is well described for the NICD, which translocates to the nucleus and binds CSL transcription factors, which can either repress or activate Notch target genes (Yuan *et al.*, 2015). There is evidence of MCAM-sh undergoing a similar process in endothelial cells, where γ-secretase-mediated proteolysis resulted in cleavage of the MCAM-ICD, which was directed to the nucleus and associated with CSL, leading to modulation of cell survival genes such as *Fas Associated Via Death Domain (FADD)* and *Bcl-xl* (Stalin *et al.*, 2016a). Similar investigations have not yet been performed in melanoma cells, which predominantly express MCAM-l.

Approach: MCAM-CTF is hypothesised to undergo further processing by PS1 and/or PS2 following ectodomain shedding. By transiently overexpressing MCAM in

HEK293 cells with knockout of either PS1, PS2, or both PS1 and PS2 (PS1/2 dKO), we aimed to confirm the involvement of these proteases in MCAM-CTF processing. Since PS1 and PS2 are components of the γ-secretase complex, we next tested whether the γ-secretase inhibitor, DAPT, had a similar effect on MCAM-CTF processing in melanoma cells. Expression of PS1 and PS2 in melanoma cells was confirmed, before attempting knockdown/knockout of each individual protease, focusing on the MM253 cell line for preliminary studies.

5.2 Materials and Methods

5.2.1 Overexpression of MCAM in HEK293 PS1/2 KO cells

The full-length WT MCAM sequence, inserted in pcDNA3.1 (Appendix J), was a kind gift by Dr Stéphane Karlen (Dermatological Clinic, Inselspital, Berne, Switzerland). Prior to transfecting cells, sequencing was performed to confirm that the plasmid contained the correct full-length MCAM sequence (see Appendix A).

To investigate the role of PS1 and PS2 in RiP of MCAM, HEK293 WT and PS1/2 dKO cells were transiently transfected with pCDNA3.1-MCAM using Lipofectamine™ 3000 (optimised reagent volumes outlined in Table 5-1). Cells were first plated in Poly-D-Lysine-coated TC plastic and cultured O/N, then transfected the following day.

To prepare DNA-lipid complexes, DNA was mixed with OptiMEM and P3000 reagent in a 1.5 mL microtube and vortexed. Lipofectamine 3000 reagent was also mixed with OptiMEM in a separate tube, then vortexed. The contents of both tubes were then combined, mixed well, and incubated at RT for 10 min, before adding to the cell media in a dropwise manner. Cells were cultured for a further 24-48 hours.

Whole cell lysates were collected the following day, and generation of the MCAM-CTF was assessed via immunoblot, using an antibody against the MCAM-CTF. Alternatively, cellular localisation of MCAM was assessed by immunofluorescence,

using transfected cells that were first plated on Poly-D-Lysine-coated coverslips. Between 24-36 h post-transfection, cells were fixed, permeabilised, and blocked, before labelling MCAM with the CC9 mAb and a fluorescent secondary antibody. Protein localisation was visualised using a Nikon A1 confocal microscope.

Table 5-1 Reagent volumes for transient transfection of HEK293 cells with MCAM construct (per well of 12, 24 well plates)

	HEK293 cells	
	12-well plate	**24-well plate**
DNA	1 µg	0.5 µg
P3000	2 µL	1 µL
OptiMEM	50 µL	25 µL
Lipofectamine™ 3000	1 µL	0.5 µL
OptiMEM	50 µL	25 µL
Volume of complex added to each well	100 µL	50 µL

5.2.2 Quantitation of PS1 and PS2 protein expression in melanoma cells

Please note the following method and multiple applications are currently in preparation for publication (Eccles *et al.*, unpublished). To enabling direct quantitation of endogenous PS1 and PS2, a synthetic PS1/2 fusion protein standard (PS Std) was designed such that it contained the antibody epitope regions for PS1 and PS2 in the same protein. The protein was recombinantly generated and purified by Genscript. The PS Std was verified as being specific for PS1 and PS2 antibodies via immunoblot. All experiments were completed in a minimum of three biological

replicates. A PS Std standard curve was run alongside the biological samples on the same PAGE and immunoblot, such that multiple replicates of the standard curve were generated. The standard curve range varied appropriately for the antibody and specific presenilin protein being detected such that the level of detected PS1 or PS2 in the biological samples were within the standard curve range. PAGE and immunoblotting was completed as described (Section 2.7).

To quantitate and directly compare PS1 and PS2 using the PS Std, band densitometry was determined using BioRad Imagelab software. The nanogram mass of PS Std used for each point on the standard curve was converted to the number of protein units (1 unit of PS Std = 30718.3 Da = 5.100843 x 10^{-11} ng). The PS Std Units were plotted against the corresponding densitometry to generate the standard curve, with the intercept set at 0, and the standard curve equation determined. The number of PS1 or PS2 protein units were calculated using the equation as determined for either the PS1 or PS2 antibody, and subsequently normalised to housekeeping protein expression and total protein loaded. The resultant output is the PS1 or PS2 protein units / µg total protein, which can then be directly compared.

5.2.3 Inhibiting γ -secretase activity in melanoma cells

Melanoma cell lines were exposed to varying concentrations of DAPT for 20-24 hours to determine the effect of inhibiting γ-secretase on MCAM-CTF processing. Briefly, cells were seeded either on TC plastic or collagen-coated coverslips and allowed to adhere O/N. The following day, DAPT was prepared to 5 µM, 10 µM and 20 µM in normal culture media and added to each well. DMSO (1/1000) was used as vehicle control. Cells were returned to the incubator and left O/N at 37ºC, 5% CO_2). Samples were collected between 20-24 hours post-treatment, either by fixing cells on coverslips and processing for I.F, as per Section 2.8, or collecting cell pellets for immunoblot, as per Section 2.7.

5.2.4 PS1 and PS2 knockdown/knockout in melanoma cells

PS1 or PS2 knockout/knockdown in MM253 melanoma cells was performed in our lab by Ms Melissa Eccles and Dr Danielle Dye, using CRISPR-Cas9. Single knockouts only were attempted for the melanoma cells (that is PS1 or PS2, not both). Briefly, guide sequences designed to target two exons within PS1 and PS2 (Table 5-2) were ligated into pSpCas9(BB)-2A-GFP (Addgene plasmid #48138), a gift from Feng Zhang (Ran *et al.*, 2013) (Appendix K); and ligations transformed into XL10-Gold ultracompetent *E.coli* cells. Plasmid DNA was amplified and purified as described (Section 2.1.3) and insertion of the correct guide sequence was confirmed by sequencing (Appendix L).

Table 5-2 PS1 and PS2 guides and screening primer sequences

Target Gene & Exon	Primer name	Primer sequence (5`- 3`)
PS1 Exon 3	Ex 3 Guide	GTTTCAACCAGCATACGAAG
	Ex 3 Screen F	CCTGTTTCTGCTCACTGTAGGT
	Ex 3 Screen R	GCTGTTTCAACCAGCATACGA
PS1 Exon 4	Ex 4 Guide	TAAAACCTATAACGTTGCTG
	Ex 4 Screen F	TGTTTAAAACCTATAACGTTGC
	Ex 4 Screen R	GGGATGTACACGTTACCATTT
PS2 Exon 1	Ex 1 Guide	GCTCCCCTACGACCCGGAGA
	Ex 1 Screen F	CTCCCCTACGACCCGGA
	Ex 1 Screen R	CTCCTCTTCCTCCAGCTCCT
PS2 Exon 4	Ex 4 Guide	ACGATCATGCACAGAGTGAC
	Ex 4 Screen F	TGACCTCCTGAGTCCCTGTA
	Ex 4 Screen R	CCACGATCATGCACAGAGTG

MM253 melanoma cells were seeded at 1 x 10^5 cells/well in a 6 well plate and cultured overnight to reach 80-90% confluence. Cells were then transfected with PS1 or PS2 pooled CRISPR plasmids. To prepare DNA-lipid complexes, DNA was mixed with OptiMEM and P3000 reagent in a 1.5 mL microtube while Lipofectamine 3000 reagent was mixed with OptiMEM in a separate tube (Table 5-3). The contents of both tubes were then combined and incubated at RT for 10 min, before adding to the cells. Cells were then cultured for 24 - 48 h prior to cell sorting.

Table 5-3 Reagent volumes for transfection of MM253 melanoma cells with PS1/PS2 CRISPR constructs (per well of 6 well plate)

MM253 Melanoma cells	
	6 well plate
DNA (pooled PS1 or PS2 plasmids)	2.5 µg
P3000	5 µL
OptiMEM	125 µL
Lipofectamine™ 3000	3.75 µL
OptiMEM	125 µL
Volume of complex added to each well	250 µL

Transfected cells were washed with PBS and detached from the tissue culture plate using 2.5 mM EDTA/PBS. Cells were resuspended in flow buffer pelleted and resuspended in 600 µL cold flow buffer containing penicillin/streptomycin (PS; 1:100). For cell collection during sorting, 14 mL round bottom polypropylene tubes were prepared with 4 mL normal culture media containing PS. Cells were sorted on GFP expression by Dr Pat Metharom using a FACs Jazz cell sorter (BD Biosciences). Cells were returned to a 6 well plate to recover for 3-5 days and were then seeded at 1 cell/well in the wells of a 96 well plate. Wells were inspected after 5-7 days and those containing a single colony were selected for further expansion and analysis.

Wells containing cells expanded from a single colony were harvested, with one quarter re-plated and three quarters used for genomic DNA extraction. Once pelleted and washed with PBS (centrifugation at 330 g for 5 min), cells were resuspended (lysed) in 50 µL of 50 mM NaOH followed by heating at 98°C for 15 min. The DNA solution was neutralised with 10 µL of 1 M Tris (pH 7.4). DNA was stored at 4^{o}C or -20^{o}C.

PCR screening was performed to identify cell clones containing genomic disruptions in each exon for PS1 or PS2. The primers were designed to amplify wild type (WT) genomic sequence but not disrupted sequence. Reactions (10 µL) consisted of 2 µL of 5x MyTaq reaction buffer (Bioline), 0.5 µL of each primer (10 µM), 0.1 µL of MyTaq polymerase (5U/µL), 1 µL of DNA and 5.9 µL of PCR grade water. Annealing temperatures were 63ºC for PS1 Exon 3, 61ºC for PS1 Exon 4, and 65ºC for PS2 Exons 1 and 4; reaction conditions were: initial denaturation (95ºC -1 min), followed by 35 cycles of denaturation (95ºC - 15s), annealing (using temperatures above – 15s), extension (72ºC - 20s), followed by a final extension (72ºC - 5 min). The PCR reactions were run on a 2% agarose gel and clones showing no amplicon for either exon (PS1- 3, 4; PS2 -1,4) were expanded, while others were discarded.

5.2.5 MCAM expression in PS1KO and PS2KO melanoma cells

Following expansion, cell lysates were prepared from each potential KO clone and protein expression of PS1 and PS2 explored by immunoblot analysis (as per standard protocol) using anti-PS1-NTF and anti-PS2-NTF antibodies, followed by anti-mouse-HRP and detection using Clarity Max ECL reagent (Biorad). Five PS1 KO clones and 10 PS2 KO clones were identified by immunoblot (Appendix M). These clones have not yet been analysed to explore potential off-target effects and are used in this thesis to further explore data generated using the γ-secretase inhibitor, DAPT.

Whole cell lysates were collected from a subset of these PS1 or PS2 KO MM253 melanoma cells and subject to immunoblot analysis, as per standard protocol, with the MCAM-CTF mAb being used to indicate whether KO affected processing of MCAM-CTF. In addition, MCAM expression was assessed by I.F, flow cytometry and qPCR (as per Sections 2.8, 2.9, and 2.12, respectively).

5.3 Results

5.3.1 The relevance of PS1 and PS2 in MCAM-CTF cleavage

A number of transmembrane proteins undergo sequential shedding of the intracellular domain following metalloproteinase-mediated cleavage of the ectodomain. Typically, this is carried out within the plane of the cell membrane by intramembrane proteases, including γ-secretase. Presenilin knockout cells (PSKO; including PS1 KO, PS2 KO and PS1/2 dKO cells) were used to investigate the possibility that the MCAM-CTF is cleaved by γ-secretase. WT HEK293 cells, PS1/2 dKO HEK293 cells, and PS1 and PS2 single KO HEK293 cells (PS1 KO and PS2 KO, respectively) were transiently transfected with MCAM and immunoblot analysis was performed on whole cell lysates. As shown in Figure 5-1A, HEK293 PS1/2 dKO cells contained higher relative levels of MCAM-CTF compared to the HEK293 WT cells. Interestingly, each of the single KO cell lines expressed lower levels of full-length MCAM but had similar total protein expression levels compared to the WT or dKO cells. When normalised to full-length MCAM, the level of MCAM-CTF was lowest in the PS2 KO and highest in the PS1/2 KO. Meanwhile, the relative amount of MCAM-CTF in PS1 KO cells was similar to HEK293 WT cells (Figure 5-1B). None of these differences in MCAM expression were significantly different compared to HEK293WT controls ($p>0.05$).

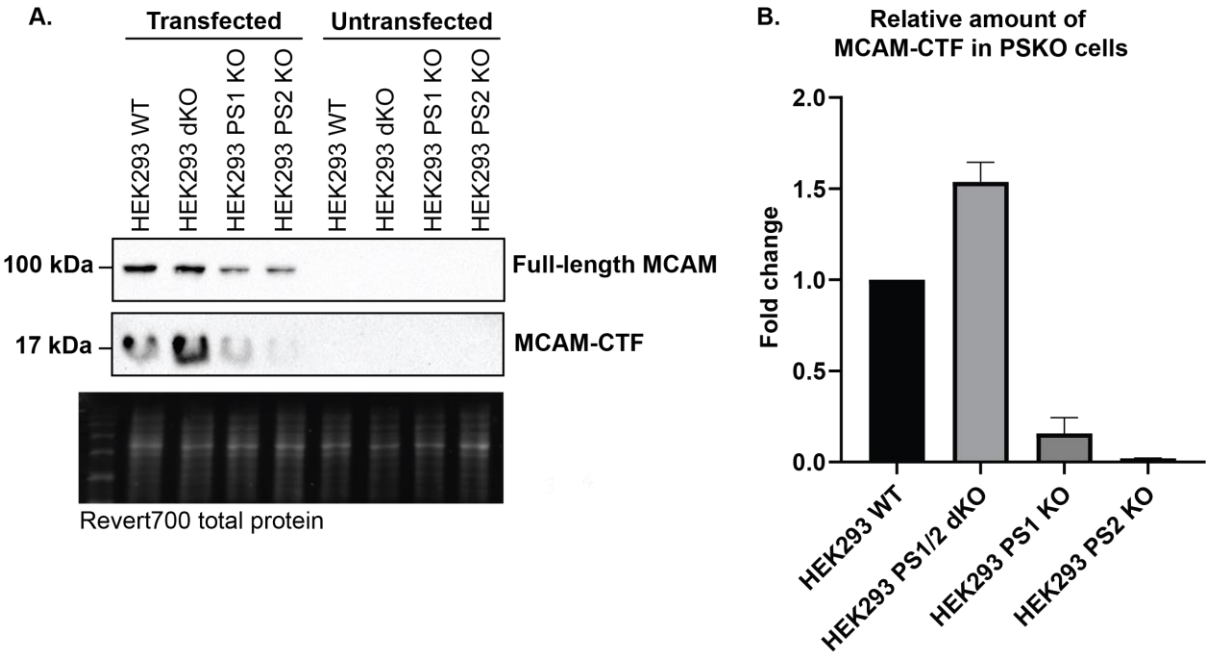

Figure 5-1 Effect of PS-1/2 knockdown on MCAM-CTF levels in HEK293 cells transiently transfected with full-length MCAM.

HEK293 WT and PS1/2 KO cells were transfected with full length MCAM and lysates harvested at 24-30 hours post-transfection (n=3). Samples were analysed by immunoblot for the presence of full length MCAM and the MCAM-CTF. HEK293 cells not transfected with MCAM were a negative control. In the transfected cels, levels of both species of MCAM were normalised to total protein loading. The amount of full length MCAM in each KO cell line was then normalised to the amount of full length MCAM in WT HEK293 cells; to generate a second normalisation factor. This was then used to express the amount of MCAM-CTF in each KO cell line relative to full length MCAM; compared to HEK293 WT. The accumulation of MCAM-CTF in the dKO cells suggests that it is a target of PS1 or PS2, such that the inability to undergo a secondary cleavage to generate the ICD fragment results in the accumulation of the larger, CTF fragment consisting of the ECD stub, TMD, and ICD. Error bars represent mean +/- SD.

Immunofluorescent labelling was then used to investigate the localisation of full-length MCAM in transfected cells, using the CC9 mAb. The staining pattern was similar in all cell lines tested, with localisation of MCAM to the cell membrane/periphery and throughout the cytoplasm (Figure 5-2). In addition, MCAM also showed some punctate staining in the nucleus in PS1 KO and PS1/2 dKO HEK293 cells, which is not commonly observed in melanoma cells.

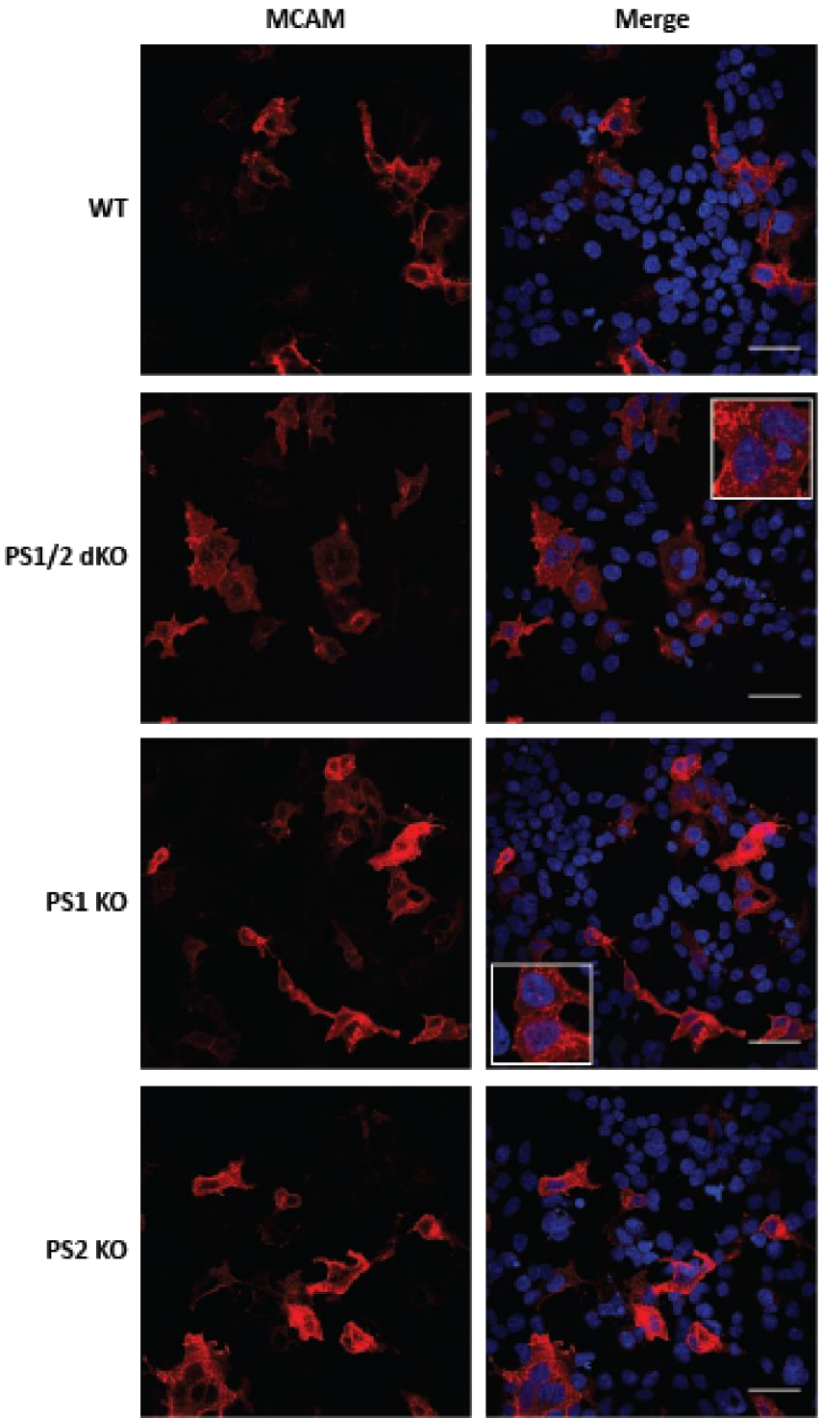

Figure 5-2 Localisation of MCAM in transfected HEK293 cell lines.

Cells were seeded into Poly-D-lysine coated wells and allowed to adhere overnight, before transfecting with full-length MCAM. Protein expression of MCAM was measured at ~24 hours post-transfection, using the CC9 mAb to probe for MCAM (n=3). There were no apparent morphological changes in transfected cells compared to untransfected cells (not shown), and all MCAM-expressing cells displayed a similar pattern of MCAM staining, which was localised to the cell membrane and throughout the cytoplasm. In some cases, there was punctate MCAM (full-length) staining also observed in the nucleus (insets) (scale bar in merged images is 50 μm).

5.3.2 Presenilin expression in melanoma cell lines

As MCAM-sh has been suggested to form part of a signalosome complex in endothelial cells, consisting of MCAM-sh, VEGFR1, VEGFR2 and PS-1 (Stalin *et al.*, 2016a), the expression of PS1 and PS2 was investigated in melanoma cells using a novel method for comparative quantitation of these proteins. This method was developed and performed by M. Eccles (Eccles *et al.,* unpublished, refer to Section 5.2.2). Three biological replicates of each cell line were used, and results are graphed as mean units (of PS1 or PS2) per µg of total protein, with mean and SD shown. Expression of PS1 was comparable between all cell lines (Figure 5-3A), taking into account the degree of variability between some replicates. In contrast, expression of PS2 was higher in MM96L, MM253, and A2058 melanoma cell lines, which are endogenous MCAM-expressing cells, and lower in SB2 and SB2 14.1 cells. The SB2 cell line, which does not express MCAM, showed the lowest level of PS2 expression. Meanwhile, SB2 14.1 cells that have been stably transfected to overexpress MCAM showed a slight increase in PS2 expression compared to their parental cell line. There was increased PS2-NTS in the MM96L and A2058 melanoma cells, but this did not reach statistical significance ($p>0.05$; non-parametric Kruskal-Wallis test) (Figure 5-3B). Representative immunoblots are shown in Figure 5-3C and Figure 5-3D.

To determine the functional relevance of PS1 and PS2 in melanoma cells, cells were initially treated with DAPT, a broad-spectrum γ-secretase inhibitor. Preliminary experiments were also carried out on MM253 cell lines with CRISPR-mediated knockout of PS1 and PS2, as shown below.

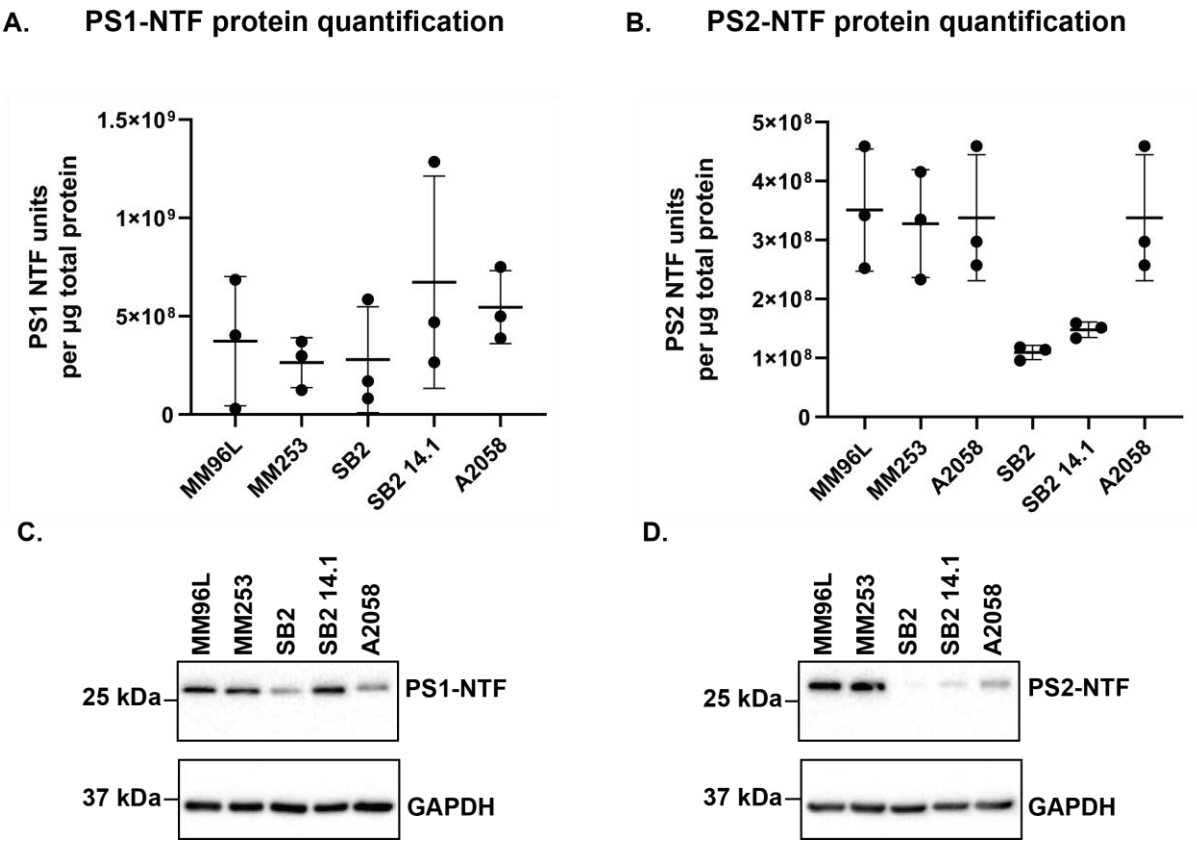

Figure 5-3 Protein expression of PS-1 and PS-2 in melanoma cell lines.

Expression of PS1 and PS2 in various melanoma cell lines was measured in whole cell lysates via immunoblot and quantitative analysis was performed (n=3; mean and SD shown). PS1 expression showed variability between individual replicates, however expression levels were relatively comparable across different cell lines (A). In contrast, there was a clear difference in the amount of PS2 expressed by endogenous MCAM-expressing cell lines, MCAM negative SB2 cells, and MCAM-overexpressing SB2 14.1 melanoma cells, but this difference was not significant ($p>0.05$) (B). A representative immunoblot is also shown for PS1-NTF detection (C) and PS2-NTF detection (D).

5.3.3 Inhibiting MCAM-CTF cleavage by blocking γ-secretase activity

Given that melanoma cells express PS1 and PS2, and that MCAM-CTF appears to be a substrate of PS1 and PS2, we next treated melanoma cell lines with DAPT, a potent γ-secretase inhibitor that effectively impairs Notch signalling (Feng *et al.*, 2019) and APP processing (Yang *et al.*, 2008). To investigate whether it affected MCAM-CTF processing, A2058, MM253 and SB2 14.1 melanoma cells were treated with increasing concentrations of DAPT (or DMSO) for ~24 hours under normal culture conditions. Immunofluorescent analysis of the MCAM-CTF revealed that treatment with DAPT typically resulted in an accumulation of MCAM-CTF in the

juxtanuclear region. Although subtle, the A2058 melanoma cells treated with DAPT appeared to have a slight increase in the amount of MCAM-CTF in the juxtanuclear region compared to DMSO-treated cells (Figure 5-4i). In MM253 melanoma cells, there was a small pool of intracellular MCAM-CTF within the juxtanuclear region of DMSO-treated cells, which became slightly more prominent in cells treated with 5-10 μM DAPT. Interestingly, these effects were not seen in cells treated with the highest concentration of DAPT (Figure 5-4ii). The effects of DAPT were most obvious in SB2 14.1 cells, where treatment with increasing concentrations of the drug were associated with an increase in the apparent amount of MCAM-CTF adjacent to the nucleus (Figure 5-4iii).

The above-mentioned results were also confirmed by immunoblot, using whole cell lysates collected from SB2 14.1, MM253, and A2058 cells treated with 0, 5, 10 and 20 μM DAPT for ~24 hours (Figure 5-5). After normalising expression based on full-length MCAM protein expression, it was apparent that DAPT-treatment led to a concentration-dependent increase in MCAM-CTF accumulation. This points towards γ-secretase being involved in MCAM proteolysis. Interestingly, despite A2058 cells not showing a clear visual increase in intracellular MCAM-CTF upon DAPT-treatment, immunoblot results suggest a concentration-dependent increase of MCAM-CTF in DAPT-treated A2058 cells. None of the changes in MCAM-CTF were statistically significant ($p>0.05$) according to the Kruskal Wallace test with Dunns multiple comparison.

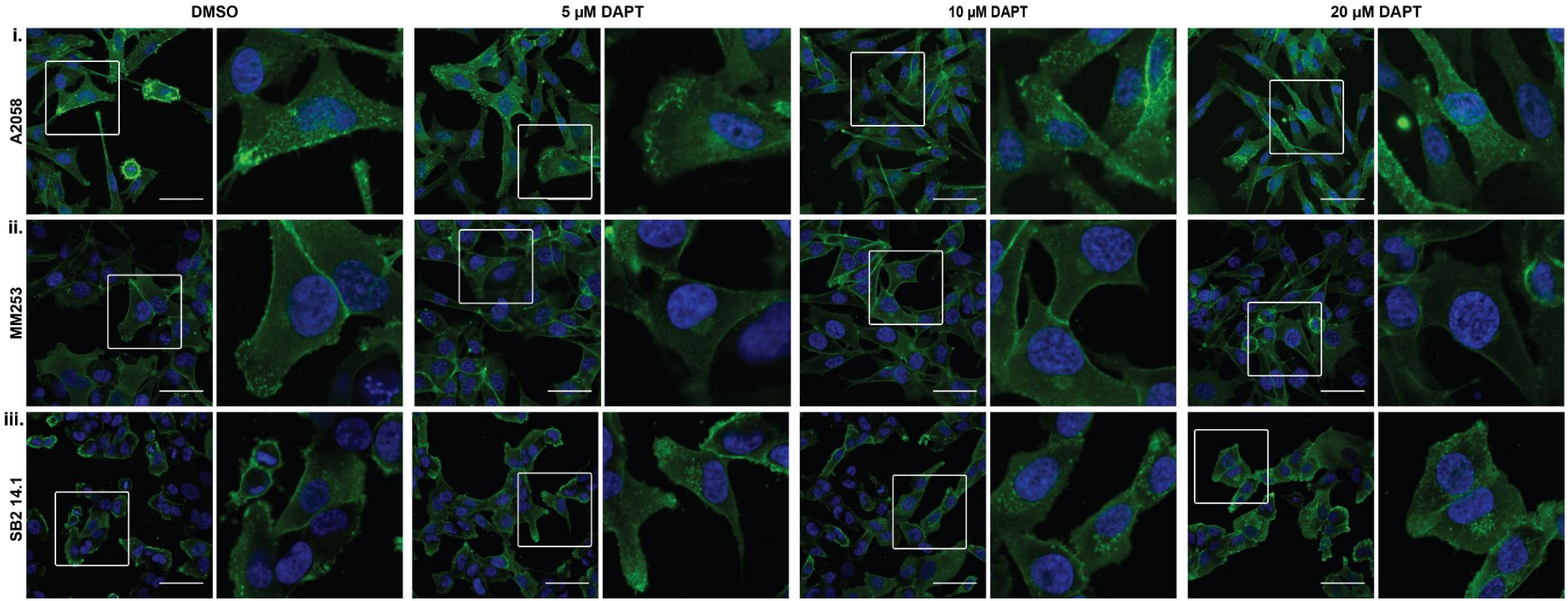

Figure 5-4 DAPT-treatment of melanoma cells leads to juxtanuclear accumulation of the MCAM-CTF.

Three melanoma cell lines were treated with increasing concentrations of DAPT for ~24 hours. The effect of DAPT on the localisation and processing of the MCAM-CTF was examined by immunofluorescent imaging (n=3). In A2058 cells (i), DAPT promoted a slight increase in the amount of intracellular MCAM-CTF in the juxtanuclear region. This was marginally clearer in MM253 cells (ii), where cells treated with 5 µM and 10 µM DAPT displayed a clearer pool of MCAM-CTF adjacent to the nucleus. In SB2 14.1 cells (iii), DAPT treatment led to a significant intracellular accumulation of MCAM-CTF in the juxtanuclear region. The scale bars in merged images are 50 µm; and boxed regions in each image are then enlarged in the next panel**.**

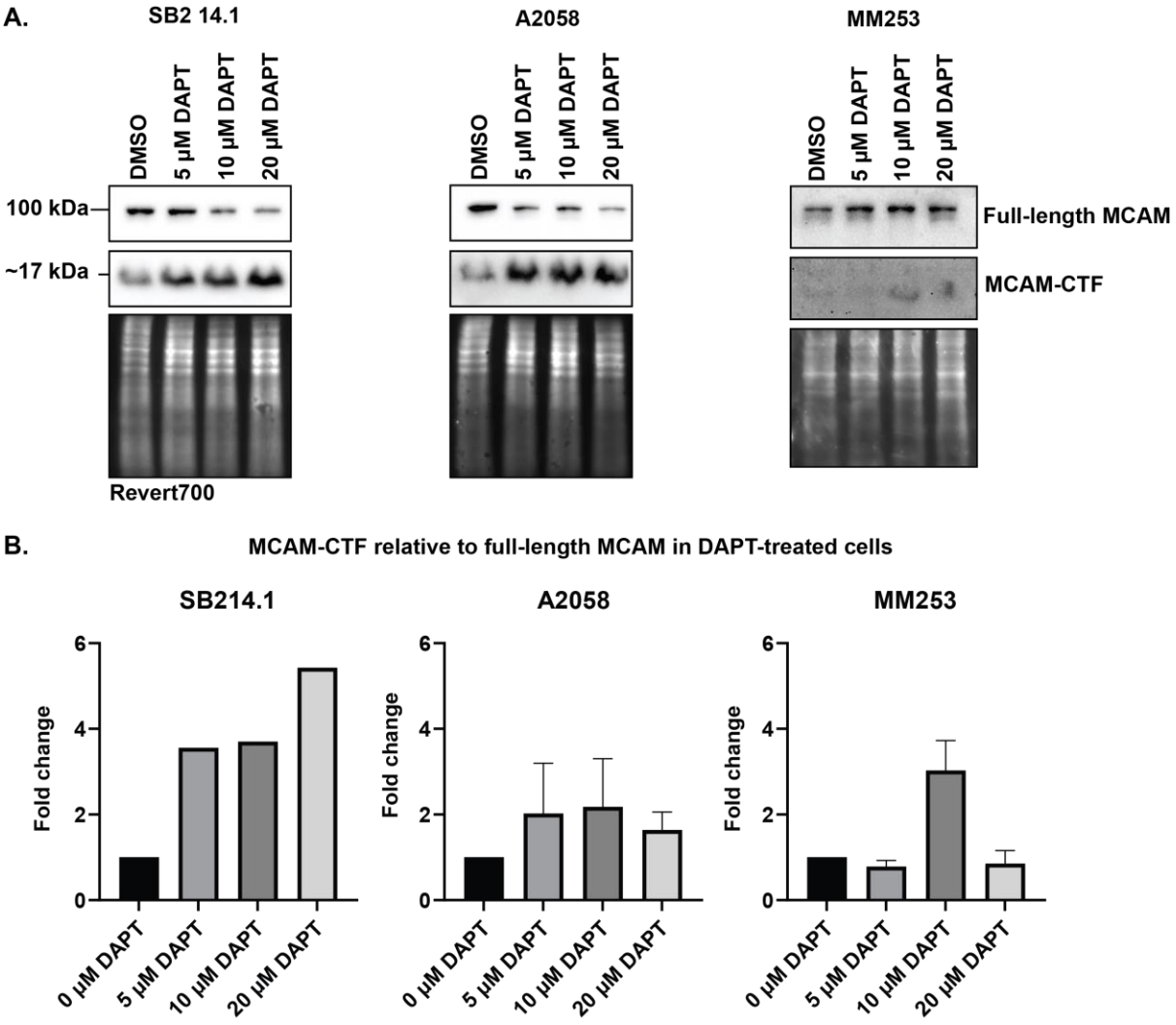

Figure 5-5 Effect of γ-secretase inhibition on the MCAM-CTF in melanoma cells.

SB214.1 (n=2), A2058 (n=3, mean and SD shown) and MM253 (n=3, mean and SD shown) melanoma cells were treated with DAPT and the effect on MCAM-CTF processing was determined by immunoblot. Accumulation of MCAM-CTF was evident in DAPT-treated samples compared to those treated with DMSO (A) The amount of MCAM-CTF was calculated relative to full-length MCAM, which showed a general trend towards MCAM-CTF accumulation following treatment with DAPT, although this was not statistically significant.

5.3.4 Knockdown of PS1 and PS2 in melanoma cells

A CRISPR/Cas9 approach was used to knockout PS1 and PS2 in MM253 melanoma cells. These cells were chosen for knockout studies, as in the initial expression screen, they were shown to express both PS1 and PS2; and we had previously explored MCAM cleavage in these cells. Knockout was performed by Dr Danielle Dye and clones chosen following PCR (data not shown) and immunoblot screening (Appendix M, see also Sections 5.2.4 and 5.2.5). Control cells were also produced

by transfecting MM253 cells with an empty vector and subjecting them to the same processing as the knockout clones.

Selected KO cell lines were used for MCAM cleavage studies, with PS expression confirmed by PCR and immunoblot. Figure 5-6 demonstrates PS1 and PS2 expression in selected KO cell lines and their respective controls. For qPCR, expression of *PSEN1* and *PSEN2* was normalised to MM253 WT cells and the non-parametric Kruskal-Wallis test and Dunns multiple comparison test were used to determine whether any differences in expression were statistically significant. Control cells expressed similar amounts of *PSEN1* and *PSEN2* compared to WT cells. *PSEN1* expression was significantly reduced (but not absent) in PS1 KO cell lines and increased in both PS2 KO lines (Figure 5-6A). *PSEN2* expression was similar between WT, control, and PS1 KO#5, was slightly lower in PS1 KO#1, and was significantly lower ($p<0.01$) in both PS2 KO cell lines (Figure 5-6B). Knockout was also confirmed at the protein level, using antibodies directed against the N-terminal fragment (NTF) of PS1 and PS2. As expected, PS1-NTF and PS2-NTF were absent from PS1 and PS2 KO cell lines, respectively (Figure 5-6C and D), except for PS2 KO#9, which showed a minimal amount of PS2 protein expression. Interestingly, both PS1 KO cells showed no protein expression despite evidence of the presence of a small amount of mRNA *PSEN1* transcript.

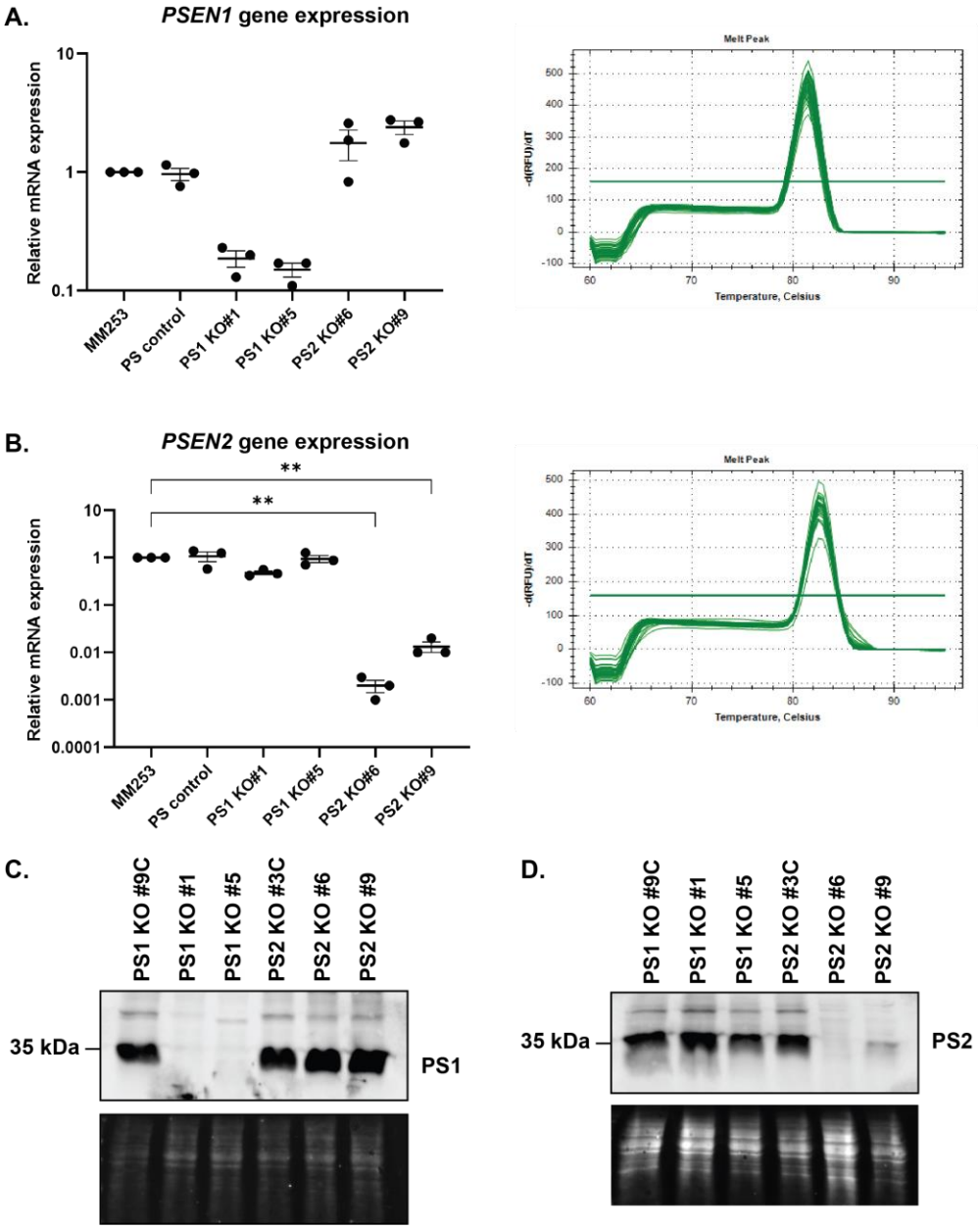

Figure 5-6 Knockdown/knockout of PS1 and PS2 in MM253 melanoma cells.

Expression of *PSEN1* and *PSEN2* in MM253 cells, including WT, control, PS1 KO and PS2 KO cell lines, was assessed using qPCR (n=3, mean and SEM shown). Knockout/down of *PSEN1* was confirmed in both PS1 KO cell lines, and there was a slight increase in *PSEN1* expression in the PS2 KO cell lines Neither of these trends were statistically significant compared to MM253 or CRISPR control cells. However, *PSEN1* expression in PS1 KO#5 (PS1 KO/KD cell line) and PS2 KO#9 (a PS2 KO cell line) was significantly different (*p<0.05). Melt curves are shown to the right (A). Knock-out/knockdown of *PSEN2* was also confirmed in PS2 KO samples, with both PS2 KO cell lines showing significantly reduced *PSEN2* expression compared to MM253 cells (**p<0.01). Melt curves are shown to the right (B). Immunoblot confirmed the level of PS1 protein was comparable between controls and PS2 KO and was absent from both PS1 KO cell lines (n=2). (C). Similarly, expression of PS2 protein was comparable between control and PS1 KO cell lines. Of the two cell lines selected from PS2 KO, PS2 KO#6 displayed complete KO, while PS2 KO#9 showed incomplete KO (n=3) (D).

5.3.5 MCAM processing in PS1KO and PS2KO MM253 cells

Once knockout/knockdown was confirmed, preliminary studies on MCAM expression were undertaken. Firstly, immunoblot was performed, using the MCAM-CTF-specific antibody to measure both full-length and MCAM-CTF expression in whole cell lysates. This demonstrated that expression of full-length MCAM was reduced in all KO cell lines tested, with the greatest reduction seen in PS1 KO#1 and PS2 KO#6. This overall trend was observed across four separate experimental replicates. Although we had hypothesized that PS KO may lead to accumulation of the MCAM-CTF, PS1 KO and PS2 KO resulted in a reduction in MCAM-CTF expression relative to the control cell lines. Non-parametric analysis using the Kruskal-Wallis test showed a significant reduction ($p<0.05$) in the relative amount of MCAM-CTF in two of the KO cell lines, PS1 KO#1 and PS2 KO#6, relative to their respective controls (Figure 5-7A). In line with immunoblot results of total MCAM levels, flow cytometric analysis of surface MCAM expression showed a notable reduction in MCAM expression on PS1 KO#1 and PS2 KO#6 MM253 cells compared to the WT and control samples. Surface MCAM expression was also reduced on MM253 PS2 KO#9 (Figure 5-7B), but to a lesser extent. Interestingly, KO of PS1 in PS1 KO#1 and PS2 in PS2 KO#6 was also associated with reduced expression of MCAM-l mRNA (Appendix N). Considering these results, MM253 PS1 KO#5 and MM253 PS2 KO#9 were selected for subsequent work investigating MCAM-CTF subcellular localisation in the presence and absence of either PS1 or PS2.

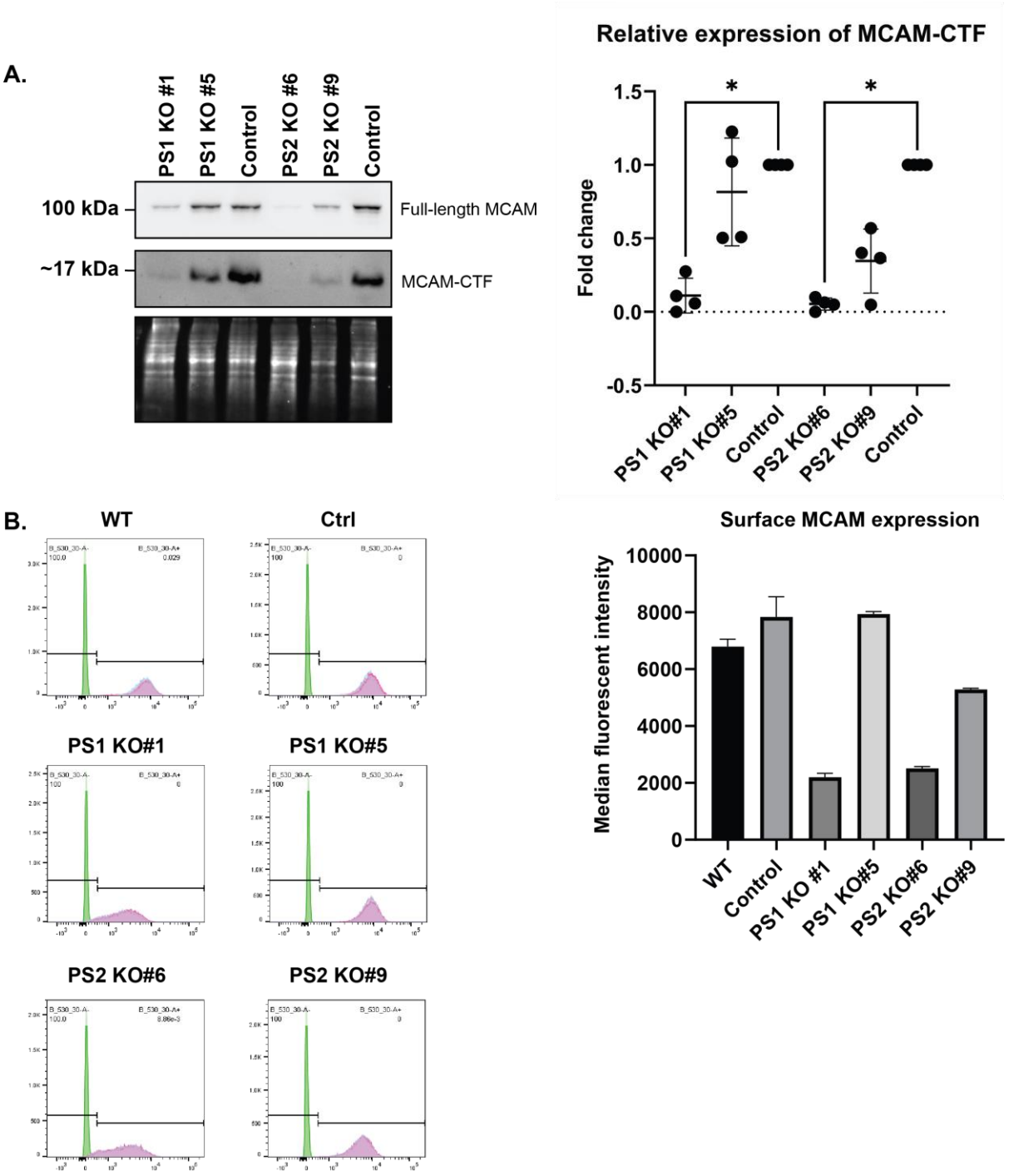

Figure 5-7 Expression of MCAM is altered in MM253 cells when expression of PS1 and PS2 is affected

The effects of PS1 and PS2 KO on MCAM expression in MM253 melanoma cells was measured by immunoblot (n=4 biological replicates) (A) and flow cytometry (n=3 technical replicates) (B). Expression of full-length MCAM at the cell surface was reduced in three of four cell lines, relative to control and WT cells. This was adjusted for when calculating the fold-change of MCAM-CTF expression. Relative to control cells, KO of PS1 led to reduced amounts of intracellular MCAM-CTF. This reduction was statistically significant in the PS1 KO#1 and PS2 KO#6 clones. Similarly, MCAM-CTF levels were greatly reduced in MM253 cells lacking PS2 expression. (Full-length MCAM exposure time 1 s; MCAM-CTF exposure time 115.9 s).

Subcellular localisation of MCAM was compared between WT (untransfected), control (transfected with empty vector), PS1 KO and PS2 KO cell lines using I.F. Both WT and control cells showed a similar staining pattern, including strong expression of MCAM at the cell surface and a low amount of intracellular MCAM that was more strongly localised to the cell projections. Importantly, the MCAM-CTF-specific antibody showed concentrated staining within the juxtanuclear region, as seen previously in melanoma cell lines (Figure 3-5), which is presumed to represent the product of MCAM ectodomain shedding (MCAM-CTF). However, it is important to note here that there was also a small amount of overlap with CC9 mAb staining in both the WT and control cells within this location (Figure 5-8; arrowheads). Meanwhile, there was little-to-no evidence of MCAM-CTF in the juxtanuclear region of PS1 KO#5 MM253 cells. Rather, these cells displayed an unusual staining pattern for MCAM-CTF, with concentrated expression within cell processes. Whilst there was some overlap with CC9 mAb, it appears that the MCAM-CTF pool detected by immunoblot may be represented by an accumulation of MCAM-CTF at the cell periphery. Expression of full-length MCAM at the cell surface was more intense at cell-cell junctions in these cells, whilst intracellular MCAM was diffuse. PS2 KO#9 showed similarities to both WT and control, and PS1 KO#5 staining, including concentrated expression of MCAM-CTF in the juxtanuclear region. However, the cytoplasmic staining pattern was comparable to PS1 KO cells, in that it was more diffuse. Regarding overall cell morphology, PS1 KO#5 cells showed the most distinct changes compared to WT and control MM253 cells. As shown with I.F. staining, these cells typically formed more short projections, whilst WT and control cells displayed a longer, more stretched out morphology. In addition, the WT and control cells had focal expression of MCAM at the leading edge - possibly within focal adhesions - which was not consistent in PS1 KO#5 cells.

LAMP2 is a marker of late endosomes and lysosomes and has been found to co-localise with MCAM in melanoma cell lines (Figure 3-7). Consistent with previous results, the MCAM-CTF localised with LAMP2-positive structures in the juxtanuclear region of MM253 WT cells. A similar degree of colocalization was seen in control cells. This is represented by overlapping staining, shown in orange (Figure 5-9; arrows). There was no evidence of MCAM-CTF localising specifically in LAMP2

positive structures in PS1 KO#5 as MCAM-CTF does not typically accumulate around the nucleus in these cells. However, in the PS2 KO#9 cells, some displayed MCAM-CTF accumulation in the perinuclear region and co-localisation with LAMP2. Importantly, there was evidence of some non-specific staining in the green channel in cells co-stained with MCAM and LAMP2. This non-specific fluorescence was mainly localised to the nucleus, as was observed in cells stained with an anti-rabbit IgG mAb isotype control (depicted in Appendix O). Consequently, it was not appropriate to perform quantitative analysis on co-localisation between MCAM-CTF and LAMP2. Importantly, the non-specific staining was not seen in cells stained with a mouse IgG2a isotype control antibody, meaning it was likely related to the rabbit antibody used in this study. Alternative lysosome markers will be considered for future studies.

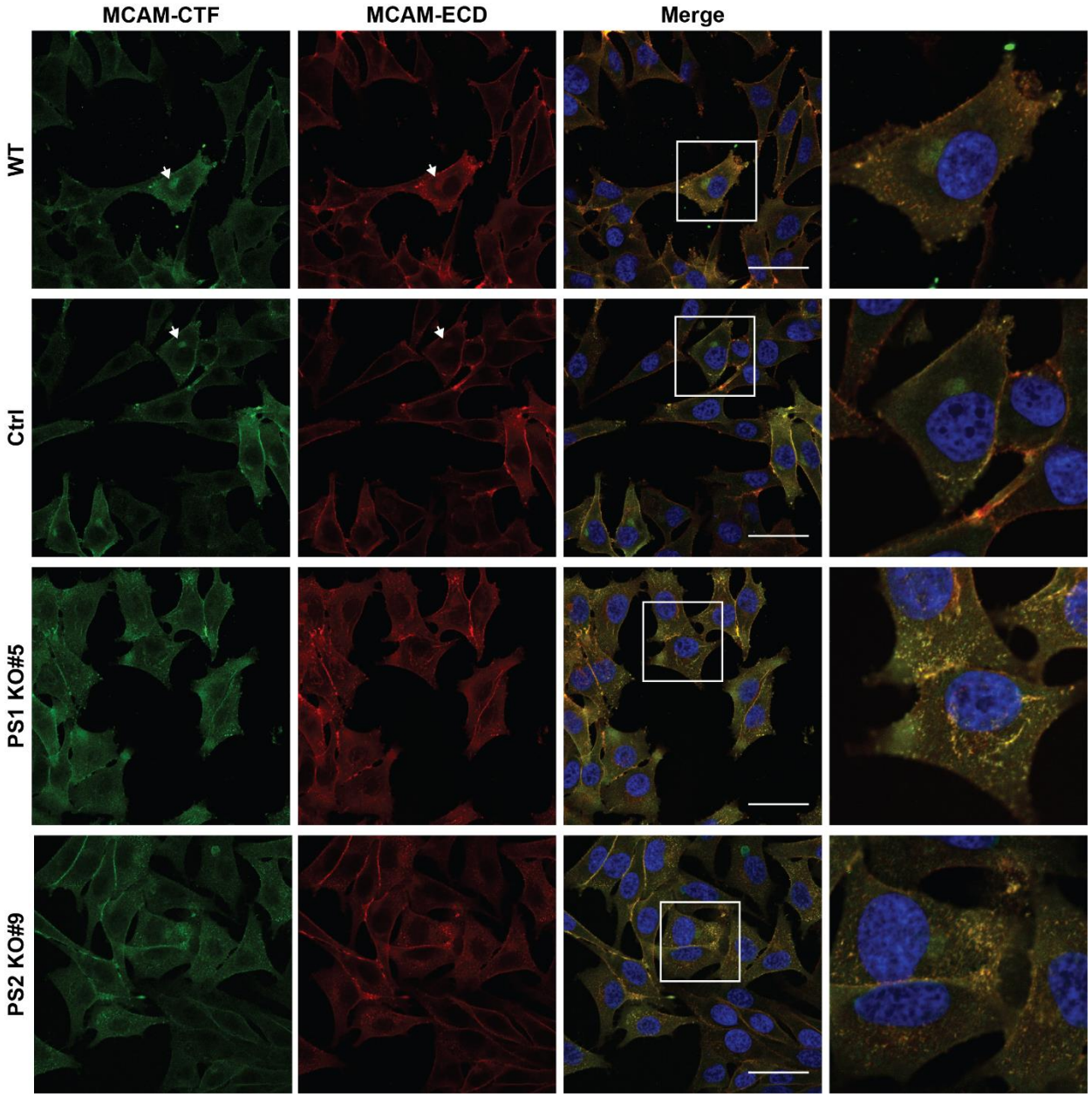

Figure 5-8 Localisation of full-length MCAM and MCAM-CTF in MM253 cells is affected by PS1 and PS2 KO

Expression and localisation of full-length MCAM and MCAM-CTF in MM253 cells was assessed using antibodies against the MCAM-ECD (red) and MCAM-CTF (green) (n=2). Overlap of the two stains, as shown in yellow/orange in the merged image, represents expression of full-length MCAM. Expression of full-length MCAM at the cell periphery was consistent in all cell lines tested but was most obvious in MM253 WT and control (ctrl) cell lines. In PS1 KO#5 and PS2 KO#6 cells, full-length MCAM was expressed throughout the cytoplasm. Arrows represent areas of MCAM-CTF accumulation, although there was a low amount of signal produced by the MCAM-ECD mAb in these areas. The scale bars in merged images are 50 µm; and boxed regions in each merged image are then enlarged in the next panel.

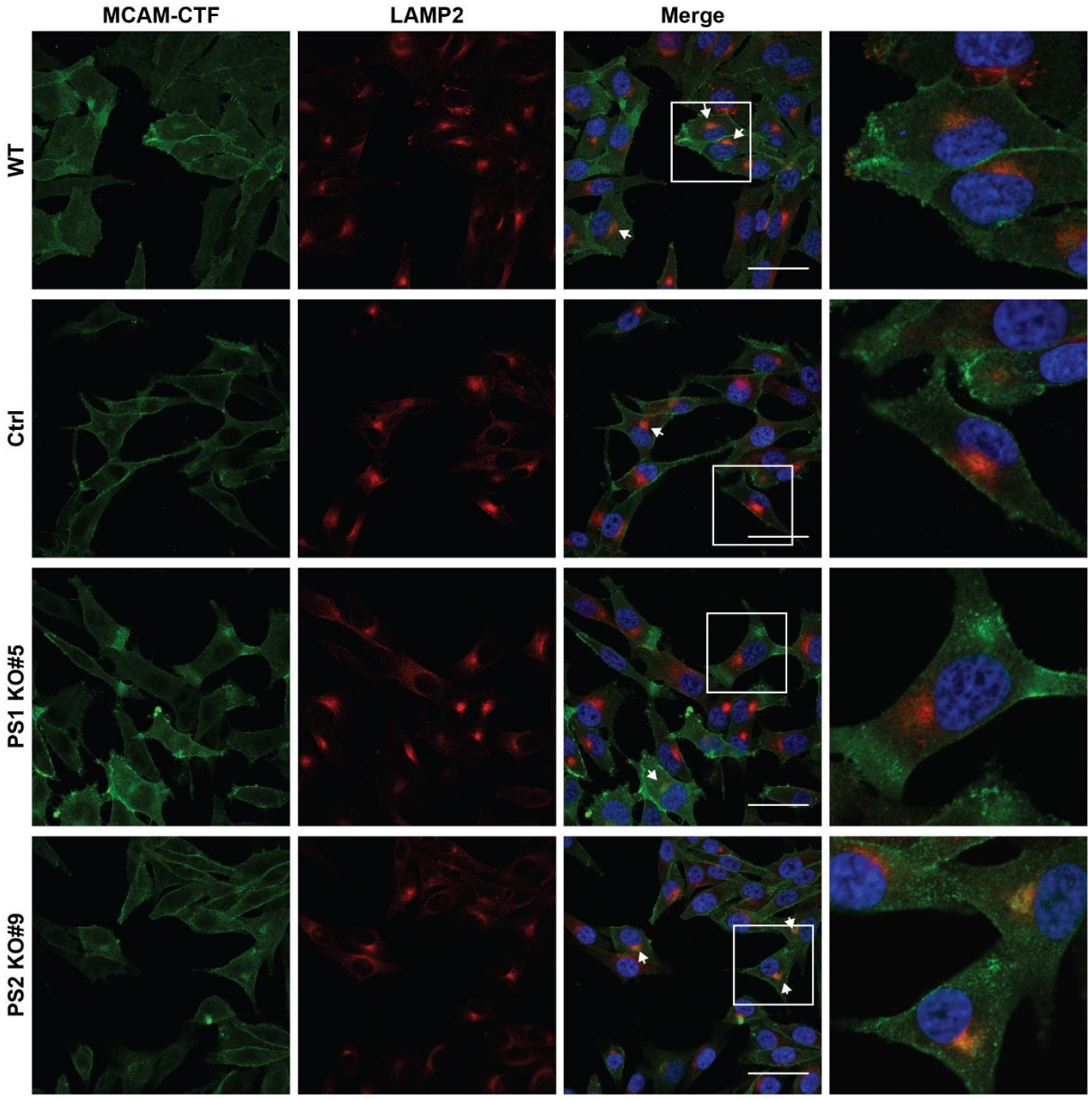

Figure 5-9 Co-localisation between MCAM-CTF and lysosomal markers is affected by PS1 and PS2 KO.

LAMP2 expression in MM253 melanoma cells was most concentrated in the juxtanuclear membrane, with some weaker staining also seen throughout the cytoplasm. MCAM-CTF localised within these structures in both WT and control (ctrl) MM253 cell lines, where there was evidence of MCAM-CTF accumulation in the juxtanuclear region (arrows and merged images). In MM253 PS1 KO#5, MCAM-CTF accumulation occurred in the cell processes and not in the juxtanuclear region, so did not co-localise with LAMP2. Similarly, PS2 KO#9 cells did not have strong evidence of MCAM-CTF expression concentrated in the juxtanuclear region, however there was some overlap with LAMP2-positive structures (red-orange staining in the magnified image). The scale bars in merged images are 50 µm; and boxed regions in each merged image are then enlarged in the next panel.

5.4 Discussion

Regulated intramembrane proteolysis is, by definition, a proteolytic event involving the sequential cleavage of membrane-spanning proteins, generating soluble extracellular and intracellular protein fragments (Brown *et al.*, 2000). The second cleavage event occurs within the plane of the cell membrane, and involves proteases collectively known as intramembrane cleaving proteases (iCliPs). These encompass γ-secretase (Güner & Lichtenthaler, 2020), signal peptide peptidases (Weihofen *et al.*, 2002), site-2 proteases (Rawson, 2013), and rhomboid-type serine proteases (Lemberg & Freeman, 2007), which cleave their respective substrates to release intracellular domains that are either destined to become functional molecules (i.e. transcription regulators), or are rapidly degraded (McCarthy *et al.*, 2017).

PS1 and PS2 are well-known proteases that form part of the γ-secretase complex and are implicated in Alzheimer's disease through processing of amyloid precursor protein (APP) (Zhang *et al.*, 2013), as well as cancer progression related to Notch processing (McCaw *et al.*, 2021). Beyond their relevance in APP and Notch processing- and indeed in processing of over 140 other membrane substrates (Güner & Lichtenthaler, 2020) - PS1 and PS2 have also been recognised for their non-proteolytic functions, independent of γ-secretase (Zhang *et al.*, 2013). In particular, a growing number of studies over recent years have reported on the involvement of both PS1 and PS2 in Ca^{2+} regulation, particularly in mitochondrial Ca^{2+} homeostasis (Rojas-Charry *et al.*, 2020) and autophagy (Fedeli *et al.*, 2019; Lee *et al.*, 2010a; Rojas-Charry *et al.*, 2020). Additionally, PS1 has been implicated in the formation and maintenance of intercellular adhesions, which mainly relies on its recruitment to the cell periphery by β-catenin (Singh *et al.*, 2001).

Importantly, among the 149 γ-secretase substrates identified in a review by Güner and Lichtenthaler (2020), MCAM/CD145/MUC18 was not listed as a known substrate, however an earlier study by Stalin *et al.* (Stalin *et al.*, 2016a) suggest that MCAM-CTF may be processed by PS1 in endothelial cells. Here, MCAM-sh was found in a cellular fraction containing VEGFR1, VEGFR2, Angiomotin p80, and PS1 which, together with MCAM-sh, were proposed to form a signalosome complex. In

addition, γ-secretase treatment prevented translocation of MCAM-sh-CTF/ICD to the nucleus, even in the presence of rsMCAM (Stalin *et al.*, 2016a). Whilst this provides evidence towards MCAM-sh being a substrate of γ-secretase, our study is the first to demonstrate the processing of MCAM-l-CTF by γ-secretase in melanoma cells.

Further, this is the only study to our knowledge that has explored the involvement of both PS1 and PS2 in MCAM processing in melanoma cells. We initially confirmed MCAM-CTF processing by PS1 and PS2 using MCAM-expressing HEK293 cells with either PS1 KO, PS2 KO, or double KO of both PS1 and PS2. Whilst KO of the individual PSs did not prevent processing of the MCAM-CTF, it was clear from PS1/2 dKO HEK293s that MCAM-CTF cleavage requires expression of either PS1 or PS2. Expression of PS1 and PS2 was then confirmed in melanoma cell lines by immunoblot, and quantification was performed using a novel model developed by Ms Melissa Eccles. This method uses a fusion protein encompassing domains of PS1 and PS2 to enable direct quantification and comparison of PS1 and PS2 protein levels (2022; personal communication). From this it was apparent that the relative expression of PS1 is consistent across multiple melanoma cell lines. Interestingly *PSEN1*, the gene encoding PS1, has been identified for its role as an anti-apoptotic gene in some malignant melanoma cell lines (Su *et al.*, 2009), however the relevance of PS1- γ-secretase in melanoma is unknown. Since PS1 is a candidate protease for γ-secretase -mediated cleavage of many other proteins and is implicated in the progression of various tumours, including gastric cancer (Li *et al.*, 2016), hepatocellular carcinoma (Shen *et al.*, 2018), bladder cancer (Deng *et al.*, 2015), and colorectal cancer (Taniguchi *et al.*, 2003), it likely also plays a role in melanoma progression - a role that may not necessarily involve MCAM-CTF cleavage.

Interestingly, endogenous expression of PS2 is reportedly higher than PS1 in certain tumour cells, including melanomas (Sannerud *et al.*, 2016). It has recently been reported that low PS1 expression may be a significant feature of aggressive melanomas (Sidor *et al.*, 2022). Of interest in the present study, the expression of PS2 was more variable between melanoma cells, particularly between endogenous

MCAM-expressing cell lines and MCAM-overexpressing cell lines. The lower level of PS2 expression in SB2 14.1 melanoma cells (and the SB2 parental cell line), coupled with the significant accumulation of MCAM-CTF in these cells (as shown in Chapter 3), is consistent with the theory that PS2 is involved in MCAM cleavage. And although we were unable to perform studies on the sub-cellular localisation of PS1 and PS2 in melanoma cells, localisation of the MCAM-CTF within LAMP2-positive structures in the juxtanuclear region of melanoma cells also provides evidence that PS2 is responsible for MCAM-CTF cleavage in melanoma cells. An elegant study performed by Sannerud *et al.* (2016) demonstrated that PS2 expression is restricted to LAMP1-positive late endosomes and lysosomes, where it performs proteolytic processing of its substrates (Sannerud *et al.*, 2016), including epithelial cell adhesion molecule (EpCAM) (Maetzel *et al.*, 2009), and a pathologically relevant intracellular pool of amyloid-β (Williamson *et al.*, 2017). LAMP1 and LAMP2 are both involved in lysosomal biogenesis and serve as markers for this organelle (Eskelinen, 2006).

Similar results were seen in MM253 melanoma cells, whereby CRISPR-mediated KO of either *PS1* or *PS2* did not appear to impair cleavage of the MCAM-CTF. Interestingly, however, it did affect the expression of full-length MCAM, such that levels of full-length MCAM were reduced in the HEK293 PS1KO and PS2KO cells, as well as in MM253 melanoma cells with KO of either *PS1* or *PS2*. The exact cause of this is unclear, however it hints that interrupting normal PS function has a global effect on protein processing and expression. Indeed, PS1 and PS2 have important roles beyond simply catalysing the cleavage of γ-secretase substrates. For example, both PS1 and PS2 are important for autophagy. This has been shown in murine neuroblastoma cells and in murine blastocysts, where PS1 mutation or KO lead to impaired autophagy due to lack of lysosomal acidification (Lee *et al.*, 2010a; Rojas-Charry *et al.*, 2020). Similarly, familial Alzheimer's disease-related mutations of PS2 have been linked to decreased recruitment of Rab7-GTPase, and subsequent impaired autophagy (Fedeli *et al.*, 2019).

Importantly, we confirmed that γ-secretase was involved in MCAM-CTF processing by treating melanoma cells with DAPT, a broad-spectrum inhibitor that is widely used to impair the proteolysis of γ-secretase substrates (Hachmeister *et al.*, 2013). Treating melanoma cells with DAPT provided similar results to the PS1/2 dKO in HEK293 cells, such that total inhibition of γ-secretase activity led to retention of the MCAM-CTF. In SB2 14.1 and MM253 melanoma cells, MCAM-CTF was predominantly localised to the juxtanuclear region of DAPT-treated cells.

Collectively, the results given in this chapter suggests that both PS1 and PS2 may be capable of cleaving MCAM. This is not an unknown concept, given the previous publication of a paper suggesting that PS1 and PS2 may act interchangeably to cleave various substrates (Kim *et al.*, 2011). Such an observation has also been made for nectin-1 processing, whereby KO of PS1 in mouse embryonic fibroblasts impaired its cleavage, but this could be partially restored by expression of PS2 (Kim *et al.*, 2011). Given that PS1 and PS2 are both expressed in melanoma cell lines, albeit at different levels, this may allow MCAM-CTF to undergo constitutive cleavage, with a preference for PS2 mediated cleavage, but potential for PS1 to cleave MCAM-CTF, in its absence.

5.5 Conclusions

Ectodomain shedding leaves behind a remnant fragment consisting of a short stub of the extracellular domain, the transmembrane domain, and the intracellular domain. Generally, removal of the ectodomain is considered essential for further proteolytic processing of transmembrane proteins by γ-secretase. In the absence of γ-secretase activity, such as through pharmacological inhibition of γ-secretase or impaired expression of PS1 or PS2 (which can occur in Alzheimer's disease), abnormal accumulation of protein CTFs is typically observed. In the present study, we demonstrated impaired processing of the MCAM-CTF in melanoma cell lines following pharmacological inhibition with DAPT. This was evident by the increased expression of MCAM-CTF relative to full-length MCAM, as measured by immunoblot, and the accumulation of MCAM-CTF in the juxtanuclear region, which was observed by I.F. staining.

Whilst we hypothesised that PS2-γ-secretase may be responsible for MCAM-CTF processing (rather than PS1-γ-secretase), initial data collected from MCAM-expressing HEK293 PS1/2 dKO cell lines indicated that KO of both PSs was required to prevent MCAM-CTF cleavage. Meanwhile, KO of a single PS did not affect the relative amount of MCAM-CTF but was associated with lowered expression of full-length MCAM. This was explored in MM253 melanoma cell lines, and a similar observation was made. Of the multiple KO cell lines generated, two of each PS1 KO and PS2 KO were selected for further study. In line with data collected from HEK293 PS1 KO and PS2 KO, the MCAM-CTF did not accumulate in MCAM-expressing MM253 cells in which either PS1 or PS2 alone had been knocked out. Interestingly, surface expression of full-length MCAM expression was also altered/decreased. This points towards 1) a possible compensatory mechanism whereby KO of one PS leads to increased activity of the other, and 2) a potential feedback mechanism whereby altered CTF processing prevents nuclear translocation of the MCAM-ICD and therefore disrupts gene transcription that is normally required for constitutive expression of MCAM. That MCAM-CTF accumulates in the juxtanuclear region within LAMP2-positive LE/lysosomes indicates that PS2 within these structures may be predominantly responsible for MCAM-CTF cleavage, however it seems apparent that PS1 can also carry out this function in the absence of PS2. Collectively, data reported on here hints towards both PS1 and PS2 being capable of further cleaving the MCAM-CTF.

Chapter 6

MCAM intracellular binding partners and regulation of shedding through post-translational modification

6.1 Introduction

The regulation of ectodomain shedding can be controlled at multiple levels, including at the substate level or, less frequently, at the sheddase level. Whilst anchorage of ADAM17 to the plasma membrane (Li *et al.*, 2007) and exposure to phosphatidylserine at the cell membrane (Veit *et al.*, 2019) have each been shown to be involved in ADAM17 activity, the ubiquitous expression of ADAMs and MMPs, along with their promiscuous cleaving nature, suggests that that cleavage is more likely to be regulated at the substrate level. This may be via extracellular factors (e.g. growth factors, cytokines) (Singh *et al.*, 2005), post-translational modifications (e.g. glycosylation, palmitoylation) (Akasaka-Manya *et al.*, 2016; Bhattacharyya *et al.*, 2013; Karabasheva *et al.*, 2014), or binding of intracellular ligands (e.g. moesin, calmodulin) (Rzeniewicz *et al.*, 2015). Additionally, substrate dimerisation may promote cleavage of transmembrane proteins, which has been reported for both CD44 and Neuregulin-1 (Hartmann *et al.*, 2015). Regardless of external regulatory factors, ectodomain shedding requires transmembrane proteins to be accessible to sheddases at the cell membrane, resulting in the release of soluble proteins. Hence, factors such as endocytosis (Basagiannis & Christoforidis, 2016) can also contribute to the regulation of ectodomain shedding.

Alternatively, soluble proteins may be a product of alternative splicing. MCAM is known to undergo alternative splicing of exon 15 to produce two transmembrane isoforms: MCAM-l and MCAM-sh (Lehmann *et al.*, 1989; Sers *et al.*, 1993). In addition, the avian homologue of MCAM, HEMCAM, also exists as a soluble isoform that is generated by alternative splicing (Vainio *et al.*, 1996). Recent evidence suggests that in humans, sMCAM can be produced by alternative splicing (Nollet *et al.*, 2022), although the main evidence thus far supports that ectodomain shedding is the main source of sMCAM (Stalin *et al.*, 2016a). Importantly, our current understanding of sMCAM production in human cells is largely based on studies performed in endothelial cells and the short isoform of MCAM. Meanwhile, there is little research into the cleavage of MCAM-l, which is the predominant isoform expressed by melanoma cells (as shown in Chapter 3).

Despite differing only in the intracellular region, the MCAM-l and MCAM-sh isoforms are both structurally and functionally distinct. Whilst both MCAM-l and MCAM-sh contain an ERM binding site and PKC phosphorylation site within the intracellular tail, only MCAM-sh possesses a PDZ domain. Meanwhile, MCAM-l has an additional phosphorylation site for PKC, a di-leucine motif, and a tyrosine/endocytosis motif (Stalin *et al.*, 2017). These distinctions can account for the different subcellular localisation of each isoform (Guezguez *et al.*, 2006), as well as cell-specific migrating capacity and signalling abilities (Guezguez *et al.*, 2007; Luo *et al.*, 2012).

Considering the additional amino acid sequence of the intracellular domain of MCAM-l compared to MCAM-sh, it is likely that ectodomain shedding of each isoform is regulated differently, at least in part. As such, understandings of the proteolytic processing of MCAM-sh in endothelial cells cannot be directly translated to melanoma cells, which predominantly express MCAM-l (see Figure 3-2). Therefore, further study into the regulation of MCAM-l ectodomain shedding in melanoma cells is warranted.

We explored the effect of glycosylation and palmitoylation on MCAM cleavage. Glycosylation is known to specifically regulate the cleavage susceptibility of substrates such as TNF-α and APP (Akasaka-Manya *et al.*, 2016; Goth *et al.*, 2015), but is also associated with protein stability, which indirectly may enhance cleavage (Yang *et al.*, 2015). Although there is limited data exploring the role of palmitoylation in regulating ectodomain cleavage, evidence suggests that palmitoylation of specific resides in APP affects cleavage (Bhattacharyya *et al.*, 2013).

MCAM has eight putative N-glycosylation sites, mainly located in the external juxtamembrane region (Wang *et al.*, 2020), which is also where ectodomain cleavage is believed to occur. Bubka *et al.* (2014) found that MCAM undergoes N-glycosylation by Golgi beta-1,4-mannosyl-glycoprotein 4-beta-N-acetyl-glucosaminyltransferase (*MGAT3*) and alpha-1,6-mannosylglycoprotein 6-beta-N-acetylglucosaminyltransferase A (*MGAT5*). Increased levels of these enzymes in melanoma cells were associated with increased amounts of bisected and β1,6

branched N-glycans on MCAM. However, the viability and motility of melanoma cells were not affected by these differences (Bubka *et al.*, 2014). Interestingly, a recent study also reported for the first time that MCAM undergoes O-glycosylation by glycosyltransferase β-1,3-galactosyl-oglycosyl-glycoprotein β-1,6-N-acetylglucosaminyltransferase-3 (GCNT3), and this modification enhanced the stability and half-life of MCAM (Sumardika *et al.*, 2018).

Palmitoylation of Cys590 in the MCAM cytoplasmic tail is associated with increased stability of MCAM in the cell membrane (Wang *et al.*, 2015). Thus, we hypothesized that inhibiting palmitoylation may decrease/destabilise MCAM surface expression and therefore alter ectodomain cleavage.

We were also interested in binding partners of the MCAM cytoplasmic tail. Moesin has previously been found to link the intracellular domain of MCAM to the cytoskeleton, promoting the formation of microvilli and associated cell migration (Luo *et al.*, 2012). Moesin was also found to promote ectodomain shedding in L-selectin, whilst calmodulin (CaM) was found to inhibit shedding (see Section 1.3.2.3) (Rzeniewicz *et al.*, 2015). It is also possible that moesin, CaM and L-selectin form a protein complex to regulate shedding (Deng *et al.*, 2013a), and this is further influenced by membrane lipid composition. Accordingly, we sought to investigate these potential regulatory mechanisms of shedding in the context of MCAM-l. We also hoped to identify new binding partners of the intracellular domain of MCAM via a pull-down assay, which may contribute to the regulation of shedding.

Approach: this chapter describes a range of experimental approaches used to explore the regulation of MCAM shedding in melanoma cell lines. Firstly, the potential for calmodulin and moesin to reciprocally regulate MCAM shedding was explored. Expression of CaM was confirmed by qPCR but was difficult to assess in melanoma cells using routine immunoblot and I.F. Further, attempting to inhibit its activity had toxic effects on both melanoma and non-melanoma cell lines. We also attempted a pull-down assay to identify additional binding partners of the intracellular domain of MCAM. Next, we investigated the effect of post-translational modifications

-glycosylation and palmitoylation- on MCAM cleavage. Whilst these were not positive findings overall, there are opportunities to further this work in the future, using the data collected here as a framework for more informed research.

6.2 Materials and Methods

6.2.1 Immunofluorescence for MCAM co-localisation

Cells were grown to confluence on collagen-coated coverslips. Wounding was performed using a P1000 pipette tip to make two parallel scratches in the monolayer. Detached cells were removed by gently rinsing the wells with warm media, then cells were incubated in normal culture media at 37^{o}C, 5% CO_2 for ~24 hours, allowing cells to migrate towards the wound. For moesin staining, cells were fixed with 4% PFA in HBS, and permeabilised using 0.1% TX-100 in HBS. Cells to be labelled for CaM were fixed and permeabilised by incubating with ice-cold methanol:acetone (1:1) for 5 min.

6.2.2 Immunoblot and qPCR for CaM expression in melanoma cells

Previously, it has been reported that reliable detection of Calmodulin on a PVDF membrane requires cross-linking of the protein to the membrane following transfer (Ivetic *et al.*, 2004; Kahn *et al.*, 1998). This was tested by either air-drying the membrane, followed by rehydration in ethanol, washing with PBS, and blocking; alternatively, membranes were washed with PBS, incubated with paraformaldehyde and washed with PBS. Membrane blocking and probing was performed as described in section 2.7.

qPCR analysis for *CALM-1, -2* and *-3* was performed as described in Section 2.12, using oligo sequences from Esteras *et al.* (2012); and normalised against the control genes *CASC3* and *RPS2.*

6.2.3 Chemical inhibition of CaM activity

Trifluoperazine dihydrochloride was serially diluted from a 100 mM stock in cell culture medium. Concentrations ranging from 0-500 µM were prepared, with DMSO was used as a vehicle control at a dilution of 1/200 in culture media. This reflected the dilution of DMSO present when trifluoperazine dihydrochloride was used at the highest concentration tested (500 µM). When SB2 14.1 (or mCHO) cells reached >70% confluence, cell culture media was removed, and monolayers were rinsed thrice with SFM to remove any traces of serum. TP was then added to each well and incubated at 37^{o}C.

6.2.4 Inhibiting protein glycosylation by Swainsonine treatment

Cells were seeded on normal TC plastic and allowed to adhere. Later the same day, cells were incubated with Swainsonine (SW)-containing media. SW inhibits Golgi α-mannosidase II, which plays a key role in the synthesis of complex N-glycans. SW was chosen as it is well tolerated by cells and leads to more subtle changes in glycan structure, compared to inhibitors such as tunicamycin which act early in glycan synthesis and can lead to endoplasmic reticulum (ER) stress. A range of concentrations of SW were tested (0.25, 0.5 and 1 µg/mL). DMSO was used as a vehicle control at a dilution of 1/200 in culture media, reflecting the dilution of DMSO present when SW was used at the highest concentration tested (1 µg/mL). After ~48 hours, media was collected, and monolayers were rinsed with PBS. Cells were detached and lysates were collected for immunoblot analysis, as described in Section 2.4 and 2.7.

6.2.5 Palmitoylation inhibition in melanoma cells

SB2 14.1 and A2058 melanoma cells were seeded on normal TC plastic and incubated O/N at 37^{o}C, 5% CO_2. The following day, cells were treated with 2-bromohexadecanoid acid (2-BP). Firstly, 2-BP was diluted from a 5M stock to a 500 mM working concentration in DMSO. Then, concentrations ranging from 10-250 µM were prepared in normal culture media and added to cells. After incubating for ~24 hours, cells were fixed, permeabilised, blocked, and immunofluorescently labelled for

the MCAM-CTF, as outlined in Section 2.8. Imaging was performed using the Nikon A1 confocal microscope.

6.3 Results

6.3.1 N-Glycosylation and palmitoylation may not regulate MCAM cleavage

Protein glycosylation has been reported to affect ectodomain shedding through altering protein stability. Since MCAM is heavily N-glycosylated and carries complex N-glycans (Bubka *et al.*, 2014), we treated melanoma cells with SW to inhibits the addition of these structures. The size of full-length MCAM in the lysate was reduced, in line with the loss of N-glycan structures (Figure 6-1), however a preliminary study indicated no significant change in the accumulation of MCAM-CTF to suggest that MCAM cleavage was upregulated due to loss of MCAM stability (Appendix P).

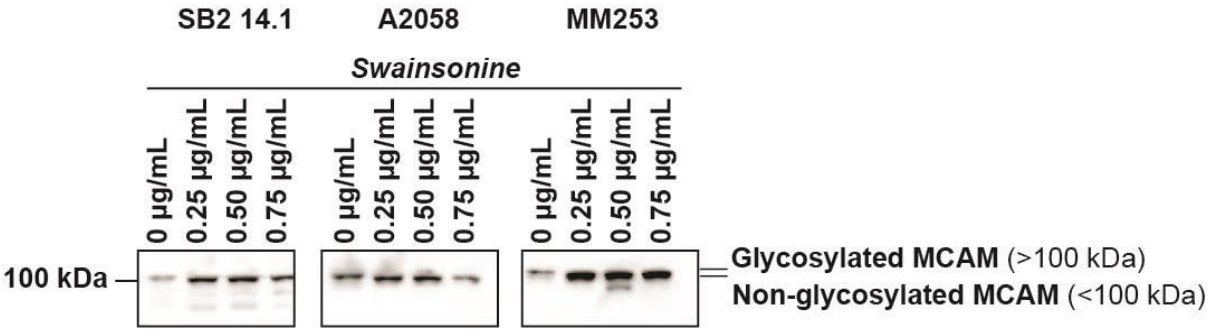

Figure 6-1 Swainsonine impaired MCAM N-glycosylation but not ectodomain shedding

SB2 14.1, MM253 and A2058 melanoma cells were incubated in the presence of increasing concentrations of Swainsonine (SW) for 48 hours to inhibit protein glycosylation (n=1). The loss of N-glycan structures was confirmed by the slightly lower molecular weight of full-length MCAM in treated cells compared to untreated cells.

In addition to N-glycosylation, MCAM can also undergo a post-translational modification process known as palmitoylation. This process involves the addition of palmitic acid to certain amino acid residues, which is important for targeting proteins to the cell membrane and stabilising them (Guan & Fierke, 2011; Shum *et al.*, 1996). MCAM can be reversibly palmitoylated at Cys590 (Wang *et al.*, 2015). Inhibition of

protein palmitoylation was achieved here by treating cells with 2-BP. Concentrations above 300 μM were found to cause loss of cell viability (data not shown), therefore concentrations between 0-250 μM were tested. Whilst 2-BP treatment appeared to affect the expression/localisation of MCAM to the cell surface, likely due to de-palmitoylation of MCAM impairing its localisation to membrane lipid rafts, it did not lead to a large increase in MCAM-CTF visualised in the juxtanuclear region of SB2 14.1 melanoma cells. This was evident in cells treated with any concentration of 2-BP Figure 6-2). Changes in cell morphology were also noted in treated vs. untreated cells, whereby cells appeared larger and flatter following incubation with 2-BP. As there were no striking differences in MCAM-CTF accumulation, experiments measuring sMCAM in media were not undertaken.

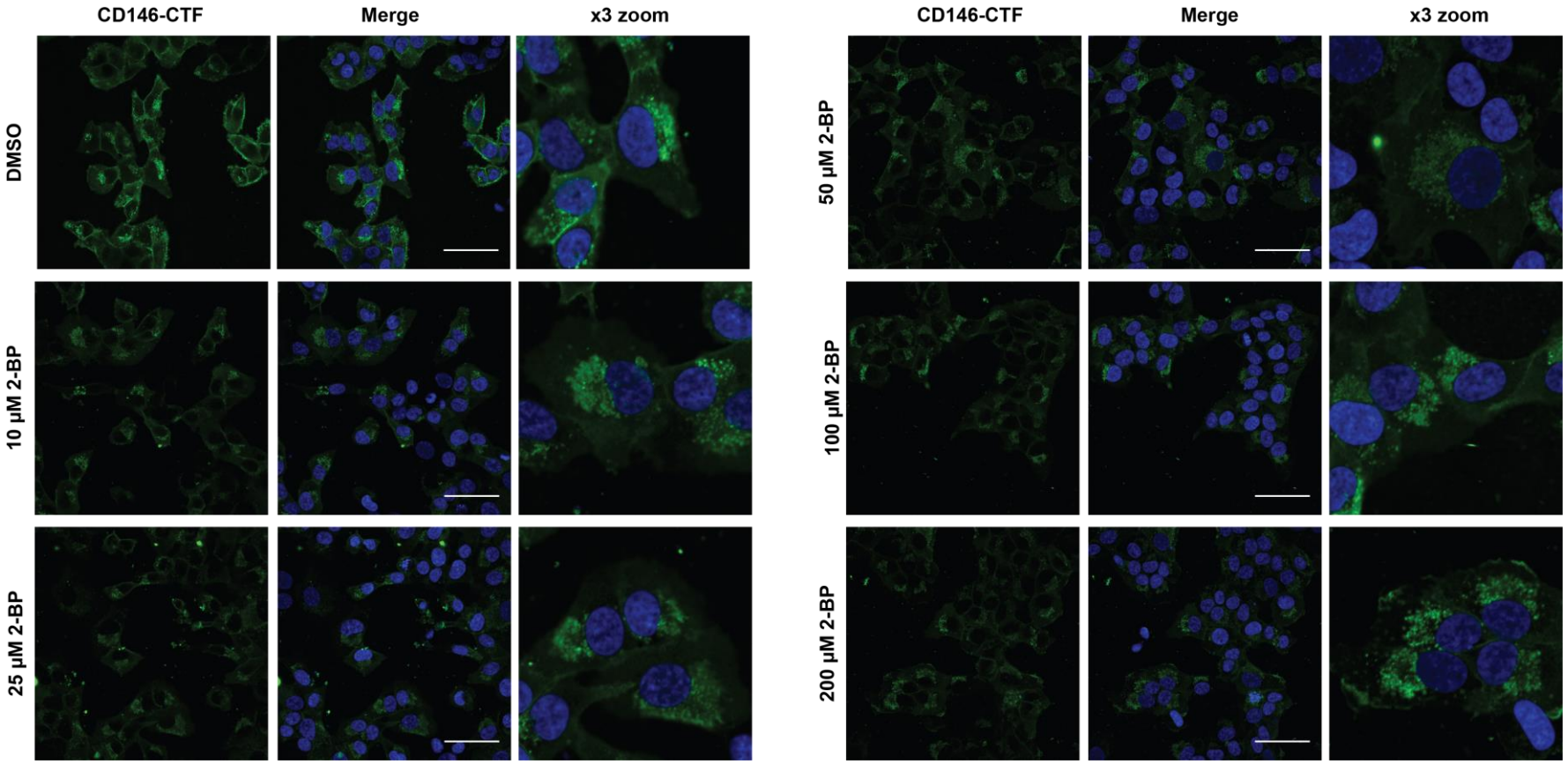

Figure 6-2 Inhibiting MCAM palmitoylation in SB2 14.1 melanoma cells affects MCAM localisation

SB2 14.1 cells were treated with 2-BP (10 – 200 µM) (n=1). Following treatment, the trafficking of full-length MCAM to the cell surface appeared to be impaired. Cells also became larger and flatter, with a less polarised morphology. The distribution of the MCAM-CTF appears to cover a larger area in the treated cells, but this is likely due to the overall morphological changes. Scale bars on images in the middle column of each panel are 50 µm; with the boxed region from the merged image enlarged in the final column of each panel.

6.3.2 Moesin co-localises with MCAM

Moesin is a member of the ERM family of actin-binding proteins. Moesin is known to interact with MCAM (Luo *et al.*, 2012) and has been proposed to promote ectodomain shedding when interacting with the intracellular domain of transmembrane proteins (Figure 6-3A). Immunofluorescent staining was used to determine the localisation of MCAM and moesin in migrating melanoma cells overexpressing either WT or mutant (MT) MCAM variants under normal culture conditions. In SB2 14.1, SB2LP #5.13 and SB2YG 3.1.2 cells, moesin showed even/regular staining throughout the cytoplasm, with strong expression at the cell surface that was particularly concentrated at the leading edge of polarised cells. Here, it co-localised with MCAM (Figure 6-3B). This co-localisation was seen in both WT and MT cells, indicating that modifying the di-leucine and tyrosine motifs did not influence MCAM-moesin interactions.

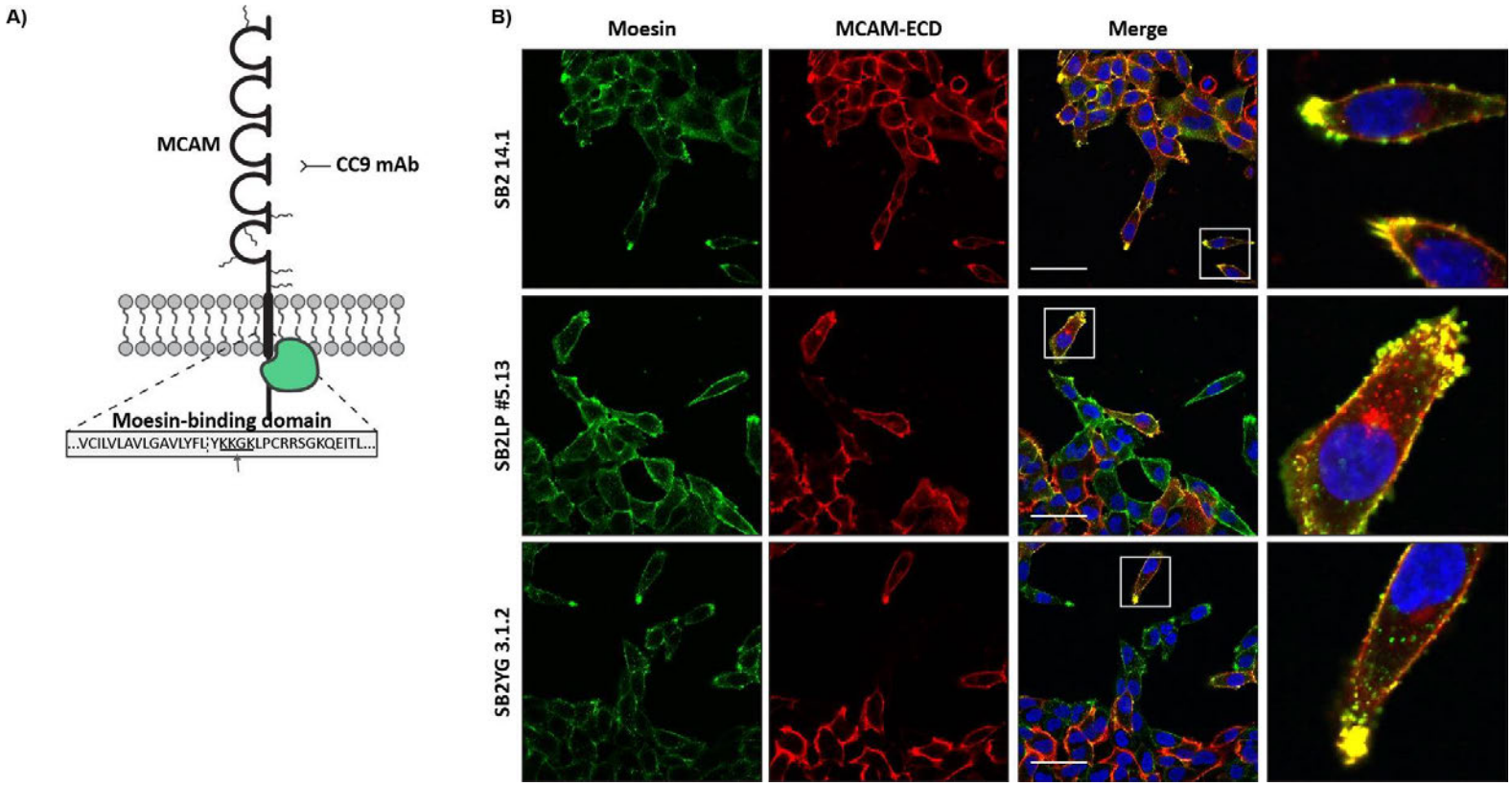

Figure 6-3 MCAM and moesin interact and co-localise at the cell periphery

Moesin is known to bind the KKGK motif within the juxtamembrane region of the MCAM-CTF (A). Migrating cells were co-stained for moesin and MCAM (using the CC9 mAb) to determine cellular location of the two proteins (n=3). MCAM and moesin were seen to co-localise predominantly at the cell periphery, with strong staining at the leading edge of migrating cells. This was consistent between all MCAM-expressing cells. Scale bars in the merged image are 50 µm; with the boxed region from the merged image enlarged in the fourth column.

6.3.3 CaM is predicted to interact with the MCAM-CTF

Calmodulin is a calcium-binding protein. It is involved in the regulation of numerous cellular processes, afforded by its ability to bind to a countless number of protein targets. Whilst there is no specific sequence that CaM binds to, CaM binding sites (also referred to as CaM recruitment signalling motifs) (Yap *et al.*, 2000) share common features, including the spacing of hydrophobic "anchor" residues, a net positive charge of the binding region, and the tendency to form amphipathic α-helix structures (Mruk *et al.*, 2014; Tidow & Nissen, 2013). The canonical CaM binding motifs that have been identified to date are outlined in (Appendix Q). Because of the lack of sequence similarity of CaM-binding sites in different proteins, experimental analysis for the identification of such sites can be troublesome. Therefore, the use of web-based prediction tools is particularly important for identifying putative CaM binding domains. To date, two online prediction tools have been published. The web-based database described by Yap *et al.* (Yap *et al.*, 2000) predicts CaM recruitment signalling motifs (CRS) within a protein sequence. Since CRS motifs share very little sequence homology, their identification is based on common biological and biophysical characteristics. Identification of a putative calmodulin binding site using this online tool takes into consideration the following features:

- Hydropathy (measure of hydrophobic or hydrophilic properties of an amino acid)
- Alpha-helical propensity
- Residue weight
- Residue charge
- Hydrophobic residue content
- Helical class
- Occurrence of particular residues

Importantly, other analysis tools/databases for the prediction of CaM binding motifs within a protein sequence have become available more recently. This includes the "**C**almodulin Database **A**nd **M**eta-Analysis" predictor (CAM) described by Mruk *et al.* (2014) is another easily accessible web-based tool that uses a script to identify every canonical CaM-binding motif within a sequence. By taking into account charge

discrimination and acknowledging that CaM binds to sites with multiple overlapping binding motifs, this database is able to more accurately predict where CaM binds in a given peptide sequence (Mruk *et al.*, 2014).

When analysing the protein sequence of MCAM (both WT and mutant; Appendix R) for putative CaM binding sites, two predicted CaM binding sites were identified. These were located between residues 575-592 and 599-613 (Figure 6-4), the first of which also contains part of the TMD. This is in line with the predicted CaM binding domain identified using the Calmodulin Database (between aa572-592). According to a paper published regarding the Calmodulin Database and Meta-Analysis predictor, the higher the number of canonical CaM motifs in a sequence segment, the greater likelihood of CaM binding to that sequence (Mruk *et al.*, 2014). Thus, we predicted that CaM may bind to MCAM in melanoma cells *in vitro*, and that it should be investigated as a potential regulator of MCAM ectodomain shedding. Pull down experiments were performed; however, CaM was not among the proteins pulled-down by the MCAM-ICD (Appendix S)

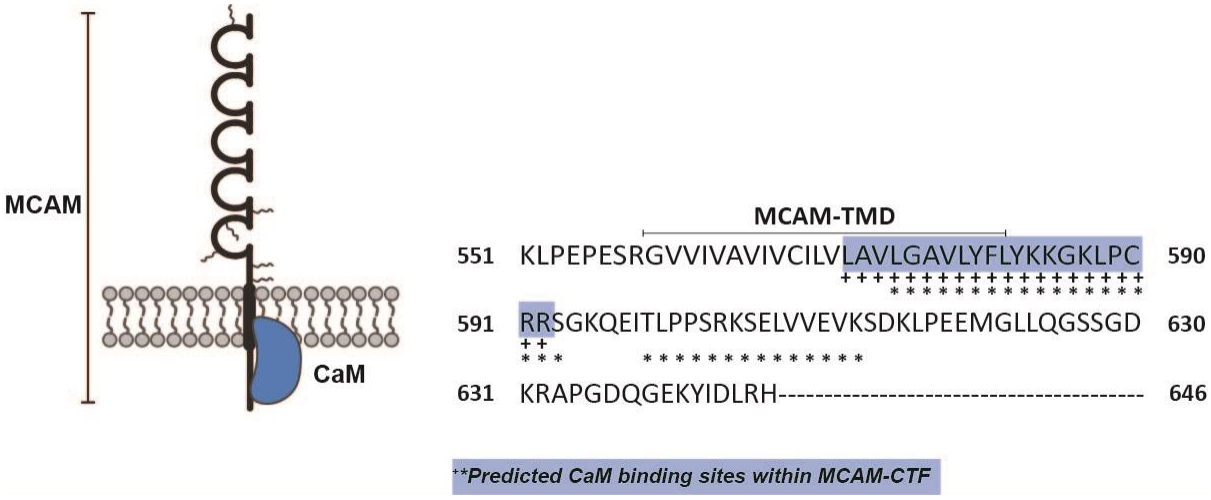

Figure 6-4 Predicted calmodulin-binding domains within MCAM-l using two different online tools

Two separate online tools were utilised to predict where CaM may bind within the CTF of human MCAM. A sequence spanning the transmembrane domain (TMD) and the juxtanuclear region of the CTF was predicted as the most likely binding site for MCAM (blue highlight). Other predicted binding sites with a lower affinity for CaM binding are also represented (*). Resources: http://calcium.uhnres.utoronto.ca/ctdb/ctdb/sequence.html and http://cam.umassmed.edu/index.php

6.3.4 CaM is expressed in melanoma cells but its relevance in MCAM cleavage is unclear

To confirm the expression of CaM in melanoma cells, I.F and immunoblot were used. However, I.F. was unsuccessful, and whilst there was limited fluorescent signal in CaM-stained cells, it did not appear to be a true representation of the amount of CaM expected to be expressed in these cells and was likely an artifact of non-specific antibody binding, as it appeared similar to the isotype control antibody used (data not shown). Further, being able to detect CaM in whole cell lysates by immunoblot required extensive troubleshooting and was difficult to reproduce. In line with previous findings by Van Eldik *et al.* (1984), cross-linking of the ~15 kDa protein was required to minimise loss of CaM during staining and washing steps (Figure 6-5). Since CaM is found ubiquitously in eukaryotic cells, the lack of staining is likely due to an antibody binding or detection issue. This theory was supported by the detection of *CALM1, CALM2, and CALM3* in a range of melanoma cells, and in HUV-EC-Cs, was confirmed by qPCR (Figure 6-6). Levels of each gene were calculated relative to SB2 14.1 melanoma cells. The expression of *CALM1* and *CALM3* showed a similar pattern, with higher expression in MM96L, SkMel28, Colo239F and HUV-EC-Cs compared to SB2 14.1 cells. Expression of *CALM2* was more variable and was lowest in MM253 cells.

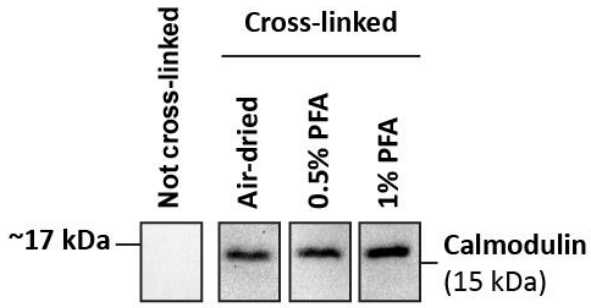

Figure 6-5 Detecting calmodulin in melanoma cells

Calmodulin protein expression in SB2 14.1 melanoma cells was confirmed by immunoblot (n=1). Protein transferred to PVDF membrane required cross-linking prior to blocking and probing. This could be achieved by air-drying and re-hydrating the membrane, or by incubating with 0.5% or 1% paraformaldehyde (PFA).

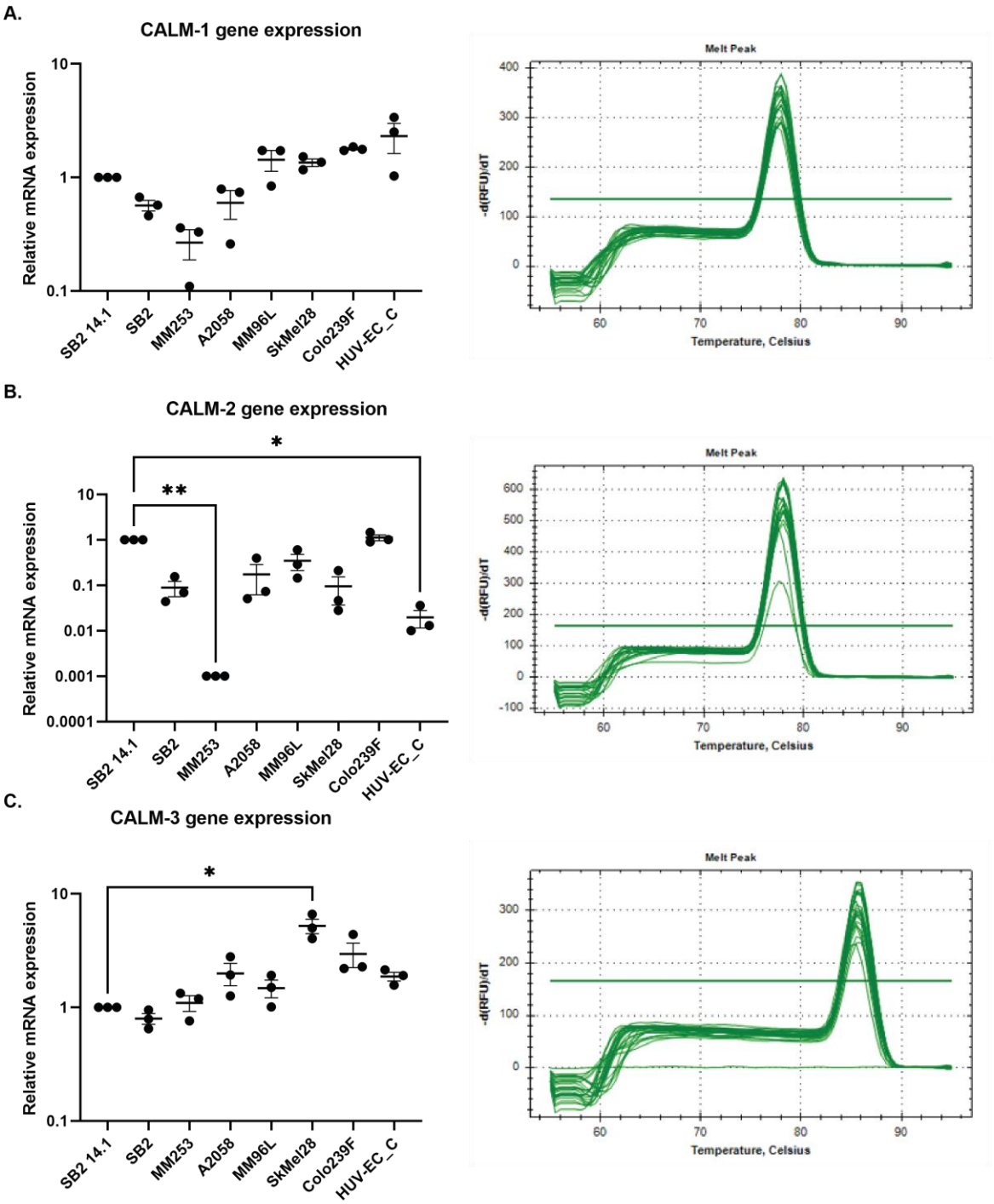

Figure 6-6 Calmodulin-encoding genes expressed in melanoma cell lines

CALM transcripts were amplified in HUV-EC-C and melanoma cells and fold changes calculated using the 2 (-ΔΔCT) method, using the reference genes *CASC3* and *RPS2*, and SB2 14.1 cells as the reference cell line for each amplicon (as these cells were used in the immunoblot experiments) (n=3). Expression of *CALM1* (A), *CALM2* (B) and *CALM3* (C) was seen in all samples tested, except for *CALM2* in MM253 cells. Each data point represents a biological replicate for each cell line; mean and SEM are also shown. The melt curve associated with each amplicon is shown on the right and indicates the presence of a single amplification product. MM253 and HUV-EC-C cells showed significantly reduced *CALM2* expression compared to SB2 14.1 cells (*p<0.05, **p< 0.01), while SkMel28 cells showed increased *CALM3* expression compared SB2 14.1 (*p<0.05).

In previous studies, co-IP and mutagenesis assays have helped to determine the CaM-protein interactions occurring *in vitro* (Kleene *et al.*, 2010; Wong *et al.*, 2004). Further, the addition of CaM inhibitors to experimental protocols are useful for determining whether CaM has a role in the negative regulation of ectodomain shedding (Horiuchi *et al.*, 2007; Lai *et al.*, 2009). The calmodulin inhibitor, trifluoperazine dihyrochloride (TP) was tested for its ability to promote MCAM shedding. However, concentrations above 10nM, which are reportedly required to effectively inhibit calmodulin, appeared to be toxic to SB2 14.1 melanoma cells. To confirm this was not melanoma-specific, Chinese hamster ovary cells modified to express MCAM were also treated with TP, resulting in a loss of viability after 2-3 hours, characterised by detachment of all cells from tissue culture plastic. Due to time constraints caused by the COVID-19 pandemic, the role of CaM in MCAM ectodomain shedding was not investigated further.

6.4 Discussion

The ectodomains of MCAM-l and MCAM-sh are identical, consisting of five immunoglobulin-like domains (V-V-C2-C2-C2) with eight potential N-glycosylation sites (Stalin *et al.*, 2017). MCAM is highly conserved, with human MCAM sharing ~81% identity with mouse and 73.8% with chicken forms of MCAM (Taira *et al.*, 2004), suggesting an important biological function. Whilst the peptide sequence of the MCAM ectodomain is identical for both isoforms, variations in post-translational modifications, sequences, or conformations may convey unique functions to each isoform. To illustrate this, Nollet *et al.* (2017) generated a tumour-specific antibody against MCAM, which was found to react with MCAM on cancer cells (including melanoma, verrucous skin carcinoma, renal carcinoma, and colonic adenocarcinoma). The inability of this antibody to react with full-length MCAM on endothelial cells indicated that post-translational modifications may indeed play an important part in developing tumour-specific antibodies (Nollet *et al.*, 2017). Further, an antibody specific for sMCAM, which did not react with MCAM on the surface of endothelial cells or tumour cells, has reportedly been developed (Stalin *et al.*, 2016) and may also rely on select modifications to distinguish between soluble and full-length, transmembrane isoforms of MCAM.

Importantly, post-translational modifications offer diversity to the proteome, and are frequent in cancer. This includes protein phosphorylation, histone epigenetic modifications, acetylation, glycosylation, sumoylation, methylation, ubiquitination, citrullination, and palmitoylation, which have all been identified in cancer cells (Liu *et al.*, 2022). Interestingly, such modifications as N-glycosylation (Pakkiriswami *et al.*, 2016), O-glycosylation (Goth *et al.*, 2015), phosphorylation (Hinkle *et al.*, 2006; Mechtersheimer *et al.*, 2001), and palmitoylation (Poggi *et al.*, 2013), have been shown to regulate ectodomain shedding of molecules, including CDCP1, TNF-α, NCAM, and L1 adhesion molecule, respectively. The overarching hypothesis is that such modifications alter the stability and/or conformation of proteins expressed on the cell surface, thereby influencing their susceptibility to proteolytic cleavage.

Using chemical inhibitors against two types of post-translational modification - palmitoylation and glycosylation - we investigated the relevance of these modifications in regulating MCAM cleavage in melanoma cell lines. As MCAM is known be glycosylated by *MGAT5* (Bubka *et al.*, 2014), which catalyses the addition of complex N-glycans, cells were treated with SW which blocks Golgi α-mannosidase II, a precursor step in the addition of these structures. Here, long-term (>48 h) treatment with SW impaired the glycosylation of full-length MCAM, which was apparent from the reduced molecular weight of the protein in SW-treated SB2 14.1 cells. Evidence that SW promoted cleavage of MCAM, however, was not as convincing, as there was no striking increase in sMCAM in the media of treated SB2 14.1 cells. In addition, the amount of MCAM-CTF in treated cells was not clearly altered, further suggesting that ectodomain shedding of MCAM may not be affected by N-glycosylation.

However, the use of SW may also drive the addition of hybrid/bisecting glycan structures (by blocking the addition of complex structures). Hybrid structures can be added by *MGAT3,* which has also been implicated in MCAM N-glycosylation (Bubka *et al.*, 2014). Therefore, glycosylation changes associated with SW treatment may have been too subtle to induce a difference in MCAM cleavage. Other inhibitors that

could be used include deoxymannojirimycin (DMJ) which inhibits α-mannosidase I, a step in the pathway prior to the actions of both *MGAT3* and *MGAT5;* or tunicamycin, which inhibits the first step in N-glycan synthesis. In addition, a recent paper described for the first time, the addition of O-glycan structures on MCAM. Sumardika *et al.* (2018), found that glycosylation of MCAM by *GCNT3* enhanced MCAM expression at the cell surface, provided protein stability, and prolonged the half-life of MCAM, and a specific inhibiter of GCNT3*,* talniflumate, has been identified (Rao *et al.*, 2016). Given that O-glycosylation has been implicated in ectodomain cleavage more strongly than N-glycosylation (Goth *et al.*, 2015), it would be interesting to explore MCAM cleavage in the presence of talniflumate.

However, the use of chemical inhibitors should be approached with caution, as these will affect all proteins modified by glycosylation, including sheddases. Indeed, a comparison of the activity of ADAM17 produced by insect versus mammalian cells found that the more heavily glycosylated mammalian-produced ADAM17 had lower activity against synthetic substrates (Chavaroche *et al.*, 2014). However, the significance of this remains to be confirmed, as ADAM17 may act differently in the cellular environment. A more elegant and informative approach would be site-specific mutation of putative glycosylation motifs (both N- and O-) of MCAM, followed by stable transection of mutant constructs into melanoma and/or endothelial cells.

Besides glycosylation, MCAM can undergo post-translational modifications involving the addition of palmitic acid (Wang *et al.*, 2015) or phosphates (Guezguez *et al.*, 2006). Here, we studied the effect of the palmitoylation inhibitor, 2-bromohexadecanoic acid (2-BP), on MCAM cleavage. As with other forms of post-translational modification, palmitoylation is important for broadening protein functionality. Previously, Wang *et al*. (2015) demonstrated that MCAM undergoes palmitoylation at Cys590, and de-palmitoylation induced by Wnt5a promotes polarised distribution of MCAM. Using the presence of the MCAM-CTF in the juxtanuclear region as an indirect read-out of ectodomain shedding, it did not appear that 2-BP treatment significantly enhanced the shedding of MCAM. As such, we did not progress to measuring sMCAM in tissue culture media. Whilst we did not

observe a polarised distribution of MCAM in response to inhibited palmitoylation (Wang *et al.*, 2015), morphological changes were noted, and were accompanied by reduced localisation of MCAM to the cell surface. Given the importance of palmitoylation in targeting proteins to lipid rafts (Guan & Fierke, 2011), this phenomenon is not unexpected, and suggests that inhibition of MCAM palmitoylation was achieved by treatment with 2-BP treatment. The relevance of palmitoylation in MCAM cleavage, however, remains unclear and requires further investigation. Again, specific mutation of Cys590 (the palmitoylated residue in MCAM) would facilitate these experiments and reduce off-target effects of global chemical inhibition.

Although protein phosphorylation has been implicated in the regulation of ectodomain shedding, we did not pursue this in our studies. Whilst phosphorylation is important in outside-in signalling cascades induced by MCAM engagement with its ligand (Anfosso *et al.*, 1998; Anfosso *et al.*, 2001), its involvement in the regulation of MCAM shedding is unclear. Given the importance of these motifs in downstream signalling, it is likely that modifying phosphorated residues on MCAM would have widespread functional effects, which may make it difficult to specifically assess ectodomain cleavage. Future studies will therefore be required.

As well as focusing on the role of the MCAM ectodomain in regulating MCAM shedding, we also investigated the relevance of the intracellular proteins, CaM and moesin, in MCAM proteolysis. Though moesin has previously been shown to interact with the KKGK motif of MCAM, where it acts as a cytoskeletal linker (Luo *et al.*, 2012), we performed I.F. and Co-IP to confirm this. Here, MCAM co-localised with moesin at the surface/periphery of SB2 14.1 melanoma cell lines, as expected. Further, co-IP identified a ~180 kDa protein that immunoprecipitated with MCAM and was detected by an anti-moesin antibody. As the expected molecular weight of moesin is around 68 kDa and MCAM is ~120 kDa, the band could represent a protein complex formed between MCAM and moesin. Since MCAM-moesin interactions have been previously established (Luo *et al.*, 2012), we did not aim to clarify this further. Interestingly, MCAM containing mutations in the di-leucine domain and a tyrosine domain did not affect MCAM-moesin co-localisation. Moreover, these

mutations did not affect shedding in our preliminary screen, although there were some differences in intracellular localisation (refer to Chapter 3 for previous discussion of these mutant constructs).

Next, we focused on identifying the potential involvement of CaM in MCAM ectodomain shedding. Whilst immunoblot and I.F did not provide reassuring evidence of CaM expression in melanoma cell lines, qPCR confirmed expression of three CaM genes - *CALM1, CALM2, and CALM-3* - at the mRNA level.

Importantly, the role of CaM in regulating ectodomain shedding of other members of the IgSF has been described. For example, CaM binding assays, surface plasmon resonance analysis, and ELISA, demonstrated that CaM can interact directly with the intracellular domain (of both the long and short isoforms) of NCAM in a calcium-dependent manner (Kleene *et al.*, 2010). Further, Wong *et al.* (2004) identified CaM as a potent inhibitor of PECAM-1 shedding, but this was reversed in the presence of the CaM inhibitor, trifluoperazine (TP). In our hands, TP had a toxic effect on melanoma cells, such that treating cells with concentrations believed to be required to achieve substantial CaM inhibition resulted in cell death. Coupled with the difficulty in sourcing a suitable antibody for detecting CaM in melanoma cells; our inability to effectively inhibit CaM meant we were unable to pursue it as a potential regulator of MCAM ectodomain shedding. However, we may speculate that the apparent stable interaction between MCAM and moesin would promote constitutive shedding of MCAM, and that inhibition of CaM may not affect sMCAM production anyway.

Overall, intramembrane processing is a highly controlled process that can be influenced by many factors. The difficulties encountered in the experiments undertaken in this chapter demonstrate the challenging nature of understanding a complex biological process *in vitro*, particularly in the disease setting. It also highlights the importance of considering factors such as protein conformation when designing experiments to investigate intracellular binding partners. This was exemplified in this chapter by the lack of proteins identified to interact with MCAM in the pull-down assay. To elaborate, MCAM has a number of known intracellular

binding partners, including hShroom1 (Dye *et al.*, 2009) and moesin (Luo *et al.*, 2012), which were not identified in the pull-down assay. As reported previously, conformation of a protein ectodomain can have a critical influence on the regulation ectodomain shedding (Hartmann *et al.*, 2015; Lichtenthaler & Meinl, 2020). Evidently, the lack of the MCAM ectodomain (since we used a vector containing only aa584-646; see Section 2.1.2) may have had a significant impact on the ability to identify biologically relevant interactions between MCAM and intracellular binding proteins. In particular, MCAM exists as monomers, homodimers and heterodimers in mammalian cells; and it is likely this influences conformation and binding properties of the intracellular domain (Wang *et al.*, 2015). However, it is interesting to note that Protein S100-A16 was identified in the pull-down assay, as various other S100 proteins have previously been discussed for their relevance in melanoma (Bresnick, 2018). In particular, the S100-A8/A9 heterodimer complex been shown to interact with MCAM to influence the growth, migration, and metastatic spread of melanoma cells (Chen *et al.*, 2019b). This may warrant further investigation into the interactions between MCAM and S100-A16 in the future.

6.5 Conclusions

Ectodomain shedding is a tightly regulated process that generates functional soluble proteins. Many factors may influence the rate and timing of ectodomain shedding, including post-translational modifications and intracellular binding proteins. To this end, we performed analysis of MCAM cleavage, measured indirectly via the amount of MCAM-CTF expressed- either by immunoblot using whole cell lysates, or by I.F- in cells treated with SW, an inhibitor of glycosylation, and in cells treated with 2-BP, an inhibitor of palmitoylation. Whilst neither approach appeared to impact MCAM cleavage, the non-specific nature of the inhibitors likely has effects on multiple proteins that may interact with MCAM and may therefore also affect cleavage processes. Additionally, we were not able to establish the potential relevance of CaM in MCAM ectodomain shedding, although it is clear that it is somehow relevant for melanoma cell survival, since inhibition with TP led to cell death. Evidently, it remains unclear how the production of sMCAM is regulated, and whilst this chapter aimed to shed light on this, it is apparent that a more targeted and nuanced approach will be necessary.

Chapter 7

Final Discussion

MCAM is a functionally diverse molecule that is well known for its role in cell adhesion and migration. Beyond promoting cell-cell and cell-matrix adhesions, MCAM is also involved in outside-in signalling (Anfosso *et al.*, 1998; Anfosso *et al.*, 2001; Jouve *et al.*, 2015), promoting cell migration through interactions with cytoskeletal proteins (Dye *et al.*, 2009; Luo *et al.*, 2012), and remodelling of ECM via upregulation of MMP2 activity (Zigler *et al.*, 2011). Owing to its relevance in melanoma, and indeed in many other cancers, it has remained an appealing therapeutic target and subject of melanoma research over many years. However, the development of clinically successful adjuvants targeting MCAM has been hindered due to the risk of off-target effects. Indeed, the physiological relevance of MCAM in vascular smooth muscle cells (Espagnolle *et al.*, 2014), vascular endothelial cells (Bardin *et al.*, 2001; Bardin *et al.*, 1998), and blood mononuclear cells (Elshal *et al.*, 2005) must be considered when researching effective ways to impair MCAM-mediated tumour metastasis. Nollet *et al.* (2017) reportedly overcame this limitation, generating an anti-MCAM antibody that bound specifically to MCAM on tumour cells *in vitro*, and impaired tumour growth and promoted apoptosis of tumour xenografts in mouse models.

Another breakthrough in the field of MCAM research has been the identification of a soluble isoform of MCAM (sMCAM) (Stalin *et al.*, 2016). This isoform was first identified in supernatants from endothelial cells (Bardin *et al.*, 1998) and was later discovered to be released from melanoma cells, as well as other tumour cells expressing MCAM (Stalin *et al.*, 2016; Stalin *et al.*, 2017). To date, sMCAM has mainly been studied in vascular endothelial cells, where it is a product of metalloproteinase-mediated cleavage (Boneberg *et al.*, 2009), and its effects are mediated through the membrane-associated binding partner, angiomotin (Stalin *et al.*, 2013). More specifically, Stalin *et al.* (2016) demonstrated that sMCAM acts through a signalosome complex consisting of angiomotin, MCAM-sh, VEGFR1, VEGFR2 and presenilin-1. Here, endothelial colony-forming cells (ECFCs; a type of endothelial progenitor) were treated with recombinant sMCAM, which was shown to bind to MCAM-sh and induce MMP-mediated cleavage of the MCAM ectodomain, followed by generation of an MCAM-ICD fragment in a γ-secretase-dependent

manner. This was linked to altered expression of proteins associated with cell survival (Stalin *et al.*, 2016a).

Importantly, it remains unclear how sMCAM is generated from melanoma cells, and much of what is known from studies in endothelial cells (Bardin *et al.*, 2003; Boneberg *et al.*, 2009; Stalin *et al.*, 2016a; Stalin *et al.*, 2013) cannot be directly translated to melanoma cells - firstly because melanoma cells express predominantly the long isoform of MCAM (Dye *et al.*, 2009). In endothelial cells, the long isoform is not processed in the same way as MCAM-sh, nor is it associated with angiogenic properties or altered cell survival following treatment with rsMCAM (Stalin *et al.*, 2016a). Secondly, the cleavage of MCAM in melanoma cells is expected to convey survival and metastatic advantages, whilst in endothelial cells, it is likely to be important for physiological functioning. Interestingly, tumour-derived sMCAM (tsMCAM) can act in both an autocrine and paracrine manner, binding to angiomotin on tumour cells and vascular endothelial cells. Its specific effects on tumour cells include upregulation of pro-survival genes and down-regulation of anti-apoptotic genes, whilst in endothelial cells, tsMCAM promotes cell proliferation and enhances tumour vascularisation (Stalin *et al.*, 2016).

A recent study by Nollet *et al.* (2022) demonstrated the release of sMCAM was due to ADAM-mediated cleavage, but also suggested there is evidence of sMCAM being a product of alternative splicing. Previously this has only been reported for the avian homologue of MCAM (Vainio *et al.*, 1996). In our hands, transmembrane isoforms of MCAM in melanoma cells included MCAM-l and MCAM-sh. While mRNA for the novel splice variants published by Nollet *et al.* (2022) were also detected, expression was minimal (i.e.10 - 1000 fold lower expression of these variants than in endothelial cells, depending on the cell line). A soluble isoform was also detected by immunoblot in this study and was distinguishable from full-length MCAM based on protein size. This is an important distinction of our work from others, which have measured sMCAM via ELISA (Bardin *et al.*, 2003; Boneberg *et al.*, 2009; Nomikou *et al.*, 2015; Stalin *et al.*, 2016a). Although ELISA allows quantification, it would not distinguish between sMCAM and MCAM-l or MCAM-sh, which may be present in the medium of

dying cells. Given the difficulties we experienced with cell viability in the presence of various chemical stimuli or inhibitors, the ability to distinguish between full-length MCAM and MCAMs is critical in investigating MCAM cleavage.

In the present study, we found that sMCAM produced by melanoma cells in culture was reliant on the presence of FBS in the cell culture media. Whether this is due to the presence of external factors, such as lysophosphatidic acid (LPA) (Hirata *et al.*, 2001) or heat-resistant proteases within the serum (since some sMCAM was detected in the media even when heat-inactivated serum was used) remains unclear. As we were unable to provide direct evidence of sMCAM production in the absence of serum, despite using well-known stimulators of ectodomain shedding (e.g. PMA, calcium ionophore- discussed below), the MCAM-CTF was used as an alternative readout of ectodomain shedding. This fragment, consisting of the TMD and ICD of MCAM- collectively referred to as the MCAM-CTF- appeared to be increased in cells following PMA stimulation, suggesting that PMA may promote cleavage of MCAM. This was shown using both I.F and immunoblot, where increased production/accumulation of the MCAM-CTF was observed in PMA-treated cells relative to cells treated with vehicle control. It is unclear why sMCAM was not detectable here, despite this evidence of increased MCAM processing. Interestingly, Lorenzen *et al.* (2016) noted that long-term treatment with PMA can interfere with sheddases function and therefore affects the production of soluble proteins, although since we collected samples after short-term (~2 hour) treatment, this may not explain the absence of sMCAM in the media. Alternatively, PMA may have an unprecedented effect on MCAM-CTF processing, without affecting ectodomain shedding. Nevertheless, it is clear that melanoma cells generate both sMCAM and MCAM-CTF, similar to findings made by Stalin *et al.* (2016) using ECFCs.

To investigate the specific proteases responsible for the cleavage of MCAM, we first attempted treatment with a broad-spectrum metalloproteinase inhibitor, GM6001 (Tsumagari *et al.*, 2017). This is a commonly used broad-spectrum inhibitor of MMPs and ADAMs and has been shown to reduce the generation of sMCAM in ECFCs (Stalin *et al.*, 2016a). Similarly, it reduced sMCAM production by SB2 14.1 cells in

normal culture media. Due to low levels of sMCAM generated by melanoma cell lines expressing endogenous MCAM, it was not feasible to test the ability of GM6001 to inhibit sMCAM production in any other cell lines at our disposal, as it would have been difficult to accurately measure the effect of the inhibitor. Using an alternative approach of overexpressing ADAM10 and ADAM17 by transient transfection, we were able to visually interpret whether ADAMs and MCAM may co-localise, using I.F. staining and confocal microscopy This was performed in A2058 cells, which have lower basal expression of both ADAM10 and ADAM17 relative to other cell lines tested, and MM253 cells, which have higher expression of ADAM17 and low-to-moderate expression of ADAM10 compared to other cell lines tested. The overexpressed proteins showed a high level of expression in the nuclear region, which may be an artefact of transient transfection, although nuclear localisation of ADAM10 has been reported in tumour cells (Lee *et al.*, 2010b). Confirming the localisation of endogenous ADAM10 and ADAM17 will be imperative in future studies, as localisation of these proteases has been shown to affect substrate cleavage (Lorenzen *et al.*, 2016; Schlöndorff *et al.*, 2000).

Both ADAM10 and ADAM17 have been implicated in the cleavage of cell adhesion molecules associated with cancer progression (Garton *et al.*, 2001; Lee *et al.*, 2007), and whilst we did not provide direct evidence for either of these sheddases being responsible for sMCAM production in melanoma cells, further in-depth studies would be expected to recognise MCAM as a substrate of ADAM10 and/or ADAM17. Interestingly, the susceptibility of MCAM to PMA-induced cleavage hints towards ADAM17 being relevant in MCAM cleavage, with evidence suggesting that PKC activation (induced by PMA) is associated with activation of ADAM17 and subsequent shedding of its specific substrates (Lorenzen *et al.*, 2016). Importantly, however, long-term exposure to PMA (>6 hours) can affect the normal recycling of ADAM17, leading to downregulation of mature ADAM17 and abolished ADAM17-mediated shedding (Lorenzen *et al.*, 2016). Thus, observations from the use of non-physiological activators of ectodomain shedding, including PMA, must be interpreted with caution. There are also several physiological stimuli of ADAMs (e.g. LPA, TNF-α, and thrombin) that could be explored. The ability to reliability stimulate higher levels of sMCAM would facilitate investigation of the effect of specific inhibitors.

The second product of ectodomain shedding, the remnant C-terminal fragment (CTF), typically consists of a short sequence of the extracellular domain, the transmembrane domain, and the intracellular domain. For MCAM, this was represented by a ~11-17 kDa fragment on immunoblot. Further proteolytic processing by an intracellular cleaving protease (iCliP) would be expected to yield a product of ~7 kDa. In endothelial cells, a product of ~6-8 kDa has been identified using an antibody against the CTF of MCAM. This was assumed to represent the MCAM-sh-ICD, with the authors commenting that this fragment was a product of γ-secretase-mediated cleavage (Lee *et al.*, 2007).

In our hands, MCAM-l-CTF also appeared to be a substrate for γ-secretase. The use of the broad-spectrum γ-secretase inhibitor, DAPT, was particularly convincing of this, with evidence of MCAM-CTF accumulation in melanoma cells treated with DAPT for ~24 hours, suggesting that DAPT treatment prevented release of the ICD (Frade, 2005; Maes *et al.*, 2014; von Rotz *et al.*, 2004). Interestingly, the localisation of the MCAM-CTF in melanoma cells to the late endosome/lysosome, but not the Golgi or ER, may hold clues towards which γ-secretase protease - PS1 or PS2 - is primarily responsible for MCAM-CTF processing. Previously, Sannerud *et al.* (2016) gave evidence for the localisation of PS2 to the late endosome/lysosome, where it was responsible for APP cleavage. Meanwhile, PS1 was mainly localised to the cell surface (Sannerud *et al.*, 2016). Whilst we did not have access to an antibody suitable for I.F. detection of PS1 and PS2 to study their localisation in melanoma cells, we were able to quantify the expression of PS1 and PS2, using a novel tool developed by Eccles *et al*. (unpublished) that enabled quantification based on protein units and facilitated a direct comparison of the quantity of PS1 vs. PS2. This demonstrated that while PS1 is expressed at a similar level across all cell lines tested, PS2 is differentially expressed by melanoma cell lines, although most cells express more PS1 than PS2. In particular, we noted higher expression of PS2 in cell lines that displayed lower levels of MCAM-CTF accumulation, and lower expression of PS2 in the SB2 14.1 cell line where MCAM-CTF accumulates in the juxtanuclear region and is not rapidly degraded.

Collectively, this points towards PS2 as a major regulator of MCAM-CTF cleavage in melanoma cells. However, knockdown of PS2 alone did not abolish MCAM-CTF processing, either in melanoma or non-melanoma cells. Similarly, knockdown of PS1 did not appear to impair MCAM-CTF cleavage. However double knockout of both PS1 and PS2 (dKO) led to an accumulation of the MCAM-CTF in HEK293 cells. Evidently, PS1 and PS2 may be equally capable of cleaving the MCAM-CTF, with a preference for PS2 mediated cleavage under standard conditions. Thus far, our results provide novel evidence that MCAM-l in melanoma cells is a substrate for metalloproteinases - potentially ADAM17 - which cleave the ectodomain to release sMCAM. This is proceeded by γ-secretase-mediated proteolysis of the CTF (Figure 7-1). Further investigation will be necessary to 1) conclusively demonstrate the involvement of ADAM17 in MCAM ectodomain shedding, and 2) confirm that MCAM-CTF is cleaved by γ-secretase and produces a functionally relevant MCAM-ICD fragment.

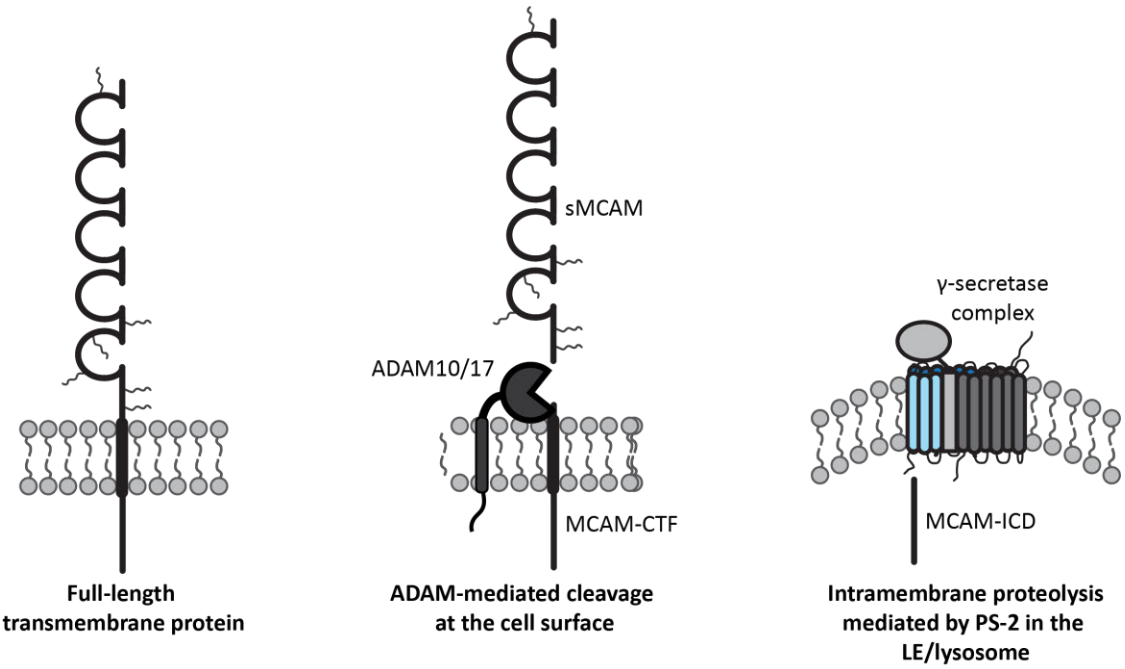

Figure 7-1 Proposed mechanism of MCAM processing

The full-length protein is expressed predominantly at the cell surface, where it is susceptible to ADAM10 and/or ADAM17-mediated cleavage. This results in release of the soluble ectodomain (sMCAM). Following ectodomain shedding, the CTF is internalised and targeted to the LE/lyso. PS-2 is present within the LE/lyso, and is capable of further processing the CTF, liberating the MCAM-ICD. The function of the MCAM-ICD in melanoma cells is yet to be determined.

The relevance of MCAM-CTF processing is of interest because substrates of γ-secretase typically yield an ICD fragment that is capable of translocating to the nucleus and acting as a transcription regulator. This has been well-established for Notch and APP (Bukhari *et al.*, 2017; von Rotz *et al.*, 2004), and Stalin *et al.* (2016) also noted that in endothelial cells, MCAM-ICD translocated to the nucleus when cells were treated with rsMCAM. This was only observed for MCAM-sh and not for MCAM-l (Stalin *et al.*, 2016a). However, it is often not possible to detect ICD expression/localisation *in vitro* due to the rapid processing of the ICD (Güner & Lichtenthaler, 2020). As we were unable to detect any product of γ-secretase-mediated cleavage of MCAM-l in melanoma cells, it is possible that the half-life of this fragment is very short.

However, we also took into consideration that MCAM-CTF localisation to the lysosome may simply mean the protein fragment is degraded, similar to transmembrane proteins such as pro-heparin-binding epidermal growth factor-like receptor (proHB-EGF) or pro-Amphiregulin (proAREG). These proteins undergo endocytosis following MMP/ADAM-mediated ectodomain shedding and are then targeted to the lysosomal degradation pathway, rather than undergoing further cleavage events (Higashiyama *et al.*, 2011). Notably, the long half-life of MCAM-CTF, even in the presence of an inhibitor of protein synthesis (i.e. cycloheximide) made it difficult to establish whether this may occur in melanoma cells. However, we believe the evidence supports our theory that MCAM-CTF undergoes γ-secretase mediated cleavage and produces an ICD fragment that may hold functional relevance to melanoma progression, particularly if it capable of translocation to the nucleus to regulate gene transcription. Indeed, in endothelial cells, MCAM-ICD has been proposed to enter the nucleus, bind to CSL, and regulate expression of *eNOS, BCl-xl, FADD,* and *MCAM-sh* (Stalin *et al.*, 2016). This warrants further investigations into expression of genes that may be up- or down-regulated in response to MCAM cleavage in melanoma cells.

Coupled with the long half-life of the MCAM-CTF, the inability to stimulate MCAM shedding in the absence of serum made investigations into the regulation of

ectodomain shedding infinitely more challenging. In addition, melanoma cells were particularly sensitive to various well-known chemical stimulators (and inhibitors) of ectodomain shedding that have been well-established to promote ectodomain shedding of other surface molecules, even under serum-free conditions. As mentioned above, PMA treatment appeared to enhance MCAM ectodomain shedding, based on measurement of the MCAM-CTF. However, another well-known stimulator, ionomycin (a calcium ionophore), clearly induced cell death at concentrations that have previously been deemed necessary to promote ectodomain shedding of MCAM in endothelial cells (Boneberg *et al.*, 2009). Although ionomycin induced cell death, and could not be used for further studies, this was important for highlighting why immunoblot is a valuable tool for confirming ectodomain shedding. To elaborate, the presence of protein detected by ELISA does not distinguish between protein size or source, and indeed Boneberg *et al.* (2009) noted that ionomycin treatment likely induced cell death when used at concentrations exceeding 10 μM.

Since calcium ionophore induces calcium influx, via the entry of extracellular Ca^{2+} and/or mobilisation from intracellular stores (Dedkova *et al.*, 2000), we propose that ionomycin promoted Ca^{2+}-induced apoptosis, as described by Orrenius *et al.* (2003). Interestingly, cells treated with a calmodulin inhibitor were similarly sensitive to treatment and exhibited signs of apoptosis after short-term treatment. This suggests that melanoma cells are surprisingly sensitive to Ca^{2+}, and impaired Ca^{2+} homeostasis promotes apoptotic cell death.

Whilst we were unable to demonstrate the relevance of post-translational modifications in regulating MCAM cleavage, this is not to say that post-translational modifications do not play a role in the regulation of MCAM ectodomain shedding. Since both glycosylation and palmitoylation have been suggested to regulate cleavage of other molecules (Bhattacharyya *et al.*, 2013; Goth *et al.*, 2015), and since MCAM is known to undergo both these forms of post-translational modification (Wang *et al.*, 2015; Wang *et al.*, 2020), further investigations may be warranted. In particular, site-directed mutagenesis of Cys590, a residue within the MCAM-CTF that

is known to be palmitoylated (Wang *et al.*, 2015), would help to elucidate the role palmitoylation has in regulating the cleavage of MCAM. Similarly, mutation of specific N- and O- glycosylation motifs within the MCAM extracellular domain may render it more susceptible to cleavage. In turn, this may have many potential downstream consequences, especially if impaired glycosylation were to promote dysregulated cleavage of MCAM.

Further, whilst the intracellular protein CaM appears to play an important role in regulated shedding of other proteins (i.e. L-selectin), it is typically considered a negative regulator of ectodomain shedding (Gifford *et al.*, 2012). Consequently, it may not interact with MCAM in melanoma cells, where constitutive shedding of MCAM is utilised to support tumour progression. Rather, MCAM may preferentially bind moesin, which has been suggested to compete with CaM for a binding site within the intracellular juxtamembrane sequence. Interactions between MCAM in moesin in melanoma cells have been well-established and were also demonstrated in the present study by I.F. and co-IP. Future studies may be required to address the relevance of CaM in MCAM shedding, and as a potential therapeutic target for modulating MCAM cleavage and tumour progression.

Overall, the data presented in this PhD thesis contribute novel findings to the ever-growing field of melanoma research. In particular, we have shown that production of sMCAM from melanoma cells is dependent on MMP/ADAM sheddase activity, and we have identified the MCAM-I-CTF as a novel substrate of γ-secretase. Additionally, we have highlighted the need for more elaborate studies to establish how ectodomain shedding is regulated at the substrate level.

7.1 Future Directions

The therapeutic landscape for melanoma has changed drastically over the past ten years (Guo *et al.*, 2021). In particular, the advent of immunotherapy has led to a significant improvement in overall survival and progression-free survival rates for patients with metastatic melanoma (Atkins *et al.*, 2022). However, not all patients

have a long-term respond to these therapies (Steininger *et al.*, 2021), meaning the identification of novel targets and alternative therapeutic strategies is still a high priority in the melanoma research field.

The aim of this thesis was to further characterise the melanoma biomarker, MCAM, to improve our understanding of its relevance as a functional biomolecule in tumour progression. Specifically, the cleavage of MCAM by metalloproteinases and γ-secretase was investigated, along with factors that may influence its susceptibility to cleavage.

In Chapter 3, we confirmed the cleavage of MCAM from melanoma cells *in vitro*, using immunoblot to demonstrate the presence of sMCAM in cell culture media and MCAM-CTF in whole cell lysates. We hypothesised that the MCAM-CTF may undergo further proteolysis to produce an ICD fragment, however, we were unable to demonstrate this via immunoblot or I.F. Other proteins that undergo RiP to produce ICD fragments are also difficult to detect due to only being transiently expressed (Wu *et al.*, 2017). Since ICD fragments are capable of translocating to the nucleus (von Rotz *et al.*, 2004; Yuan *et al.*, 2015), and since MCAM-sh-ICD has been shown to do this in endothelial cells (Stalin *et al.*, 2016a), it may be necessary to investigate the expression of genes that have been shown to be upregulated by MCAM cleavage. These include *eNOS, Bcl-xl, and FADD,* which are all potential target genes that are upregulated by rsMCAM treatment in endothelial cells (Stalin *et al.*, 2016a), and myc/max, Erk, Amot p80, Bcl-xl, and sirtuin-1, which are induced by autocrine binding of sMCAM to tumour cells (Stalin *et al.*, 2016). The expression of genes influenced by MCAM cleavage could then be compared to cells that have been treated with γ-secretase inhibitors, since these appear to inhibit the cleavage of MCAM-CTF (see Chapter 5).

Further, in Chapter 3 we demonstrated the localisation of full-length MCAM at the cell surface and MCAM-CTF in the perinuclear region by immunofluorescence. Specifically, MCAM-CTF localised with LAMP2, a marker of the LE/lysosome. As the LE/lysosome also contains PS2 (Sannerud *et al.*, 2016), it would be relevant to

investigate whether MCAM-CTF localises with PS2 in melanoma cells, either by I.F or co-IP.

The focus of chapter 4 was on investigating the potential role of members of the metalloproteinase family in MCAM ectodomain shedding. By inhibiting the production of sMCAM through GM6001 treatment, we provided evidence that MCAM is a substrate for metalloproteinases in melanoma cell lines. Despite it being previously reported that MCAM is a cleaved by MMP3 in endothelial cells (Boneberg *et al.*, 2009), we were unable to reproduce these results in melanoma cell lines using targeted MMP inhibitors (MMP-inhibitor I and MMP-inhibitor III). Rather, our results hint towards the involvement of ADAMs in MCAM ectodomain shedding, which is in line with recent reports of MCAM being cleaved by ADAM10 and ADAM17 (Nollet *et al.*, 2022). To further strengthen our data and confirm whether ADAM10 and/orADAM17 are involved in MCAM ectodomain shedding in melanoma cells, it will be necessary to inhibit/block their activity. There are reports of inhibitors that can selectively block either ADAM10 or ADAM17 (Ludwig *et al.*, 2005; Tateishi *et al.*, 2021), which would be interesting to test in melanoma cells *in vitro*. Alternatively, an siRNA approach would ensure targeted inhibition of the selected ADAM protease.

In chapter 5, the intramembrane proteolysis of MCAM was investigated. Specifically, cleavage of the MCAM-CTF by the proteolytic components of the γ-secretase complex, PS1 and PS2, was scrutinised. This led to the discovery of MCAM as a novel substrate of γ-secretase in melanoma cells, with evidence that both PS1 and PS2 are capable of cleaving the MCAM-CTF. As mentioned above, I.F. using antibodies against PS2 (as well as PS1) would be useful for determining whether the MCAM-CTF co-localises with these proteases. Whilst MCAM-CTF may predominantly be cleaved by PS2 under normal culture conditions, our data provides evidence that it may also be cleaved by PS1, particularly where PS2 expression/activity is impaired. Interestingly, there are controversial reports in the literature as to whether the PSs have compensatory capabilities (Arber *et al.*, 2019; Kimberly *et al.*, 2000), so to help strengthen our conclusion that both PS1 and PS2

are able to cleave MCAM, it would be beneficial to treat the PS KO cell lines with DAPT and measure MCAM-CTF levels.

Finally, in Chapter 6 we attempted to establish whether MCAM cleavage is regulated via post-translational modifications and/or binding of intracellular proteins. Post-translational modifications are important for the regulation of substrate cleavage (Bhattacharyya *et al.*, 2013; Goth *et al.*, 2015; Janes *et al.*, 2009; Shirakabe *et al.*, 2017), and MCAM undergoes multiple post-translational modifications including glycosylation (Bubka *et al.*, 2014; Sumardika *et al.*, 2018), phosphorylation (Guezguez *et al.*, 2006), and palmitoylation (Wang *et al.*, 2015). Unfortunately, in this thesis, no link was found between post-translational modification and MCAM shedding up- or down-regulation in melanoma cells. Additional studies that could be performed include using site-directed mutagenesis to mutate a known palmitoylation site (Cys590) (Wang *et al.*, 2015), followed by measurement of MCAM cleavage. Similarly, site-directed mutagenesis of predicted glycosylation sites may help to establish the relevance of N- and O-glycosylation in MCAM cleavage.

References

Adelheid, K., Wei, C. H., Jonas, S., Zakaria, M., Maike, L., Russ, B., Carlyne, C., Martin, Z., & Laima, T. S. (2013). Endothelial cell adhesion molecule CD146: implications for its role in the pathogenesis of COPD. *The Journal of Pathology, 230*(4), 388-398 https://doi.org/10.1002/path.4197

Adler, N. R., Haydon, A., McLean, C. A., Kelly, J. W., & Mar, V. J. (2017). Metastatic pathways in patients with cutaneous melanoma. *Pigment Cell & Melanoma Research, 30*(1), 13-27 https://doi.org/https://doi.org/10.1111/pcmr.12544

Ainscough, J. S., Gerberick, G. F., Kimber, I., & Dearman, R. J. (2015). Interleukin-1β processing is dependent on a calcium-mediated interaction with calmodulin. *Journal of Biological Chemistry, 290*(52), 31151-31161 https://doi.org/10.1074/jbc.M115.680694

Akasaka-Manya, K., Kawamura, M., Tsumoto, H., Saito, Y., Tachida, Y., Kitazume, S., Hatsuta, H., Miura, Y., Hisanaga, S.-i., Murayama, S., Hashimoto, Y., Manya, H., & Endo, T. (2016). Excess APP O-glycosylation by GalNAc-T6 decreases Aβ production. *The Journal of Biochemistry, 161*(1), 99-111 https://doi.org/10.1093/jb/mvw056

Akasaka-Manya, K., & Manya, H. (2020). The role of APP O-glycosylation in Alzheimer's Disease. *Biomolecules, 10*(11), 1569 https://doi.org/https://doi.org/10.3390/biom10111569

Albelda, S. M., Muller, W. A., Buck, C. A., & Newman, P. J. (1991). Molecular and cellular properties of PECAM-1 (endoCAM/CD31): a novel vascular cell-cell adhesion molecule. *The Journal of Cell Biology, 114*(5), 1059-1068 https://doi.org/10.1083/jcb.114.5.1059

Aldovini, D., Demichelis, F., Doglioni, C., Vizio, D. D., Galligioni, E., Brugnara, S., Zeni, B., Griso, C., Pegoraro, C., Zannoni, M., Gariboldi, M., Balladore, E., Mezzanzanica, D., Canevari, S., & Barbareschi, M. (2006). MCAM expression as marker of poor prognosis in epithelial ovarian cancer. *International Journal of Cancer, 119*(8), 1920-1926 https://doi.org/10.1002/ijc.22082

Amore, A., Knott, B. C., Supekar, N. T., Shajahan, A., Azadi, P., Zhao, P., Wells, L., Linger, J. G., Hobdey, S. E., Wall, T. A. V., Shollenberger, T., Yarbrough, J. M., Tan, Z., Crowley, M. F., Himmel, M. E., Decker, S. R., Beckham, G. T., & Taylor, L. E. (2017). Distinct roles of N- and O-glycans in cellulase activity and stability. *Proceedings of the National Academy of Sciences, U.S.A., 114*(52), 13667-13672 https://doi.org/10.1073/pnas.1714249114

Anfosso, F., Bardin, N., Francès, V., Vivier, E., Camoin-Jau, L., Sampol, J., & Dignat-George, F. (1998). Activation of human endothelial cells via S-Endo-1 antigen

(CD146) stimulates the tyrosine phosphorylation of focal adhesion kinase p125FAK. *Journal of Biological Chemistry, 273*(41), 26852-26856 https://doi.org/10.1074/jbc.273.41.26852

Anfosso, F., Bardin, N., Vivier, E., Sabatier, F., Sampol, J., & Dignat-George, F. (2001). Outside-in signalling pathway linked to CD146 engagement in human endothelial cells. *Journal of Biological Chemistry, 276*(2), 1564-1569. http://www.jbc.org/content/276/2/1564.abstract

Arber, C., Villegas-Llerena, C., Toombs, J., Pocock, J. M., Ryan, N. S., Fox, N. C., Zetterberg, H., Hardy, J., & Wray, S. (2019). Amyloid precursor protein processing in human neurons with an allelic series of the PSEN1 intron 4 deletion mutation and total presenilin-1 knockout. *Brain Communications, 1*(1), fxz024. https://doi.org/10.1093/braincomms/fcz024

Arnold, M., Singh, D., Laversanne, M., Vignat, J., Vaccarella, S., Meheus, F., Cust, A. E., de Vries, E., Whiteman, D. C., & Bray, F. (2022). Global burden of cutaneous melanoma in 2020 and projections to 2040. *JAMA Dermatology, 158*(5), 495-503 https://doi.org/10.1001/jamadermatol.2022.0160

Artym, V. V., Zhang, Y., Seillier-Moiseiwitsch, F., Yamada, K. M., & Mueller, S. C. (2006). Dynamic interactions of cortactin and membrane type 1 matrix metalloproteinase at invadopodia: defining the stages of invadopodia formation and function. *Cancer Research, 66*(6), 3034-3043 https://doi.org/10.1158/0008-5472.can-05-2177

Atkins, M. B., Lee, S. J., Chmielowski, B., Tarhini, A. A., Cohen, G. I., Truong, T. G., Moon, H. H., Davar, D., O'Rourke, M., Stephenson, J. J., Curti, B. D., Urba, W. J., Brell, J. M., Funchain, P., Kendra, K. L., Ikeguchi, A. P., Jaslowski, A., Bane, C. L., Taylor, M. A., Bajaj, M., Conry, R. M., Ellis, R. J., Logan, T. F., Laudi, N., Sosman, J. A., Crockett, D. G., Pecora, A. L., Okazaki, I. J., Reganti, S., Chandra, S., Guild, S., Chen, H. X., Streicher, H. Z., Wolchok, J. D., Ribas, A., & Kirkwood, J. M. (2022). Combination dabrafenib and trametinib versus combination nivolumab and ipilimumab for patients with advanced BRAF-mutant melanoma: the DREAMseq trial-ECOG-ACRIN EA6134. *Journal of Clinical Oncology, 41*(2), 186-197 https://doi.org/10.1200/jco.22.01763

Australian Institute of Health and Welfare. (2021a). Cancer Data In Australia. Cancer series no. 133. Cat.no. CAN 144. Canberra: AIHW. https://doi.org/10.25816/ye05-nm50

Australian Institute of Health and Welfare. (2021b). *Cancer in Australia 2021*. https://www.aihw.gov.au/reports/cancer/cancer-in-australia-2021/summary

Balkwill, F. R., Capasso, M., & Hagemann, T. (2012). The tumor microenvironment at a glance. *Journal of Cell Science, 125*(23), 5591-5596 https://doi.org/10.1242/jcs.116392

Bann, J. G., Peyton, D. H., & Bächinger, H. P. (2000). Sweet is stable: glycosylation stabilizes collagen. *FEBS Lett, 473*(2), 237-240 https://doi.org/10.1016/s0014-5793(00)01493-9

Bardin, N., Anfosso, F., Massé, J.-M., Cramer, E., Sabatier, F., Bivic, A. L., Sampol, J., & Dignat-George, F. (2001). Identification of CD146 as a component of the endothelial junction involved in the control of cell-cell cohesion. *Blood, 98*(13), 3677-3684.

Bardin, N., Blot-Chabaud, M., Despoix, N., Kebir, A., Harhouri, K., Arsanto, J.-P., Espinosa, L., Perrin, P., Robert, S., Vely, F., Sabatier, F., Bivic, A. L., Kaplanski, G., Sampol, J., & Dignat-George, F. (2009). CD146 and its soluble form regulate monocyte transendothelial migration. *Arteriosclerosis, Thrombosis and Vascular Biology, 29*, 746-753.

Bardin, N., Francès, V., Combes, V., Sampol, J., & Dignat-George, F. (1998). CD146: biosynthesis and production of a soluble form in human cultured endothelial cells. *FEBS Letters, 421*(1), 12-14. //www.sciencedirect.com/science/article/pii/S0014579397014555

Bardin, N., Moal, V., Anfosso, F., Daniel, L., Brunet, P., Sampol, J., & George, F. D. (2003). Soluble CD146, a novel endothelial marker, is increased in physiopathological settings linked to endothelial junctional alteration. *Thrombosis and Haemostasis, 90*(11), 915-920 https://doi.org/10.1160/TH02-11-0285

Bardin, N., Reumaux, D., Geboes, K., Francois Colombel, J., Blot-Chabaud, M., Sampol, J., Duthilleul, P., & Dignat-George, F. (2006). Increased expression of CD146, a new marker of the endothelial junction in active inflammatory bowel disease. *Inflammatory Bowel Disease, 12*(1), 16-21 https://doi.org/10.1097/01.MIB.0000194181.46930.88

Basagiannis, D., & Christoforidis, S. (2016). Constitutive endocytosis of VEGFR2 protects the receptor against shedding. *The Journal of Biological Chemistry, 29*(32), 16892–16903 https://doi.org/10.1074/jbc.M116.730309

Bastian, B. C. (2014). The molecular pathology of melanoma: an integrated taxonomy of melanocytic neoplasia. *Annual Reviews Pathology, 9*, 239-271 https://doi.org/10.1146/annurev-pathol-012513-104658

Bell, J. H., Herrera, A. H., Li, Y., & Walcheck, B. (2007). Role of ADAM17 in the ectodomain shedding of TNF-α and its receptors by neutrophils and macrophages. *Journal of Leukocyte Biology, 82*(1), 173-176 https://doi.org/https://doi.org/10.1189/jlb.0307193

Bendell, J., Sharma, S., Patel, M. R., Windsor, K. S., Wainberg, Z. A., Gordon, M., Chaves, J., Berlin, J., Brachmann, C. B., Zavodovskaya, M., Liu, J., Thai, D., Bhargava, P., Shah, M. A., Khan, S. A., & Starodub, A. (2020). Safety and efficacy of andecaliximab (GS-5745) plus gemcitabine and nab-paclitaxel in patients with

advanced pancreatic adenocarcinoma: results from a phase I study. *Oncologist, 25*(11), 954-962 https://doi.org/10.1634/theoncologist.2020-0474

Berchtold, M. W., & Villalobo, A. (2014). The many faces of calmodulin in cell proliferation, programmed cell death, autophagy, and cancer. *Biochimica et Biophysica Acta (BBA) - Molecular Cell Research, 1843*(2), 398-435 https://doi.org/https://doi.org/10.1016/j.bbamcr.2013.10.021

Bertolotto, C. (2013). Melanoma: from melanocyte to genetic alterations and clinical options. *Scientifica, 2013*, 635203 https://doi.org/10.1155/2013/635203

Bhattacharyya, R., Barren, C., & Kovacs, D. M. (2013). Palmitoylation of amyloid precursor protein regulates amyloidogenic processing in lipid rafts. *The Journal of Neuroscience, 33*(27), 11169-11183 https://doi.org/10.1523/JNEUROSCI.4704-12.2013

Black, R. A., Rauch, C. T., Kozlosky, C. J., Peschon, J. J., Slack, J. L., Wolfson, M. F., Castner, B. J., Stocking, K. L., Reddy, P., Srinivasan, S., Nelson, N., Boiani, N., Schooley, K. A., Gerhart, M., Davis, R., Fitzner, J. N., Johnson, R. S., Paxton, R. J., March, C. J., & Cerretti, D. P. (1997). A metalloproteinase disintegrin that releases tumour-necrosis factor-alpha from cells. *Nature, 385*(6618), 729-733.

Bolduc, D. M., Montagna, D. R., Gu, Y., Selkoe, D. J., & Wolfe, M. S. (2016). Nicastrin functions to sterically hinder γ-secretase–substrate interactions driven by substrate transmembrane domain. *Proceedings of the National Academy of Sciences, U.S.A., 113*(5), E509-E518 https://doi.org/10.1073/pnas.1512952113

Bollmann, M., Pap, T., Lohmann, C. H., & Bertrand, J. (2019). Matrix metalloproteinase mediated shedding of Syndecan-4 under osteoarthritis conditions. *Osteoarthritis and Cartilage, 27*(1), S196-S197 https://doi.org/10.1016/j.joca.2019.02.304

Boneberg, E.-M., Illges, H., Legler, D. F., & Fürstenberger, G. (2009). Soluble CD146 is generated by ectodomain shedding of membrane CD146 in a calcium-induced, matrix metalloprotease-dependent process. *Microvascular Research, 78*(3), 325-331 https://doi.org/http://dx.doi.org/10.1016/j.mvr.2009.06.012

Borggrefe, T., Lauth, M., Zwijsen, A., Huylebroeck, D., Oswald, F., & Giaimo, B. D. (2016). The Notch intracellular domain integrates signals from Wnt, Hedgehog, TGFβ/BMP and hypoxia pathways. *Biochimica et Biophysica Acta (BBA) - Molecular Cell Research, 1863*(2), 303-313 https://doi.org/https://doi.org/10.1016/j.bbamcr.2015.11.020

Braley, A., Kwak, T., Jules, J., Harja, E., Landgraf, R., & Hudson, B. I. (2016). Regulation of receptor for advanced glycation end products (RAGE) ectodomain shedding and its role in cell function. *Journal of Biological Chemistry, 291*(23), 12057-12073 https://doi.org/10.1074/jbc.M115.702399

Bresnick, A. R. (2018). S100 proteins as therapeutic targets. *Biophysical Reviews, 10*(6), 1617-1629 https://doi.org/10.1007/s12551-018-0471-y

Bringans, S., Eriksen, S., Kendrick, T., Gopalakrishnakone, P., Livk, A., Lock, R., & Lipscombe, R. (2008). Proteomic analysis of the venom of heterometrus longimanus (Asian black scorpion). *Proteomics, 8*(5), 1081-1096 https://doi.org/https://doi.org/10.1002/pmic.200700948

Brown, M. S., Ye, J., Rawson, R. B., & Goldstein, J. L. (2000). Regulated intramembrane proteolysis: a control mechanism conserved from bacteria to humans. *Cell, 100*(4), 391-398 https://doi.org/10.1016/S0092-8674(00)80675-3

Bu, P., Zhuang, J., Feng, J., Yang, D., Shen, X., & Yan, X. (2007). Visualization of CD146 dimerization and its regulation in living cells. *Biochimica et Biophysica Acta (BBA) - Molecular Cell Research, 1773*(4), 513-520 https://doi.org/https://doi.org/10.1016/j.bbamcr.2007.01.009

Bubka, M., Link-Lenczowski, P., Janik, M., Pocheć, E., & Lityńska, A. (2014). Overexpression of N-acetylglucosaminyltransferases III and V in human melanoma cells. Implications for MCAM N-glycosylation. *Biochimie, 103*, 37-49 https://doi.org/http://dx.doi.org/10.1016/j.biochi.2014.04.003

Buchanan, P. C., Boylan, K. L. M., Walcheck, B., Heinze, R., Geller, M. A., Argenta, P. A., & Skubitz, A. P. N. (2017). Ectodomain shedding of the cell adhesion molecule Nectin-4 in ovarian cancer is mediated by ADAM10 and ADAM17. *The Journal of Biological Chemistry, 292*(15), 6339-6351 https://doi.org/10.1074/jbc.M116.746859

Bukhari, H., Glotzbach, A., Kolbe, K., Leonhardt, G., Loosse, C., & Müller, T. (2017). Small things matter: Implications of APP intracellular domain AICD nuclear signalling in the progression and pathogenesis of Alzheimer's disease. *Progress in Neurobiology, 156*, 189-213 https://doi.org/https://doi.org/10.1016/j.pneurobio.2017.05.005

Bussard, K. M., Mutkus, L., Stumpf, K., Gomez-Manzano, C., & Marini, F. C. (2016). Tumor-associated stromal cells as key contributors to the tumor microenvironment. *Breast Cancer Research, 18*(1), 84 https://doi.org/10.1186/s13058-016-0740-2

Calligaris, M., Cuffaro, D., Bonelli, S., Spanò, D. P., Rossello, A., Nuti, E., & Scilabra, S. D. (2021). Strategies to target ADAM17 in disease: from Its discovery to the iRhom revolution. *Molecules, 26*(4), 944 https://doi.org/https://10.3390/molecules26040944

Campbell, W. A., Reed, M. L. O., Strahle, J., Wolfe, M. S., & Xia, W. (2003). Presenilin endoproteolysis mediated by an aspartyl protease activity pharmacologically distinct from γ-secretase. *Journal of Neurochemistry, 85*(6), 1563-1574 https://doi.org/https://doi.org/10.1046/j.1471-4159.2003.01799.x

Castro-Castro, A., Marchesin, V., Monteiro, P., Lodillinsky, C., Rosse, C., & Chavrier, P. (2015). Cellular and molecular mechanisms of MT1-MMP-dependent cancer cell invasion. *Annual Review of Cell and Developmental Biology, 32*(1), 1-22 https://doi.org/10.1146/annurev-cellbio-111315-125227

Cathcart, J., Pulkoski-Gross, A., & Cao, J. (2015). Targeting matrix metalloproteinases in cancer: bringing new life to old ideas. *Genes and Diseases, 2*, 26-34 https://doi.org/http://dx.doi.org/10.1016/j.gendis.2014.12.002

Cavallaro, U., & Dejana, E. (2011). Adhesion molecule signalling: not always a sticky business. *Nature Reviews Molecular Cell Biology, 12*(3), 189-197 https://doi.org/10.1038/nrm3068

Chakrabarti, A., & Mukhopadhyay, D. (2012). Novel adaptors of amyloid precursor protein intracellular domain and their functional implications. *Genomics, proteomics & bioinformatics, 10*(4), 208-216 https://doi.org/10.1016/j.gpb.2012.07.002

Chavaroche, A., Cudic, M., Giulianotti, M., Houghten, R. A., Fields, G. B., & Minond, D. (2014). Glycosylation of a disintegrin and metalloprotease 17 affects its activity and inhibition. *Analytical Biochemistry, 449*, 68-75 https://doi.org/10.1016/j.ab.2013.12.018

Chen, J., Luo, Y., Huang, H., Wu, S., Feng, J., Zhang, J., & Yan, X. (2018). CD146 is essential for PDGFRβ-induced pericyte recruitment. *Protein & Cell, 9*(8), 743-747 https://doi.org/10.1007/s13238-017-0484-5

Chen, X. B., Li, W., & Chu, A. X. (2019a). MicroRNA-133a inhibits gastric cancer cells growth, migration, and epithelial-mesenchymal transition process by targeting presenilin 1. *Journal of cellular biochemistry, 120*(1), 470-480 https://doi.org/10.1002/jcb.27403

Chen, Y., Sumardika, I. W., Tomonobu, N., Winarsa Ruma, I. M., Kinoshita, R., Kondo, E., Inoue, Y., Sato, H., Yamauchi, A., Murata, H., Yamamoto, K.-i., Tomida, S., Shien, K., Yamamoto, H., Soh, J., Liu, M., Futami, J., Sasai, K., Katayama, H., Kubo, M., Putranto, E. W., Hibino, T., Sun, B., Nishibori, M., Toyooka, S., & Sakaguchi, M. (2019b). Melanoma cell adhesion molecule is the driving force behind the dissemination of melanoma upon S100A8/A9 binding in the original skin lesion. *Cancer Letters, 452*, 178-190 https://doi.org/https://doi.org/10.1016/j.canlet.2019.03.023

Cheng, Y., Lin, L., Li, X., Lu, A., Hou, C., Wu, Q., Hu, X., Zhou, Z., Chen, Z., & Tang, F. (2021). ADAM10 is involved in the oncogenic process and chemo-resistance of triple-negative breast cancer via regulating Notch1 signalling pathway, CD44 and PrPc. *Cancer Cell International, 21*(1), 32 https://doi.org/10.1186/s12935-020-01727-5

Chiang, P.-M., Fortna, R. R., Price, D. L., Li, T., & Wong, P. C. (2012). Specific domains in anterior pharynx-defective 1 determine its intramembrane interactions with nicastrin and presenilin. *Neurobiology of Aging, 33*(2), 277-285 https://doi.org/10.1016/j.neurobiolaging.2009.12.028

Christensen, J., & Shastri, V. P. (2015). Matrix-metalloproteinase-9 is cleaved and activated by cathepsin K. *BMC Research Notes, 8*, 322-322 https://doi.org/10.1186/s13104-015-1284-8

Christensen, J. N., Schmidt, H., Steiniche, T., & Madsen, M. (2020). Identification of robust reference genes for studies of gene expression in FFPE melanoma samples and melanoma cell lines. *Melanoma Research, 30*(1), 26-38

Cireap, N., & Narita, D. (2013). Molecular profiling of ADAM12 and ADAM17 genes in human malignant melanoma. *Pathology Oncology Research, 19*(4), 755-762 https://doi.org/10.1007/s12253-013-9639-8

Codony-Servat, J., Albanell, J., Lopez-Talavera, J. C., Arribas, J., & Baselga, J. (1999). Cleavage of the HER2 ectodomain is a pervanadate-activable process that is inhibited by the tissue inhibitor of metalloproteases-1 in breast cancer cells. *Cancer Research, 59*(6), 1196-1201 http://cancerres.aacrjournals.org/content/canres/59/6/1196.full.pdf

Colomb, F., Wang, W., Simpson, D., Zafar, M., Beynon, R., Rhodes, J. M., & Yu, L.-G. (2017). Galectin-3 interacts with the cell-surface glycoprotein CD146 (MCAM, MUC18) and induces secretion of metastasis-promoting cytokines from vascular endothelial cells *Journal of Biological Chemistry, 292*, 8381-8389 https://doi.org/10.1074/jbc.M117.783431

Conibear, E., & Davis, N. G. (2010). Palmitoylation and depalmitoylation dynamics at a glance. *Journal of Cell Science, 123*(Pt 23), 4007-4010 https://doi.org/10.1242/jcs.059287

Connacher, M. K., Tay, J. W., & Ahn, N. G. (2017). Rear-polarized Wnt5a-receptor-actin-myosin-polarity (WRAMP) structures promote the speed and persistence of directional cell migration. *Mol Biol Cell, 28*(14), 1924-1936 https://doi.org/10.1091/mbc.e16-12-0875

Curti, B. D., & Faries, M. B. (2021). Recent advances in the treatment of melanoma. *The New England Journal of Medicine, 384*(23), 2229-2240 https://doi.org/10.1056/NEJMra2034861

Curtin, J. A., Fridlyand, J., Kageshita, T., Patel, H. N., Busam, K. J., Kutzner, H., Cho, K.-H., Aiba, S., Bröcker, E.-B., LeBoit, P. E., Pinkel, D., & Bastian, B. C. (2005). Distinct sets of genetic alterations in melanoma. *New England Journal of Medicine, 353*(20), 2135-2147 https://doi.org/10.1056/NEJMoa050092

D'Arcy, C., & Kiel, C. (2021). Cell adhesion molecules in normal skin and melanoma. *Biomolecules, 11*(8), 2-21. https://doi.org/doi:10.3390/biom11081213

Dahmani, A., & Delisle, J.-S. (2018). TGF-β in T cell biology: implications for cancer immunotherapy. *Cancers, 10*(6), 194 https://doi.org/10.3390/cancers10060194

Dang, M., Armbruster, N., Miller, M. A., Cermeno, E., Hartmann, M., Bell, G. W., Root, D. E., Lauffenburger, D. A., Lodish, H. F., & Herrlich, A. (2013). Regulated ADAM17-dependent EGF family ligand release by substrate-selecting signalling pathways. *Proceedings of the National Academy of Sciences, U.S.A, 110*(24), 9776-9781 https://doi.org/10.1073/pnas.1307478110 %J

Danyukova, T., Schöneck, K., & Pohl, S. (2022). Site-1 and site-2 proteases: a team of two in regulated proteolysis. *Biochimica et Biophysica Acta (BBA) - Molecular Cell Research, 1869*(1), 119138 https://doi.org/https://doi.org/10.1016/j.bbamcr.2021.119138

Davis, L. E., Shalin, S. C., & Tackett, A. J. (2019). Current state of melanoma diagnosis and treatment. *Cancer Biology and Therapy, 20*(11), 1366-1379 https://doi.org/10.1080/15384047.2019.1640032

de Oca, B., Montes, P., Malardé, V., Proust, R., Dautry-Varsat, A., & Gesbert, F. (2010). Ectodomain shedding of interleukin-2 receptor β and generation of an intracellular functional fragment. *The Journal of Biological Chemistry, 285*(29), 22050-22058 https://doi.org/10.1074/jbc.M109.093088

Dedkova, E. N., Sigova, A. A., & Zinchenko, V. P. (2000). Mechanism of action of calcium ionophores on intact cells: ionophore-resistant cells. *Membrane and Cell Biology, 13*(3), 357-368

Deng, H., Lv, L., Li, Y., Zhang, C., Meng, F., Pu, Y., Xiao, J., Qian, L., Zhao, W., Liu, Q., Zhang, D., Wang, Y., Zhang, H., He, Y., & Zhu, J. (2015). The miR-193a-3p regulated PSEN1 gene suppresses the multi-chemoresistance of bladder cancer. *Biochimica et Biophysica Acta (BBA) - Molecular Basis of Disease, 1852*(3), 520-528 https://doi.org/https://doi.org/10.1016/j.bbadis.2014.12.014

Deng, W., Cho, S., & Li, R. (2013a). FERM domain of moesin desorbs the basic-rich cytoplasmic domain of L-selectin from the anionic membrane surface. *Journal of Molecular Biology, 425*(18) https://doi.org/10.1016/j.jmb.2013.06.008

Deng, W., Putkey, J. A., & Li, R. (2013b). Calmodulin adopts an extended conformation when interacting with L-selectin in membranes. *PLOS ONE, 8*(5), e62861 https://doi.org/10.1371/journal.pone.0062861

Deng, W., Srinivasan, S., Zheng, X., Putkey, J. A., & Li, R. (2011). Interaction of calmodulin with L-selectin at the membrane interface: implication on the regulation of L-selectin shedding. *Journal of Molecular Biology, 411*(1), 220-233 https://doi.org/http://dx.doi.org/10.1016/j.jmb.2011.05.041

Deryugina, E. I., Ratnikov, B. I., Postnova, T. I., Rozanov, D. V., & Strongin, A. Y. (2002). Processing of integrin αv subunit by membrane type 1 matrix metalloproteinase stimulates migration of breast carcinoma cells on vitronectin and enhances tyrosine phosphorylation of focal adhesion kinase. *Journal of Biological Chemistry, 277*(12), 9749-9756 https://doi.org/10.1074/jbc.M110269200

Deschenes, Robert J. “Protein Palmitoylation”. In *Encyclopedia of Biological Chemistry (Second Edition),* edited by William J. Lennarz and M. Daniel Lane, 645-647. Cambridge, MA: Academic Press, 2013. https://doi.org/https://doi.org/10.1016/B978-0-12-378630-2.00022-0

Díaz-Fernández, A., Miranda-Castro, R., de-los-Santos-Álvarez, N., & Lobo-Castañón, M. J. (2018). Post-translational modifications in tumor biomarkers: the next challenge for aptamers? *Analytical and Bioanalytical Chemistry, 410*(8), 2059-2065 https://doi.org/10.1007/s00216-018-0861-9

Diestel, S., Hinkle, C. L., Schmitz, B., & Maness, P. F. (2005). NCAM140 stimulates integrin-dependent cell migration by ectodomain shedding. *Journal of Neurochemistry, 95*, 1777-1784 https://doi.org/10.1111/j.1471-4159.2005.03475.x

Dudzik, P., Trojan, S. E., Ostrowska, B., Lasota, M., Dulińska-Litewka, J., Laidler, P., & Kocemba-Pilarczyk, K. A. (2019a). Aberrant promoter methylation may be responsible for the control of CD146 (MCAM) gene expression during breast cancer progression*. *The Journal of the Polish Biochemical Society and of the Polish Academy of Sciences, 66*(4), 619-625 https://doi.org/https://doi.org/10.18388/abp.2019_2907

Dudzik, P., Trojan, S. E., Ostrowska, B., Zemanek, G., Dulińska-Litewka, J., Laidler, P., & Kocemba-Pilarczyk, K. A. (2019b). The epigenetic modifier 5-aza-2-deoxycytidine triggers the expression of *CD146 g*ene in prostate cancer cells. *Anticancer research, 39*(5), 2395-2403 https://doi.org/10.21873/anticanres.13357

Dwivedi, A., Slater, S. C., & George, S. J. (2009). MMP-9 and -12 cause N-cadherin shedding and thereby β-catenin signalling and vascular smooth muscle cell proliferation. *Cardiovascular Research, 81*(1), 178-186 https://doi.org/10.1093/cvr/cvn278

Dye, D. E. (2007). *The role of MCAM in melanoma and metastasis* [PhD Thesis, University of Western Australia]. Perth, Western Australia.

Dye, D. E., Karlen, S., Rohrbach, B., Staub, O., Braathen, L. R., Eidne, K. A., & Coombe, D. R. (2009). hShroom1 links a membrane bound protein to the actin cytoskeleton. *Cellular and Molecular Life Sciences, 66*(4), 681-696 https://doi.org/10.1007/s00018-009-8645-1

Ebsen, H., Lettau, M., Kabelitz, D., & Janssen, O. (2015). Subcellular localization and activation of ADAM proteases in the context of FasL shedding in T lymphocytes. *Molecular Immunology, 65*(2), 416-428 https://doi.org/10.1016/j.molimm.2015.02.008

Eggermont, A. M. M., & Kirkwood, J. M. (2004). Re-evaluating the role of dacarbazine in metastatic melanoma: what have we learned in 30 years? *European Journal of Cancer, 40*(12), 1825-1836 https://doi.org/https://doi.org/10.1016/j.ejca.2004.04.030

Elshal, M. F., Khan, S. S., Takahashi, Y., Solomon, M. A., & McCoy, J. P. (2005). CD146 (Mel-CAM), an adhesion marker of endothelial cells, is a novel marker of lymphocyte subset activation in normal peripheral blood. *Blood, 106*(8), 2923-2924 https://doi.org/10.1182/blood-2005-06-2307

Emmanouilidi, A., Paladin, D., Greening, D. W., & Falasca, M. (2019). Oncogenic and non-malignant pancreatic exosome cargo reveal distinct expression of oncogenic and prognostic factors involved in tumor invasion and metastasis. *Proteomics, 19*(8) https://doi.org/10.1002/pmic.201800158

Endo, K., Takino, T., Miyamori, H., Kinsen, H., Yoshizaki, T., Furukawa, M., & Sato, H. (2003). Cleavage of syndecan-1 by membrane type matrix metalloproteinase-1 stimulates cell migration. *Journal of Biological Chemistry, 278*(42), 40764-40770 https://doi.org/10.1074/jbc.M306736200

Endres, K., Anders, A., Kojro, E., Gilbert, S., Fahrenholz, F., & Postina, R. (2003). Tumor necrosis factor-α converting enzyme is processed by proprotein-convertases to its mature form which is degraded upon phorbol ester stimulation. *European Journal of Biochemistry, 270*(11), 2386-2393 https://doi.org/https://doi.org/10.1046/j.1432-1033.2003.03606.x

Escrevente, C., Morais, V. A., Keller, S., Soares, C. M., Altevogt, P., & Costa, J. (2008). Functional role of N-glycosylation from ADAM10 in processing, localization and activity of the enzyme. *Biochimica et Biophysica Acta (BBA)- General Subjects, 1780*(6), 905-913 https://doi.org/https://doi.org/10.1016/j.bbagen.2008.03.004

Eskelinen, E. L. (2006). Roles of LAMP-1 and LAMP-2 in lysosome biogenesis and autophagy. *Molecular Aspects of Medicine, 27*(5-6), 495-502 https://doi.org/10.1016/j.mam.2006.08.005

Espagnolle, N., Guilloton, F., Deschaseaux, F., Gadelorge, M., Sensébé, L., & Bourin, P. (2014). CD146 expression on mesenchymal stem cells is associated with their

vascular smooth muscle commitment. *Journal of Cellular and Molecular Medicine, 18*(1), 104-114. http://dx.doi.org/10.1111/jcmm.12168

Esteras, N., Muñoz, Ú., Alquézar, C., Bartolomé, F., Bermejo-Pareja, F., & Martín-Requero, Á. (2012). Altered calmodulin degradation and signalling in non-neuronal cells from alzheimer's disease patients *Current Alzheimer Research, 9*(3), 267-277. https://doi.org/DOI://10.2174/156720512800107564

Facey, A., Pinar, I., Arthur, J. F., Qiao, J., Jing, J., Mado, B., Carberry, J., Andrews, R. K., & Gardiner, E. E. (2016). A-Disintegrin-And-Metalloproteinase (ADAM) 10 activity on resting and activated platelets. *Biochemistry, 55*(8), 1187-1194. https://doi.org/10.1021/acs.biochem.5b01102

Fan, D., Takawale, A., Shen, M., Samokhvalov, V., Basu, R., Patel, V., Wang, X., Fernandez-Patron, C., Seubert, J. M., Oudit, G. Y., & Kassiri, Z. (2016). A disintegrin and metalloprotease-17 regulates pressure overload-induced myocardial hypertrophy and dysfunction through proteolytic processing of integrin β1. *Hypertension, 68*(4), 937-948. https://doi.org/10.1161/HYPERTENSIONAHA.116.07566

Fedeli, C., Filadi, R., Rossi, A., Mammucari, C., & Pizzo, P. (2019). PSEN2 (presenilin 2) mutants linked to familial Alzheimer disease impair autophagy by altering Ca(2+) homeostasis. *Autophagy, 15*(12), 2044-2062. https://doi.org/10.1080/15548627.2019.1596489

Feng, J., Wang, J., Liu, Q., Li, J., Zhang, Q., Zhuang, Z., Yao, X., Liu, C., Li, Y., Cao, L., Li, C., Gong, L., Li, D., Zhang, Y., & Gao, H. (2019). DAPT, a γ-secretase inhibitor, suppresses tumorigenesis, and progression of growth hormone-producing adenomas by targeting notch signalling. *Frontiers in Oncology, 9*, 809. https://doi.org/10.3389/fonc.2019.00809

Fitzgerald, M. L., Wang, Z., Park, P. W., Murphy, G., & Bernfield, M. (2000). Shedding of syndecan-1 and -4 ectodomains is regulated by multiple signalling pathways and mediated by a Timp-3–sensitive metalloproteinase. *The Journal of Cell Biology, 148*(4), 811-824. https://doi.org/10.1083/jcb.148.4.811

Flanagan, K., Fitzgerald, K., Baker, J., Regnstrom, K., Gardai, S., Bard, F., Mocci, S., Seto, P., You, M., Larochelle, C., Prat, A., Chow, S., Li, L., Vandevert, C., Zago, W., Lorenzana, C., Nishioka, C., Hoffman, J., Botelho, R., Willits, C., Tanaka, K., Johnston, J., & Yednock, T. (2012). Laminin-411 is a vascular ligand for MCAM and Ffcilitates TH17 cell entry into the CNS. *PLoS One, 7*(7), e40443 https://doi.org/10.1371/journal.pone.0040443

Frade, J. M. (2005). Nuclear translocation of the p75 neurotrophin receptor cytoplasmic domain in response to neurotrophin binding. *The Journal of neuroscience : the official journal of the Society for Neuroscience, 25*(6), 1407-1411 https://doi.org/10.1523/JNEUROSCI.3798-04.2005

Franco, P. I. R., Rodrigues, A. P., de Menezes, L. B., & Miguel, M. P. (2020). Tumor microenvironment components: allies of cancer progression. *Pathology - Research and Practice, 216*(1), 152729 https://doi.org/https://doi.org/10.1016/j.prp.2019.152729

Fröhlich, C., Klitgaard, M., Noer, J., Kotzsch, A., Nehammer, C., Kronqvist, P., Berthelsen, J., Blobel, C., Kveiborg, M., Albrechtsen, R., & Wewer, U. (2013). ADAM12 is expressed in the tumour vasculature and mediates ectodomain shedding of several membrane-anchored endothelial proteins. *The Biochemical Journal, 452*(1), 97-109 https://doi.org/10.1042/BJ20121558

Gangemi, R., Amaro, A., Gino, A., Barisione, G., Fabbi, M., Pfeffer, U., Brizzolara, A., Queirolo, P., Salvi, S., Boccardo, S., Gualco, M., Spagnolo, F., Jager, M. J., Mosci, C., Rossello, A., & Ferrini, S. (2014). ADAM10 correlates with uveal melanoma metastasis and promotes in vitro invasion. *Pigment Cell & Melanoma Research, 27*(6), 1138-1148 https://doi.org/10.1111/pcmr.12306

Gao, Q., Zhang, J., Wang, X., Liu, Y., He, R., Liu, X., Wang, F., Feng, J., Yang, D., Wang, Z., Meng, A., & Yan, X. (2017). The signalling receptor MCAM coordinates apical-basal polarity and planar cell polarity during morphogenesis. *Nature Communications*, 8(15279), 1-13. https://doi.org/10.1038/ncomms15279

Garton, K. J., Gough, P. J., Blobel, C. P., Murphy, G., Greaves, D. R., Dempsey, P. J., & Raines, E. W. (2001). Tumor Necrosis Factor-α-converting Enzyme (ADAM17) mediates the cleavage and shedding of fractalkine (CX3CL1). *Journal of Biological Chemistry, 276*(41), 37993-38001. http://www.jbc.org/content/276/41/37993.abstract

Garton, K. J., Gough, P. J., Philalay, J., Wille, P. T., Blobel, C. P., Whitehead, R. H., Dempsey, P. J., & Raines, E. W. (2003). Stimulated shedding of vascular cell adhesion molecule 1 (VCAM-1) is mediated by tumor necrosis factor-converting enzyme (ADAM 17). *The Journal of Biological Chemistry, 278*(39), 37459-37464 https://doi.org/10.1074/jbc.M305877200

Gearing, A. J. H., Beckett, P., Christodoulou, M., Churchill, M., Clements, J., Davidson, A. H., Drummond, A. H., Galloway, W. A., Gilbert, R., Gordon, J. L., Leber, T. M., Mangan, M., Miller, K., Nayee, P., Owen, K., Patel, S., Thomas, W., Wells, G., Wood, L. M., & Woolley, K. (1994). Processing of tumour necrosis factor-α precursor by metalloproteinases. *Nature, 370*, 555 https://doi.org/10.1038/370555a0

Gershenwald, J. E., Scolyer, R. A., Hess, K. R., Sondak, V. K., Long, G. V., Ross, M. I., Lazar, A. J., Faries, M. B., Kirkwood, J. M., McArthur, G. A., Haydu, L. E., Eggermont, A. M. M., Flaherty, K. T., Balch, C. M., & Thompson, J. F. (2017). Melanoma staging: evidence-based changes in the American Joint Committee on Cancer eighth edition cancer staging manual. *CA: A Cancer Journal for Clinicians, 67*(6), 472-492 https://doi.org/https://doi.org/10.3322/caac.21409

Gifford, J. L., Ishida, H., & Vogel, H. J. (2012). Structural insights into calmodulin-regulated L-selectin ectodomain shedding. *The Journal of Biological Chemistry, 287*(32), 26513-26527 https://doi.org/10.1074/jbc.M112.373373

Golubkov, V. S., & Strongin, A. Y. (2012). Insights into ectodomain shedding and processing of protein-tyrosine pseudokinase 7 (PTK7). *The Journal of Biological Chemistry, 287*(50), 42009-42018 https://doi.org/10.1074/jbc.M112.371153

Gooz, M. (2010). ADAM-17: the enzyme that does it all. *Critical Reviews in Biochemistry and Molecular Biology, 45*(2), 146-169 https://doi.org/10.3109/10409231003628015

Goth, C. K., Halim, A., Khetarpal, S. A., Rader, D. J., Clausen, H., & Schjoldager, K. T. B. G. (2015). A systematic study of modulation of ADAM-mediated ectodomain shedding by site-specific O-glycosylation. *Proceedings of the National Academy of Sciences, U.S.A., 112*(47), 14623-14628 https://doi.org/10.1073/pnas.1511175112

Groth, E., Pruessmeyer, J., Babendreyer, A., Schumacher, J., Pasqualon, T., Dreymueller, D., Higashiyama, S., Lorenzen, I., Grötzinger, J., Cataldo, D., & Ludwig, A. (2016). Stimulated release and functional activity of surface expressed metalloproteinase ADAM17 in exosomes. *Biochimica et Biophysica Acta (BBA)- Molecular Cell Research, 1863*(11), 2795-2808 https://doi.org/https://doi.org/10.1016/j.bbamcr.2016.09.002

Gschwind, A., Hart, S., Fischer, O. M., & Ullrich, A. (2003). TACE cleavage of proamphiregulin regulates GPCR-induced proliferation and motility of cancer cells. *The EMBO Journal, 22*(10), 2411-2421 https://doi.org/10.1093/emboj/cdg231

Guan, X., & Fierke, C. A. (2011). Understanding protein palmitoylation: biological significance and enzymology. *Science China Chemistry, 54*(12), 1888-1897 https://doi.org/10.1007/s11426-011-4428-2

Guezguez, B., Vigneron, P., Alais, S., Jaffredo, T., Gavard, J., Mège, R.-M., & Dunon, D. (2006). A dileucine motif targets MCAM-l cell adhesion molecule to the basolateral membrane in MDCK cells. *FEBS Letters, 580*(15), 3649-3656. https://doi.org/10.1016/j.febslet.2006.05.048

Guezguez, B., Vigneron, P., Lamerant, N., Kieda, C., Jaffredo, T., & Dunon, D. (2007). Dual Role of Melanoma Cell Adhesion Molecule (MCAM)/CD146 in lymphocyte endothelium interaction: MCAM/CD146 promotes rolling via microvilli induction in lymphocyte and is an endothelial adhesion receptor. *The Journal of Immunology, 179*(10), 6673-6685.

Güner, G., & Lichtenthaler, S. F. (2020). The substrate repertoire of γ-secretase/presenilin. *Seminars in Cell & Developmental Biology, 105*, 27-42 https://doi.org/https://doi.org/10.1016/j.semcdb.2020.05.019

Guo, W., Wang, H., & Li, C. (2021). Signal pathways of melanoma and targeted therapy. *Signal Transduction and Targeted Therapy, 6*(1), 424 https://doi.org/10.1038/s41392-021-00827-6

Gutwein, P., Mechtersheimer, S., Riedle, S., Stoeck, A., Gast, D., Joumaa, S., Zentgraf, H., Fogel, M., & Altevogt, P. (2003). ADAM10-mediated cleavage of L1 adhesion molecule at the cell surface and in released membrane vesicles. *The FASEB Journal, 17*(2), 292-294 https://doi.org/10.1096/fj.02-0430fje

Gutwein, P., Stoeck, A., Riedle, S., Gast, D., Runz, S., Condon, T. P., Marmé, A., Phong, M.-C., Linderkamp, O., Skorokhod, A., & Altevogt, P. (2005). Cleavage of L1 in exosomes and apoptotic membrane vesicles released from ovarian carcinoma cells. *Clinical Cancer Research, 11*(7), 2492 https://doi.org/10.1158/1078-0432.CCR-04-1688

Haapasalo, A., & Kovacs, D. M. (2011). The many substrates of presenilin/γ-secretase. *Journal of Alzheimer's Disease, 25*(1), 3-28 https://doi.org/10.3233/JAD-2011-101065

Hachmeister, M., Bobowski, K. D., Hogl, S., Dislich, B., Fukumori4, A., Eggert, C., Mack, B., Kremling, H., Sarrach, S., Coscia, F., Zimmermann, W., Steiner, H., Lichtenthaler, S. F., & Gires, O. (2013). Regulated intramembrane proteolysis and degradation of murine Epithelial Cell Adhesion Molecule mEpCAM. *PLoS One, 8*(8), e71836 https://doi.org/10.1371/journal.pone.0071836

Hackett, M., Guo, L., Shabanowitz, J., Hunt, D. F., & Hewlett, E. L. (1994). Internal lysine palmitoylation in adenylate cyclase toxin from *Bordetella pertussis*. *Science, 266*(5184), 433-435 https://doi.org/doi:10.1126/science.7939682

Haqq, C., Nosrati, M., Sudilovsky, D., Crothers, J., Khodabakhsh, D., Pulliam, B. L., Federman, S., Miller, J. R., Allen, R. E., Singer, M. I., Leong, S. P. L., Ljung, B.-M., Sagebiel, R. W., & Kashani-Sabet, M. (2005). The gene expression signatures of melanoma progression. *Proceedings of the National Academy of Sciences, U.S.A., 102*(17), 6092-6097 https://doi.org/10.1073/pnas.0501564102

Harhouri, K., Kebir, A., Guillet, B., Foucault-Bertaud, A., Voytenko, S., Piercecchi-Marti, M.-D., Berenguer, C., Lamy, E., Vely, F. d. r., Pisano, P., Ouafik, L. H., Sabatier, F., Sampol, J., Bardin, N., Dignat-George, F. o., & Blot-Chabaud, M. (2010). Soluble CD146 displays angiogenic properties and promotes neovascularization in experimental hind-limb ischemia. *Vascular Biology, 115*(18), 3843-3851 https://doi.org/10.1182/blood-2009-06-229591

Hartmann, D., de Strooper, B., Serneels, L., Craessaerts, K., Herreman, A., Annaert, W., Umans, L., Lübke, T., Lena Illert, A., von Figura, K., & Saftig, P. (2002). The disintegrin/metalloprotease ADAM 10 is essential for Notch signalling but not for α-secretase activity in fibroblasts. *Human Molecular Genetics, 11*(21), 2615-2624 https://doi.org/10.1093/hmg/11.21.2615

Hartmann, M., Herrlich, A., & Herrlich, P. (2013). Who decides when to cleave an ectodomain? *Trends in Biochemical Sciences, 38*(3), 111-120 https://doi.org/http://dx.doi.org/10.1016/j.tibs.2012.12.002

Hartmann, M., Parra, L. M., Ruschel, A., Lindner, C., Morrison, H., Herrlich, A., & Herrlich, P. (2015). Inside-out regulation of ectodomain cleavage of cluster-of-differentiation-44 (CD44) and of neuregulin-1 requires substrate dimerization. *The Journal of Biological Chemistry, 290*(28), 17041-17054 https://doi.org/10.1074/jbc.M114.610204

Hayashida, K., Bartlett, A. H., Chen, Y. E., & Park, P. W. (2010). Molecular and Cellular Mechanisms of Ectodomain Shedding. *Anatomical Record, 293*(6), 925-937 https://doi.org/10.1002/ar.20757

Hayashida, K., Stahl, P. D., & Park, P. W. (2008). Syndecan-1 ectodomain shedding is regulated by the small GTPase Rab5. *Journal of Biological Chemistry, 283*(51), 35435-35444 https://doi.org/https://doi.org/10.1074/jbc.M804172200

Hayward, N. K., Wilmott, J. S., Waddell, N., Johansson, P. A., Field, M. A., Nones, K., Patch, A. M., Kakavand, H., Alexandrov, L. B., Burke, H., Jakrot, V., Kazakoff, S., Holmes, O., Leonard, C., Sabarinathan, R., Mularoni, L., Wood, S., Xu, Q., Waddell, N., Tembe, V., Pupo, G. M., De Paoli-Iseppi, R., Vilain, R. E., Shang, P., Lau, L. M. S., Dagg, R. A., Schramm, S. J., Pritchard, A., Dutton-Regester, K., Newell, F., Fitzgerald, A., Shang, C. A., Grimmond, S. M., Pickett, H. A., Yang, J. Y., Stretch, J. R., Behren, A., Kefford, R. F., Hersey, P., Long, G. V., Cebon, J., Shackleton, M., Spillane, A. J., Saw, R. P. M., López-Bigas, N., Pearson, J. V., Thompson, J. F., Scolyer, R. A., & Mann, G. J. (2017). Whole-genome landscapes of major melanoma subtypes. *Nature, 545*(7653), 175-180 https://doi.org/10.1038/nature22071

Hedemann, N., Rogmans, C., Sebens, S., Wesch, D., Reichert, M., Schmidt-Arras, D., Oberg, H.-H., Pecks, U., van Mackelenbergh, M., Weimer, J., Arnold, N., Maass, N., & Bauerschlag, D. O. (2018). ADAM17 inhibition enhances platinum efficiency in ovarian cancer. *Oncotarget, 9*(22) https://doi.org/https://doi.org/10.18632/oncotarget.24682

Higashiyama, S., Nanba, D., Nakayama, H., Inoue, H., & Fukuda, S. (2011). Ectodomain shedding and remnant peptide signalling of EGFRs and their ligands. *The Journal of Biochemistry, 150*(1), 15-22 https://doi.org/10.1093/jb/mvr068

Hinkle, C. L., Diestel, S., Lieberman, J., & Maness, P. F. (2006). Metalloprotease-induced ectodomain shedding of neural cell adhesion molecule (NCAM). *Journal of Neurobiology, 66*(12), 1378-1395 https://doi.org/10.1002/neu.20257

Hirata, M., Umata, T., Takahashi, T., Ohnuma, M., Miura, Y., Iwamoto, R., & Mekada, E. (2001). Identification of serum factor inducing ectodomain shedding of proHB-EGF and studies of noncleavable mutants of proHB-EGF. *Biochemical and Biophysical Research Communications, 283*, 915-922 https://doi.org/10.1006/bbrc.2001.4879

Hofmann, U. B., Eggert, A. A. O., Blass, K., Bröcker, E.-B., & Becker, J. C. (2003). Expression of matrix metalloproteinases in the microenvironment of spontaneous and experimental melanoma metastases reflects the requirements for tumor formation. *Cancer Research, 63*(23), 8221-8225.

Hofmann, U. B., Westphal, J. R., van Muijen, G. N. P., & Ruiter, D. J. (2000). Matrix metalloproteinases in human melanoma. *Journal of Investigative Dermatology, 115*(3), 337-344 https://doi.org/10.1046/j.1523-1747.2000.00068.x

Homrich, M., Gotthard, I., Wobst, H., & Diestel, S. (2016). Cell adhesion molecules and ubiquitination- functions and significance. *Biology, 5*(1), 1-107 https://doi.org/10.3390/biology5010001

Horiuchi, K., Gall, S. L., Schulte, M., Yamaguchi, T., Reiss, K., Murphy, G., Toyama, Y., Hartmann, D., Saftig, P., & Blobel, C. P. (2007). Substrate selectivity of epidermal growth factor-receptor ligand sheddases and their regulation by phorbol esters and calcium influx. *Molecular Biology of the Cell, 18*, 176-188 https://doi.org/10.1091/mbc.e06-01-0014

Hu, X., Li, D., Zhang, W., Zhou, J., Tang, B., & Li, L. (2012). Matrix metalloproteinase-9 expression correlates with prognosis and involved in ovarian cancer cell invasion. *Gynecologic Oncology, 286*, 1537-1543 https://doi.org/10.1007/s00404-012-2456-6

Huang, A. C., & Zappasodi, R. (2022). A decade of checkpoint blockade immunotherapy in melanoma: understanding the molecular basis for immune sensitivity and resistance. *Nature Immunology, 23*(5), 660-670 https://doi.org/10.1038/s41590-022-01141-1

Ilie, M., Long, E., Hofman, V., Selva, E., Bonnetaud, C., Boyer, J., nissac, N. V., Sanfiorenzo, C., Ferrua, B., Marquette, C.-H., Mouroux, J., & Hofman, P. (2014). Clinical value of circulating endothelial cells and of soluble CD146 levels in patients undergoing surgery for non-small cell lung cancer. *British Journal of Cancer, 110*(5), 1236-1243 https://doi.org/10.1038/bjc.2014.11

Image analysis and quantitation for western blotting. (2022). BioRad Laboratories Inc. Retrieved April 02, 2022 from https://www.bio-rad.com/en-au/applications-technologies/image-analysis-quantitation-for-western-blotting?ID=PQEERM9V5F6X

Ishikawa, T., Wondimu, Z., Oikawa, Y., Gentilcore, G., Kiessling, R., Egyhazi Brage, S., Hansson, J., & Patarroyo, M. (2014). Laminins 411 and 421 differentially promote tumor cell migration via α6β1 integrin and MCAM (CD146). *Matrix biology : journal of the International Society for Matrix Biology, 38*, 69-83 https://doi.org/10.1016/j.matbio.2014.06.002

Itoh, Y. (2015). Membrane-type matrix metalloproteinases: their functions and regulations. *Matrix Biology, 44-46*, 207-223 https://doi.org/https://doi.org/10.1016/j.matbio.2015.03.004

Ivetic, A. (2018). A head-to-tail view of L-selectin and its impact on neutrophil behaviour. *Cell and Tissue Research, 371*(3), 437-453 https://doi.org/10.1007/s00441-017-2774-x

Ivetic, A., Florey, O., Deka, J., Haskard, D. O., Ager, A., & Ridley, A. J. (2004). Mutagenesis of the Ezrin-Radixin-Moesin binding domain of L-selectin tail affects shedding, microvillar positioning, and leukocyte tethering. *The Journal of Biological Chemistry, 279*(32), 33263-33272.

Iwagishi, R., Tanaka, R., Seto, M., Takagi, T., Norioka, N., Ueyama, T., Kawamura, T., Takagi, J., Ogawa, Y., & Shirakabe, K. (2020). Negatively charged amino acids in the stalk region of membrane proteins reduce ectodomain shedding. *Journal of Biological Chemistry, 295*(35), 12343-12352 https://doi.org/10.1074/jbc.RA120.013758

Izumi, Y., Hirata, M., Hasuwa, H., Iwamoto, R., Umata, T., Miyado, K., Tamai, Y., Kurisaki, T., Sehara-Fujisawa, A., Ohno, S., & Mekada, E. (1998). A metalloprotease-disintegrin, MDC9/meltrin-gamma/ADAM9 and PKCdelta are involved in TPA-induced ectodomain shedding of membrane-anchored heparin-binding EGF-like growth factor. *The EMBO Journal, 17*(24), 7260-7272 https://doi.org/10.1093/emboj/17.24.7260

Jackson, H. W., Defamie, V., Waterhouse, P., & Khokha, R. (2016). TIMPs: versatile extracellular regulators in cancer. *Nature Reviews Cancer, 17*, 38-53 https://doi.org/10.1038/nrc.2016.115

Jackson, L. F., Qiu, T. H., Sunnarborg, S. W., Chang, A., Zhang, C., Patterson, C., & Lee, D. C. (2003). Defective valvulogenesis in HB-EGF and TACE-null mice is associated with aberrant BMP signalling. *The EMBO Journal, 22*(11), 2704-2716 https://doi.org/10.1093/emboj/cdg264

Janes, P. W., Wimmer-Kleikamp, S. H., Frangakis, A. S., Treble, K., Griesshaber, B., Sabet, O., Grabenbauer, M., Ting, A. Y., Saftig, P., Bastiaens, P. I., & Lackmann, M. (2009). Cytoplasmic relaxation of active Eph controls ephrin shedding by ADAM10. *PLOS Biology, 7*(10), e1000215-e1000215 https://doi.org/10.1371/journal.pbio.1000215

Jenkins, R. W., & Fisher, D. E. (2021). Treatment of advanced melanoma in 2020 and beyond. *The Journal of Investigative Dermatology, 141*(1), 23-31 https://doi.org/10.1016/j.jid.2020.03.943

Jeon, Y. H., Ha, M., Kim, S. W., Kim, M. J., Lee, C.-S., Oh, C.-K., Han, M.-E., Oh, S.-O., & Kim, Y. H. (2019). Evaluation of the prognostic significances of γ-secretase genes in pancreatic cancer. *Oncology Letters, 17*(5), 4614-4620 https://doi.org/10.3892/ol.2019.10113

Jiang, G., Zhang, L., Zhu, Q., Bai, D., Zhang, C., & Wang, X. (2016). CD146 promotes metastasis and predicts poor prognosis of hepatocellular carcinoma. *Journal of Experimental & Clinical Cancer Research, 35*(38), 1-12 https://doi.org/10.1186/s13046-016-0313-3

Jiang, J., Yang, J., Feng, P., Zuo, B., Dong, N., Wu, Q., & He, Y. (2014). N-glycosylation is required for matriptase-2 autoactivation and ectodomain shedding. *Journal of Biological Chemistry, 289*(28), 19500-19507 https://doi.org/10.1074/jbc.M114.555110

Jiang, T., Zhuang, J., Duan, H., Luo, Y., Zeng, Q., Fan, K., Yan, H., Lu, D., Ye, Z., Hao, J., Feng, J., Yang, D., & Yan, X. (2012). CD146 is a co-receptor for VEGFR-2 in tumor angiogenesis. *Blood, 120*(11), 2330-2339 https://doi.org/10.1182/blood-2012-01-406108

Johnson, J. P., Bar-Eli, M., Jansen, B., & Markhof, E. (1997). Melanoma progression–associated glycoprotein MUC18/MCAM mediates homotypic cell adhesion through interaction with a heterophilic ligand. *International Journal of Cancer, 73*(5), 769-774 https://doi.org/10.1002/(SICI)1097-0215(19971127)73:5%3C769::AID-IJC26%3E3.0.CO;2-%23

Johnson, N., Březinová, J., Stephens, E., Burbridge, E., Freeman, M., Adrain, C., & Strisovsky, K. (2017). Quantitative proteomics screen identifies a substrate repertoire of rhomboid protease RHBDL2 in human cells and implicates it in epithelial homeostasis. *Nature Scientific Reports, 7*(7283), 1-13 https://doi.org/10.1038/s41598-017-07556-3

Jouve, N., Bachelier, R., Despoix, N., Blin, M. G., Matinzadeh, M. K., Poitevin, S., Aurrand-Lions, M., Fallague, K., Bardin, N., Blot-Chabaud, M., Vely, F., Dignat-George, F., & Leroyer, A. S. (2015). CD146 mediates VEGF-induced melanoma cell extravasation through FAK activation. *International Journal of Cancer, 137*, 50-60 https://doi.org/10.1002/ijc.29370

Jouve, N., Despoix, N., Espeli, M., Gauthier, L., Cypowyj, S., Fallague, K., Schiff, C., Dignat-George, F., Vély, F., & Leroyer, A. S. (2013). The involvement of CD146 and its novel ligand galectin-1 in apoptotic regulation of endothelial cells. *Journal of Biological Chemistry, 288*, 2571-2579 https://doi.org/10.1074/jbc.M112.418848

Jovanovic, P., Mihajlovic, M., Djordjevic-Jocic, J., Vlajkovic, S., Cekic, S., & Stefanovic, V. (2013). Ocular melanoma: an overview of the current status. *International Journal Clinical and Experimental Pathology, 6*(7), 1230-1244

Kahn, J., Ingraham, R. H., Shirley, F., Migaki, G. I., & Kishimoto, T. K. (1994). Membrane proximal cleavage of L-selectin: identification of the cleavage site and a 6-kD transmembrane peptide fragment of L-selectin. *The Journal of Cell Biology, 125*(2), 461-470

Kahn, J., Walcheck, B., Migaki, G. I., Jutila, M. A., & Kishimoto, T. K. (1998). Calmodulin regulates L-selectin adhesion molecule expression and function through a protease-dependent mechanism. *Cell, 92*(6), 809-818 https://doi.org/http://dx.doi.org/10.1016/S0092-8674(00)81408-7

Kajita, M., Itoh, Y., Chiba, T., Mori, H., Okada, A., Kinoh, H., & Seiki, M. (2001). Membrane-type 1 matrix metalloproteinase cleaves CD44 and promotes cell migration. *The Journal of Cell Biology, 153*(5), 893-904 https://doi.org/http://www.jcb.org/cgi/content/full/153/5/893

Kalinich, M., Murphy, W., Wongvibulsin, S., Pahalyants, V., Yu, K.-H., Lu, C., Wang, F., Zubiri, L., Naranbhai, V., Gusev, A., Kwatra, S. G., Reynolds, K. L., & Semenov, Y. R. (2021). Prediction of severe immune-related adverse events requiring hospital admission in patients on immune checkpoint inhibitors: study of a population level insurance claims database from the USA. *Journal for ImmunoTherapy of Cancer, 9*(3), e001935 https://doi.org/10.1136/jitc-2020-001935

Kalus, I., Bormann, U., Mzoughi, M., Schachner, M., & Kleene, R. (2006). Proteolytic cleavage of the neural cell adhesion molecule by ADAM17/TACE is involved in neurite outgrowth. *Journal of Neurochemistry, 98*, 78-88 https://doi.org/10.1111/j.1471-4159.2006.03847.x

Kalus, I., Schnegelsberg, B., Seidah, N. G., Kleene, R., & Schachner, M. (2003). The proprotein convertase PC5A and a metalloprotease are involved in the proteolytic processing of the neural adhesion molecule L1. *Journal of Biological Chemistry, 278*(12), 10381-10388 https://doi.org/10.1074/jbc.M208351200

Kannan, S. (2016). *4 easy steps to analyze your qPCR data using double delta Ct analysis*. Retrieved June 24, 2020 from https://bitesizebio.com/24894/4-easy-steps-to-analyze-your-qpcr-data-using-double-delta-ct-analysis/

Karabasheva, D., Cole, N. B., & Donaldson, J. G. (2014). Roles for trafficking and O-Linked glycosylation in the turnover of model cell surface proteins. *The Journal of Biological Chemistry, 289*(28), 19477-19490 https://doi.org/10.1074/jbc.M114.564666

Karlen, S., & Braathen, L. (1999). Regulation of the melanoma cell adhesion molecule gene in melanoma: modulation of mRNA synthesis by cyclic adenosine monophosphate, phorbol ester, and stem cell factor/c-kit signalling. *The Journal of Investigative Dermatology, 113*, 711-719 https://doi.org/10.1046/j.1523-1747.1999.00746.x

Kato, T., Hagiyama, M., & Ito, A. (2018). Renal ADAM10 and 17: their physiological and medical meanings. *Frontiers in Cell and Developmental Biology, 6*(153), 1-8 https://doi.org/10.3389/fcell.2018.00153

Kawaguchi, K., Yoshida, S., Hatano, R., & Asano, S. (2017). Pathophysiological roles of ezrin/radixin/moesin proteins. *Biological & Pharmaceutical Bulletin, 40*, 381-390 https://doi.org/10.1248/bpb.b16-01011

Kebir, A., Harhouri, K., Guillet, B., Liu, J. W., Foucault-Bertaud, A., Lamy, E., Kaspi, E., Elganfoud, N., Vely, F., Sabatier, F., Sampol, J., Pisano, P., Kruithof, E. K. O., Bardin, N., Dignat-George, F., & Blot-Chabaud, M. (2010). CD146 short isoform increases the proangiogenic potential of endothelial progenitor cells in vitro and in vivo. *Cellular Biology, 107*(1), 66-75 https://doi.org/10.1161/circresaha.109.213827

Kessenbrock, K., Plaks, V., & Werb, Z. (2010). Matrix metalloproteinases: regulators of the tumor microenvironment. *Cell, 141*(1), 52-67 https://doi.org/https://doi.org/10.1016/j.cell.2010.03.015

Killock, D., & Ivetić, A. (2010). The cytoplasmic domains of TNFα-converting enzyme (TACE/ADAM17) and L-selectin are regulated differently by p38 MAPK and PKC to promote ectodomain shedding. *Biochemical Journal, 428*(2), 293-304. https://doi: 10.1042/BJ20091611

Killock, D., Parsons, M., Zarrouk, M., Ameer-Beg, S., Ridley, A., Haskard, D., Zvelebil, M., & Ivetić, A. (2009). *In vitro* and *in vivo* characterization of molecular interactions between calmodulin, Ezrin/Radixin/Moesin, and L-selectin. *The Journal of Biological Chemistry, 284*(13), 8833-8845 https://doi.org/10.1074/jbc.M806983200

Kim, J., Chang, A., Dudak, A., Federoff, H. J., & Lim, S. T. (2011). Characterization of nectin processing mediated by presinilin-dependent gamma-secretase. *Journal of Neurochemistry, 119*(5), 945-956 https://doi.org/10.1111/j.1471-4159.2011.07479.x

Kim, Y.-H., & Jung, J.-C. (2012). Suppression of tunicamycin-induced CD44v6 ectodomain shedding and apoptosis is correlated with temporal expression patterns of active ADAM10, MMP-9 and MMP-13 proteins in Caki-2 renal carcinoma cells. *Oncology Reports, 28*(5), 1869-1874 https://doi.org/10.3892/or.2012.1986

Kimberly, W. T., Xia, W., Rahmati, T., Wolfe, M. S., & Selkoe, D. J. (2000). The transmembrane aspartates in presenilin 1 and 2 are obligatory for γ-secretase activity and amyloid β-protein generation. *Journal of Biological Chemistry, 275*(5), 3173-3178 https://doi.org/10.1074/jbc.275.5.3173

Kirshner, Z. Z., & Gibbs, R. B. (2018). Use of the REVERT(®) total protein stain as a loading control demonstrates significant benefits over the use of housekeeping proteins when analyzing brain homogenates by Western blot: An analysis of samples representing different gonadal hormone states. *Molecular and Cellular Endocrinology, 473*, 156-165 https://doi.org/10.1016/j.mce.2018.01.015

Kivisaari, A. K., Kallajoki, M., Ala-aho, R., McGrath, J. A., Bauer, J. W., Königová, R., Medvecz, M., Beckert, W., Grénman, R., & Kähäri, V. M. (2010). Matrix

metalloproteinase-7 activates heparin-binding epidermal growth factor-like growth factor in cutaneous squamous cell carcinoma. *British Journal of Dermatology, 163*(4), 726-735 https://doi.org/10.1111/j.1365-2133.2010.09924.x

Kleene, R., Mzoughi, M., Joshi, G., Kalus, I., Bormann, U., Schulze, C., Xiao, M.-F., Dityatev, A., & Schachner, M. (2010). NCAM-induced neurite outgrowth depends on binding of calmodulin to NCAM and on nuclear import of NCAM and fak fragments. *The Journal of Neuroscience, 30*(32), 10784-10798 https://doi.org/10.1523/jneurosci.0297-10.2010

Kleuss, C., & Krause, E. (2003). Gαs is palmitoylated at the N-terminal glycine. *The EMBO Journal, 22*(4), 826-832 https://doi.org/https://doi.org/10.1093/emboj/cdg095

Knäuper, V., Will, H., López-Otin, C., Smith, B., Atkinson, S. J., Stanton, H., Hembry, R. M., & Murphy, G. (1996). Cellular mechanisms for human procollagenase-3 (MMP-13) activation: evidence that MT1-MMP (MMP-14) and gelatinase A (MMP-2) are able to enerate active enzyme. *Journal of Biological Chemistry, 271*(29), 17124-17131 https://doi.org/10.1074/jbc.271.29.17124

Kobata, A., & Amano, J. (2005). Altered glycosylation of proteins produced by malignant cells, and application for the diagnosis and immunotherapy of tumours. *Immunology and Cell Biology, 83*(4), 429-439 https://doi.org/http://dx.doi.org/10.1111/j.1440-1711.2005.01351.x

Korycka, J., Łach, A., Heger, E., Bogusławska, D. M., Wolny, M., Toporkiewicz, M., Augoff, K., Korzeniewski, J., & Sikorski, A. F. (2012). Human DHHC proteins: a spotlight on the hidden player of palmitoylation. *European Journal of Cell Biology, 91*(2), 107-117 https://doi.org/https://doi.org/10.1016/j.ejcb.2011.09.013

Krauthammer, M., Kong, Y., Bacchiocchi, A., Evans, P., Pornputtapong, N., Wu, C., McCusker, J. P., Ma, S., Cheng, E., Straub, R., Serin, M., Bosenberg, M., Ariyan, S., Narayan, D., Sznol, M., Kluger, H. M., Mane, S., Schlessinger, J., Lifton, R. P., & Halaban, R. (2015). Exome sequencing identifies recurrent mutations in NF1 and RASopathy genes in sun-exposed melanomas. *Nature Genetics, 47*(9), 996-1002 https://doi.org/10.1038/ng.3361

Kryczka, J., Stasiak, M., Dziki, L., Mik, M., Dziki, A., & Cierniewski, C. S. (2012). Matrix metalloproteinase-2 cleavage of the β1 integrin ectodomain facilitates colon cancer cell motility. *Journal of Biological Chemistry, 287*(43), 36556-36566 https://doi.org/10.1074/jbc.M112.384909

Kuhn, P.-H., Colombo, A. V., Schusser, B., Dreymueller, D., Wetzel, S., Schepers, U., Herber, J., Ludwig, A., Kremmer, E., Montag, D., Müller, U., Schweizer, M., Saftig, P., Bräse, S., & Lichtenthaler, S. F. (2016). Systematic substrate identification indicates a central role for the metalloprotease ADAM10 in axon targeting and synapse function. *eLife, 5*, e12748 https://doi.org/10.7554/eLife.12748

Kuhn, P.-H., Wang, H., Dislich, B., Colombo, A., Zeitschel, U., Ellwart, J. W., Kremmer, E., Roßner, S., & Lichtenthaler, S. F. (2010). ADAM10 is the physiologically relevant, constitutive α-secretase of the amyloid precursor protein in primary neurons. *The EMBO Journal, 29*(17), 3020-3032 https://doi.org/10.1038/emboj.2010.167

Lai, Z. W., Lew, R. A., Yarski, M. A., Mu, F.-T., Andrews, R. K., & Smith, A. I. (2009). The identification of a calmodulin-binding domain within the cytoplasmic tail of angiotensin-converting enzyme-2. *Endocrinology, 150*(5), 2376-2381 https://doi.org/10.1210/en.2008-1274

Lal, M., & Caplan, M. (2011). Regulated intramembrane proteolysis: signalling pathways and biological functions. *Physiology, 26*(1), 34-44 https://doi.org/10.1152/physiol.00028.2010

Lambert, D. W., Clarke, N. E., Hooper, N. M., & Turner, A. J. (2008). Calmodulin interacts with angiotensin-converting enzyme-2 (ACE2) and inhibits shedding of its ectodomain. *FEBS Letters, 582*(2), 385-390 https://doi.org/http://dx.doi.org/10.1016/j.febslet.2007.11.085

Lammich, S., Okochi, M., Takeda, M., Kaether, C., Capell, A., Zimmer, A.-K., Edbauer, D., Walter, J., Steiner, H., & Haass‡, C. (2002). Presenilin-dependent intramembrane proteolysis of CD44 leads to the liberation of its intracellular domain and the secretion of an Aβ-like peptide. *The Journal of Biological Chemistry, 277*(47), 44754-44759 https://doi.org/10.1074/jbc.M206872200

Laurent, S. A., Hoffmann, F. S., Kuhn, P.-H., Cheng, Q., Chu, Y., Schmidt-Supprian, M., Hauck, S. M., Schuh, E., Krumbholz, M., Rübsamen, H., Wanngren, J., Khademi, M., Olsson, T., Alexander, T., Hiepe, F., Pfister, H.-W., Weber, F., Jenne, D., Wekerle, H., Hohlfeld, R., Lichtenthaler, S. F., & Meinl, E. (2015). γ-secretase directly sheds the survival receptor BCMA from plasma cells. *Nature Communications, 6*(1), 7333 https://doi.org/10.1038/ncomms8333

Le Gall, S. M., Maretzky, T., Issuree, P. D. A., Niu, X.-D., Reiss, K., Saftig, P., Khokha, R., Lundell, D., & Blobel, C. P. (2010). ADAM17 is regulated by a rapid and reversible mechanism that controls access to its catalytic site. *Journal of Cell Science, 123*(22), 3913 https://doi.org/10.1242/jcs.069997

Lee, H. S., Qi, Y., & Im, W. (2015). Effects of N-glycosylation on protein conformation and dynamics: Protein Data Bank analysis and molecular dynamics simulation study. *Scientific Reports, 5*(1), 8926 https://doi.org/10.1038/srep08926

Lee, J.-H., Yu, W. H., Kumar, A., Lee, S., Mohan, P. S., Peterhoff, C. M., Wolfe, D. M., Martinez-Vicente, M., Massey, A. C., Sovak, G., Uchiyama, Y., Westaway, D., Cuervo, A. M., & Nixon, R. A. (2010a). Lysosomal proteolysis and autophagy require presenilin 1 and are disrupted by Alzheimer-related PS1 mutations. *Cell, 141*(7), 1146-1158 https://doi.org/https://doi.org/10.1016/j.cell.2010.05.008

Lee, K. H., Choi, E. Y., Hyun, M. S., Jang, B. I., Kim, T. N., Kim, S. W., Song, S. K., Kim, J. H., & Kim, J. R. (2007). Association of extracellular cleavage of E-cadherin mediated by MMP-7 with HGF-induced in vitro invasion in human stomach cancer cells. *European Surgical Research, 39*(4), 208-215 https://doi.org/10.1159/000101452

Lee, S.-F., Srinivasan, B., Sephton, C. F., Dries, D. R., Wang, B., Yu, C., Wang, Y., Dewey, C. M., Shah, S., Jiang, J., & Yu, G. (2011). γ-Secretase-regulated proteolysis of the Notch receptor by mitochondrial intermediate peptidase. *Journal of Biological Chemistry, 286*(31), 27447-27453 https://doi.org/10.1074/jbc.M111.243154

Lee, S., Schramme, A., Doberstein, K., Dummer, R., Abdel-Bakky, M. S., Keller, S., Altevogt, P., Oh, S. T., Reichrath, J., Oxmann, D., Pfeilschifter, J., Mihic-Probst, D., & Gutwein, P. (2010b). ADAM10 is upregulated in melanoma metastasis compared with primary melanoma. *Journal of Investigative Dermatology, 130*(3), 763-773 https://doi.org/https://doi.org/10.1038/jid.2009.335

Lehmann, J. M., Holzmann, B., Breitbart, E. W., Schmiegelow, P., Riethmüller, G., & Johnson, J. P. (1987). Discrimination between benign and malignant cells of melanocytic lineage by two novel antigens, a glycoprotein with a molecular weight of 113,000 and a protein with a molecular weight of 76,000. *Cancer Research, 47*(3), 841-845

Lehmann, J. M., Riethmüller, G., & Johnson, J. P. (1989). MUC18, a marker of tumor progression in human melanoma, shows sequence similarity to the neural cell adhesion molecules of the immunoglobulin superfamily. *Proceedings of the National Academy of Sciences, U.S.A., 86*(24), 9891-9895 https://doi.org/10.1073/pnas.86.24.9891

Lehti, K., Lohi, J., Valtanen, H., & Keski-Oja, J. (1998). Proteolytic processing of membrane-type-1 matrix metalloproteinase is associated with gelatinase A activation at the cell surface. *The Biochemical Journal, 334* (2), 345-353 https://doi.org/10.1042/bj3340345

Lemberg, M. K., & Freeman, M. (2007). Cutting proteins within lipid bilayers: rhomboid structure and mechanism. *Molecular Cell, 28*(6), 930-940 https://doi.org/10.1016/j.molcel.2007.12.003

LI-COR. (2017). *Revert™ total protein stain normalization protocol*. Retrieved March 1, 2022 from https://www.licor.com/documents/1q6nvqiov23om7n80hco046w9mpfqz3s

Li, G., Kalabis, J., Xu, X., Meier, F., Oka, M., Bogenrieder, T., & Herlyn, M. (2003). Reciprocal regulation of MelCAM and AKT in human melanoma. *Oncogene, 22*(44), 6891-6899. http://dx.doi.org/10.1038/sj.onc.1206819

Li, K., Tay, F. R., & Yiu, C. K. Y. (2020). The past, present and future perspectives of matrix metalloproteinase inhibitors. *Pharmacology & Therapeutics, 207*(107465), 1-13 https://doi.org/doi.org/10.1016/j.pharmthera.2019.107465

Li, L.-H., Tu, Q.-Y., Deng, X.-H., Xia, J., Hou, D.-R., Guo, K., & Zi, X.-H. (2017). Mutant presenilin2 promotes apoptosis through the p53/miR-34a axis in neuronal cells. *Brain Research, 1662*, 57-64 https://doi.org/https://doi.org/10.1016/j.brainres.2017.01.034

Li, P., Lin, X., Zhang, J.-R., Li, Y., Lu, J., Huang, F.-C., Zheng, C.-H., Xie, J.-W., Wang, J.-B., & Huang, C.-M. (2016). The expression of presenilin 1 enhances carcinogenesis and metastasis in gastric cancer. *Oncotarget, 7*(9), 10650-10662 https://doi.org/10.18632/oncotarget.7298

Li, X., Pérez, L., Pan, Z., & Fan, H. (2007). The transmembrane domain of TACE regulates protein ectodomain shedding. *Cell Research, 17*(12), 985-998 https://doi.org/10.1038/cr.2007.98

Li, Y., & Galileo, D. S. (2010). Soluble L1CAM promotes breast cancer cell adhesion and migration in vitro, but not invasion. *Cancer Cell International, 10*, 34 https://doi.org/10.1186/1475-2867-10-34

Lichtenthaler, S. F. (2006). Ectodomain shedding of the amyloid precursor protein: cellular control mechanisms and novel modifiers. *Neurodegenerative Diseases, 3*(4-5), 262-269 https://doi.org/10.1159/000095265

Lichtenthaler, S. F., Lemberg, M. K., & Fluhrer, R. (2018). Proteolytic ectodomain shedding of membrane proteins in mammals- hardware, concepts, and recent developments. *The EMBO Journal, 37*(15), e99456 https://doi.org/10.15252/embj.201899456

Lichtenthaler, S. F., & Meinl, E. (2020). To cut or not to cut: new rules for proteolytic shedding of membrane proteins. *Journal of Biological Chemistry, 295*(35), 12353-12355 https://doi.org/10.1074/jbc.H120.015304

Liu, F., Xu, K., Xu, Z., de las Rivas, M., Wang, C., Li, X., Lu, J., Zhou, Y., Delso, I., Merino, P., Hurtado-Guerrero, R., Zhang, Y., & Wu, F. (2017). The small molecule luteolin inhibits N-acetyl-α-galactosaminyltransferases and reduces mucin-type O-glycosylation of amyloid precursor protein. *Journal of Biological Chemistry, 292*(52), 21304-21319 https://doi.org/https://doi.org/10.1074/jbc.M117.814202

Liu, J., Wang, Q., Kang, Y., Xu, S., & Pang, D. (2022). Unconventional protein post-translational modifications: the helmsmen in breast cancer. *Cell & Bioscience, 12*(1), 22 https://doi.org/10.1186/s13578-022-00756-z

Liu, P., Liu, X., Li, Y., Covington, M., Wynn, R., Huber, R., Hillman, M., Yang, G., Ellis, D., Marando, C., Katiyar, K., Bradley, J., Abremski, K., Stow, M., Rupar, M., Zhuo, J., Li,

Y.-L., Lin, Q., Burns, D., Xu, M., Zhang, C., Qian, D.-Q., He, C., Sharief, V., Weng, L., Agrios, C., Shi, E., Metcalf, B., Newton, R., Friedman, S., Yao, W., Scherle, P. A., Hollis, G., & Burn, T. C. (2006). Identification of ADAM10 as a major source of HER2 ectodomain sheddase activity in HER2 overexpressing breast cancer cells. *Cancer Research and Therapy, 5*(6), 657-664.

Liu, X., Zhao, J., Zhang, Y., Ubarretxena-Belandia, I., Forth, S., Lieberman, R. L., & Wang, C. (2020). Substrate–enzyme interactions in intramembrane proteolysis: γ-secretase as the prototype. *Frontiers in Molecular Neuroscience, 13*, 1-15. https://doi.org/10.3389/fnmol.2020.00065

Liu, Y., Sun, X., Feng, J., Deng, L.-L., Liu, Y., Li, B., Zhu, M., Lu, C., & Zhou, L. (2016). MT2-MMP induces proteolysis and leads to EMT in carcinomas. *Oncotarget, 7*(30), 48193-48205. https://doi.org/10.18632/oncotarget.10194

Lo, S. N., Scolyer, R. A., & Thompson, J. F. (2018). Long-term survival of patients with thin (T1) cutaneous melanomas: a Breslow thickness cut point of 0.8 mm separates higher-risk and lower-risk tumors. *Annals of Surgical Oncology, 25*(4), 894-902 https://doi.org/10.1245/s10434-017-6325-1

Lorenzen, I., Lokau, J., Korpys, Y., Oldefest, M., Flynn, C. M., Künzel, U., Garbers, C., Freeman, M., Grötzinger, J., & Düsterhöft, S. (2016). Control of ADAM17 activity by regulation of its cellular localisation. *Scientific Reports, 6*, 35067-35067 https://doi.org/10.1038/srep35067

Louvet-Vallée, S. (2000). ERM proteins: from cellular architecture to cell signalling. *Biology of the Cell, 92*, 305-316 https://doi.org/10.1016/s0248-4900(00)01078-9

Ludwig, A., Hundhausen, C., Lambert, M. H., Broadway, N., Andrews, R. C., Bickett, D. M., Leesnitzer, M. A., & Becherer, J. D. (2005). Metalloproteinase inhibitors for the disintegrin-like metalloproteinases ADAM10 and ADAM17 that differentially block constitutive and phorbol ester-inducible shedding of cell surface molecules. *Comb Chem High Throughput Screen, 8*(2), 161-171 https://doi.org/10.2174/1386207053258488

Luo, W.-j., Wang, H., Li, H., Kim, B. S., Shah, S., Lee, H.-J., Thinakaran, G., Kim, T.-W., Yu, G., & Xu, H. (2003). PEN-2 and APH-1 coordinately regulate proteolytic processing of presenilin 1. *Journal of Biological Chemistry, 278*(10), 7850-7854 https://doi.org/10.1074/jbc.C200648200

Luo, Y., Zheng, C., Zhang, J., Lu, D., Zhuang, Xing, S., Feng, J., Yang, D., & Yan, X. (2012). Recognition of CD146 as an ERM-binding protein offers novel mechanisms for melanoma cell migration. *Oncogene, 31*, 306-321 https://doi.org/10.1038/onc.2011.244

Maes, H., Kuchnio, A., Peric, A., Moens, S., Nys, K., De Bock, K., Quaegebeur, A., Schoors, S., Georgiadou, M., Wouters, J., Vinckier, S., Vankelecom, H., Garmyn, M., Vion, A.-C., Radtke, F., Boulanger, C., Gerhardt, H., Dejana, E., Dewerchin, M., Ghesquière, B., Annaert, W., Agostinis, P., & Carmeliet, P. (2014). Tumor vessel normalization by chloroquine independent of autophagy. *Cancer Cell, 26*(2), 190-206 https://doi.org/https://doi.org/10.1016/j.ccr.2014.06.025

Maetzel, D., Denzel, S., Mack, B., Canis, M., Went, P., Benk, M., Kieu, C., Papior, P., Baeuerle, P. A., Munz, M., & Gires, O. (2009). Nuclear signalling by tumour-associated antigen EpCAM. *Nature Cell Biology, 11*(2), 162-171 https://doi.org/10.1038/ncb1824

Marambaud, P., Shioi, J., Serban, G., Georgakopoulos, A., Sarner, S., Nagy, V., Baki, L., Wen, P., Efthimiopoulos, S., Shao, Z., Wisniewski, T., & Robakis, N. K. (2002). A presenilin-1/γ-secretase cleavage releases the E-cadherin intracellular domain and regulates disassembly of adherens junctions. *The EMBO Journal, 21*(8), 1948-1956 https://doi.org/10.1093/emboj/21.8.1948

Maretzky, T., Reiss, K., Ludwig, A., Buchholz, J., Scholz, F., Proksch, E., de Strooper, B., Hartmann, D., & Saftig, P. (2005). ADAM10 mediates E-cadherin shedding and regulates epithelial cell-cell adhesion, migration, and β-catenin translocation. *Proceedings of the National Academy of Sciences, U.S.A., 102*(26), 9182-9187 https://doi.org/10.1073/pnas.0500918102

McCarthy, A. J., Coleman-Vaughan, C., & McCarthy, J. V. (2017). Regulated intramembrane proteolysis: emergent role in cell signalling pathways. *Biochemical Society Transactions, 45*(6), 1185-1202 https://doi.org/https://doi.org/10.1042/BST20170002

McCaw, T. R., Inga, E., Chen, H., Jaskula-Sztul, R., Dudeja, V., Bibb, J. A., Ren, B., & Rose, J. B. (2021). Gamma secretase inhibitors in cancer: a current perspective on clinical performance. *Oncologist, 26*(4), e608-e621 https://doi.org/10.1002/onco.13627

McGary, E. C., Lev, D. C., & Bar-Eli, M. (2002). Cellular adhesion pathways and metastatic potential of human melanoma. *Cancer Biology and Therapy, 1*(5), 459-465 https://doi.org/10.4161/cbt.1.5.158

Mechtersheimer, S., Gutwein, P., Agmon-Levin, N., Stoeck, A., Oleszewski, M., Riedle, S., Postina, R., Fahrenholz, F., Fogel, M., Lemmon, V., & Altevogt, P. (2001). Ectodomain shedding of L1 adhesion molecule promotes cell migration by autocrine binding to integrins. *The Journal of Cell Biology, 155*(4), 661-674 https://doi.org/10.1083/jcb.200101099

Mehner, C., Hockla, A., Miller, E., Ran, S., Radisky, D. C., & Radisky, E. S. (2014). Tumor cell-produced matrix metalloproteinase 9 (MMP-9) drives malignant progression and metastasis of basal-like triple negative breast cancer. *Oncotarget, 5*(9), 2736-2749 https://doi.org/10.18632/oncotarget.1932

Meliso, F. M., Micali, D., Silva, C. T., Sabedot, T. S., Coetzee, S. G., Koch, A., Fahlbusch, F. B., Noushmehr, H., Schneider-Stock, R., & Jasiulionis, M. G. (2017). SIRT1 regulates Mxd1 during malignant melanoma progression. *Oncotarget, 8*(70), 114540-114553 https://doi.org/10.18632/oncotarget.21457

Meloty-Kapella, L., Shergill, B., Kuon, J., Botvinick, E., & Weinmaster, G. (2012). Notch ligand endocytosis generates mechanical pulling force dependent on dynamin, epsins, and actin. *Developmental Cell, 22*(6), 1299-1312 https://doi.org/10.1016/j.devcel.2012.04.005

Meng, F., Qian, L., Lv, L., Ding, B., Zhou, G., Cheng, X., Niu, S., & Liang, Y. (2016). miR-193a-3p regulation of chemoradiation resistance in oesophageal cancer cells via the PSEN1 gene. *Gene, 579*(2), 139-145 https://doi.org/10.1016/j.gene.2015.12.060

Mentrup, T., Cabrera-Cabrera, F., Fluhrer, R., & Schröder, B. (2020). Physiological functions of SPP/SPPL intramembrane proteases. *Cellular and Molecular Life Sciences, 77*(15), 2959-2979 https://doi.org/10.1007/s00018-020-03470-6

Merino, A., Hoogduijn, M. J., Molina-Molina, M., Arias-Salgado, E. G., Korevaar, S. S., Baan, C. C., & Montes-Worboys, A. (2021). Membrane particles from mesenchymal stromal cells reduce the expression of fibrotic markers on pulmonary cells. *PLoS One, 16*(3), e0248415 https://doi.org/10.1371/journal.pone.0248415

Migaki, G. I., Kahn, J., & Kishimoto, T. K. (1995). Mutational analysis of the membrane-proximal cleavage site of L- selectin: relaxed sequence specificity surrounding the cleavage site. *Journal of Experimental Medicine, 182*(2), 549-557

Miller, M. A., Sullivan, R. J., & Lauffenburger, D. A. (2017). Molecular pathways: receptor ectodomain shedding in treatment, resistance, and monitoring of cancer. *Clinical Cancer Research, 23*(3), 623-629.

Mills, L., Tellez, C., Huang, S., Baker, C., McCarty, M., Green, L., Gudas, J. M., Feng, X., & Bar-Eli, M. (2002). Fully human antibodies to MCAM/MUC18 inhibit tumor growth and metastasis of human melanoma. *Cancer Research, 62*(17), 5106-5114

Mintz-Weber, C. S., & Johnson, J. P. (2000). Identification of the elements regulating the expression of the cell adhesion molecule MCAM/MUC18: loss of AP-2 is not required for MCAM expression in melanoma cell lines*. *Journal of Biological Chemistry, 275*(44), 34672-34680 https://doi.org/https://doi.org/10.1074/jbc.M003812200

Moreno-Fortuny, A., Bragg, L., Cossu, G., & Roostalu, U. (2017). MCAM contributes to the establishment of cell autonomous polarity in myogenic and chondrogenic differentiation. *Biology Open, 6*(11), 1592-1601 https://doi.org/10.1242/bio.027771

Mort, R. L., Jackson, I. J., & Patton, E. E. (2015). The melanocyte lineage in development and disease. *Development, 142*(4), 620-632 https://doi.org/10.1242/dev.106567

Motulsky, H. J. (2023). *Principles of statistics, GraphPad statistics guide*. Retrieved March 01, 2023 from https://www.graphpad.com/guides/prism/7/statistics/index.htm

Motwani, J., & Eccles, M. R. (2021). Genetic and genomic pathways of melanoma development, invasion and metastasis. *Genes, 12*(10), 1543 https://doi.org/https://doi.org/10.3390/genes12101543

Mruk, K., Farley, B. M., Ritacco, A. W., & Kobertz, W. R. (2014). Calmodulation meta-analysis: predicting calmodulin binding via canonical motif clustering. *Journal of General Physiology, 144*(1), 105-114 https://doi.org/10.1085/jgp.201311140

Müller, T., Meyer, H. E., Egensperger, R., & Marcus, K. (2008). The amyloid precursor protein intracellular domain (AICD) as modulator of gene expression, apoptosis, and cytoskeletal dynamics—Relevance for Alzheimer's disease. *Progress in Neurobiology, 85*(4), 393-406 https://doi.org/https://doi.org/10.1016/j.pneurobio.2008.05.002

Muller, W. A., Weigl, S. A., Deng, X., & Phillips, D. M. (1993). PECAM-1 is required for transendothelial migration of leukocytes. *The Journal of Experimental Medicine, 178*(2), 449-460 https://doi.org/10.1084/jem.178.2.449

Mullooly, M., McGowan, P. M., Kennedy, S. A., Madden, S. F., Crown, J., O' Donovan, N., & Duffy, M. J. (2015). ADAM10: a new player in breast cancer progression? *British Journal of Cancer, 113*(6), 945-951 https://doi.org/10.1038/bjc.2015.288

Nagano, O., & Saya, H. (2004). Mechanism and biological significance of CD44 cleavage. *Cancer Science, 95*(12), 930-935 https://doi.org/10.1111/j.1349-7006.2004.tb03179.x

Nagase, H. (1998). Cell surface activation of progelatinase A (proMMP-2) and cell migration. *Cell Research, 8*(3), 179-186 https://doi.org/10.1038/cr.1998.18

Naik, P. P. (2021). Role of biomarkers in the integrated management of melanoma. *Disease Markers, 2021*(6238317), 1-13 https://doi.org/10.1155/2021/6238317

Najy, A. J., Day, K. C., & Day, M. L. (2008a). ADAM15 supports prostate cancer metastasis by modulating tumor cell–endothelial cell interaction. *Cancer Research, 68*(4), 1092-1099 https://doi.org/10.1158/0008-5472.CAN-07-2432

Najy, A. J., Day, K. C., & Day, M. L. (2008b). The ectodomain sedding of E-cadherin by ADAM15 supports ErbB receptor activation. *The Journal of Biological Chemistry, 283*(26), 18393-18401 https://doi.org/10.1074/jbc.M801329200

National Cancer Control Indicators. (2019). *Relative survival by stage at diagnosis (melanoma)*. https://ncci.canceraustralia.gov.au/outcomes/relative-survival-rate/relative-survival-stage-diagnosis-melanoma

Naus, S., Richter, M., Wildeboer, D., Moss, M., Schachner, M., & Bartsch, J. W. (2004). Ectodomain shedding of the neural recognition molecule CHL1 by the metalloprotease-disintegrin ADAM8 promotes neurite outgrowth and suppresses neuronal cell death. *Journal of Biological Chemistry, 279*(16), 16083-16090 https://doi.org/10.1074/jbc.M400560200

Neisch, A. L., & Fehon, R. G. (2011). Ezrin, radixin and moesin: key regulators of membrane-cortex interactions and signalling. *Current opinion in Cell Biology, 23*(4), 377-382 https://doi.org/10.1016/j.ceb.2011.04.011

Nhan, H. S., Chiang, K., & Koo, E. H. (2015). The multifaceted nature of amyloid precursor protein and its proteolytic fragments: friends and foes. *Acta Neuropathologica, 129*(1), 1-19 https://doi.org/10.1007/s00401-014-1347-2

Nielsen, M. I., de Haan, N., Kightlinger, W., Ye, Z., Dabelsteen, S., Li, M., Jewett, M. C., Bagdonaite, I., Vakhrushev, S. Y., & Wandall, H. H. (2022). Global mapping of GalNAc-T isoform-specificities and O-glycosylation site-occupancy in a tissue-forming human cell line. *Nature Communications, 13*(1), 6257 https://doi.org/10.1038/s41467-022-33806-8

Nikkola, J., Vihinen, P., Vuoristo, M.-S., Kellokumpu-Lehtinen, P., Kähäri, V.-M., & Pyrhönen, S. (2005). High serum levels of matrix metalloproteinase-9 and matrix metalloproteinase-1 are associated with rapid progression in patients with metastatic melanoma. *Clinical Cancer Research, 11*(14), 5158-5166 https://doi.org/10.1158/1078-0432.Ccr-04-2478

Nishizawa, Y., Okui, Y., Inaba, M., Okuno, S., Yukioka, K., Miki, T., Watanabe, Y., & Morii, H. (1988). Calcium/calmodulin-mediated action of calcitonin on lipid metabolism in rats. *Journal of Clinical Investigation, 82*(4), 1165-1172 https://doi.org/10.1172/JCI113713

Nodomi, S., Umeda, K., Saida, S., Kinehara, T., Hamabata, T., Daifu, T., Kato, I., Hiramatsu, H., Watanabe, K. i., Kuwahara, Y., Iehara, T., Adachi, S., Konishi, E., Nakahata, T., Hosoi, H., & Heike, T. (2016). CD146 is a novel marker for highly tumorigenic cells and a potential therapeutic target in malignant rhabdoid tumor. *Oncogene, 35*(40), 5317-5327 https://doi.org/10.1038/onc.2016.72

Nollet, M., Bachelier, R., Joshkon, A., Traboulsi, W., Mahieux, A., Moyon, A., Muller, A., Somasundaram, I., Simoncini, S., Peiretti, F., Leroyer, A. S., Guillet, B., Granel, B., Dignat-George, F., Bardin, N., Foucault-Bertaud, A., & Blot-Chabaud, M. (2022). Multiple variants of soluble CD146 are involved in systemic sclerosis: identification of

a novel pro-fibrotic factor. *Arthritis & Rheumatology, n/a*(n/a) https://doi.org/https://doi.org/10.1002/art.42063

Nollet, M., Stalin, J., Moyon, A., Traboulsi, W., Essaadi, A., Robert, S., Malissen, N., Bachelier, R., Daniel, L., Foucault-Bertaud, A., Gaudy-Marqueste, C., Lacroix, R., Leroyer, A. S., Guillet, B., Bardin, N., Dignat-George, F., & Blot-Chabaud1, M. (2017). A novel anti-CD146 antibody specifically targets cancer cells by internalizing the molecule. *Oncotarget, 8*(68), 112283-112296 https://doi.org/DOI: 10.18632/oncotarget.22736

Nomikou, E., Alexopoulou, A., Vasilieva, L., Agiasotelli, D., Pavlou, E., Theodossiades, G., & Dourakis, S. P. (2015). Soluble CD146, a novel endothelial marker, is related to the severity of liver disease. *Scandinavian Journal of Gastroenterology, 50*(5), 577-583 https://doi.org/10.3109/00365521.2014.985706

Ohnishi, H., Kobayashi, H., Okazawa, H., Ohe, Y., Tomizawa, K., Sato, R., & Matozaki, T. (2004). Ectodomain shedding of SHPS-1 and its role in regulation of cell migration. *Journal of Biological Chemistry, 279*(27), 27878-27887 https://doi.org/10.1074/jbc.M313085200

Okamoto, I., Kawano, Y., Murakami, D., Sasayama, T., Araki, N., Miki, T., Wong, A. J., & Saya, H. (2001). Proteolytic release of CD44 intracellular domain and its role in the CD44 signalling pathway. *The Journal of Cell Biology, 155*(5), 755-762 https://doi.org/10.1083/jcb.200108159

Orme, J. J., Jazieh, K. A., Xie, T., Harrington, S., Liu, X., Ball, M., Madden, B., Charlesworth, M. C., Azam, T. U., Lucien, F., Wootla, B., Li, Y., Villasboas, J. C., Mansfield, A. S., Dronca, R. S., & Dong, H. (2020). ADAM10 and ADAM17 cleave PD-L1 to mediate PD-(L)1 inhibitor resistance. *OncoImmunology, 9*(1), 1744980 https://doi.org/10.1080/2162402X.2020.1744980

Orrenius, S., Zhivotovsky, B., & Nicotera, P. (2003). Regulation of cell death: the calcium–apoptosis link. *Nature Reviews Molecular Cell Biology, 4*(7), 552-565 https://doi.org/10.1038/nrm1150

Ortega, A., & Morán, J. (2011). Role of cytoskeleton proteins in the morphological changes during apoptotic cell death of cerebellar granule neurons. *Neurochemical Research, 36*(1), 93-102 https://doi.org/10.1007/s11064-010-0269-1

Pach, E., Kümper, M., Fromme, J. E., Zamek, J., Metzen, F., Koch, M., Mauch, C., & Zigrino, P. (2021). Extracellular matrix remodeling by fibroblast-MMP14 regulates melanoma growth. *International Journal of Molecular Sciences, 22*(22), 12276 https://doi.org/10.3390/ijms222212276

Pakkiriswami, S., Couto, A., Nagarajan, U., & Georgiou, M. (2016). Glycosylated notch and cancer. *Frontiers in Oncology, 6*(37), 1-8. https://doi.org/10.3389/fonc.2016.00037

Pandey, K. N. (2009). Functional roles of short sequence motifs in the endocytosis of membrane receptors. *Frontiers in Bioscience (Landmark Edition), 14*, 5339-5360 https://doi.org/10.2741/3599

Pearl, R. A., Pacifico, M. D., Richman, P. I., Wilson, G. D., & Grover, R. (2008). Stratification of patients by melanoma cell adhesion molecule (MCAM) expression on the basis of risk: implications for sentinel lymph node biopsy. *Journal of Plastic, Reconstructive & Aesthetic Surgery, 61*(3), 265-271 https://doi.org/10.1016/j.bjps.2007.04.010

Peltonen, H. M., Haapasalo, A., Hiltunen, M., Kataja, V., Kosma, V.-M., & Mannermaa, A. (2013). γ-Secretase Components as predictors of breast cancer outcome. *PLOS ONE, 8*(11), e79249 https://doi.org/10.1371/journal.pone.0079249

Peschon, J. J., Slack, J. L., Reddy, P., Stocking, K. L., Sunnarborg, S. W., Lee, D. C., Russell, W. E., Castner, B. J., Johnson, R. S., Fitzner, J. N., Boyce, R. W., Nelson, N., Kozlosky, C. J., Wolfson, M. F., Rauch, C. T., Cerretti, D. P., Paxton, R. J., March, C. J., & Black, R. A. (1998). An essential role for ectodomain shedding in mammalian development. *Science, 282*(5392), 1281-1284. https://doi.org/10.1126/science.282.5392.1281

Pires da Silva, I., Ahmed, T., McQuade, J. L., Nebhan, C. A., Park, J. J., Versluis, J. M., Serra-Bellver, P., Khan, Y., Slattery, T., Oberoi, H. K., Ugurel, S., Haydu, L. E., Herbst, R., Utikal, J., Pföhler, C., Terheyden, P., Weichenthal, M., Gutzmer, R., Mohr, P., Rai, R., Smith, J. L., Scolyer, R. A., Arance, A. M., Pickering, L., Larkin, J., Lorigan, P., Blank, C. U., Schadendorf, D., Davies, M. A., Carlino, M. S., Johnson, D. B., Long, G. V., Lo, S. N., & Menzies, A. M. (2022). Clinical models to define response and survival with anti-pd-1 antibodies alone or combined with ipilimumab in metastatic melanoma. *Journal of Clinical Oncology, 40*(10), 1068-1080 https://doi.org/10.1200/jco.21.01701

Plesca, D., Mazumder, S., & Almasan, A. (2008). DNA damage response and apoptosis. *Methods in Enzymology, 446*, 107-122 https://doi.org/10.1016/S0076-6879(08)01606-6

Poggi, M., Kara, I., Brunel, J.-M., Landrier, J.-F., Govers, R., Bonardo, B., Fluhrer, R., Haass, C., Alessi, M.-C., & Peiretti, F. (2013). Palmitoylation of TNF alpha is involved in the regulation of TNF receptor 1 signalling. *Biochimica et Biophysica Acta (BBA) - Molecular Cell Research, 1833*(3), 602-612 https://doi.org/https://doi.org/10.1016/j.bbamcr.2012.11.009

Potrony, M., Badenas, C., Aguilera, P., Puig-Butille, J. A., Carrera, C., Malvehy, J., & Puig, S. (2015). Update in genetic susceptibility in melanoma. *Annals of Translational Medicine, 3*(15), 210 https://doi.org/10.3978/j.issn.2305-5839.2015.08.11

Prevost, J. M., Pelley, J. L., Zhu, W., D'Egidio, G. E., Beaudry, P. P., Pihl, C., Neely, G. G., Claret, E., Wijdenes, J., & Brown, C. B. (2002). Granulocyte-macrophage colony-

stimulating factor (GM-CSF) and inflammatory stimuli up-regulate secretion of the soluble GM-CSF receptor in human monocytes: evidence for ectodomain shedding of the cell surface GM-CSF receptor α subunit. *The Journal of Immunology, 169*(10), 5679-5688 https://doi.org/10.4049/jimmunol.169.10.5679

Qian, Y. N., Luo, Y. T., Duan, H. X., Feng, L. Q., Bi, Q., Wang, Y. J., & Yan, X. Y. (2014). Adhesion molecule CD146 and its soluble form correlate well with carotid atherosclerosis and plaque instability. *CNS Neuroscience & Therapeutics, 20*(5), 438-445 https://doi.org/10.1111/cns.12234

Quintero-Fabián, S., Arreola, R., Becerril-Villanueva, E., Torres-Romero, J. C., Arana-Argáez, V., Lara-Riegos, J., Ramírez-Camacho, M. A., & Alvarez-Sánchez, M. E. (2019). Role of matrix metalloproteinases in angiogenesis and cancer. *Frontiers in Oncology, 9,* 1-21. https://doi.org/10.3389/fonc.2019.01370

Ra, H.-J., & Parks, W. C. (2007). Control of matrix metalloproteinase catalytic activity. *Matrix Bbiology : Journal of the International Society for Matrix Biology, 26*(8), 587-596 https://doi.org/10.1016/j.matbio.2007.07.001

Ramel, D., Wang, X., Laflamme, C., Montell, D. J., & Emery, G. (2013). Rab11 regulates cell–cell communication during collective cell movements. *Nature Cell Biology, 15*, 317 https://doi.org/10.1038/ncb2681

Ran, F. A., Hsu, P. D., Wright, J., Agarwala, V., Scott, D. A., & Zhang, F. (2013). Genome engineering using the CRISPR-Cas9 system. *Nature Protocols, 8*(11), 2281-2308 https://doi.org/10.1038/nprot.2013.143

Rao, C. V., Janakiram, N. B., Madka, V., Kumar, G., Scott, E. J., Pathuri, G., Bryant, T., Kutche, H., Zhang, Y., Biddick, L., Gali, H., Zhao, Y. D., Lightfoot, S., & Mohammed, A. (2016). Small-molecule Inhibition of GCNT3 disrupts mucin biosynthesis and malignant cellular behaviors in pancreatic cancer. *Cancer Research, 76*(7), 1965-1974 https://doi.org/10.1158/0008-5472.Can-15-2820

Rashed, M. H., Bayraktar, E., Helal, G. K., Abd-Ellah, M. F., Amero, P., Chavez-Reyes, A., & Rodriguez-Aguayo, C. (2017). Exosomes: from garbage bins to promising therapeutic targets. *International Journal of Molecular Sciences, 18*(3), 538 https://doi.org/10.3390/ijms18030538

Rawlings, N. D., Barrett, A. J., Thomas, P. D., Huang, X., Bateman, A., & Finn, R. D. (2017). The MEROPS database of proteolytic enzymes, their substrates and inhibitors in 2017 and a comparison with peptidases in the PANTHER database. *Nucleic Acids Research, 46*(D1), D624-D632 https://doi.org/10.1093/nar/gkx1134

Rawson, R. B. (2013). The site-2 protease. *Biochimica et Biophysica Acta (BBA) - Biomembranes, 1828*(12), 2801-2807 https://doi.org/https://doi.org/10.1016/j.bbamem.2013.03.031

Rebecca, V. W., Somasundaram, R., & Herlyn, M. (2020). Pre-clinical modeling of cutaneous melanoma. *Nature Communications, 11*(1), 2858 https://doi.org/10.1038/s41467-020-15546-9

Reglero-Real, N., Colom, B., Bodkin, J. V., & Nourshargh, S. (2016). Endothelial cell junctional adhesion molecules: role and regulation of expression in inflammation. *Arteriosclerosis, Thrombosis, and Vascular Biology, 36*(10), 2048-2057 https://doi.org/10.1161/ATVBAHA.116.307610

Reily, C., Stewart, T. J., Renfrow, M. B., & Novak, J. (2019). Glycosylation in health and disease. *Nature Reviews: Nephrology, 15*(6), 346-366 https://doi.org/10.1038/s41581-019-0129-4

Reiss, K., & Bhakdi, S. (2017). The plasma membrane: penultimate regulator of ADAM sheddase function. *Biochimica et Biophysica Acta (BBA) - Molecular Cell Research, 1864*, 2082-2087 https://doi.org/https://doi.org/10.1016/j.bbamcr.2017.06.006

Reiss, K., Maretzky, T., Ludwig, A., Tousseyn, T., de Strooper, B., Hartmann, D., & Saftig, P. (2005). ADAM10 cleavage of N-cadherin and regulation of cell–cell adhesion and β-catenin nuclear signalling. *The EMBO Journal, 24*(4), 742-752 https://doi.org/10.1038/sj.emboj.7600548

Reiss, K., & Saftig, P. (2009). The “A Disintegrin And Metalloprotease” (ADAM) family of sheddases: Physiological and cellular functions. *Seminars in Cell & Developmental Biology, 20*(2), 126-137 https://doi.org/https://doi.org/10.1016/j.semcdb.2008.11.002

Richetta, A. G., Valentini, V., Marraffa, F., Paolino, G., Rizzolo, P., Silvestri, V., Zelli, V., Carbone, A., Di Mattia, C., Calvieri, S., Frascione, P., Donati, P., & Ottini, L. (2018). Metastases risk in thin cutaneous melanoma: prognostic value of clinical-pathologic characteristics and mutation profile. *Oncotarget, 9*(63), 32173-32181 https://doi.org/10.18632/oncotarget.25864

Riethmueller, S., Somasundaram, P., Ehlers, J. C., Hung, C.-W., Flynn, C. M., Lokau, J., Agthe, M., Düsterhöft, S., Zhu, Y., Grötzinger, J., Lorenzen, I., Koudelka, T., Yamamoto, K., Pickhinke, U., Wichert, R., Becker-Pauly, C., Rädisch, M., Albrecht, A., Hessefort, M., Stahnke, D., Unverzagt, C., Rose-John, S., Tholey, A., & Garbers, C. (2017). Proteolytic origin of the soluble human IL-6R *in vivo* and a decisive role of N-glycosylation. *PLOS Biology, 15*(1), e2000080 https://doi.org/10.1371/journal.pbio.2000080

Rojas-Charry, L., Calero-Martinez, S., Morganti, C., Morciano, G., Park, K., Hagel, C., Marciniak, S. J., Glatzel, M., Pinton, P., & Sepulveda-Falla, D. (2020). Susceptibility to cellular stress in PS1 mutant N2a cells is associated with mitochondrial defects and altered calcium homeostasis. *Scientific Reports, 10*(1), 6455 https://doi.org/10.1038/s41598-020-63254-7

Roomi, M. W., Monterrey, J. C., Kalinovsky, T., Rath, M., & Niedzwiecki, A. (2009). Patterns of MMP-2 and MMP-9 expression in human cancer cell lines. *Oncology Reports, 21*(5), 1323-1333.

Roostalu, U., Aldeiri, B., Albertini, A., Humphreys, N., Simonsen-Jackson, M., Wong, J. K. F., & Cossu, G. (2018). Distinct cellular mechanisms underlie smooth muscle turnover in vascular development and repair. *Circulation Research, 122*(2), 267-281 https://doi.org/10.1161/CIRCRESAHA.117.312111

Rotte, A. (2019). Combination of CTLA-4 and PD-1 blockers for treatment of cancer. *Journal of Experimental & Clinical Cancer Research, 38*(1), 255 https://doi.org/10.1186/s13046-019-1259-z

Ruma, I. M., Putranto, E. W., Kondo, E., Murata, H., Watanabe, M., Huang, P., Kinoshita, R., Futami, J., Inoue, Y., Yamauchi, A., Sumardika, I. W., Youyi, C., Yamamoto, K., Nasu, Y., Nishibori, M., Hibino, T., & Sakaguchi, M. (2016). MCAM, as a novel receptor for S100A8/A9, mediates progression of malignant melanoma through prominent activation of NF-κB and ROS formation upon ligand binding. *Clinical Experimental Metastasis, 33*(6), 609-627 https://doi.org/10.1007/s10585-016-9801-2

Rzeniewicz, K., Newe, A., Rey Gallardo, A., Davies, J., Holt, M. R., Patel, A., Charras, G. T., Stramer, B., Molenaar, C., Tedder, T. F., Parsons, M., & Ivetic, A. (2015). L-selectin shedding is activated specifically within transmigrating pseudopods of monocytes to regulate cell polarity in vitro. *Proceedings of the National Academy of Sciences, U.S.A., 112*(12), E1461-E1470 https://doi.org/10.1073/pnas.1417100112

Saad, S., Gottlieb, D. J., Bradstock, K. F., Overall, C. M., & Bendall, L. J. (2002). Cancer cell-associated fibronectin induces release of matrix metalloproteinase-2 from normal fibroblasts. *Cancer Research, 62*(1), 283-289

Sahai, E., Astsaturov, I., Cukierman, E., DeNardo, D. G., Egeblad, M., Evans, R. M., Fearon, D., Greten, F. R., Hingorani, S. R., Hunter, T., Hynes, R. O., Jain, R. K., Janowitz, T., Jorgensen, C., Kimmelman, A. C., Kolonin, M. G., Maki, R. G., Powers, R. S., Puré, E., Ramirez, D. C., Scherz-Shouval, R., Sherman, M. H., Stewart, S., Tlsty, T. D., Tuveson, D. A., Watt, F. M., Weaver, V., Weeraratna, A. T., & Werb, Z. (2020). A framework for advancing our understanding of cancer-associated fibroblasts. *Nature Reviews Cancer, 20*(3), 174-186 https://doi.org/10.1038/s41568-019-0238-1

Sahin, U., Weskamp, G., Kelly, K., Zhou, H.-M., Higashiyama, S., Peschon, J., Hartmann, D., Saftig, P., & Blobel, C. P. (2004). Distinct roles for ADAM10 and ADAM17 in ectodomain shedding of six EGFR ligands. *Journal of Cell Biology, 164*(5), 769-779 https://doi.org/10.1083/jcb.200307137

Sanchez-Vega, F., Mina, M., Armenia, J., Chatila, W. K., Luna, A., La, K. C., Dimitriadoy, S., Liu, D. L., Kantheti, H. S., Saghafinia, S., Chakravarty, D., Daian, F., Gao, Q., Bailey, M. H., Liang, W. W., Foltz, S. M., Shmulevich, I., Ding, L., Heins, Z., Ochoa, A.,

Gross, B., Gao, J., Zhang, H., Kundra, R., Kandoth, C., Bahceci, I., Dervishi, L., Dogrusoz, U., Zhou, W., Shen, H., Laird, P. W., Way, G. P., Greene, C. S., Liang, H., Xiao, Y., Wang, C., Iavarone, A., Berger, A. H., Bivona, T. G., Lazar, A. J., Hammer, G. D., Giordano, T., Kwong, L. N., McArthur, G., Huang, C., Tward, A. D., Frederick, M. J., McCormick, F., Meyerson, M., Van Allen, E. M., Cherniack, A. D., Ciriello, G., Sander, C., & Schultz, N. (2018). Oncogenic signalling pathways in the cancer genome atlas. *Cell, 173*(2), 321-337.e310 https://doi.org/10.1016/j.cell.2018.03.035

Sanderson, M. P., Keller, S., Alonso, A., Riedle, S., Dempsey, P. J., & Altevogt, P. (2008). Generation of novel, secreted epidermal growth factor receptor (EGFR/ErbB1) isoforms via metalloprotease-dependent ectodomain shedding and exosome secretion. *Journal of Cellular Biochemistry, 103*(6), 1783-1797 https://doi.org/10.1002/jcb.21569

Sannerud, R., Esselens, C., Ejsmont, P., Mattera, R., Rochin, L., Tharkeshwar, Arun K., De Baets, G., De Wever, V., Habets, R., Baert, V., Vermeire, W., Michiels, C., Groot, Arjan J., Wouters, R., Dillen, K., Vints, K., Baatsen, P., Munck, S., Derua, R., Waelkens, E., Basi, Guriqbal S., Mercken, M., Vooijs, M., Bollen, M., Schymkowitz, J., Rousseau, F., Bonifacino, Juan S., Van Niel, G., De Strooper, B., & Annaert, W. (2016). Restricted location of PSEN2/γ-secretase determines substrate specificity and generates an intracellular Aβ pool. *Cell, 166*(1), 193-208 https://doi.org/https://doi.org/10.1016/j.cell.2016.05.020

Sato, H., Takino, T., Okada, Y., Cao, J., Shinagawa, A., Yamamoto, E., & Seiki, M. (1994). A matrix metalloproteinase expressed on the surface of invasive tumour cells. *Nature, 370*, 61-65 https://doi.org/10.1038/370061a0

Schägger, H., & von Jagow, G. (1987). Tricine-sodium dodecyl sulfate-polyacrylamide gel electrophoresis for the separation of proteins in the range from 1 to 100 kDa. *Analytical Biochemistry, 166*(2), 368-379 https://doi.org/https://doi.org/10.1016/0003-2697(87)90587-2

Schlagbauer-Wadl, H., Jansen, B., Muler, M., Polterauer, P., Wolff, K., Hans-Georg-Eichler, Pehamberger, H., Konak, E., & Johnson, J. P. (1999). Influence of MUC18/MCAM/CD146 expression on human melanoma growth and metastasis in SCID mice. *International Journal of Cancer, 81*(6), 951-955. https://doi.org/https://doi.org/10.1186/s12935-014-0147-z

Schlöndorff, J., Becherer, J. D., & Blobel, C. P. (2000). Intracellular maturation and localization of the tumour necrosis factor alpha convertase (TACE). *The Biochemical Journal, 347*(1), 131-138 https://doi.org/10.1042/0264-6021:3470131

Schlöndorff, J., Lum, L., & Blobel, C. P. (2001). Biochemical and pharmacological criteria define two shedding activities for TRANCE/OPGL that are distinct from the Tumor Necrosis Factor α Convertase *. *Journal of Biological Chemistry, 276*(18), 14665-14674 https://doi.org/10.1074/jbc.M010741200

Schneider-Poetsch, T., Ju, J., Eyler, D. E., Dang, Y., Bhat, S., Merrick, W. C., Green, R., Shen, B., & Liu, J. O. (2010). Inhibition of eukaryotic translation elongation by cycloheximide and lactimidomycin. *Nature Chemical Biology, 6*(3), 209-217 https://doi.org/10.1038/nchembio.304

Schneider, B. J., Naidoo, J., Santomasso, B. D., Lacchetti, C., Adkins, S., Anadkat, M., Atkins, M. B., Brassil, K. J., Caterino, J. M., Chau, I., Davies, M. J., Ernstoff, M. S., Fecher, L., Ghosh, M., Jaiyesimi, I., Mammen, J. S., Naing, A., Nastoupil, L. J., Phillips, T., Porter, L. D., Reichner, C. A., Seigel, C., Song, J. M., Spira, A., Suarez-Almazor, M., Swami, U., Thompson, J. A., Vikas, P., Wang, Y., Weber, J. S., Funchain, P., & Bollin, K. (2021). Management of immune-related adverse events in patients treated with immune checkpoint inhibitor therapy: Asco guideline update. *Journal of Clinical Oncology, 39*(36), 4073-4126 https://doi.org/10.1200/jco.21.01440

Schroeter, E. H., Kisslinger, J. A., & Kopan, R. (1998). Notch-1 signalling requires ligand-induced proteolytic release of intracellular domain. *Nature, 393*(6683), 382-386 https://doi.org/10.1038/30756

Schummer, P., Schilling, B., & Gesierich, A. (2020). Long-term outcomes in BRAF-mutated melanoma treated with combined targeted therapy or immune checkpoint blockade: are we approaching a true cure? *American Journal of Clinical Dermatology, 21*(4), 493-504 https://doi.org/10.1007/s40257-020-00509-z

Sciarrillo, R., Wojtuszkiewicz, A., Assaraf, Y. G., Jansen, G., Kaspers, G. J. L., Giovannetti, E., & Cloos, J. (2020). The role of alternative splicing in cancer: from oncogenesis to drug resistance. *Drug Resistance Updates, 53*, 100728 https://doi.org/https://doi.org/10.1016/j.drup.2020.100728

Selkoe, D. J., & Wolfe, M. S. (2007). Presenilin: running with scissors in the membrane. *Cell, 131*(2), 215-221 https://doi.org/10.1016/j.cell.2007.10.012

Sers, C., Kirsch, K., Rothbächer, U., Riethmüller, G., & Johnson, J. P. (1993). Genomic organization of the melanoma-associated glycoprotein MUC18: implications for the evolution of the immunoglobulin domains. *Proceedings of the National Academy of Sciences, U.S.A., 90*(18), 8514-8518. https://doi.org/10.1073/pnas.90.18.8514

Shah, S., Lee, S.-F., Tabuchi, K., Hao, Y.-H., Yu, C., LaPlant, Q., Ball, H., Dann, C. E., Südhof, T., & Yu, G. (2005). Nicastrin Functions as a γ-secretase-substrate receptor. *Cell, 122*(3), 435-447 https://doi.org/https://doi.org/10.1016/j.cell.2005.05.022

Shain, A. H., & Bastian, B. C. (2016). From melanocytes to melanomas. *Nature Reviews Cancer, 16*(6), 345-358 https://doi.org/10.1038/nrc.2016.37

Shain, A. H., Joseph, N. M., Yu, R., Benhamida, J., Liu, S., Prow, T., Ruben, B., North, J., Pincus, L., Yeh, I., Judson, R., & Bastian, B. C. (2018). Genomic and transcriptomic

analysis reveals incremental disruption of key signalling pathways during melanoma evolution. *Cancer Cell, 34*(1), 45-55.e44 https://doi.org/10.1016/j.ccell.2018.06.005

Shay, G., Lynch, C. C., & Fingleton, B. (2015). Moving targets: Emerging roles for MMPs in cancer progression and metastasis. *Matrix Biology, 44-46*, 200-206 https://doi.org/https://doi.org/10.1016/j.matbio.2015.01.019

Shen, Y., Yin, Y., Peng, Y., Lv, D., Miao, F., Dou, F., & Zhang, J. (2018). Modulation of the gamma-secretase activity as a therapy against human hepatocellular carcinoma. *Journal of Cancer Research and Therapeutics, 14*, 473 https://doi.org/10.4103/0973-1482.174542

Shih, I. M., Speicher, D., Hsu, M. Y., Levine, E., & Herlyn, M. (1997). Melanoma cell-cell interactions are mediated through heterophilic Mel-CAM/ligand adhesion. *Cancer Research, 57*(17), 3835-3840

Shirakabe, K., Omura, T., Shibagaki, Y., Mihara, E., Homma, K., Kato, Y., Yoshimura, A., Murakami, Y., Takagi, J., Hattori, S., & Ogawa, Y. (2017). Mechanistic insights into ectodomain shedding: susceptibility of CADM1 adhesion molecule is determined by alternative splicing and O-glycosylation. *Scientific Reports, 7*(1), 46174 https://doi.org/10.1038/srep46174

Shteinman, E. R., Wilmott, J. S., da Silva, I. P., Long, G. V., Scolyer, R. A., & Vergara, I. A. (2022). Causes, consequences and clinical significance of aneuploidy across melanoma subtypes. *Fronteirs in Oncology, 12*, 988691 https://doi.org/10.3389/fonc.2022.988691

Shum, L., Turck, C. W., & Derynck, R. (1996). Cysteines 153 and 154 of transmembrane transforming growth factor-α are palmitoylated and mediate cytoplasmic protein association. *Journal of Biological Chemistry, 271*(45), 28502-28508 https://doi.org/10.1074/jbc.271.45.28502

Sidor, J., Gillette, M., Dezi, L. A., Untiveros, G., & Strizzi, L. (2022). Role of presenilin-1 in aggressive human melanoma. *International Journal of Molecular Sciences, 23*(9), 4904 https://doi.org/10.3390/ijms23094904

Singh, N., Talalayeva, Y., Tsiper, M., Romanov, V., Dranovsky, A., Colflesh, D., Rudamen, G., Vitek, M. P., Shen, J., Yang, X., Goldgaber, D., & Schwarzman, A. L. (2001). The role of Alzheimer's disease-related presenilin 1 in intercellular adhesion. *Experimental Cell Research, 263*(1), 1-13 https://doi.org/https://doi.org/10.1006/excr.2000.5098

Singh, R. J. R., Mason, J. C., Lidington, E. A., Edwards, D. R., Nuttall, R. K., Khokha, R., Knauper, V., Murphy, G., & Gavrilovic, J. (2005). Cytokine stimulated vascular cell adhesion molecule-1 (VCAM-1) ectodomain release is regulated by TIMP-3.

Cardiovascular Research, 67(1), 39-49 https://doi.org/10.1016/j.cardiores.2005.02.020

Slack, B. E., Siniaia, M. S., & Blusztajn, J. K. (2006). Collagen type I selectively activates ectodomain shedding of the discoidin domain receptor 1: involvement of Src tyrosine kinase. *Journal of Cellular Biochemistry, 98*(3), 672-684 https://doi.org/10.1002/jcb.20812

Soto-Gamez, A., Chen, D., Nabuurs, A. G. E., Quax, W. J., Demaria, M., & Boersma, Y. L. (2020). A bispecific inhibitor of the EGFR/ADAM17 axis decreases cell proliferation and migration of EGFR-dependent cancer cells. *Cancers, 12*(2), 411 https://doi.org/10.3390/cancers12020411

Spasic, D., & Annaert, W. (2008). Building γ-secretase – the bits and pieces. *Journal of Cell Science, 121*(4), 413-420 https://doi.org/10.1242/jcs.015255 %J

Speck, O., Hughes, S. C., Noren, N. K., Kulikauskas, R. M., & Fehon, R. G. (2003). Moesin functions antagonistically to the Rho pathway to maintain epithelial integrity. *Nature, 421*, 83-87 https://doi.org/10.1038/nature01295

Stalin, J., Harhouri, K., Hubert, L., Garrigue, P., Nollet, M., Essaadi, A., Muller, A., Foucault-Bertaud, A., Bachelier, R., Sabatier, F., Pisano, P., Peiretti, F., Leroyer, A. S., Guillet, B., Bardin, N., Dignat-George, F., & Blot-Chabaud, M. (2016a). Soluble CD146 boosts therapeutic effect of endothelial progenitors through proteolytic processing of short CD146 isoform. *Cardiovascular Research, 111*(3), 240-251 https://doi.org/10.1093/cvr/cvw096

Stalin, J., Harhouri, K., Hubert, L., Subrini, C., Lafitte, D., Lissitzky, J.-C., Elganfoud, N., Robert, S., Foucault-Bertaud, A., Kaspi, E., Sabatier, F., Aurrand-Lions, M., Bardin, N., Holmgren, L., Dignat-George, F., & Blot-Chabaud, M. (2013). Soluble melanoma cell adhesion molecule (sMCAM/sCD146) promotes angiogenic effects on endothelial progenitor cells through angiomotin. *The Journal of Biological Chemistry, 288*(13), 8991-9000 https://doi.org/10.1074/jbc.M112.446518

Stalin, J., Nollet, M., Garigue, P., Fernandez, S., Vivancos, L., Essaadi, A., Muller, A., Bachelier, R., Foucault-Bertaud, A., Fugazza, L., Leroyer, A., Bardin, N., Guillet, B., Dignat-George, F., & Blot-Chabaud, M. (2016). Targeting soluble CD146 with a neutralizing antibody inhibits vascularization, growth and survival of CD146-positive tumors. *Oncogene, 35*(42), 5489-5500 https://doi.org/10.1038/onc.2016.83

Stalin, J., Traboulsi, W., Vivancos-Stalin, L., Nollet, M., Joshkon, A., Bachelier, R., Guillet, B., Lacroix, R., Foucault-Bertaud, A., Leroyer, A. S., Dignat-George, F., Bardin, N., & Blot-Chabaud, M. (2020). Therapeutic targeting of soluble CD146/MCAM with the M2J-1 monoclonal antibody prevents metastasis development and procoagulant activity in CD146-positive invasive tumors. *International Journal of Cancer, 147*(6), 1666-1679 https://doi.org/10.1002/ijc.32909

Stalin, J, L. Vivancos, N. Bardin, F. Dignat-George, and M. Blot-Chabaud. '"MCAM and Its Isoforms as Novel Targets in Angiogenesis Research and Therapy"'. In Physiologic and Pathologic Angiogenesis - Signalling Mechanisms and Targeted Therapy. Edited by Dan Simionescu and Agneta Simionescu, InTech. Vienna, Austria. 2017. https://doi.org/10.5772/66765

Steininger, J., Gellrich, F. F., Schulz, A., Westphal, D., Beissert, S., & Meier, F. (2021). Systemic therapy of metastatic melanoma: on the road to cure. *Cancers, 13*(6), 1430 https://doi.org/10.3390/cancers13061430

Sternlicht, M. D., Sunnarborg, S. W., Kouros-Mehr, H., Yu, Y., Lee, D. C., & Werb, Z. (2009). Mammary ductal morphogenesis requires paracrine activation of stromal EGFR via ADAM17-dependent shedding of epithelial amphiregulin. *Development, 132*(17), 3923-3933 https://doi.org/10.1242/dev.01966

Stoeck, A., Keller, S., Riedle, S., Sanderson, Michael P., Runz, S., Le Naour, F., Gutwein, P., Ludwig, A., Rubinstein, E., & Altevogt, P. (2006). A role for exosomes in the constitutive and stimulus-induced ectodomain cleavage of L1 and CD44. *Biochemical Journal, 393*(3), 609-618 https://doi.org/10.1042/BJ20051013

Stoletov, K., Kato, H., Zardouzian, E., Kelber, J., Yang, J., Shattil, S., & Klemke, R. (2010). Visualizing extravasation dynamics of metastatic tumor cells. *Journal of Cell Science, 123*(13), 2332-2341 https://doi.org/10.1242/jcs.069443 %J

Stowell, S. R., Ju, T., & Cummings, R. D. (2015). Protein glycosylation in cancer. *Annual Review of Pathology: Mechanisms of Disease, 10*(1), 473-510 https://doi.org/10.1146/annurev-pathol-012414-040438

Struhl, G., & Adachi, A. (1998). Nuclear access and action of notch *in vivo*. *Cell, 93*(4), 649-660 https://doi.org/https://doi.org/10.1016/S0092-8674(00)81193-9

Su, D. M., Zhang, Q., Wang, X., He, P., Zhu, Y. J., Zhao, J., Rennert, O. M., & Su, Y. A. (2009). Two types of human malignant melanoma cell lines revealed by expression patterns of mitochondrial and survival-apoptosis genes: implications for malignant melanoma therapy. *Molecular Cancer Therapeutics, 8*(5), 1292-1304 https://doi.org/10.1158/1535-7163.MCT-08-1030

Sumardika, I. W., Youyi, C., Kondo, E., Inoue, Y., Ruma, I. M. W., Murata, H., Kinoshita, R., Yamamoto, K.-I., Tomida, S., Shien, K., Sato, H., Yamauchi, A., Futami, J., Putranto, E. W., Hibino, T., Toyooka, S., Nishibori, M., & Sakaguchi, M. (2018). β-1,3-Galactosyl-O-Glycosyl-Glycoprotein β-1,6-N-Acetylglucosaminyltransferase 3 increases MCAM stability, which enhances S100A8/A9-mediated cancer motility. *Oncology Research, 26*(3), 431-444 https://doi.org/10.3727/096504017X15031557924123

Switzer, B., Puzanov, I., Skitzki, J. J., Hamad, L., & Ernstoff, M. S. (2022). Managing metastatic melanoma in 2022: a clinical review. *JCO Oncology Practice, 18*(5), 335-351 https://doi.org/10.1200/OP.21.00686

Taira, E., Kohama, K., Tsukamoto, Y., Okumura, S., & Miki, N. (2004). Characterization of Gicerin/MUC18/CD146 in the rat nervous system. *Journal of Cellular Physiology, 198*(3), 377-387 https://doi.org/https://doi.org/10.1002/jcp.10413

Taira, E., Takaha, N., Taniura, H., Kim, C.-H., & Miki, N. (1994). Molecular cloning and functional expression of gicerin, a novel cell adhesion molecule that binds to neurite outgrowth factor. *Neuron, 12*(4), 861-872 https://doi.org/https://doi.org/10.1016/0896-6273(94)90338-7

Takashima, A., Sato, M., Mercken, M., Tanaka, S., Kondo, S., Honda, T., Sato, K., Murayama, M., Noguchi, K., Nakazato, Y., & Takahashi, H. (1996). Localization of alzheimer-associated presenilin 1 in transfected COS-7 cells. *Biochemical and Biophysical Research Communications, 227*(2), 423-426 https://doi.org/https://doi.org/10.1006/bbrc.1996.1523

Talantov, D., Mazumder, A., Yu, J. X., Briggs, T., Jiang, Y., Backus, J., Atkins, D., & Wang, Y. (2005). Novel genes associated with malignant melanoma but not benign melanocytic lesions. *Clinical Cancer Research, 11*(20), 7234-7242 https://doi.org/10.1158/1078-0432.Ccr-05-0683

Tamura, K., Taniguchi, Y., Minoguchi, S., Sakai, T., Tun, T., Furukawa, T., & Honjo, T. (1995). Physical interaction between a novel domain of the receptor Notch and the transcription factor RBP-Jκ/Su(H). *Current Biology, 5*(12), 1416-1423 https://doi.org/10.1016/S0960-9822(95)00279-X

Taniguchi, Y., Kim, S.-H., & Sisodia, S. S. (2003). Presenilin-dependent "γ-secretase" processing of deleted in colorectal cancer (DCC). *Journal of Biological Chemistry, 278*(33), 30425-30428 https://doi.org/10.1074/jbc.C300239200

Taniura, H., Kuo, C. H., Hayashi, Y., & Miki, N. (1991). Purification and characterization of an 82-kD membrane protein as a neurite outgrowth factor binding protein: possible involvement of NOF binding protein in axonal outgrowth in developing retina. *The Journal of Cell Biology, 112*(2), 313-322 https://doi.org/10.1083/jcb.112.2.313

Tateishi, H., Tateishi, M., Radwan, M. O., Masunaga, T., Kawatashiro, K., Oba, Y., Oyama, M., Inoue-Kitahashi, N., Fujita, M., Okamoto, Y., & Otsuka, M. (2021). A new inhibitor of ADAM17 composed of a zinc-binding dithiol moiety and a specificity pocket-binding appendage. *Chemical & Pharmaceutical Bulletin, 69*(11), 1123-1130 https://doi.org/10.1248/cpb.c21-00701

Tawbi, H. A., Schadendorf, D., Lipson, E. J., Ascierto, P. A., Matamala, L., Castillo Gutiérrez, E., Rutkowski, P., Gogas, H. J., Lao, C. D., De Menezes, J. J., Dalle, S., Arance, A.,

Grob, J.-J., Srivastava, S., Abaskharoun, M., Hamilton, M., Keidel, S., Simonsen, K. L., Sobiesk, A. M., Li, B., Hodi, F. S., Long, G. V., & Investigators, R.-. (2022). Relatlimab and nivolumab versus nivolumab in untreated advanced melanoma. *The New England Journal of Medicine, 386*(1), 24-34 https://doi.org/10.1056/NEJMoa2109970

Tian, X., Liu, Z., Niu, B., Zhang, J., Tan, T. K., Lee, S. R., Zhao, Y., Harris, D. C. H., & Zheng, G. (2011). E-cadherin/β-catenin complex and the epithelial barrier. *Journal of Biomedicine and Biotechnology, 2011*, 567305 https://doi.org/10.1155/2011/567305

Tidow, H., & Nissen, P. (2013). Structural diversity of calmodulin binding to its target sites. *The FEBS Journal, 280*, 5551-5565 https://doi.org/10.1111/febs.12296

To, M. D., Gokgoz, N., Doyle, T. G., Donoviel, D. B., Knight, J. A., Hyslop, P. S., Bernstein, A., & Andrulis, I. L. (2006). Functional characterization of novel presenilin-2 variants identified in human breast cancers. *Oncogene, 25*(25), 3557-3564 https://doi.org/10.1038/sj.onc.1209397

Toricelli, M., Melo, F. H. M., Peres, G. B., Silva, D. C. P., & Jasiulionis, M. G. (2013). Timp1 interacts with beta-1 integrin and CD63 along melanoma genesis and confers anoikis resistance by activating PI3-K signalling pathway independently of Akt phosphorylation. *Molecular Cancer, 12*(1), 1095 https://doi.org/10.1186/1476-4598-12-22

Tsumagari, K., Shirakabe, K., Ogura, M., Sato, F., Ishihama, Y., & Sehara-Fujisawa, A. (2017). Secretome analysis to elucidate metalloprotease-dependent ectodomain shedding of glycoproteins during neuronal differentiation. *Genes to Cells, 22*(2), 237-244 https://doi.org/https://doi.org/10.1111/gtc.12466

Tu, T., Zhang, C., Yan, H., Luo, Y., Kong, R., Wen, P., Ye, Z., Chen, J., Feng, J., Liu, F., Wu, J. Y., & Yan, X. (2015). CD146 acts as a novel receptor for netrin-1 in promoting angiogenesis and vascular development. *Cell Research, 25*(3), 275-287. Retrieved 03//print, from http://dx.doi.org/10.1038/cr.2015.15

Tung, H. H., & Lee, S. L. (2017). Physical binding of endothelial MCAM and neural transmembrane protease matriptase-novel cell adhesion in neural stem cell vascular niche. *Scientific Reports, 7*(1), 4946 https://doi.org/10.1038/s41598-017-05131-4

Twito, T., Chen, Z., Khatri, I., Wong, K., Spaner, D., & Gorczynski, R. (2013). Ectodomain shedding of CD200 from the B-CLL cell surface is regulated by ADAM28 expression. *Leukemia Research, 37*(7), 816-821 https://doi.org/https://doi.org/10.1016/j.leukres.2013.04.014

Uemura, K., Kihara, T., Kuzuya, A., Okawa, K., Nishimoto, T., Ninomiya, H., Sugimoto, H., Kinoshita, A., & Shimohama, S. (2006). Characterization of sequential N-cadherin

cleavage by ADAM10 and PS1. *Neuroscience Letters, 402*(3), 278-283 https://doi.org/https://doi.org/10.1016/j.neulet.2006.04.018

Vääräniemi, J., Huotari, V., Lehto, V. P., & Eskelinen, S. (1997). Effect of PMA on the integrity of the membrane skeleton and morphology of epithelial MDCK cells is dependent on the activity of amiloride-sensitive ion transporters and membrane potential. *European Journal of Cell Biology, 74*(3), 262-272

Vainio, O., Dunon, D., Aïssi, F., Dangy, J. P., McNagny, K. M., & Imhof, B. A. (1996). HEMCAM, an adhesion molecule expressed by c-kit+ hemopoietic progenitors. *The Journal of Cell Biology, 135*(6 Pt 1), 1655-1668 https://doi.org/10.1083/jcb.135.6.1655

Van Eldik, L. J., & Wolchok, S. R. (1984). Conditions for reproducible detection of calmodulin and S100β in immunoblots. *Biochemical and Biophysical Research Communications, 124*(3), 752-759 https://doi.org/https://doi.org/10.1016/0006-291X(84)91022-2

Van Wart, H. E., & Birkedal-Hansen, H. (1990). The cysteine switch: a principle of regulation of metalloproteinase activity with potential applicability to the entire matrix metalloproteinase gene family. *Proceedings of the National Academy of Sciences, U.S.A., 87*(14), 5578-5582 https://doi.org/10.1073/pnas.87.14.5578

Vandyck, H. H. L. D., Hillen, L. M., Bosisio, F. M., van den Oord, J., zur Hausen, A., & Winnepenninckx, V. (2021). Rethinking the biology of metastatic melanoma: a holistic approach. *Cancer and Metastasis Reviews, 40*(2), 603-624 https://doi.org/10.1007/s10555-021-09960-8

Vawter, M. P., Usen, N., Thatcher, L., Ladenheim, B., Zhang, P., VanderPutten, D. M., Conant, K., Herman, M. M., van Kammen, D. P., Sedvall, G., Garver, D. L., & Freed, W. J. (2001). Characterization of human cleaved N-CAM and association with schizophrenia. *Experimental Neurology, 172*(1), 29-46 https://doi.org/https://doi.org/10.1006/exnr.2001.7790

Veit, M., Ahrens, B., Seidel, J., Sommer, A., Bhakdi, S., & Reiss, K. (2019). Mutagenesis of the ADAM17-phosphatidylserine-binding motif leads to embryonic lethality in mice. *Life Science Alliance, 2*(5), e201900430 https://doi.org/10.26508/lsa.201900430

Verhulst, E., Garnier, D., De Meester, I., & Bauvois, B. (2022). Validating cell surface proteases as drug targets for cancer therapy: what do we know, and where do we go? *Cancers, 14*(3), 1-32 https://doi.org/10.3390/cancers14030624

Vilmos, P., Kristó, I., Szikora, S., Jankovics, F., Lukácsovich, T., Kari, B., & Erdélyi, M. (2016). The actin-binding ERM protein Moesin directly regulates spindle assembly and function during mitosis. *Cell Biology International, 40*(6), 696-707 https://doi.org/10.1002/cbin.10607

Visse, R., & Nagase, H. (2003). Matrix metalloproteinases and tissue inhibitors of metalloproteinases. *Circulation Research, 92*(8), 827-839 https://doi.org/10.1161/01.RES.0000070112.80711.3D

von Burstin, J., Bachhuber, F., Paul, M., Schmid, R. M., & Rustgi, A. K. (2017). The TALE homeodomain transcription factor MEIS1 activates the pro-metastatic melanoma cell adhesion molecule Mcam to promote migration of pancreatic cancer cells. *Molecular Carcinogenesis, 56*(3), 936-944 https://doi.org/https://doi.org/10.1002/mc.22547

von Rotz, R. C., Kohli, B. M., Bosset, J., Meier, M., Suzuki, T., Nitsch, R. M., & Konietzko, U. (2004). The APP intracellular domain forms nuclear multiprotein complexes and regulates the transcription of its own precursor. *Journal of Cell Science, 117*(19), 4435-4448 https://doi.org/10.1242/jcs.01323

Wang, W., Runkle, K. B., Terkowski, S. M., Ekaireb, R. I., & Witze, E. S. (2015). Protein depalmitoylation is induced by Wnt5a and promotes polarized cell behavior. *The Journal of Biological Chemistry, 290*(25), 15707-15716 https://doi.org/10.1074/jbc.M115.639609

Wang, X., Spandidos, A., Wang, H., & Seed, B. (2011). PrimerBank: a PCR primer database for quantitative gene expression analysis, 2012 update. *Nucleic Acids Research, 40*(D1), D1144-D1149 https://doi.org/10.1093/nar/gkr1013

Wang, Z., Xu, Q., Zhang, N., Du, X., Xu, G., & Yan, X. (2020). CD146, from a melanoma cell adhesion molecule to a signalling receptor. *Signal Transduction and Targeted Therapy, 5*(1), 148. https://doi.org/10.1038/s41392-020-00259-8

Wang, Z., & Yan, X. (2013). CD146, a multi-functional molecule beyond adhesion. *Cancer Letters, 330*(2), 150-162. https://doi.org/https://doi.org/10.1016/j.canlet.2012.11.049

Weber, S., & Saftig, P. (2012). Ectodomain shedding and ADAMs in development. *Development, 139*(20), 3693-3709.

Weihofen, A., Binns, K., Lemberg, M. K., Ashman, K., & Martoglio, B. (2002). Identification of signal peptide peptidase, a presenilin-type aspartic protease. *Science, 296*(5576), 2215-2218. https://doi.org/10.1126/science.1070925

Weihofen, A., & Martoglio, B. (2003). Intramembrane-cleaving proteases: controlled liberation of proteins and bioactive peptides. *Trends in Cell Biology, 13*(2), 71-78. https://doi.org/https://doi.org/10.1016/S0962-8924(02)00041-7

Wessely, A., Steeb, T., Berking, C., & Heppt, M. V. (2021). How neural crest transcription factors contribute to melanoma heterogeneity, cellular plasticity, and treatment resistance. *International Journal of Molecular Sciences, 22*(11), 5761. https://doi.org/10.3390/ijms22115761

Williams, H., Johnson, J. L., Jackson, C. L., White, S. J., & George, S. J. (2010). MMP-7 mediates cleavage of N-cadherin and promotes smooth muscle cell apoptosis. *Cardiovascular Research, 87*(1), 137-146 https://doi.org/10.1093/cvr/cvq042

Williamson, R. L., Laulagnier, K., Miranda, A. M., Fernandez, M. A., Wolfe, M. S., Sadoul, R., & Di Paolo, G. (2017). Disruption of amyloid precursor protein ubiquitination selectively increases amyloid β (Aβ) 40 levels via presenilin 2-mediated cleavage. *The Journal of Biological Chemistry, 292*(48), 19873-19889 https://doi.org/10.1074/jbc.M117.818138

Witze, E. S., Connacher, M. K., Houel, S., Schwartz, M. P., Morphew, M. K., Reid, L., Sacks, D. B., Anseth, K. S., & Ahn, N. G. (2013). Wnt5a directs polarized calcium gradients by recruiting cortical endoplasmic reticulum to the cell trailing edge. *Developmental Cell, 26*, 645-657 https://doi.org/http://dx.doi.org/10.1016/j.devcel.2013.08.019

Witze, E. S., Litman, E. S., Argast, G. M., Moon, R. T., & Ahn, N. G. (2008). Wnt5a control of cell polarity and directional movement by polarized redistribution of adhesion receptors. *Science, 320*(5874), 365-369 https://doi.org/10.1126/science.1151250

Won, S. J., Cheung See Kit, M., & Martin, B. R. (2018). Protein depalmitoylases. *Critical Reviews in Biochemistry and Molecular Biology, 53*(1), 83-98 https://doi.org/10.1080/10409238.2017.1409191

Wong, K. K., Zhu, F., Khatri, I., Huo, Q., Spaner, D. E., & Gorczynski, R. M. (2016). Characterization of CD200 ectodomain shedding. *PLOS ONE, 11*(4), e0152073 https://doi.org/10.1371/journal.pone.0152073

Wong, M.-X., Harbour, S. N., Wee, J. L., Lau, L.-M., Andrews, R. K., & Jackson, D. E. (2004). Proteolytic cleavage of platelet endothelial cell adhesion molecule-1 (PECAM-1/CD31) is regulated by a calmodulin-binding motif. *FEBS Letters, 568*(1), 70-78 https://doi.org/https://doi.org/10.1016/j.febslet.2004.04.094

Wright, S. C., Schellenberger, U., Ji, L., Wang, H., & Larrick, J. W. (1997). Calmodulin-dependent protein kinase II mediates signal transduction in apoptosis. *The FASEB Journal, 11*(11), 843-849 https://doi.org/10.1096/fasebj.11.11.9285482

Wrobel, T., Mazur, G., Wolowiec, D., Jazwiec, B., Sowinska, E., & Kulizkowski, K. (2006). sVE-cadherin and sCD146 serum levels in patients with multiple myeloma. *Clinical & Laboratory Haematology, 28*(1), 36-39 https://doi.org/10.1111/j.1365-2257.2006.00756.x

Wu, B., Cui, J., Yang, X.-M., Liu, Z.-Y., Song, F., Li, L., Jiang, J.-L., & Chen, Z.-N. (2017). Cytoplasmic fragment of CD147 generated by regulated intramembrane proteolysis contributes to HCC by promoting autophagy. *Cell Death and Disease, 8*, e2925 https://doi.org/10.1038/cddis.2017.251

Wu, G.-J., Fu, P., Wang, S.-W., & Wu, M.-W. H. (2008). Enforced expression of MCAM/MUC18 increases in vitro motility and invasiveness and in vivo metastasis of two melanoma K1735 sublines in a syngeneic mouse model. *Molecular Cancer Research, 6*(11), 1666-1677.

Wu, G.-J., Wu, M.-W. H., Wang, S.-W., Liu, Z., Qu, P., Peng, Q., Yang, H., Varma, V. A., Sun, Q. C., Petros, J. A., Lim, S. D., & Amin, M. B. (2001). Isolation and characterization of the major form of human MUC18 cDNA gene and correlation of MUC18 over-expression in prostate cancer cell lines and tissues with malignant progression. *Gene, 279*(1), 17-31 https://doi.org/http://dx.doi.org/10.1016/S0378-1119(01)00736-3

Wu, J.-D., Hong, C.-Q., Huang, W.-H., Wei, X.-L., Zhang, F., Zhuang, Y.-X., Zhang, Y.-Q., & Zhang, G.-J. (2018). L1 cell adhesion molecule and its soluble form sL1exhibit poor prognosis in primary breast cancer patients. *Clinical Breast Cancer, 18*(5), e851-e861 https://doi.org/https://doi.org/10.1016/j.clbc.2017.12.011

Xie, S., Luca, M., Huang, S., Gutman, M., Reich, R., Johnson, J. P., & Bar-Eli, M. (1997). Expression of MCAM/MUC18 by human melanoma cells leads to increased tumor growth and metastasis. *Cancer Research, 57*(11), 2295-2303

Xie, T., Dong, B., Yan, Y., Hu, G., & Xu, Y. (2016). Association between MMP-2 expression and prostate cancer: A meta-analysis. *Biomedical Reports, 4*(2), 241-245 https://doi.org/10.3892/br.2015.553

Xing, Y., Xu, Q., & Lee, C. (2003). Widespread production of novel soluble protein isoforms by alternative splicing removal of transmembrane anchoring domains. *FEBS Letters, 555*(3), 572-578 https://doi.org/https://doi.org/10.1016/S0014-5793(03)01354-1

Yan, H., Zhang, C., Wang, Z., Tu, T., Duan, H., Luo, Y., Feng, J., Liu, F., & Yan, X. (2017). CD146 is required for VEGF-C-induced lymphatic sprouting during lymphangiogenesis. *Scientific Reports, 7*(1), 7442 https://doi.org/10.1038/s41598-017-06637-7

Yan, X., Lin, Y., Yang, D., Shen, Y., Yuan, M., Zhang, Z., Li, P., Xia, H., Li, L., Luo, D., Liu, Q., Mann, K., & Bader, B. L. (2003). A novel anti-CD146 monoclonal antibody, AA98, inhibits angiogenesis and tumor growth. *Blood, 102*(1), 184-191 https://doi.org/10.1182/blood-2002-04-1004

Yang, H., Wang, S., Liu, Z., Wu, M. H., McAlpine, B., Ansel, J., Armstrong, C., & Wu, G. (2001). Isolation and characterization of mouse MUC18 cDNA gene, and correlation of MUC18 expression in mouse melanoma cell lines with metastatic ability. *Gene, 265*(1-2), 133-145 https://doi.org/10.1016/s0378-1119(01)00349-3

Yang, L., Dutta, S. M., Troyer, D. A., Lin, J. B., Lance, R. A., Nyalwidhe, J. O., Drake, R. R., & Semmes, O. J. (2015). Dysregulated expression of cell surface glycoprotein CDCP1 in prostate cancer. *Oncotarget, 6*(41), 43743-43758 https://doi.org/https://doi.org/10.18632/oncotarget.6193

Yang, T., Arslanova, D., Gu, Y., Augelli-Szafran, C., & Xia, W. (2008). Quantification of gamma-secretase modulation differentiates inhibitor compound selectivity between two substrates notch and amyloid precursor protein. *Molecular Brain, 1*(1), 15 https://doi.org/10.1186/1756-6606-1-15

Yap, K. L., Kim, J., Truong, K., Sherman, M., Yuan, T., & Ikura, M. (2000). Calmodulin target database. *Journal of Structural and Functional Genomics, 1*(1), 8-14 https://doi.org/10.1023/A:1011320027914

Yokozeki, T., Wakatsuki, S., Hatsuzawa, K., Black, R. A., Wada, I., & Sehara-Fujisawa, A. (2007). Meltrin β (ADAM19) mediates ectodomain shedding of Neuregulin β1 in the Golgi apparatus: fluorescence correlation spectroscopic observation of the dynamics of ectodomain shedding in living cells. *Genes to Cells, 12*(3), 329-343 https://doi.org/10.1111/j.1365-2443.2007.01060.x

Yuan, J. S., Reed, A., Chen, F., & Stewart, C. N. (2006). Statistical analysis of real-time PCR data. *BMC Bioinformatics, 7*(1), 85 https://doi.org/10.1186/1471-2105-7-85

Yuan, X., Wu, H., Xu, H., Xiong, H., Chu, Q., Yu, S., Wu, G. S., & Wu, K. (2015). Notch signalling: an emerging therapeutic target for cancer treatment. *Cancer Letters, 369*(1), 20-27 https://doi.org/https://doi.org/10.1016/j.canlet.2015.07.048

Yun, H. M., Park, M. H., Kim, D. H., Ahn, Y. J., Park, K. R., Kim, T. M., Yun, N. Y., Jung, Y. S., Hwang, D. Y., Yoon, D. Y., Han, S. B., & Hong, J. T. (2014). Loss of presenilin 2 is associated with increased iPLA2 activity and lung tumor development. *Oncogene, 33*(44), 5193-5200 https://doi.org/10.1038/onc.2014.128

Zabouo, G., Imbert, A.-M., Jacquemier, J., Finetti, P., Moreau, T., Esterni, B., Birnbaum, D., Bertucci, F., & Chabannon, C. (2009). CD146 expression is associated with a poor prognosis in human breast tumors and with enhanced motility in breast cancer cell lines. *Breast Cancer Research, 11*(1), R1 https://doi.org/10.1186/bcr2215

Zeng, Q., Li, W., Lu, D., Wu, Z., Duan, H., Luo, Y., Feng, J., Yang, D., Fu, L., & Yan, X. (2012). CD146, an epithelial-mesenchymal transition inducer, is associated with triple-negative breast cancer. *Proceedings of the National Academy of Sciences, U.S.A., 109*(4), 1127-1132 https://doi.org/10.1073/pnas.1111053108

Zhang, L., Bukulin, M., Kojro, E., Roth, A., Metz, V. V., Fahrenholz, F., Nawroth, P. P., Bierhaus, A., & Postina, R. (2008a). Receptor for advanced glycation end products is subjected to protein ectodomain shedding by metalloproteinases. *Journal of Biological Chemistry, 283*(51), 35507-35516 https://doi.org/10.1074/jbc.M806948200

Zhang, L., Luo, Y., Teng, X., Wu, Z., Li, M., Xu, D., Wang, Q., Wang, F., Feng, J., Zeng, X., & Yan, X. (2018). CD146: a potential therapeutic target for systemic sclerosis. *Protein & Cell, 9*(12), 1050-1054 https://doi.org/10.1007/s13238-018-0531-x

Zhang, S., Zhang, M., Cai, F., & Song, W. (2013). Biological function of Presenilin and its role in AD pathogenesis. *Translational Neurodegeneration, 2*(1), 15 https://doi.org/10.1186/2047-9158-2-15

Zhang, X., Guo, L., Collage, R. D., Stripay, J. L., Tsung, A., Lee, J. S., & Rosengart, M. R. (2011). Calcium/calmodulin-dependent protein kinase (CaMK) Iα mediates the macrophage inflammatory response to sepsis. *Journal of Leukocyte Biology, 90*(2), 249-261 https://doi.org/10.1189/jlb.0510286

Zhang, Y., Zheng, C., Zhang, J., Yang, D., Feng, J., Lu, D., & Yan, X. (2008b). Generation and characterization of a panel of monoclonal antibodies against distinct epitopes of human CD146. *Hybridoma, 27*(5), 345-352 https://doi.org/10.1089/hyb.2008.0034

Zheng, C., Qiu, Y., Zeng, Q., Zhang, Y., Lu, D., Yang, D., Feng, J., & Yan, X. (2009). Endothelial CD146 is required for in vitro tumor-induced angiogenesis: the role of a disulfide bond in signalling and dimerization. *The International Journal of Biochemistry & Cell Biology, 41*(11), 2163-2172 https://doi.org/https://doi.org/10.1016/j.biocel.2009.03.014

Zhu, G., Zhang, X., Wang, Y., Xiong, H., Zhao, Y., Wang, J., & Sun, F. (2015). Prognostic value of melanoma cell adhesion molecule expression in cancers: a meta-analysis. *International Journal of Clinical and Experimental Medicine, 8*(8), 12056-12063

Ziegler, W. H., Tigges, U., Zieseniss, A., & Jockusch, B. M. (2002). A lipid-regulated docking site on vinculin for Protein Kinase C*. *Journal of Biological Chemistry, 277*(9), 7396-7404 https://doi.org/https://doi.org/10.1074/jbc.M110008200

Zigler, M., Villares, G. J., Dobroff, A. S., Wang, H., Huang, L., Braeuer, R. R., Kamiya, T., Melnikova, V. O., Song, R., Friedman, R., Alani, R. M., & Bar-Eli, M. (2011). Expression of Id-1 is regulated by MCAM/MUC18: a missing link in melanoma progression. *Cancer Research, 71*(10), 3494-3504 https://doi.org/10.1158/0008-5472.can-10-3555

Zunke, F., & Rose-John, S. (2017). The shedding protease ADAM17: physiology and pathophysiology. *Biochimica et Biophysica Acta (BBA) - Molecular Cell Research, 1864*(11), 2059-2070 https://doi.org/https://doi.org/10.1016/j.bbamcr.2017.07.001

Appendix A

Plasmid sequencing results

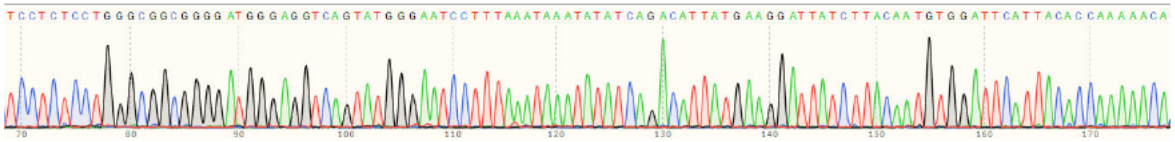

Appendix A- i pcDNA3-ADAM10-HA (Addgene plasmid #65106)- *forward*

Chromatogram (upper) and sequence alignment (lower) demonstrate correct sequencing of the plasmid in the "forward direction". The blue highlight is the sequence represented in chromatogram.

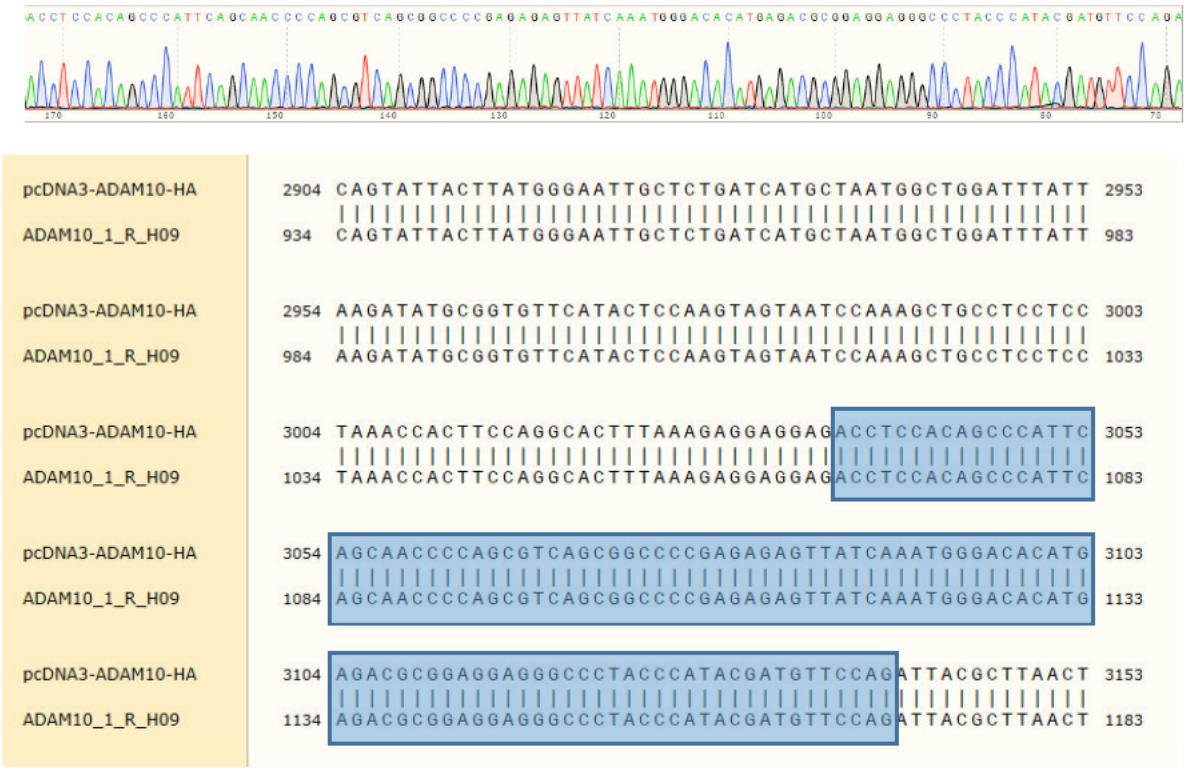

Appendix A- ii pcDNA3-ADAM10-HA (Addgene plasmid #65106)- *reverse*

Chromatogram (upper) and sequence alignment (lower) demonstrate correct sequencing of the plasmid in the "reverse direction". The blue highlight is the sequence represented in chromatogram.

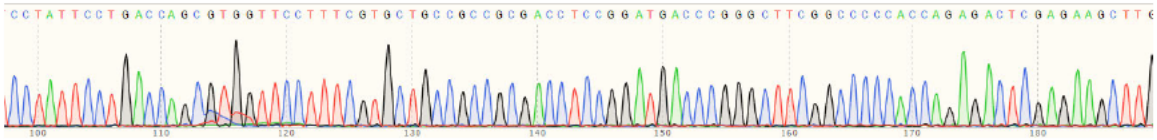

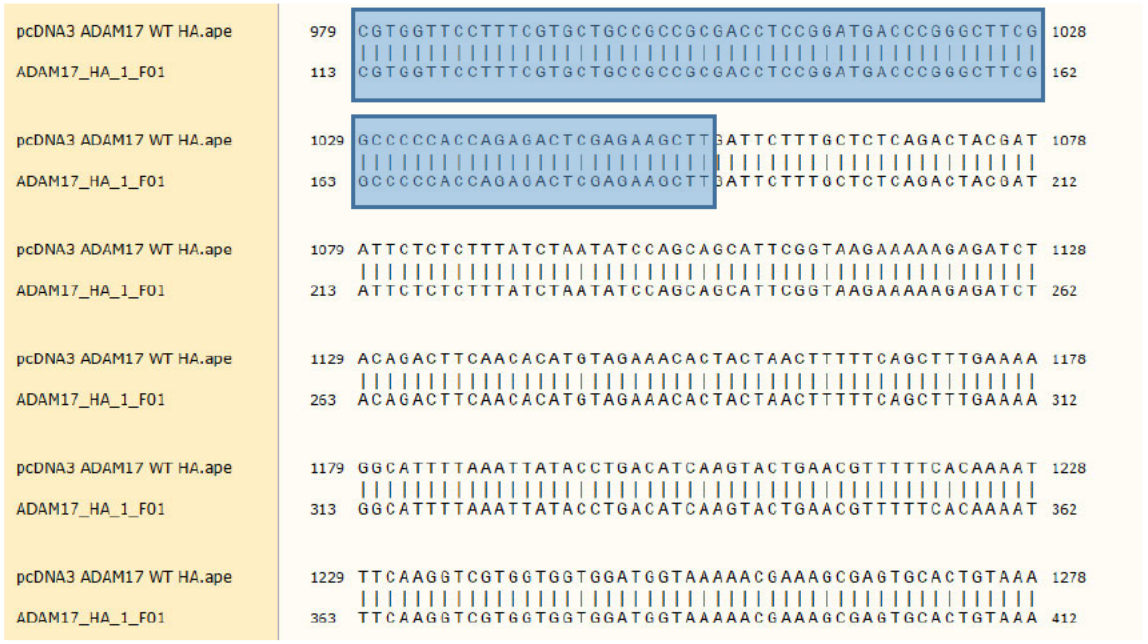

Appendix A- iii pcDNA3-ADAM17-HA (Addgene plasmid #65105)- *forward*

Chromatogram (upper) and sequence alignment (lower) demonstrate correct sequencing of the plasmid in the "forward direction". The blue highlight is the sequence represented in chromatogram.

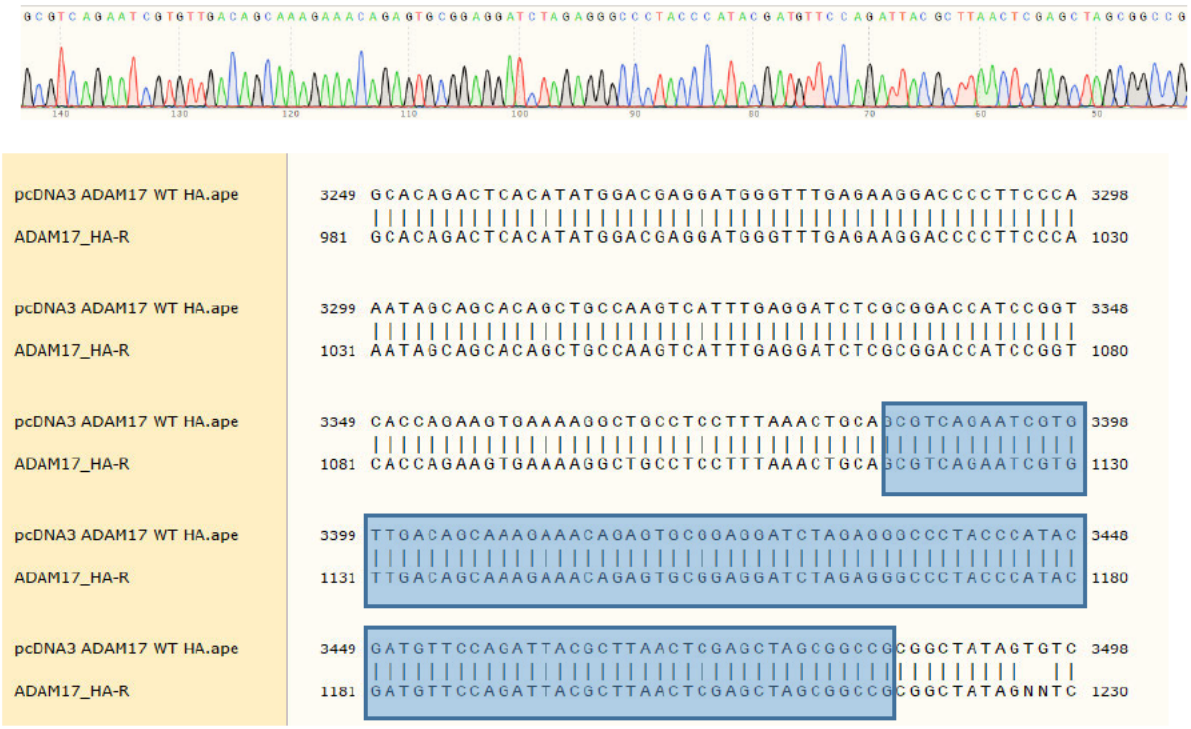

Appendix A- iv pcDNA3-ADAM17-HA (Addgene plasmid #65105)- *reverse*

Chromatogram (upper) and sequence alignment (lower) demonstrate correct sequencing of the plasmid in the "reverse direction". The blue highlight is the sequence represented in chromatogram.

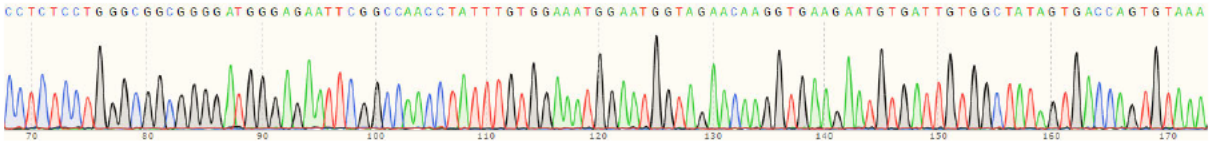

pcDNA3-Delta(ProMP)-ADAM10-HA	942	CCTGGGCGGCGGGGATGGGAGAATTCGGCCAACCTATTTGTGGAAATGGA	991
Delta(ProMP)ADAM10_HA_F	73	CCTGGGCGGCGGGGATGGGAGAATTCGGCCAACCTATTTGTGGAAATGGA	122
pcDNA3-Delta(ProMP)-ADAM10-HA	992	ATGGTAGAACAAGGTGAAGAATGTGATTGTGGCTATAGTGACCAGTGTAA	1041
Delta(ProMP)ADAM10_HA_F	123	ATGGTAGAACAAGGTGAAGAATGTGATTGTGGCTATAGTGACCAGTGTAA	172
pcDNA3-Delta(ProMP)-ADAM10-HA	1042	AGATGAATGCTGCTTCGATGCAAATCAACCAGAGGGAAGAAAATGCAAAC	1091
Delta(ProMP)ADAM10_HA_F	173	AGATGAATGCTGCTTCGATGCAAATCAACCAGAGGGAAGAAAATGCAAAC	222
pcDNA3-Delta(ProMP)-ADAM10-HA	1092	TGAAACCTGGGAAACAGTGCAGTCCAAGTCAAGGTCCTTGTTGTACAGCA	1141
Delta(ProMP)ADAM10_HA_F	223	TGAAACCTGGGAAACAGTGCAGTCCAAGTCAAGGTCCTTGTTGTACAGCA	272
pcDNA3-Delta(ProMP)-ADAM10-HA	1142	CAGTGTGCATTCAAGTCAAAGTCTGAGAAGTGTCGGGATGATTCAGACTG	1191
Delta(ProMP)ADAM10_HA_F	273	CAGTGTGCATTCAAGTCAAAGTCTGAGAAGTGTCGGGATGATTCAGACTG	322
pcDNA3-Delta(ProMP)-ADAM10-HA	1192	TGCAAGGGAAGGAATATGTAATGGCTTCACAGCTCTCTGCCCAGCATCTG	1241
Delta(ProMP)ADAM10_HA_F	323	TGCAAGGGAAGGAATATGTAATGGCTTCACAGCTCTCTGCCCAGCATCTG	372

Appendix A- v pcDNA3-Delta(ProMP)-ADAM10-HA (Addgene plasmid #65107)- *forward*

Chromatogram (upper) and sequence alignment (lower) demonstrate correct sequencing of the plasmid in the "forward direction". The blue highlight is the sequence represented in chromatogram.

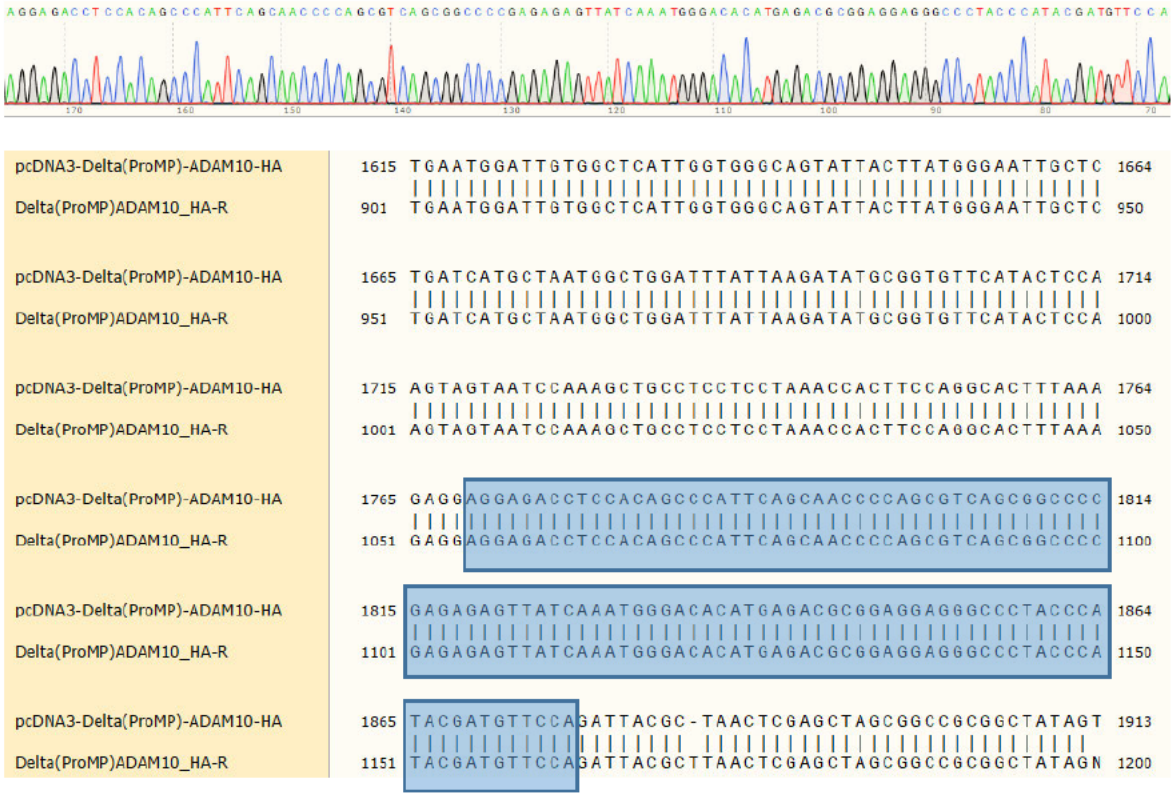

Appendix A- vi pcDNA3-Delta(ProMP)-ADAM10-HA (Addgene plasmid #65107)- *reverse*

Chromatogram (upper) and sequence alignment (lower) demonstrate correct sequencing of the plasmid in the "reverse direction". The blue highlight is the sequence represented in chromatogram.

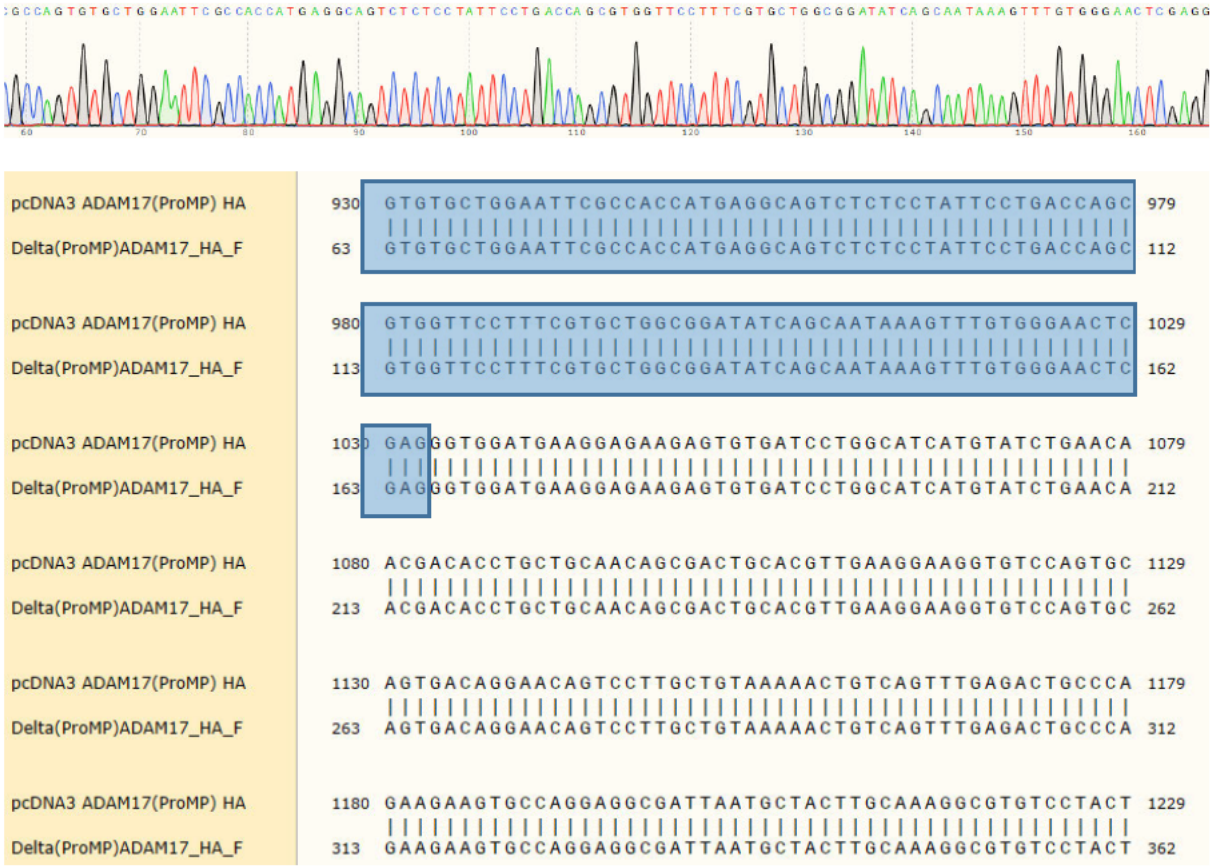

Appendix A- vii pcDNA3-Delta(ProMP)-ADAM17-HA (Addgene plasmid #65221)- *forward*

Chromatogram (upper) and sequence alignment (lower) demonstrate correct sequencing of the plasmid in the "forward direction". The blue highlight is the sequence represented in chromatogram.

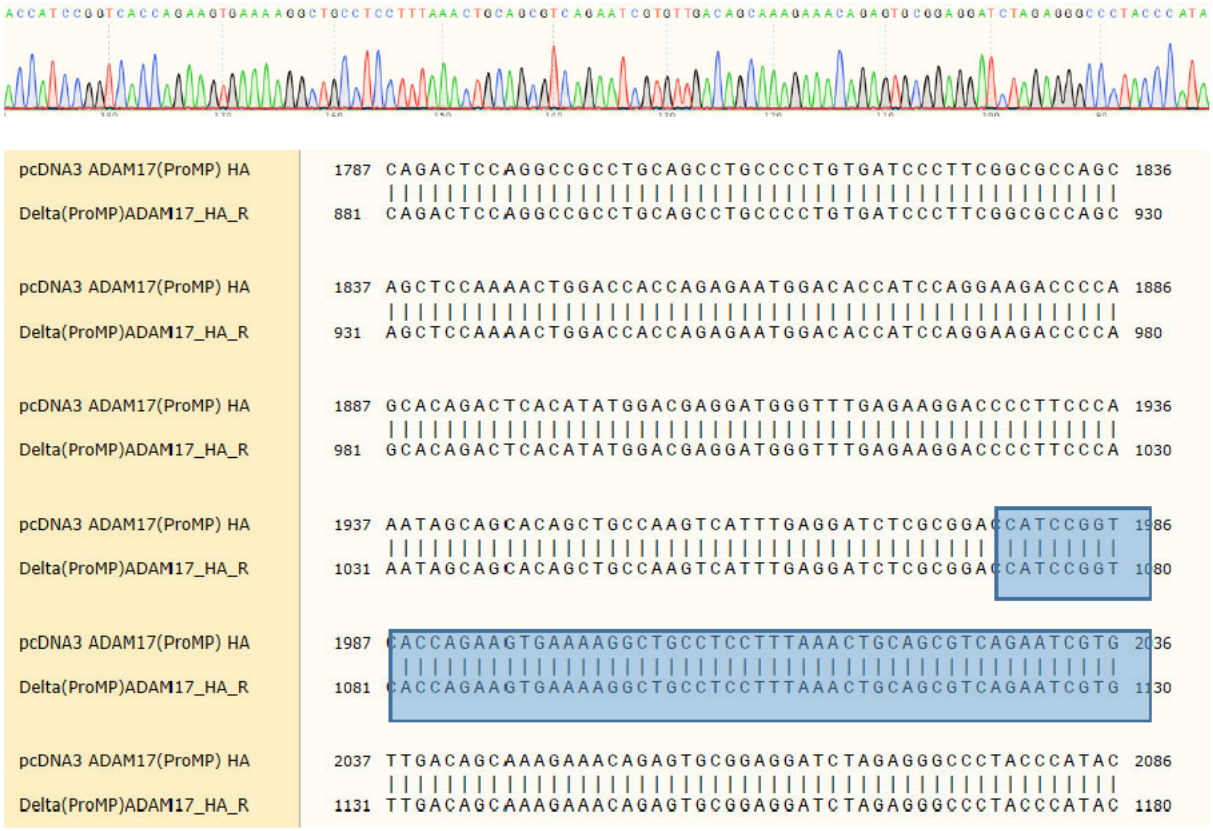

Appendix A- viii pcDNA3-Delta(ProMP)-ADAM17-HA (Addgene plasmid #65221)- *reverse*

Chromatogram (upper) and sequence alignment (lower) demonstrate correct sequencing of the plasmid in the "reverse direction". The blue highlight is the sequence represented in chromatogram.

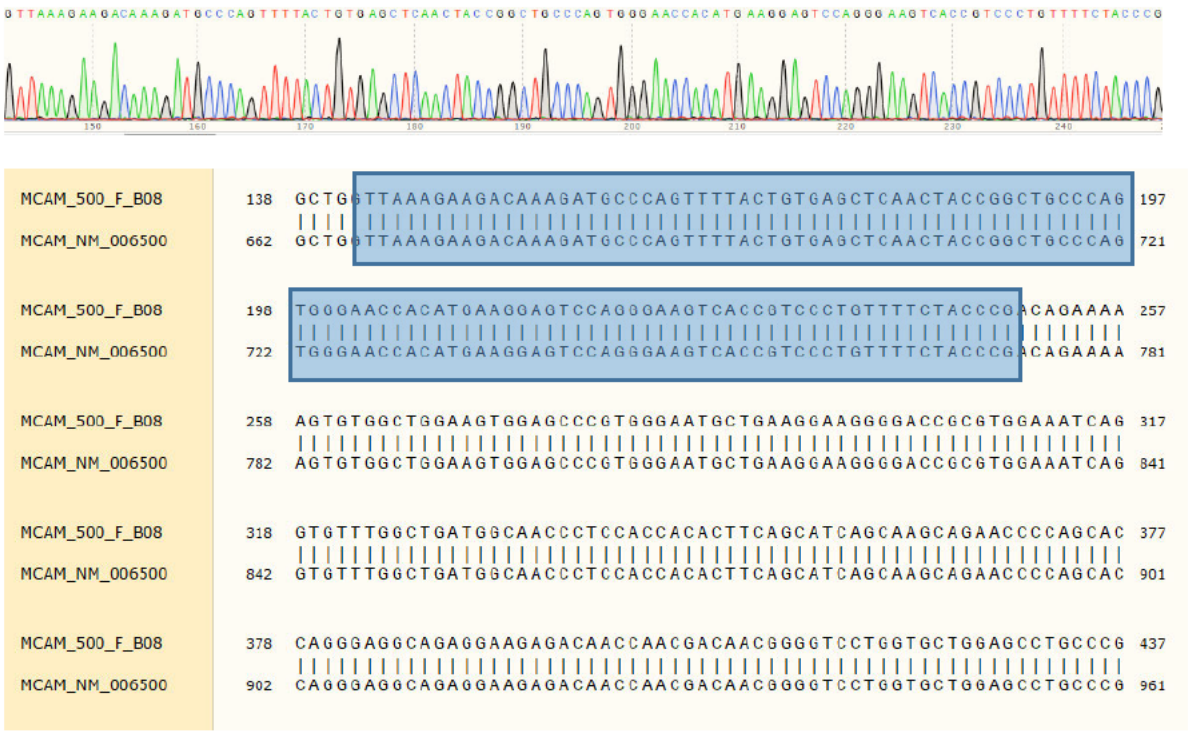

Appendix A- ix pcDNA3.1-MCAM ECD (forward)

Chromatogram (upper) and sequence alignment (lower) demonstrate correct sequencing of the plasmid in the "forward direction". The blue highlight is the sequence represented in chromatogram.

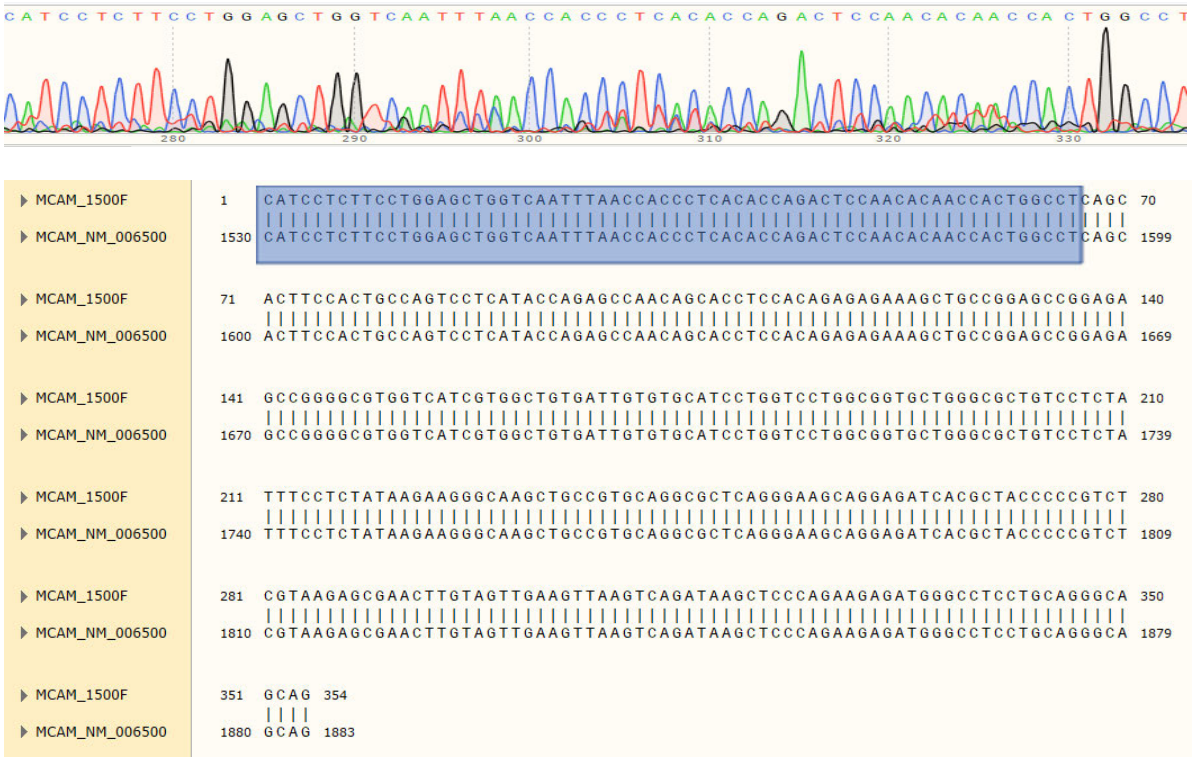

Appendix A- x pcDNA3.1-MCAM ICD (forward)

Chromatogram (upper) and sequence alignment (lower) demonstrate correct sequencing of the plasmid in the "forward direction". The blue highlight is the sequence represented in chromatogram.

Appendix B

Point mutations to MCAM-ICD

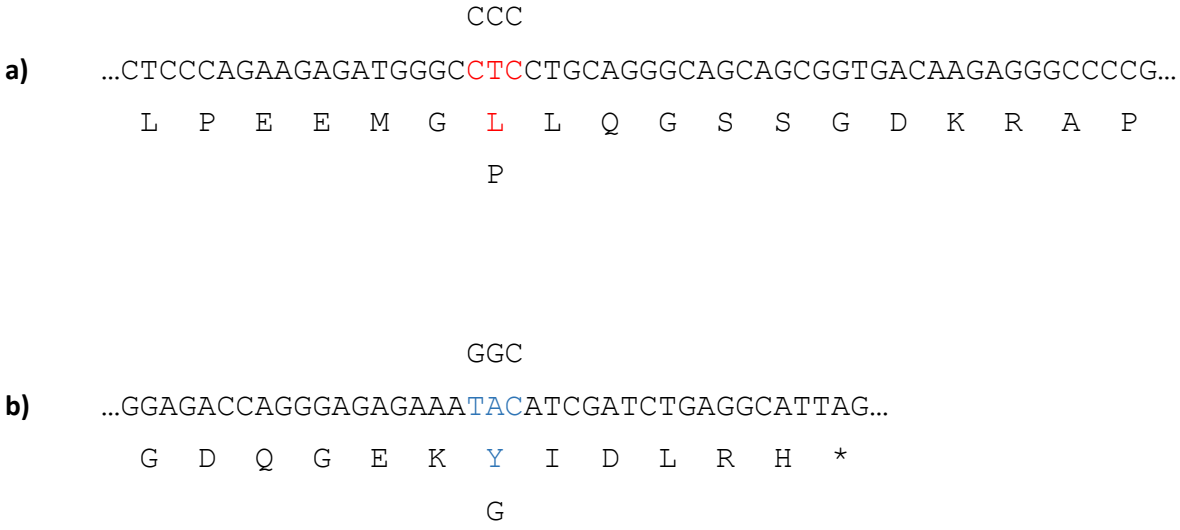

Site-directed mutagenesis was used to introduce mutations to the MCAM-ICD. These mutations affected (a) the di-leucine motif, converting Leu623 to Pro, and (b) the tyrosine motif, converting Tyr641 to Gly. Stable transfection of SB2 melanoma cells to generate the MCAM-expressing SB214.1, SB2LP, and SB2YG cell lines was performed by Dr. Danielle Dye.

Appendix C

Mycoplasma testing results

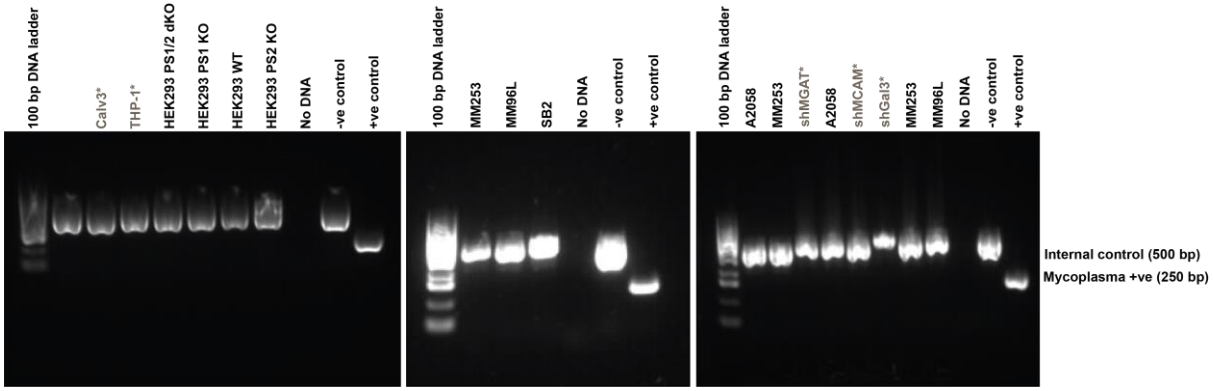

Cell culture media was routinely tested by PCR to ensure cells were not contaminated with Mycoplasma. An internal control was added to each sample (500 base pairs; bp) and a positive control was run on each gel (250 bp).

**Denotes samples not relevant to study*

Appendix D

Cell line authentication

STR loci	Cell line						
	A2058	MM253	SkMel28	MM96L	Colo239F	SB2	SB2 14.1
AMEL	X, Y	X, X	X, Y	XX	XX	XY	XY
CSF1PO	10, 11	10 ,11	10, 12	12,12	10,12	11,12	11,12
D13S317	13, 14	11, 12	11, 12	11, 14	11, 11	8, 11	8, 11
D16S539	9, 13	11, 11	9, 12	11, 12	8, 11	9, 13	9, 13
D21S11	29, 30.2	29 ,29	28, 29	28, 29	28, 29	29,32.2	29,32.2
D5S818	9, 12	11,12	11,12,13	11, 13	10, 13	12 ,12	12 ,12
D7S820	11, 11	8, 10	10,10	8, 11	10, 11	8,10	8,10
TH01	7, 9	9.3, 9.3	7, 7	7, 7	7, 9	6, 8	6, 8
TPOX	8, 8	8, 11	8, 12	8, 10	9, 10	8, 9	8, 9
vWA	14, 18	16, 18	16, 19	17, 18	15, 18	14, 18	14, 18

Short tandem repeat (STR) profiling of melanoma cells was performed by the AGRF using the Promega GenePrint10 system.

Cell line STR data was compared to publicly available data, where this was available

- A2058; https://web.expasy.org/cellosaurus/CVCL_1059; all STRs match
- MM253; https://web.expasy.org/cellosaurus/CVCL_2604; all STRs match
- SkMel28: https://web.expasy.org/cellosaurus/CVCL_0526; all STRs match; except our cells have an extra different allele for D5S818 (database lists 11, 13 or 11, 11)

The MM96L, Colo239F and SB2 cells did not have publicly available STR data.

- STR data from MM96L and Colo239F cells was obtained from Professor Nick Hayward (QIMR Berghofer, Brisbane, Australia)
- Both of these cells matched across 6 STR's in common between the Promega GenePrint10 panel used to analyze our cells, and an in-house panel used in Professor Nick Haywards's Laboratory (AMEL, D13S317, D21S11, D5S818, D7S820, vWA)

STR data for the SB2 and MCAM variant SB2 14.1 cells was not available for comparison.

Appendix E

Primer efficiency calculations

i. Control genes

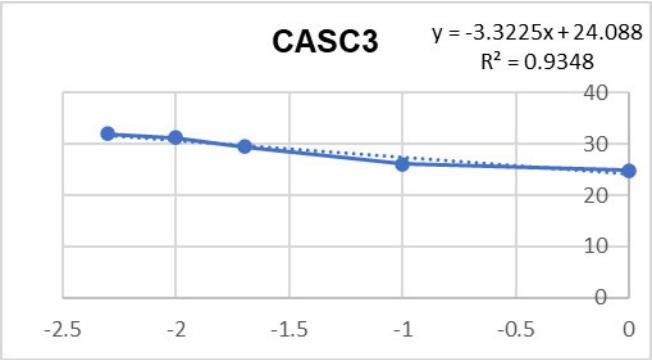

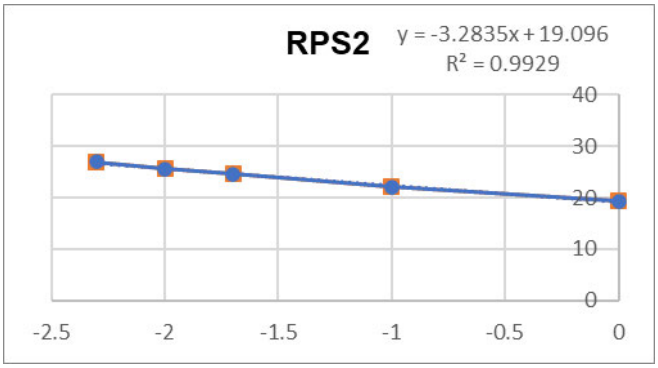

ii. Test genes

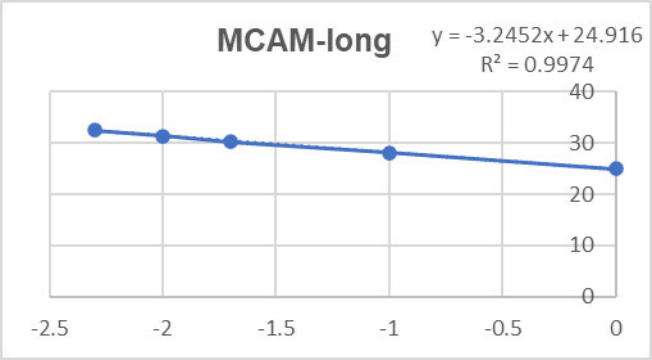

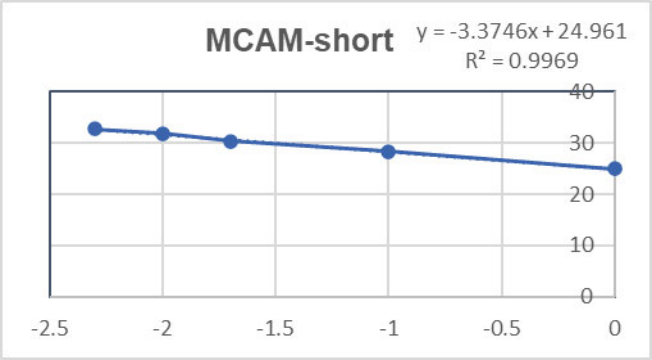

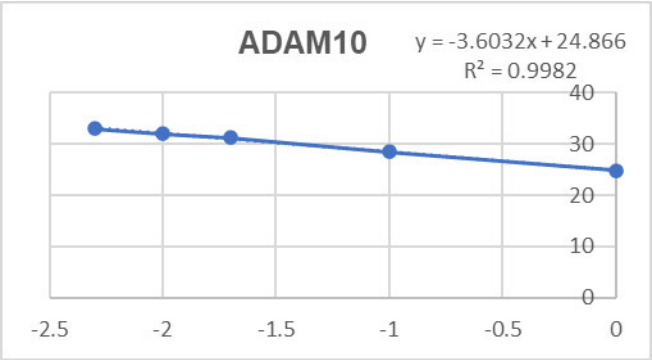

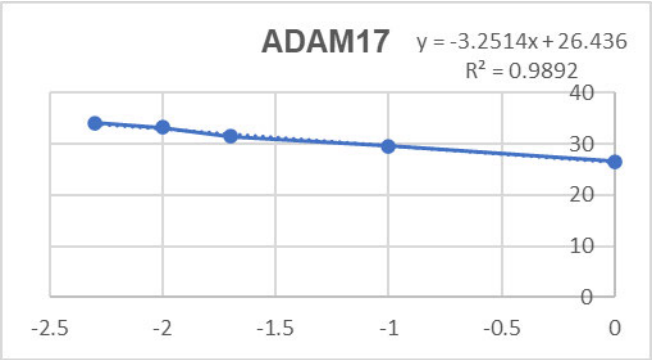

Test genes cont.

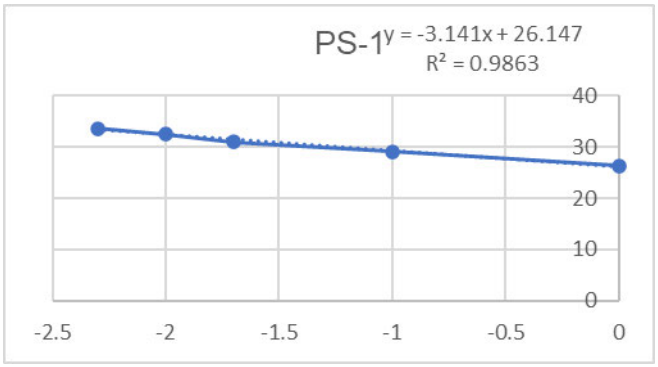

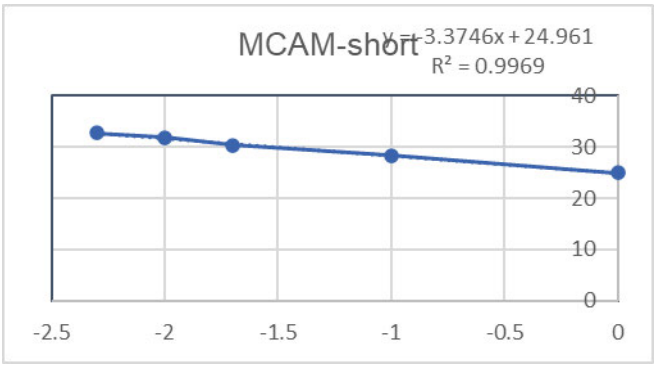

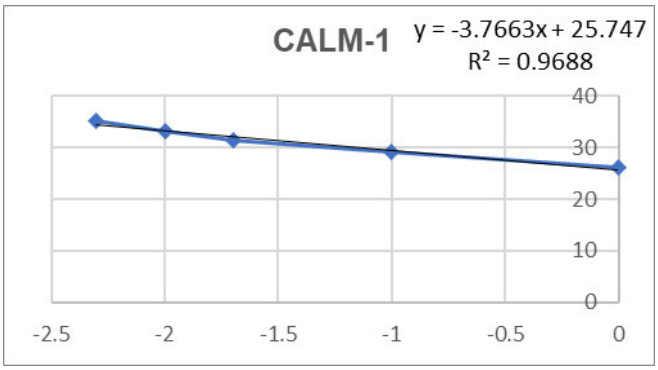

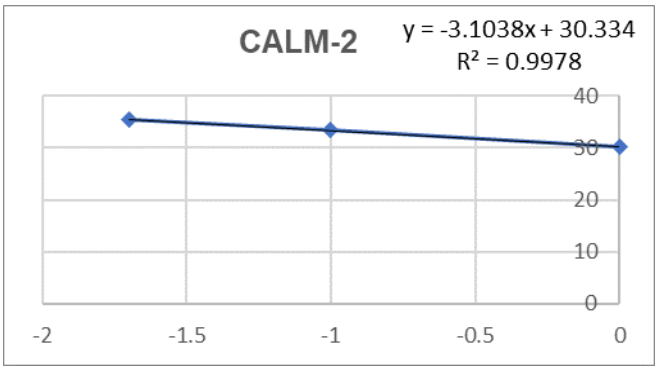

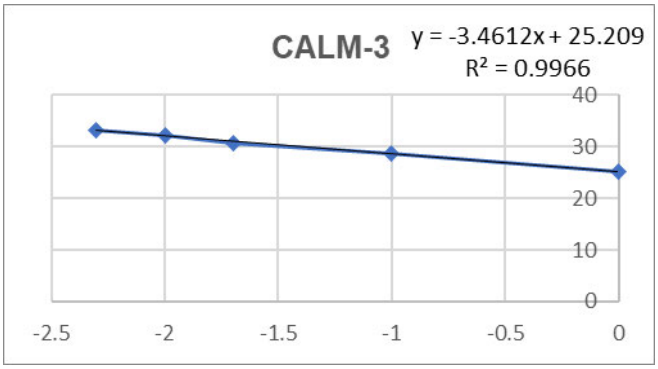

Gene	**Efficiency value** (10^(-1/The Slope Value)-1)*100
RPS2	102%
CASC3	100%
MCAM-l	103%
MCAM-s	102%
ADAM-10	90%
ADAM-17	103%
PS-1	108%
PS-2	106%
CALM-1	84%
CALM-2	110%
CALM-3	95%

Appendix F
Immunoblot for MCAM under different culture conditions

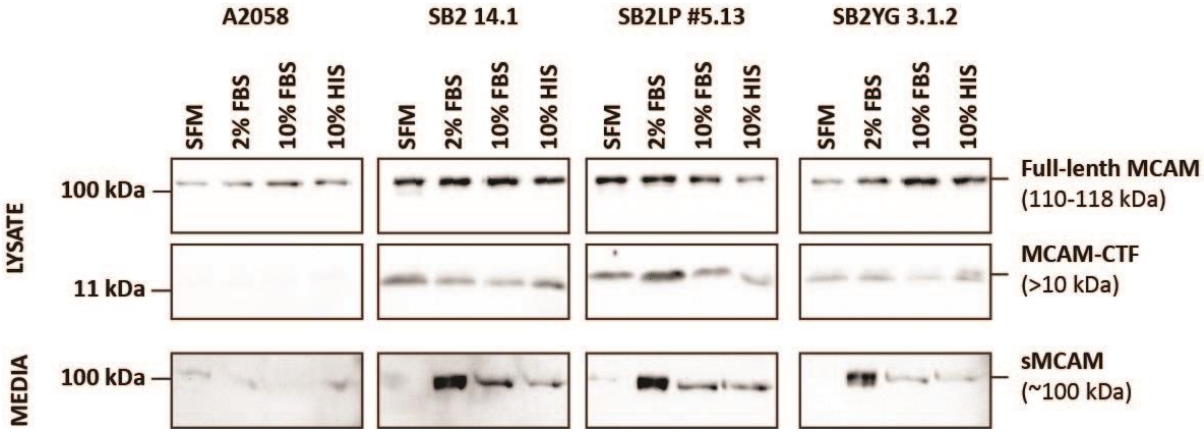

sMCAM production was compared under different conditions, including in the absence of serum (SFM), or in the presence of 2% FBS, 10% FBS, or 10% heat inactivated serum (HIS). There was minimal sMCAM under serum-free conditions. In the presence of serum, sMCAM appeared higher in samples incubated with 2% FBS. This was consistent between SB2 14.1, SB2 LP, and SB2 YG cell lines. In the below example, shedding of MCAM from A2058s was minimal under all conditions tested. A loading control (e.g. β-tubulin or Revert total protein stain) was not used here, however, all samples were collected and prepared concurrently. Equal amounts of total protein were loaded per well, based on BCA results.

Appendix G

Tris-tricine gel for MCAM-ICD

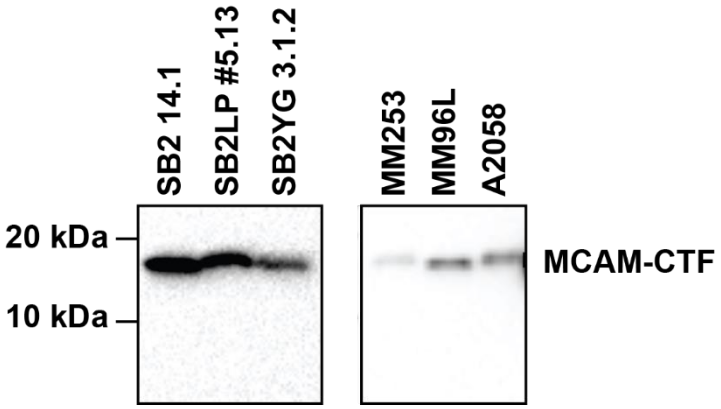

A tris-tricine gel was used to separate smaller protein fragments in melanoma cell lysates. The presence of MCAM-CTF was confirmed, however a smaller ICD fragment was not detected (expected size 6-8 kDa) in any melanoma cell lines tested. Tris-tricine gels were prepared and run by Ms Melissa Eccles.

Appendix H

Maps for plasmids containing ADAM10 and ADAM17 sequences

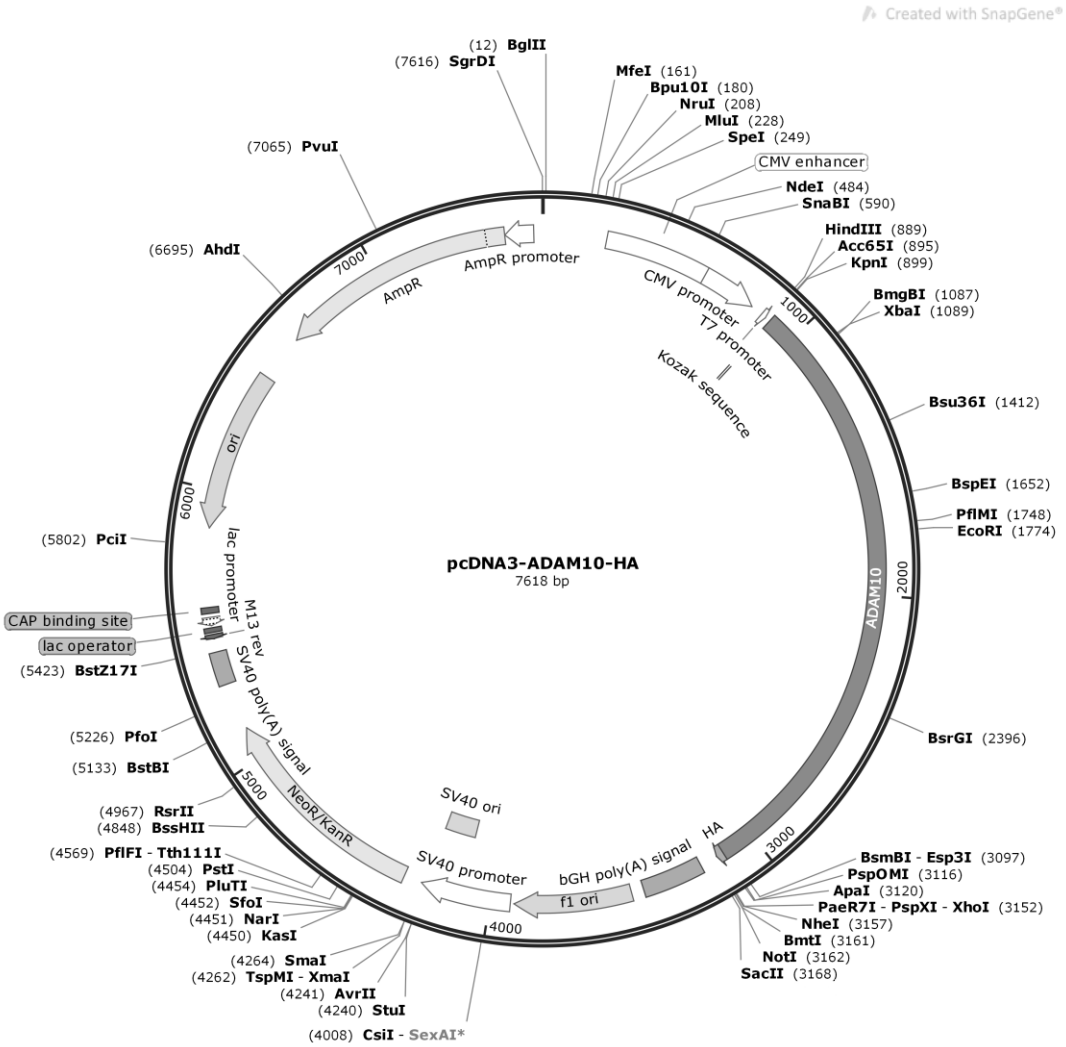

Appendix H-i pcDNA3-ADAM10-HA plasmid map

Addgene plasmid #65106. Deposited by Axel Ullrich (Gschwind *et al.*, 2003).

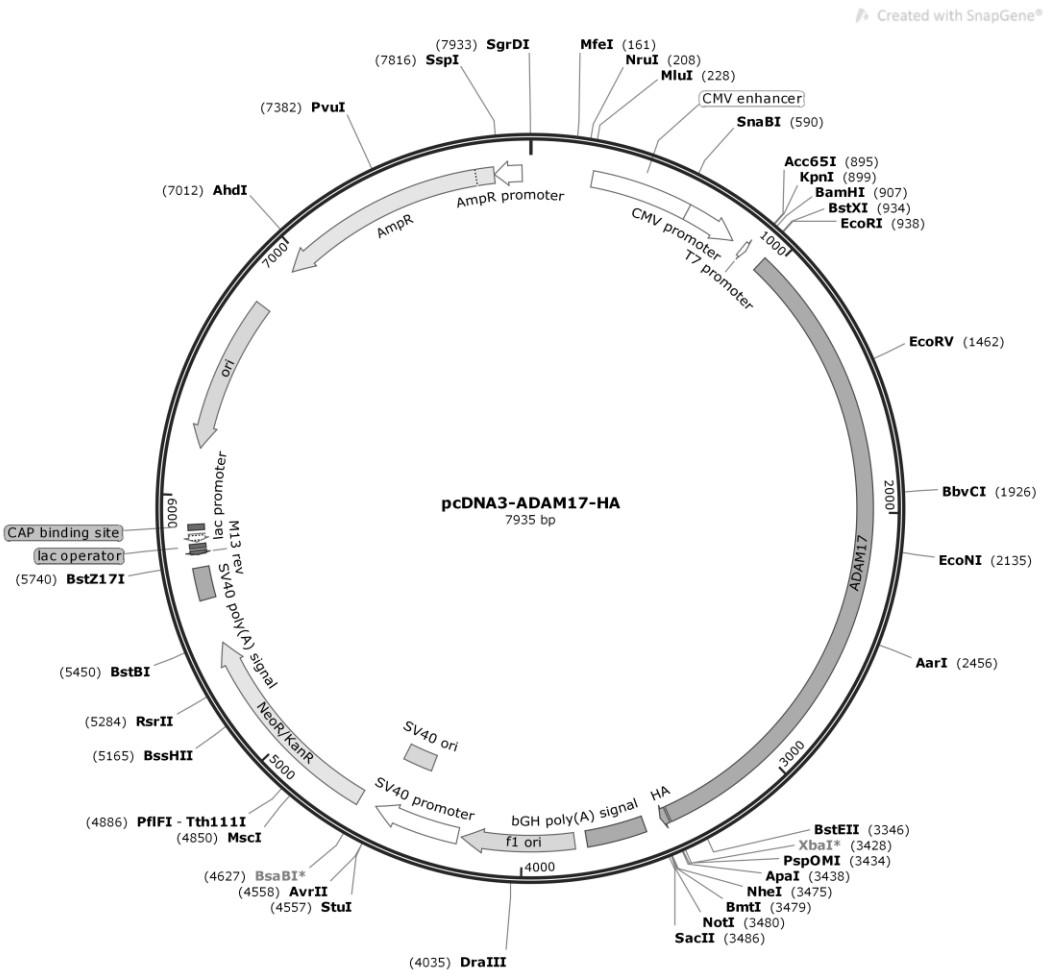

Appendix H-ii pcDNA3-ADAM17-HA plasmid map

Addgene plasmid #65105. Deposited by Axel Ullrich (Gschwind *et al.*, 2003).

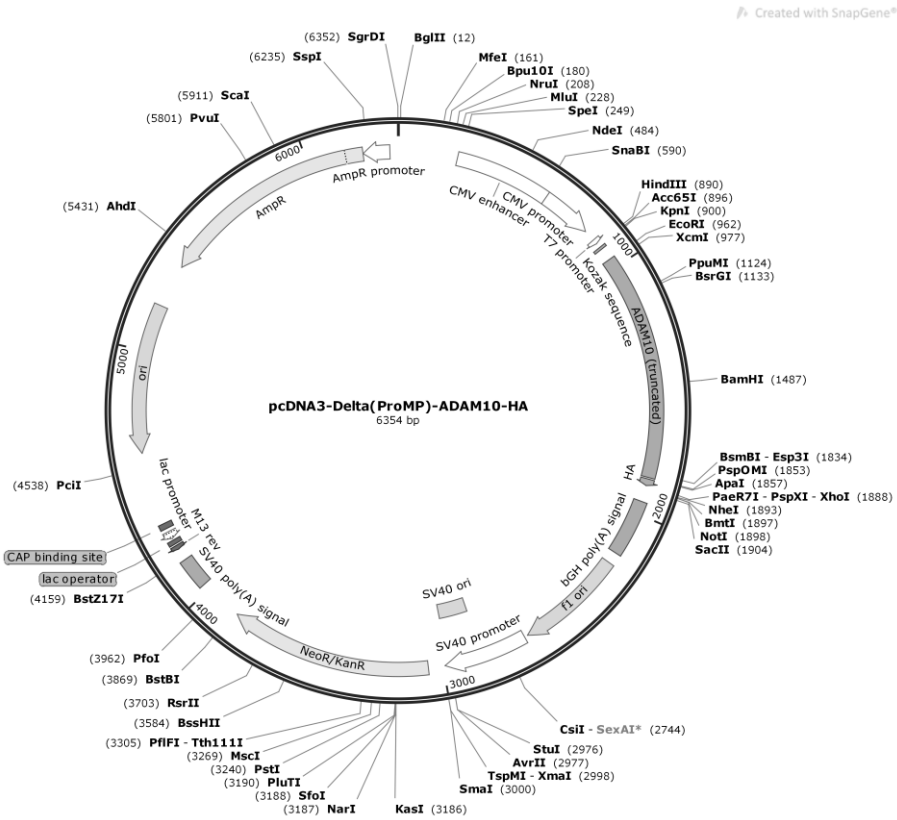

Appendix H-iii pCDNA3-Delta(ProMP)-ADAM10-HA plasmid map

Addgene plasmid #65107. Deposited by Axel Ullrich (Gschwind *et al.*, 2003).

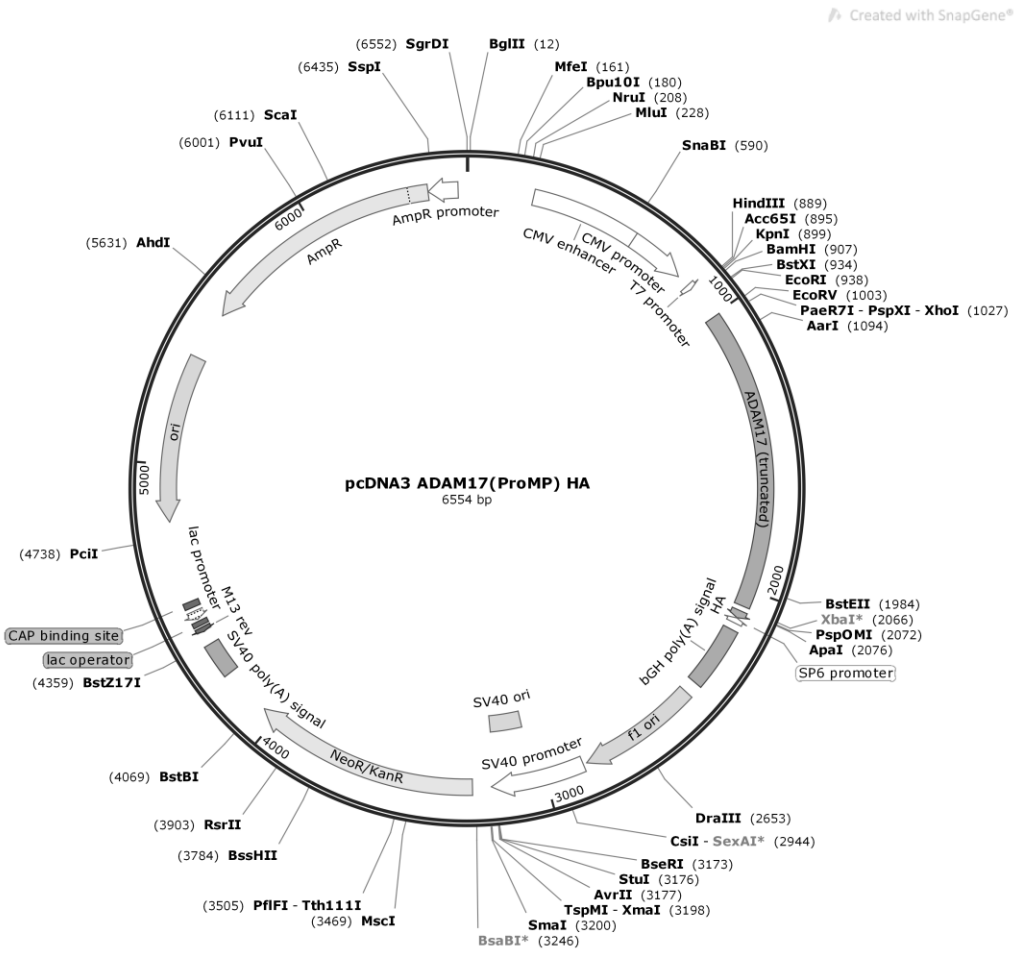

Appendix H-iv pCDNA3-Delta(ProMP)-ADAM17-HA plasmid map

Addgene plasmid #65221. Deposited by Axel Ullrich (Gschwind *et al.*, 2003).

Appendix I

Immunofluorescent labeling of MCAM and HA-tagged ADAMs

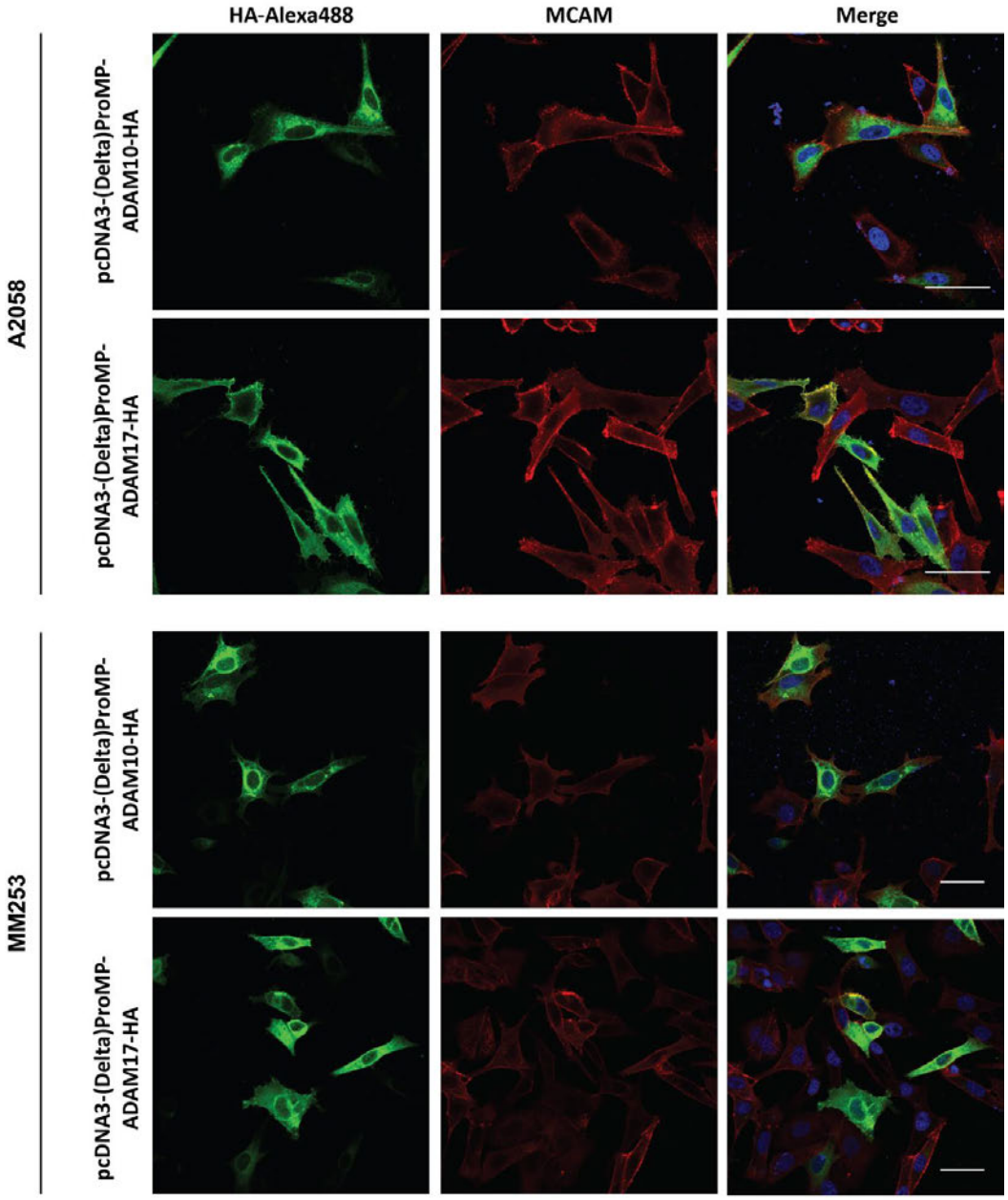

Localisation of MCAM in relation to pcDNA3-DeltaPro(MP)-ADAM10-HA and pcDNA3-DeltaPro(MP)-ADAM17-HA in transiently transfected melanoma cells (note 40x objective used for MM253 cells, 60x objective used for A2058).

Appendix J

Map for pcDNA 3.1 vector containing MCAM insert

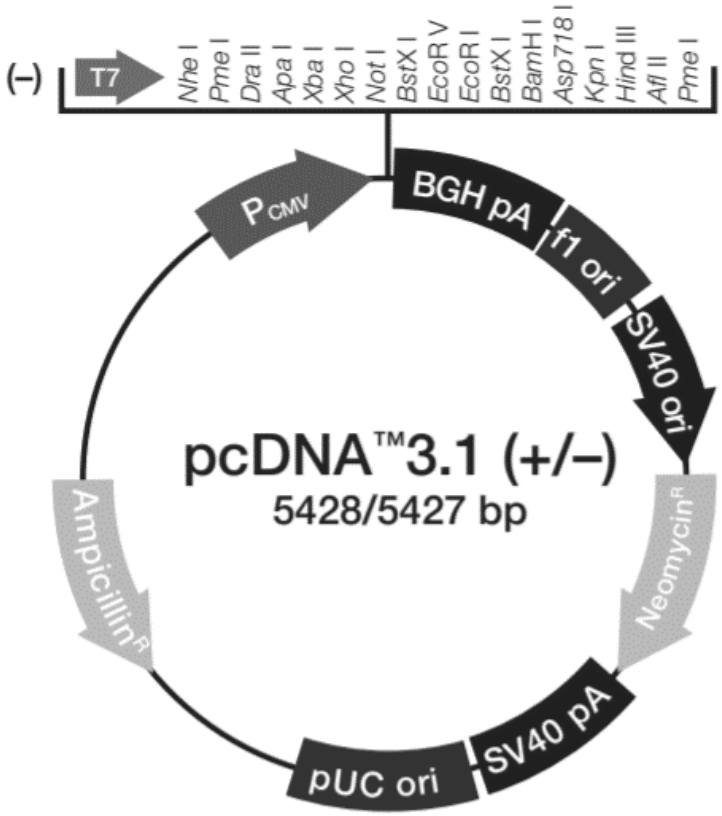

pCDNA3.1- MCAM plasmid map.

pcDNA3.1-MCAM contains full-length MCAM cDNA inserted into the MCS of pcDNA3.1 (-) between the *Xba*1 and *Not*1 restriction enzyme sites. Image of pcDNA3.1 was obtained from http://tools.thermofisher.com/content/sfs/vectors/pcdna3.1-.pdf

Appendix K

Map for CRISPR knockout plasmid

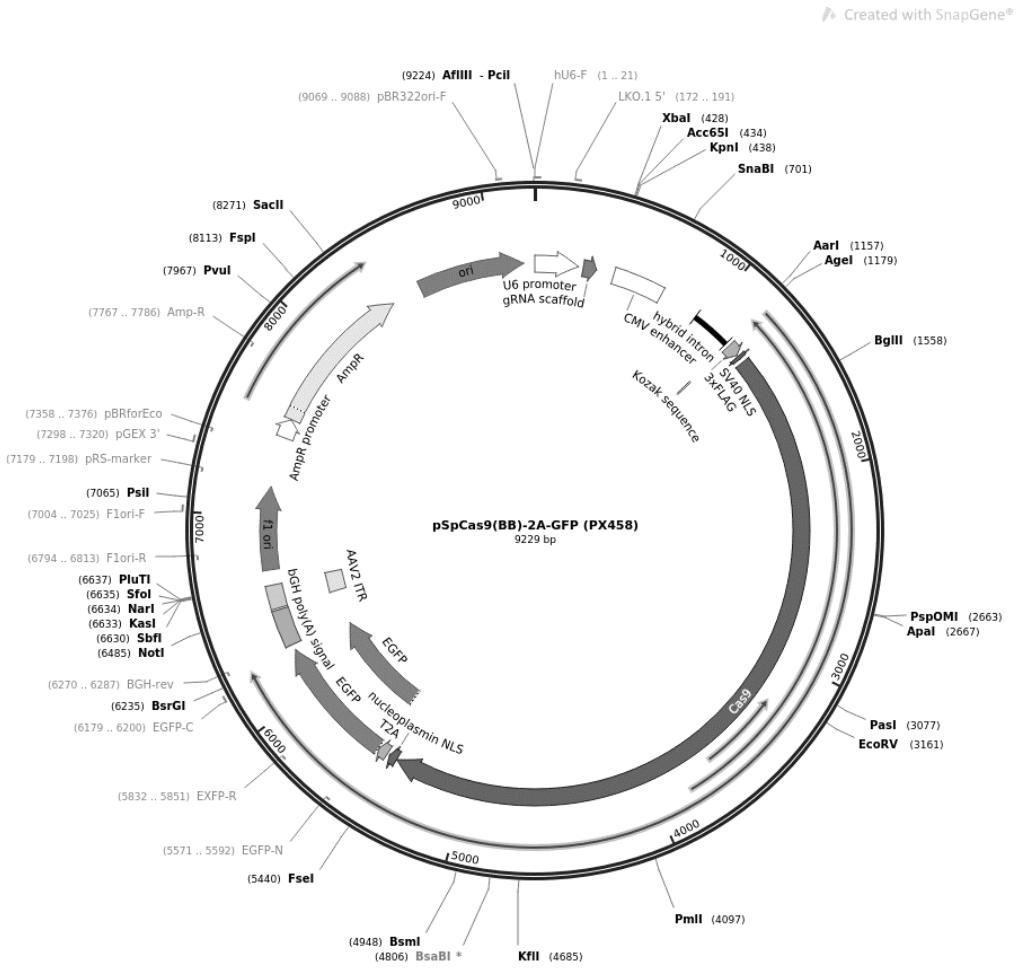

pSpCas9(BB)-2A-GFP plasmid map

Addgene plasmid #65221. PS1 and PS2 guide sequences were inserted into the BbsI sites of pSpCas9(BB)-2A-GFP using the protocol described by (Ran *et al.*, 2013). Cloning performed by Ms Melissa Eccles.

Appendix L
Sequencing of guide RNA
for PS1 and PS2 CRISPR knockout

Guide sequence #3 for CRISPR-KO of PS1

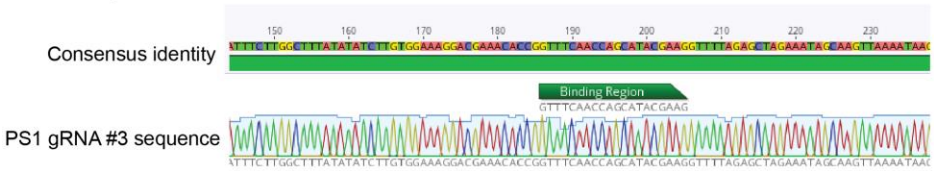

Guide sequence #4 for CRISPR-KO of PS1

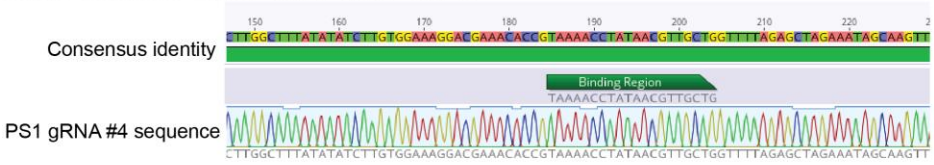

Guide sequence #1 for CRISPR-KO of PS2

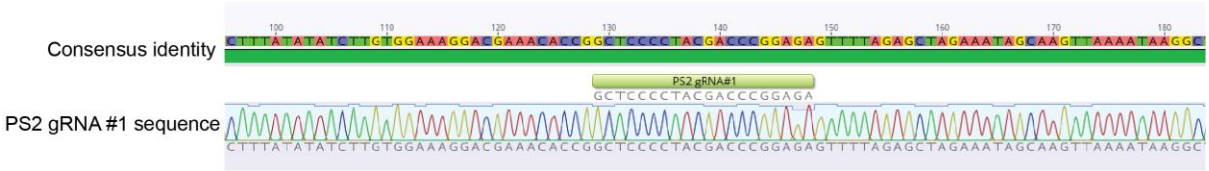

Guide sequence #4 for CRISPR-KO of PS2

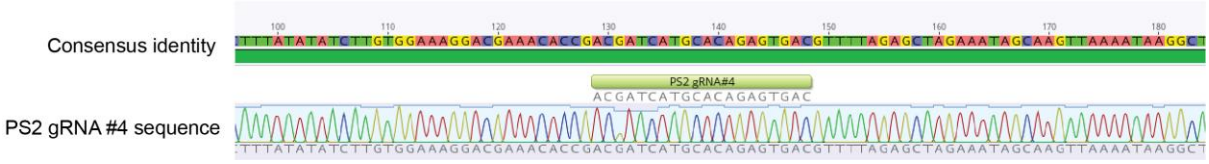

Sequencing was performed on CRISPR/Cas9 plasmids, using primers designed against the guide RNA sequence. Once the correct sequence was confirmed, cells were transfected and used in downstream applications.

Appendix M

Presenilin-NTF protein expression in MM253 melanoma cells to confirm KO

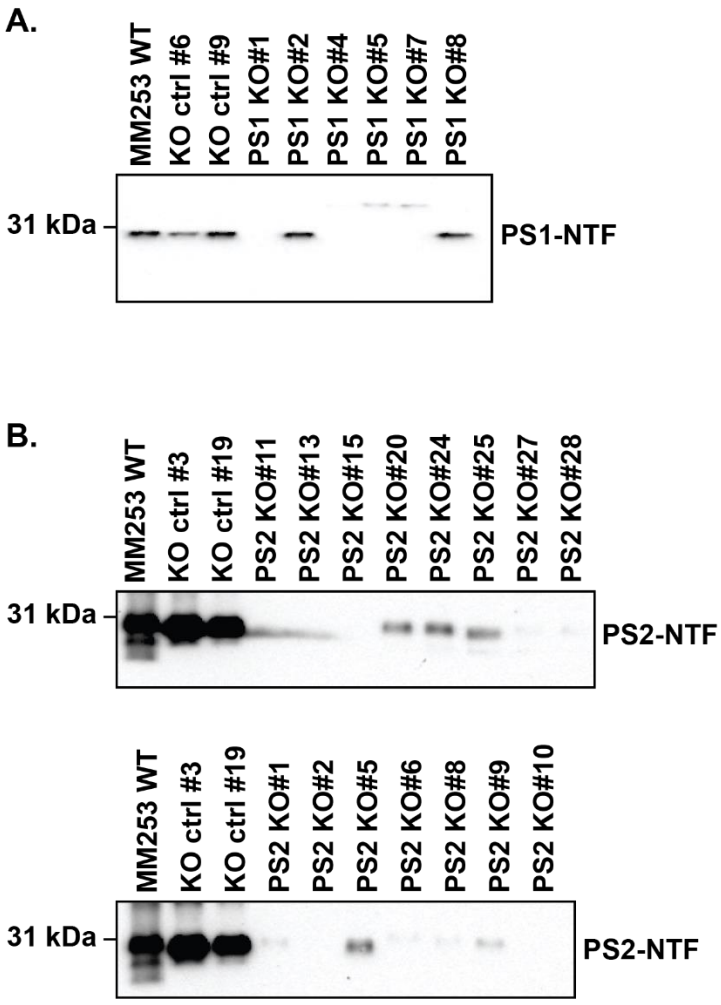

MM253 melanoma cells were screened for KO of PS1 (A) and PS2 (B) at the protein level. Whole cell lysates were collected and analysed via immunoblot, and absence of either the PS1 of PS2 N-terminal fragment was used to confirm KO (or knockdown) of the respective proteins.

Appendix N

MCAM-I mRNA expression in MM253 PS1 and PS2 KO

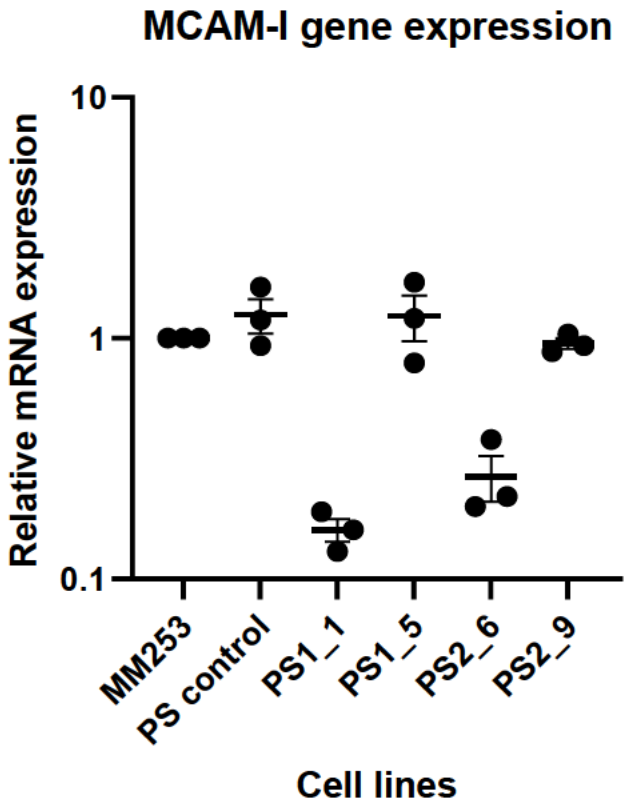

Expression of MCAM-I mRNA was determined suing qPCR. In line with immunoblot and flow cytometry results, the expression of MCAM-I was lower in some PS KO MM253 cell lines. The lowest expression was in PS1 KO#1 and PS2 KO#6.

Appendix O

Non-specific staining of cells labelled with LAMP2

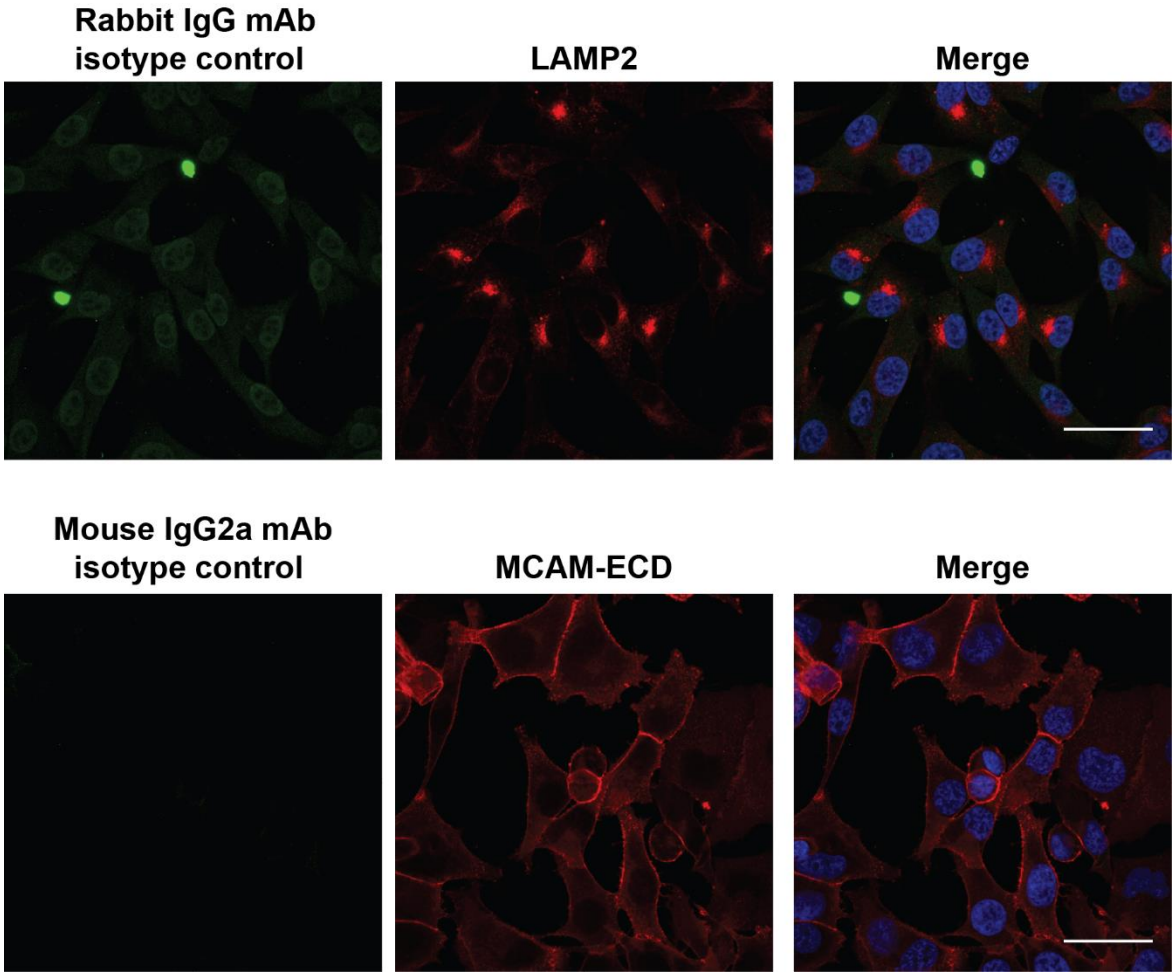

Non-specific staining in MM253 cells labelled with rabbit IgG mAb isotype control and AF488, followed by LAMP2 (mouse IgG) and AF555. Despite the use of different isotypes, staining with LAMP2, a hybridoma antibody, produced non-specific staining, predominantly within the nucleus, but also intracytoplasmic staining. This was not apparent when MCAM-ECD-specific antibody (mouse IgG2a isotype) was used in place of LAMP2, indicating the issue is related to LAMP2.

Appendix P

Impaired glycosylation did not appear to enhance MCAM-CTF cleavage

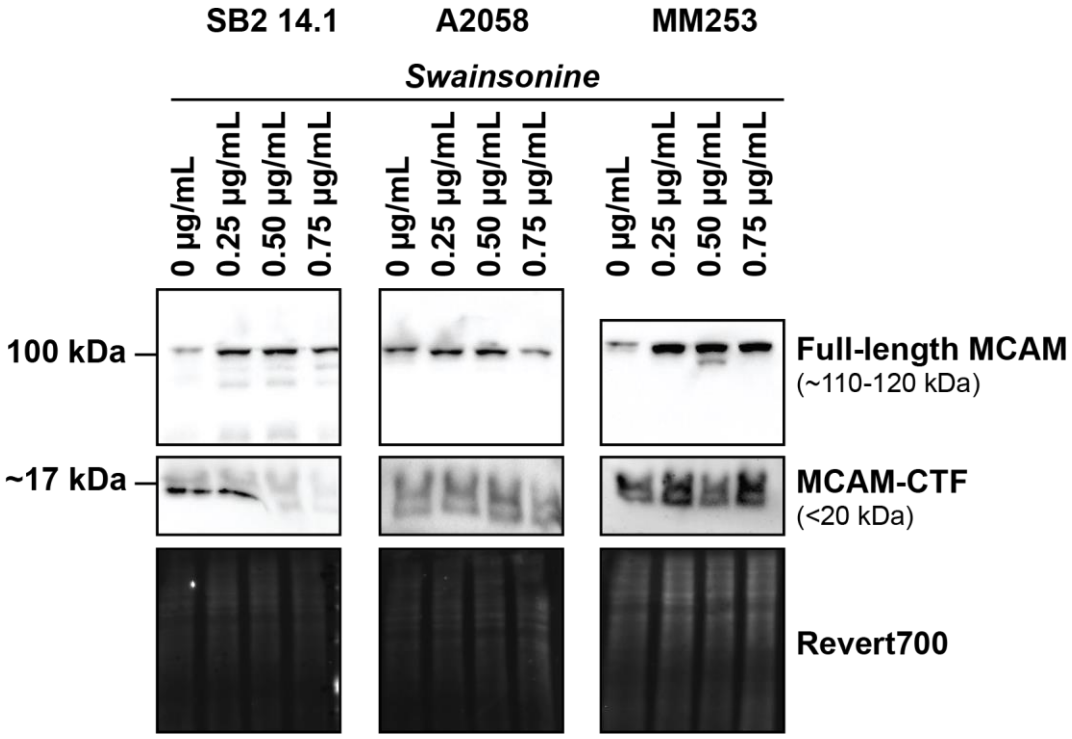

A preliminary study (n=1) was performed in three melanoma cell lines to investigate whether glycosylation of MCAM affected its cleavage. Cells treated with increasing concentrations of Swainsonine did not appear to accumulate MCAM-CTF, suggesting that impaired glycosylation did not significantly enhance MCAM shedding.

Appendix Q

Canonical CaM-binding motifs

Canonical CaM-binding motifs

Motif	Sequence
Ca^{2+} dependent	
1–10	[FILVW]xxxxxxxx[FILVW]
1–5–10	[FILVW]xxx[FAILVW]xxxx[FILVW]
Basic 1–5–10	[RK][RK][RK][FAILVW]xxx[FILV]xxxx[FILVW]
1–12	[FILVW]xxxxxxxxxx[FILVW]
1–14	[FILVW]xxxxxxxxxxxx[FILVW]
1–8–14	[FILVW]xxxxxx[FAILVW]xxxxx[FILVW]
1–5–8–14	[FILVW]xxx[FAILVW]xx[FAILVW]xxxxx[FILVW]
Basic 1–8–14	[RK][RK][RK][FILVW]xxxxxx[FAILVW]xxxxx[FILVW]
1–16	[FILVW]xxxxxxxxxxxxxx[FILVW]
Ca^{2+} independent	
IQ	[FILV]Qxxx[RK]Gxxx[RK]xx[FILVWY]
IQ-like[a]	[FILV]Qxxx[RK]xxxxxxxx
IQ-2A	[IVL]QxxxRxxxx[VL][KR]xW
IQ-2B	[IL]QxxCxxxxKxRxW
IQ unconventional	[IVL]QxxxRxxxx[RK]xx[FILVWY]

Numbers for the Ca^{2+}-dependent motifs indicate the positions that require a hydrophobic residue. Residues in the brackets can substitute for each other; x indicates any amino acid residue.
[a]Some IQ-like motifs require Ca^{2+} for CaM binding.

Canonical CaM-binding motifs have been described previously. Table taken from (Mruk *et al.*, 2014)

Appendix R

Predicted CaM binding sites within the MCAM-l cytoplasmic tail

The motif score is the number of times a single residue is predicted to be included in a calmodulin binding motif (# 0-9 times; A=10, B=11, C=12, D=13, E=14, F=15, Z=>15 times). Each residue that makes up part of a particular CaM binding motif is also designated a numerical value based on the number of times a single residue is part of a particular canonical binding motif (shown below the sequence). Each of the motif types are listed on the left side ($^{+}$denotes the motifs that are Ca^{2+} independent. IQ-like motifs can be both Ca^{2+}- dependent and Ca^{2+}- independent). Within the WT MCAM-l sequence, a motif spanning the TMD and juxtamembrane region of the ICD was identified. Sequences containing substitution mutations within the MCAM-ICD were also assessed. The first sequence has a Tyrosine (Y) to Glycine (G) substitution (^) at position 641. This mutation does not affect the predicted CaM binding motifs. However, a mutation to the dileucine motif (Leucine (L) to Proline (P) at position 623) may lead to weaker MCAM-CaM interactions. Although this mutation does not alter the predicted binding motifs, the substitution of a L to P seemingly interrupts some of the canonical CaM-binding motifs. CaM is still predicted to interact with the mutated MCAM tail, albeit with a lower affinity.

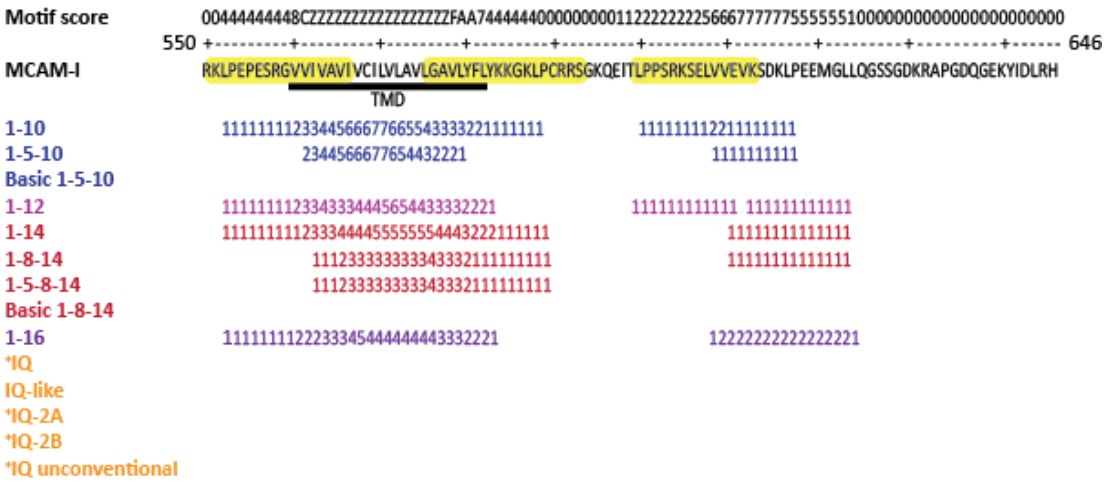

Appendix Q- i Predicted CaM binding sites in WT MCAM

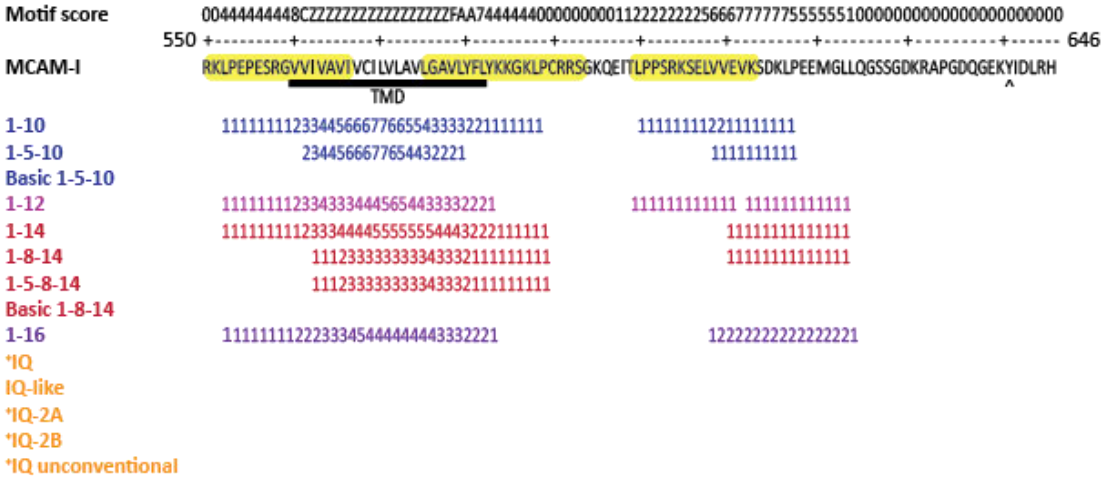

Appendix Q- ii Predicted CaM binding sites in MCAM with a Tyr (T) to Gly (G) mutation

Appendix Q- iii Predicted CaM binding sites in MCAM with a Leu (L) to Pro (P) mutation

Appendix S
Pull-down experiments for MCAM-ICD-binding proteins

Method

Protein production and pull-down

A plasmid expressing the MCAM-l cytoplasmic tail (aa584-646), inserted in the pGex.4T vector (BamHI/NotI restriction sites; pGex-MCAM), was previously constructed in our lab. This plasmid produces the MCAM cytoplasmic tail linked to Glutathione S-Transferase (GST). pGex.4T lacking an insert (pGex-empty) was used as a negative control. These plasmids were transformed into XL10 Gold chemically competent *E.coli* cells and grown on LB-Amp agar plates. Single colonies were selected and expanded in a mini culture, then plasmid DNA was purified from the culture, digested (BamHI and NotI), and checked on a gel.

Once the correct plasmid was confirmed, the DNA was transformed into chemically competent BL-21 *E.coli* cells for protein expression. For this, 100 µL bacterial cells were transferred to a 1.5 mL tube, on ice. 2 µL of plasmid DNA was added and mixed by gently flicking. Tubes were incubated on ice for 30 min, then cells were heat-shocked by immersing in a 50^{o}C water bath for 45 s followed by recovery on ice for 5 min. The transformed cells were plated on LB agar plates with 100 µg/mL ampicillin and incubated O/N at 37^{o}C. Single colonies were selected and expanded in LB-Amp liquid media culture with ampicillin O/N at 37^{o}C, with shaking at 220 rpm. For protein induction, 2 mL of O/N culture was first expanded in 100 mL LB-Agar. The optical density of the culture was measured at regular intervals until it reached 0.6 - 1.0 arbitraty units when measured at 600 nM using a spectrophotometer. A small “uninduced” sample was collected, then 0.5 mM IPTG was added to the culture and incubated for 3 hours to allow MCAM-GST protein expression to occur. Cultures were centrifuged at 500 g for 5 min, 4^{o}C to pellet cells. *E.coli* cell pellets were stored at -20^{o}C until needed.

BL-21 cell pellets were thawed and washed twice in ice-cold PBS, then resuspended in lysis buffer containing PBS, 5 mM DTT, 100 µg/mL Lysozyme, and 1x CPI. Cells were lysed on ice 20 min, then sonicated for 20 pulses at 80 Volts. The duration of each pulse was 10 s, followed by a 20 s break. This process was repeated twice. The bacterial lysates were kept on ice as much as possible. Following sonication, lysed cells were passed through an 18G and 23G needle to sheer DNA, then incubated with 1% (v/v) TritonX-100 for 30 min at 4ºC with end-over-end mixing. Debris was pelleted by centrifugation (2000 x g for 15 min at 4ºC). The clarified supernatant was then incubated with pre-washed gluthathione sepharose beads (GE170756, Sigma Aldrich) with end-over-end mixing at 4ºC, to enable the MCAM-GST fusion protein to bind to the beads. Meanwhile, SB2 14.1 cell lysates were prepared, as described in section 2.11.2.

The GST beads (now linked to MCAM-GST fusion protein) were pelleted and washed twice with HBS (pelleting beads at 330 x g for 1 min). SB2 14.1 lysates were added and mixed with beads/MCAM-GST for 24 hours at 4ºC with end-over-end mixing. Proteins within the SB2 14.1 lysates that interact with the MCAM fusion protein should form a receptor-ligand compex, bound to the glutathione beads.

SDS-PAGE for bound and un-bound proteins

Samples from pull-down experiments (descrbed above) that were used for SDS-PAGE were processed as follows: after overnight incubation with whole cell lysates, the GST beads were pelleted and washed three times with ice-cold HBS to remove un-bound proteins. To elute bound proteins from beads, samples were resuspended in SDS-loading buffer and boiled for 5 min at 90ºC. Samples were processed using SDS-PAGE and immunoblot, as detailed in section 2.7. Membranes were probed for moesin (known to interact with MCAM-ICD at the KKGK motif). The anti-MCAM mAb CC9 was also used to confirm the presence of MCAM in the lysate.

Mass-spectrometry for MCAM-binding proteins

For samples to be analysed by mass-spectrometry, beads were pelleted and washed three times with ice-cold PBS. Proteins were then eluted from the beads by incubating with 10 mM L-glutathione in Tris (pH 8.0) for 10 min on a rocking platform. The beads were pelleted by gentle centrifugation and supernatants were recovered. Four volumes of acetone (kept at -20^{o}C) was added to each sample and incubated at -20^{o}C for 1 hour to precipitate the proteins. Samples were centrifuged at ~15,600 x g for 10 min and acetone was removed. Pelleted proteins were air-dried at room temp to allow residual acetone to evaporate, then transferred to -20^{o}C for storage. Further processing and analysis were conducted at Proteomics International, Harry Perkins Institute of Medical Research, Perth, Western Australia, as described below.

Samples were analysed by electrospray ionisation mass-spec using the Shimadzu Prominence nano HPLC system (Shimadzu, Kyoto, Japan) coupled to a 5600 TripleTOF mass spectrometer (Sciex, Framingham, MA). Peptides (5 µg) were loaded onto an Agilent Zorbax 300SB-C18, 3.5 µm (Agilent Technologies, Santa Clara, CA) and separated with a linear gradient of water/acetonitrile/0.1% formic acid (v/v).

Spectral data were analysed using ProteinPilot™ 5.0 Software (Sciex) against:

Database: SwissProt

Taxonomy: *Homo sapiens* (Human)

Version: April 2017; 20,199 sequences

Proteins that had an unused ProtScore of >1.3, with at least one peptide that had greater than 95% confidence of coverage were predicted to bind to the MCAM-ICD.

Results

Twelve proteins met the criteria to be classified as an MCAM-ICD-binding protein, including an unused ProtScore of >1.3. Evidently, this is not a true representation of all MCAM-binding proteins, as proteins known to interact with MCAM (such as moesin). Amongst the proteins that were pulled down from melanoma cell lysates by the MCAM-ICD were a transcription factor for myotube development, a splicing factor, proteins involved in signal transduction pathways, and components of microtubules that are associated with cell migration.

Prediction of proteins binding to the MCAM-ICD

Proteins bound specifically to MCAM-ICD	# of peptides	Unused (ProtScore)	% coverage
Nascent polypeptide-associated complex subunit alpha, muscle-specific form	3	6.01	1.9
Glutathione S-transferase P	2	3.35	20
Serine/arginine-rich splicing factor 2	2	3.24	14.9
Crk-like protein	1	2.18	4
LanC-like protein 1	1	2.12	5.5
Tubulin β-2B chain	1	2.02	3.4
Chromodomain-helicase-DNA-binding protein 5	1	2.00	0.5
Serine-threonine kinase receptor-associated protein	1	2.00	4.6
Protein S100-A16	1	2.00	10.7
G-rich sequence factor 1	2	2.00	4.6
High mobility group protein B1	1	2.00	7.4
Importin subunit α-6	1	2.00	2.4